
Electronic Thesis and Dissertation Repository

9-13-2024 11:00 AM

A Study on Biochar Properties Toward their Effects on Adsorption Mechanisms for Aromatic Organic Compounds in Water

Griffin Loeb sack, *Western University*

Supervisor: Yeung, Ken., *The University of Western Ontario*


Co-Supervisor: Berruti, Franco., *The University of Western Ontario*

Co-Supervisor: Klinghoffer, Naomi., *The University of Western Ontario*

A thesis submitted in partial fulfillment of the requirements for the Doctor of Philosophy degree in Chemistry

© Griffin Loeb sack 2024

Follow this and additional works at: <https://ir.lib.uwo.ca/etd>

 Part of the [Analytical Chemistry Commons](#), [Environmental Chemistry Commons](#), and the [Physical Chemistry Commons](#)

Recommended Citation

Loeb sack, Griffin, "A Study on Biochar Properties Toward their Effects on Adsorption Mechanisms for Aromatic Organic Compounds in Water" (2024). *Electronic Thesis and Dissertation Repository*. 10439. <https://ir.lib.uwo.ca/etd/10439>

This Dissertation/Thesis is brought to you for free and open access by Scholarship@Western. It has been accepted for inclusion in Electronic Thesis and Dissertation Repository by an authorized administrator of Scholarship@Western. For more information, please contact wlsadmin@uwo.ca.

Abstract

Biochar, a carbon-rich by-product of the pyrolytic processing of lignocellulosic biomass in a zero or low-oxygen environment, has the potential application as a promising adsorbent for the elimination of a variety of pollutants. This work proposes and outlines a detailed method to investigate the adsorption mechanisms of biochar towards organic compounds in water, which was used to investigate a range of biochars with the objective of determining what compounds biochars are best suited to adsorb in real-world applications. Ibuprofen, acetaminophen, methyl orange and methylene blue were selected as four test compounds that are representative of organic pollutants and were used to investigate biochars produced by four woody and four non-woody biomasses under different pyrolysis temperatures and flow gases, N₂ and CO₂. While biochars that had mainly hydroxyl functional groups showed good adsorption of aromatic compounds with electron-withdrawing groups, biochars with carbonyl groups were found to have greater adsorption capacities for aromatic compounds with electron-donating groups. This suggests that the electrostatic interactions and π - π EDA interactions are both heavily influenced by the same functional groups, resulting in possible competition between the mechanisms. Subsequently, further investigation of the effect of the physical properties on adsorption mechanisms of biochar was performed where HNO₃, H₂O₂, and KOH, post-treatment on different woody biochars prepared under CO₂ at 800°C were chosen for further study. While the mineral content was not seen to have a significant role in these interactions, oxygen-functional groups dominated in contributing to negatively charged sites and thus electrostatic interactions of biochar. It was also found that OH groups increased electrostatic interactions for all the biochars, while increasing π - π electron donor-acceptor interactions with compounds with electron-withdrawing groups, as was seen for biochars activated with CO₂. Carbonyl functional groups increased these interactions with compounds containing electron-donating groups. Overall, five types of adsorption mechanisms were identified. Five of these biochars were selected that displayed each of these five main mechanisms, which were investigated for adsorption with complex mixtures of aromatic compounds, which is more representative of wastewater. The oxygen-containing functional groups had the largest influence on competitive adsorption, as they often provide the greatest number of adsorption sites for organic compounds via both electrostatic and π - π electron donor-acceptor interactions. In general, the biochars with different oxygen-containing functional groups, carbonyl

and hydroxyl in particular, had greater synergetic adsorption when combining compounds. Finally, a bio-magnetic adsorbent was produced from different biomasses via co-pyrolysis with iron-rich red mud, a waste product of the aluminum industry that is rich in iron oxide, for easier removal post adsorption. The resulting biochar-red mud composite material demonstrated good adsorption and had magnetic properties. Mixing ratios of biomass and RM were also tested to determine optimal composition for magnetic and adsorptive properties of the composites, where better adsorption performance was found with a ratio of 1:2 for RM/biomass. A threshold of biomass to RM ratio was also found to maintain magnetic properties, where the magnetic properties of the adsorbents decreased gradually when a greater ratio of biomass to RM was used, with the 1:9 RM:DF having the optimal properties of all composites tested in this study.

Keywords: Biochar, Pyrolysis, Adsorption Mechanisms, Water treatment, Competitive adsorption, Bio-magnetic adsorbent.

Summary for Lay Audience

Biochar is a charcoal-like product that is made by decomposing farm, food, and other waste products in high-heat environments in the absence of oxygen to prevent combustion. This process is referred to as pyrolysis, and the biochar that is produced can be used to adsorb a variety of pollutants in water sources including drugs and other small molecules that may have detrimental effects on health and the environment. Since biochar may have different chemical bonds on its surface, as well as different pore sizes and surface areas depending on what is used to produce the biochar, many biochars can adsorb different molecules better than others. This thesis first proposes a method to investigate what makes biochar able to adsorb aromatic molecules, which are common pharmaceutical compounds in water sources. This is done by using common drugs such as Ibuprofen and acetaminophen, as well as common dyes including methyl orange and methylene blue as test molecules to see how biochars made from woods and grasses behave differently in terms of adsorption. It was found that biochars with bonds to oxygen atoms tended to have higher adsorption capacities of aromatic molecules (containing carbon ring structures), attributed to a charge transfer between the adsorbing molecule and the biochar. This was because oxygen groups can both donate or withdraw electrons from the biochar, allowing it to attract molecules of opposing charge. This highlights the importance of both aromatic and oxygen groups on biochar surfaces in terms of adsorption. This was confirmed when the biochars were purposefully altered to have more of these oxygen groups by post-treatment with oxidizing acidic and basic chemicals. It was then found that when the oxygen groups were bonded to hydrogens there was a decrease in adsorption of negatively charged molecules, as these were repelled by the oxygen groups. Overall, five types of adsorption were identified, all of which were investigated for their adsorption in mixtures of two molecules together. In general, it was found that the biochars with different kinds of oxygen groups had the most favourable adsorption results as molecules did not compete for adsorption sites with both types of groups. Finally, a bio-magnetic adsorbent was produced from biomasses mixed with iron-rich red mud, a waste product of the aluminum industry rich in iron oxide. The processes were shown to be successful in converting all biomass species and demonstrated good adsorption and magnetic properties of the produced composites, with the best being the 1:9 RM: DF composite.

Statement of Authorship

The contents and some of the data of Chapter 2 have been submitted to be published in the Journal of Waste Management. This includes the adsorption results and physical characterization of the Douglas fir-derived biochars. The author of this thesis was responsible for a majority of the work herein, including experimental design and execution including biochar characterization, adsorption experimentation, data processing and analysis, as well as the writing of the manuscript and participating in the editing and review of the manuscript along with supervisors Dr. Yeung, Dr. Berruti and Dr. Klinghoffer.

The contents and some of the data of Chapter 3 have been submitted to be published in the Journal of Waste Management. This includes the adsorption results and physical characterization of the Douglas fir-derived biochars. The author of this thesis was responsible for a majority of the work herein, including experimental design and execution including biochar characterization, adsorption experimentation, data processing and analysis, as well as the writing of the manuscript and participating in the editing and review of the manuscript along with supervisors Dr. Yeung, Dr. Berruti and Dr. Klinghoffer.

The contents and some of Chapter 4 have been submitted to be published in the journal, Chemosphere. The author of this thesis was responsible for a majority of the work herein, including experimental design and execution including biochar characterization, adsorption experimentation, data processing and analysis, as well as the writing of the manuscript and participating in the editing and review of the manuscript along with supervisors Dr. Yeung, Dr. Berruti and Dr. Klinghoffer.

The contents and data Chapter 5 have been published in the journals of Waste Management, Analytical and Applied Pyrolysis, and the Canadian journal of Chemical Engineering under a title of the references shown below. The author of this thesis was responsible for a majority of the work herein, including experimental design and execution biochar characterization, adsorption experimentation, data processing and analysis, as well as the writing of the manuscript and participating in the editing and review of the manuscript. The author also aided Dr. Kang in the initial preparation and synthesis of composites. Dr. Sarchami

helped to perform some elemental analysis including CHNS-O and ICP analysis, and some of the pyrolysis and physical activation of samples were performed by Dr.Papari. Magnetic susceptibility tests were performed by Dr. Bartoli, Dr. Torsello, and Dr. Gerbaldo. Editing and revision was done with the help of supervisors Dr. Yeung, Dr. Berruti and Dr. Klinghoffer.

Acknowledgments

I would like to extend my sincere gratitude to the many people whose support and guidance were invaluable in the preparation of this thesis. First and foremost, I would like to thank my supervisors Dr. Ken Yeung, Dr. Franco Berruti, and Dr. Naomi Klinghoffer who have each offered invaluable advice, guidance, support and expertise throughout my research. I would also like to thank all of the members of Dr. Berruti's research group, past and present, for all of their help and valuable discussions, with a special thanks to Ms. Heejin Lee and Ms. Neha Batta for their extremely valuable knowledge and insight. Dr. Kang Kang, thank you for your mentorship, guidance and kindness over the years, much of this work could not have been done without your valuable help and advice. To Dr, Tahereh Sarchami, Mr. Lu Liu and Ms. Megan Parkes, thank you for your expertise in analytical equipment, your technical support and your patience when managing our analytical lab. I would also thank my fellow graduate students for their friendship, many discussions and advice towards my research and future, with particular thanks to Ms. Mahsa Dolatkah Ouch Bolagh and Mr. Michael Thompson.

I would like to thank my committee members and graduate school advisors. Dr. Lars Konermann, Dr. Martin Stillman, Dr. Silvia Fiore, and Dr. Mauro Giorcelli, thank you for reading my thesis, testing my knowledge, and providing valuable advice.

I would also like to thank Ms. Rebecca Sarazen, and Mr. Ivan Barker for their instruction and help during analytical analysis with FTIR, TGA, and SEM microscopy. Furthermore, I would like to thank the rest of the team at Surface Science Western for their collaboration and help using analytical instruments, without which this work could not have been done.

Finally, I would like to thank my incredible friends and family, Bethany, Dale, Jeffrey, Kruti, Mackenzie, Meaghan and Samantha for always being there for me when I needed it. To Matthew, thank you for your never-ending love and support, I would not have done it without you by my side.

Table of Contents

Abstract.....	ii
Summary for Lay Audience.....	iv
Statement of Authorship.....	v
Acknowledgments.....	vii
Table of Contents.....	viii
List of Tables.....	xii
List of Figures.....	xiii
List of Abbreviations.....	xvii
Chapter 1.....	1
1 Background Motivation and Introduction to Pyrolysis.....	1
1.1 Environmental Motivation.....	2
1.2 Introduction to Pyrolysis.....	3
1.3 Biochar Characterization Methods.....	6
1.3.1 BET Surface Area Analysis.....	7
1.3.2 Attenuated Total Reflectance (ATR)-FTIR Spectroscopy.....	10
1.3.3 Proximate and CHNS-O Elemental Analysis.....	12
1.3.4 Scanning Electron Microscope (SEM) – Energy Dispersive X-Ray (EDX) Spectroscopy.....	13
1.3.5 Thermogravimetric Analysis.....	16
1.4 Motivation and Objectives.....	17
1.5 Thesis Outline.....	18
1.6 References.....	20
Chapter 2.....	27
2 Method for the Investigation of Biochar Adsorption Mechanisms for Aqueous Aromatic Organic Compounds.....	27
2.1 Statement of Authorship.....	27
2.2 Chapter Abstract.....	28
2.3 Introduction.....	28
2.4 Materials and Methods.....	32
2.4.1 Materials.....	32
2.4.2 Procedure for Pyrolysis.....	33
2.4.3 Methodology for Investigation of Biochar Adsorption Mechanisms for Aqueous Aromatic Compounds.....	33
2.4.4 Adsorption Experiments.....	36

2.4.5	Biochar Characterization Methods	37
2.4.5.1	Proximate and CHNS-O Elemental Analysis	37
2.4.5.2	ATR-FTIR Spectroscopy	37
2.4.5.3	BET Surface Analysis	37
2.4.5.4	SEM-EDX Spectroscopy	38
2.4.5.5	Thermogravimetric Analysis.....	38
2.5	Results and Discussion	38
2.5.1	Effect of N ₂ and CO ₂ Pyrolysis Flow Gas on Adsorption Mechanisms of Biochars for Aromatic Compounds.....	38
2.5.2	Effect of Pyrolysis Temperature on Adsorption Mechanisms of Woody and Non-Woody Biochar for Aromatic Compounds.....	46
2.5.3	Effect of Biomass on Adsorption Mechanisms of Biochar for Aromatic Compounds	54
2.6	Conclusions.....	64
2.7	References.....	67
Chapter 3	73
3	Investigation of Effect of Physical Properties on Adsorption Mechanisms for Aqueous Organic Compounds by Biochar after Oxidative Post-Treatments using HNO ₃ , H ₂ O ₂ , and KOH	73
3.1	Statement of Authorship	73
3.3	Chapter Abstract.....	74
3.4	Introduction.....	74
3.5	Materials and Methods.....	76
3.5.1	Materials	76
3.5.2	Biochar Preparation and Post-Treatment Procedures	77
3.5.3	HNO ₃ Post Treatment	77
3.5.4	H ₂ O ₂ Post-Treatment.....	77
3.5.5	KOH Post-Treatment	77
3.5.6	Biochar Characterization Methods	78
3.5.6.1	Proximate and elemental analysis.....	78
3.5.6.2	ATR-FTIR spectroscopy	78
3.5.6.3	BET Surface Analysis	78
3.5.6.4	SEM-EDX Spectroscopy	78
3.5.7	Test for Adsorption Mechanisms	79
3.6	Results and Discussion	79

3.6.1	Effect of HNO ₃ Post Treatment on Adsorption Mechanisms	82
3.6.2	Effect of H ₂ O ₂ Post Treatment on Adsorption Mechanisms	84
3.6.3	Effect of KOH Post Treatment on Adsorption Mechanisms	91
3.7	Conclusion	98
3.8	References	101
Chapter 4	106
4	Competitive Adsorption of Acetaminophen, Methyl Orange and Methylene Blue by Five Biochars with Different Adsorption Mechanisms	106
4.1	Statement of Authorship	106
4.3	Chapter Abstract.....	107
4.4	Introduction.....	107
4.5	Materials and Methods.....	109
4.5.1	Materials	109
4.5.2	Preparation of Biochars.....	109
4.5.3	H ₂ O ₂ Post-Treatment.....	109
4.5.4	KOH Post-Treatment	110
4.5.5	Biochar Characterization Methods	110
4.5.5.1	CHNS-O Elemental Analysis.....	110
4.5.5.2	ATR-FTIR Spectroscopy	110
4.5.5.3	BET Surface Area	110
4.5.6	Adsorption Mechanisms Tests	111
4.5.7	Competitive Adsorption Tests.....	111
4.6	Results and Discussion	112
4.6.1	Adsorption Mechanisms of Biochars.....	112
4.6.2	Competitive Adsorption of Methyl Orange and Methylene Blue.....	117
4.6.3	Competitive Adsorption Methyl Orange and Acetaminophen.....	120
4.6.4	Competitive Adsorption of Acetaminophen and Methylene Blue	123
4.7	Conclusion	125
4.8	References.....	128
Chapter 5	133
5	Production of Magnetic Biochar via Co-Pyrolysis with Red Mud and Investigation of Adsorption Mechanisms	133
5.1	Statement of Authorship	133
5.2	Chapter Abstract.....	134

5.3	Introduction.....	134
5.4	Materials and Methods.....	136
5.4.1	Materials	136
5.4.2	Co-Pyrolysis Procedure	136
5.4.3	H ₂ O ₂ Post Treatment.....	137
5.4.4	Biochar Characterization Methods	137
5.4.4.1	BET Surface area	137
5.4.4.2	ATR-FTIR Spectroscopy	137
5.4.4.3	SEM-EDX Spectroscopy	137
5.4.4.4	CHNS-O, ICP and Proximate analysis	138
5.4.5	Magnetic Susceptibility Tests	138
5.4.6	Adsorption Mechanisms Tests	139
5.5	Results and Discussion	139
5.5.1	Investigation of Physical Characteristics of Biochar RM Composite	140
5.5.2	Investigation on Effect of Pyrolysis Temperature on Biochar RM Composite ..	146
5.5.3	Investigation of Adsorption Properties of Biochar RM Composites	148
5.5.4	Effect of H ₂ O ₂ Post-Treatments on Biochar RM Composites	151
5.5.5	Optimization of RM and Biomass Ratio for Adsorptive and Magnetic Properties for Biochar RM Composite.....	153
5.6	Conclusion	157
5.7	References.....	158
Chapter 6	162
6	Conclusions and Future Work.....	162
6.1	Conclusions.....	163
6.2	Future Work	166
6.3	References.....	168
Curriculum Vitae	169

List of Tables

Table 2.1 Physical characteristics of aromatic compounds used as adsorbates for investigation of adsorption mechanisms of biochar.....	33
Table 2.2 Proximate and elemental analysis, and textural properties of biochars	43
Table 2.3 Summary of biochar adsorption mechanisms, physical characteristics and pyrolysis .	65
Table 3.1 Proximate and elemental analysis, and textural properties of biochars	79
Table 3.2 Summary of biochar adsorption mechanisms, physical characteristics and pyrolysis conditions.....	99
Table 4.1 Adsorption mechanisms, elemental composition and surface parameters of biochars	113
Table 4.2 Simplified summary of changes in adsorption capacities of aromatic adsorbates when adsorbed in solution with other aromatic compounds	126
Table 5.1 Elemental composition of red mud and biomasses	140
Table 5.2 Yields, physical properties, and adsorption capacities of biochar and composite adsorbents	144

List of Figures

Figure 1.1 Schematic diagram of pyrolysis in a) fixed bed and b) fluidized bed reactors	6
Figure 1.2 Adsorption isotherms for classification of BET isotherm results of concentration plotted against amount of adsorbate gas adsorbed by the sample	9
Figure 1.3 Illustration of evanescent wave in ATR crystal penetrating into sample for adsorption in ATR-FTIR spectroscopy (57).....	12
Figure 1.4 Block diagram of instrumentation for elemental CHNS-O analysis (61)	13
Figure 1.5 Schematic for the principal design of scanning electron microscope (62).....	15
Figure 1.6 Schematic of principle for x-rays produced from electron guns in energy dispersive x-ray spectroscopy (65).....	16
Figure 1.7 Block Diagram of instrumentation of thermogravimetric analysis (67)	17
Figure 2.1 Schematic illustration of biochar adsorption mechanisms towards aromatic compounds in water	32
Figure 2.2 Structure of a) ibuprofen (IBU), b) acetaminophen (ACT), c) methyl orange (MO), and d) methylene blue (MB) at pH below and above individual pKa values (28,30,31,33)	36
Figure 2.3 TGA and DTG curves of a) RC and b) PH biomasses pyrolyzed under 2L/min CO ₂ and N ₂ pyrolytic gases	40
Figure 2.4 100X Magnification SEM images and EDX spectra of a) RC800-CO ₂ , b) RC800-N ₂ , c) PH800-CO ₂ , and d) PH800-N ₂	42
Figure 2.5 ATR-FTIR spectra of a) RC and b) PH derived biochars pyrolyzed at 800°C under CO ₂ and N ₂ pyrolytic gases.....	45
Figure 2.6 Adsorption capacities of IBU, ACT, MO, and MB with increasing pH for a) PH800-CO ₂ , b) PH800-N ₂ , c) RC800-CO ₂ , and d) RC800-N ₂ where adsorption was performed using 50ppm of compounds and 50 mg of biochar in 15mL solutions	46
Figure 2.7 Adsorption capacities of IBU, ACT, MO, and MB with increasing pH for a) RC500-CO ₂ , b) RC800-CO ₂ , c) DF500-CO ₂ , d) DF800-CO ₂ , e) PH500-CO ₂ , f) PH800-CO ₂ , g) MC500-CO ₂ , and g) MC800-CO ₂ where adsorption was performed using 50 ppm of compounds and 50 mg of compounds and 50mg of biochar in 15 mL solutions	48
Figure 2.8 100X SEM images and EDX spectra of a) RC500-CO ₂ , b) RC800-CO ₂ , c) DF500-CO ₂ , d) DF800-CO ₂ , e) PH500-CO ₂ , f) PH800-CO ₂ , g) MC500-CO ₂ , and h) MC800-CO ₂	51

Figure 2.9 ATR-FTIR spectra of a) RC500-CO ₂ , b) RC800-CO ₂ , c) DF500-CO ₂ , d) DF800-CO ₂ , e) PH500-CO ₂ , f) PH800-CO ₂ , g) MC500-CO ₂ , and h) MC800-CO ₂	52
Figure 2.10 Adsorption capacities of IBU, ACT, MO, and MB with increasing pH for a) MC800-CO ₂ , b) SG800-CO ₂ , c) RC800-CO ₂ , d) DF800-CO ₂ , e) PW800-CO ₂ , and f) PH800-CO ₂ where adsorption was performed using 50ppm of compounds and 50 mg of biochar in 15mL solutions	55
Figure 2.11 ATR-FTIR spectra of RC800-CO ₂ , DF800-CO ₂ , PW800-CO ₂ , PH800-CO ₂ , MC800-CO ₂ , and SG800-CO ₂	57
Figure 2.12 TGA and DTG curves of RC, DF, PW, PH, MC, and PH biomasses pyrolyzed under 2L/min of CO ₂	58
Figure 2.13 Pyrolytic decomposition mechanisms of a) hemicellulose, b) cellulose and c) lignin	62
Figure 3.1 Adsorption capacities of IBU, ACT, MO, and MB with increasing pH for a) RC500-CO ₂ , b) RC500-CO ₂ -HNO ₃ , c) DF500-CO ₂ , and d) DF500-CO ₂ -HNO ₃	83
Figure 3.2 ATR-FTIR spectra of a) RC500-CO ₂ , b) RC500-CO ₂ -HNO ₃ , c) DF500-CO ₂ , and d) DF500-CO ₂ -HNO ₃	84
Figure 3.3 ATR-FTIR spectra of a) RC500-CO ₂ and RC500-CO ₂ -H ₂ O ₂ , b) DF500-CO ₂ and DF500-CO ₂ -H ₂ O ₂ , c) RC800-CO ₂ and RC800-CO ₂ -H ₂ O ₂ , and d) DF800-CO ₂ , and DF800-CO ₂ -H ₂ O ₂	86
Figure 3.4 100X SEM images and EDX spectra of a) RC500-CO ₂ , b) RC800-CO ₂ , c) RC500-CO ₂ -H ₂ O ₂ , d) RC800-CO ₂ -H ₂ O ₂ , e) DF500-CO ₂ , f) DF800-CO ₂ , g) DF500-CO ₂ -H ₂ O ₂ , h) DF800-CO ₂ -H ₂ O ₂	88
Figure 3.5 Adsorption capacities of IBU, ACT, MO, and MB with increasing pH for	90
Figure 3.6 100X SEM images of a) RC500-CO ₂ , b) RC800-CO ₂ , c) RC500-CO ₂ -KOH d) RC800-CO ₂ -KOH, e) DF500-CO ₂ , f) DF800-CO ₂ , g) DF500-CO ₂ -KOH, h) DF800-CO ₂ -KOH	94
Figure 3.7 ATR-FTIR spectra of a) RC500-CO ₂ and RC500-CO ₂ -KOH, and b) RC800-CO ₂ , and RC800-CO ₂ -KOH, c) DF500-CO ₂ and DF500-CO ₂ -KOH, and d) DF800-CO ₂ , and DF800-CO ₂ -KOH.....	95
Figure 3.8 Adsorption capacities of IBU, ACT, MO, and MB with increasing pH for	98
Figure 4.1 ATR-FTIR spectra of DF500-CO ₂ , DF800-CO ₂ , DF800-CO ₂ -H ₂ O ₂ , DF800-CO ₂ -KOH, and MC500-CO ₂	114

Figure 4.2 Adsorption capacities of IBU, ACT, MO, and MB with increasing pH for a) DF500-CO ₂ -KOH, b) DF800-CO ₂ , c) DF800-CO ₂ -H ₂ O ₂ , d) DF800-CO ₂ -KOH, and e) MC500-CO ₂ where adsorption was performed using 50ppm of compounds and 50 mg of biochar in 15mL solutions	115
Figure 4.3 Schematic of possible intermolecular interactions between a) MO and MB, b) MO and ACT, and c) ACT and MB	117
Figure 4.4 Adsorption Capacities of biochar in a solution containing MO, MB or mixtures of these compounds for biochars a) DF500-CO ₂ -KOH, b) MC500-CO ₂ , c) DF800-CO ₂ , d) DF800-CO ₂ -H ₂ O ₂ , and e) DF800-CO ₂ -KOH.....	119
Figure 4.5 Adsorption Capacities of biochar in a solution containing MO, ACT or mixtures of these compounds for biochars a) DF500-CO ₂ -KOH, b) MC500-CO ₂ , c) DF800-CO ₂ , d) DF800-CO ₂ -H ₂ O ₂ , and e) DF800-CO ₂ -KOH.....	122
Figure 4.6 Adsorption Capacities of biochar in a solution containing MB, ACT or mixtures of these compounds for biochars a) DF500-CO ₂ -KOH, b) MC500-CO ₂ , c) DF800-CO ₂ , d) DF800-CO ₂ -H ₂ O ₂ , and e) DF800-CO ₂ -KOH.....	125
Figure 5.1 SEM images at 100X and 400X Magnification of a) RM/RC-1/1, b) RM/DF-1/1, c) RM/PW-1/1, d) RM/MC-1/1, e) RM/PH-1/1, and f) RM/SG-1/1	141
Figure 5.2 100X magnification SEM images and EDX spectra of a) RM/RC-1/1, b) RM/DF-1/1, c) RM/PW-1/1, d) RM/MC-1/1, e) RM/PH-1/1, and f) RM/SG-1/1	143
Figure 5.3 FTIR spectra of a) RC800-CO ₂ , DF800-CO ₂ , PW800-CO ₂ , MC800-CO ₂ , PH800-CO ₂ , and SG800-CO ₂ and b) RM, and RM/biochar composites	146
Figure 5.4 a) TGA and b) DTG curves for RM, RC, DF, PW, MC, PH, and SG up to 800°C ...	148
Figure 5.5 Adsorption capacities for RM/biochar composites of a) ibuprofen, b) acetaminophen, c) methyl orange, and d) methylene blue with increasing pH	149
Figure 5.6 Adsorption capacities of IBU, ACT, MO, and MB with increasing pH for	151
Figure 5.7 Adsorption capacities of IBU, ACT, MO, and MB with increasing pH for a) RM/PW-1/1, and b) RM/PW-1/1-H ₂ O ₂	152
Figure 5.8 Adsorption capacity of ACT in 15 mL solution with 50 ppm ACT at neutral pH with 10 mg of a) RM/MC adsorbents and MC800-CO ₂ , and b) RM/PW adsorbents and PW800-CO ₂ with different RM to biomass mass ratios	154

Figure 5.9 SEM images and EDX spectra at 400X Magnification for a) a) RM/PW, and b) RM/MC	156
Figure 5.10 Magnetic susceptibility properties of a) RM/MC, and b) RM/PW adsorbents prepared with different RM to biomass mass ratios	156

List of Abbreviations

ACT	Acetaminophen
ATR	Attenuated total reflectance
BET	Braunn-Emmett and Teller
CHNS-O	Carbon, hydrogen, nitrogen, sulphur and oxygen (elemental analysis)
DF	Douglas Fir
DTG	Differential thermogravimetry
EDA	Electron donor-acceptor
EDG	Electron donating group
EDX	Electron desorption x-ray spectroscopy
EWG	Electron withdrawing group
FTIR	Fourier-transform infrared
GC	Gas Chromatography
HL	Hemlock
IBU	Ibuprofen
MB	Methylene blue
MC	Miscanthus
MO	Methyl orange
PFAS	Per and polyfluoroalkyl substances
PH	Phragmites
PW	Pinewood
RC	Red cedar
RH	Rice husk
SEM	Scanning electron microscope
SG	Switch Grass
TEM	Transmission electron microscope
TGA	Thermogravimetric analysis
VM	Volatile matter

Chapter 1

1 Background Motivation and Introduction to Pyrolysis

1.1 Environmental Motivation

Various water sources for water treatment are facing enormous threats due to increasing contamination from a wide range of organic and aromatic pollutants raising concerns about public health (1–3). Excessive human activity, including agricultural activities, industrialization, and simply pollution without sufficient regulative measures introduced many organic pollutants into the water environment (4–6). These compounds can include antibiotics (7), dyes (5), hormones, petroleum hydrocarbons, and persistent organic matter (6) which can have highly detrimental effects on human and animal health and the whole ecosystem. Organic compounds such as dyes or antibiotics can damage the immune systems of aquatic organisms and cause human cell abnormalities due to poor biodegradability and high carcinogenicity (1,8,9). To counter this, many wastewater treatment techniques such as adsorption, photocatalytic degradation, and advanced oxidation processes have been studied; however, adsorption is considered the most economical and effective (1,10). Adsorption has been found to be a simple, low-cost, low energy-demanding and highly efficient method for removal of a wide range of challenging organic compounds, including dyes, pharmaceuticals, per- and poly-fluoroalkyl substances (PFAS), and phenols (11–14). Among different adsorbents, biochar has recently been the focus of many publications for removing organic and aromatic compounds as it can be produced from a wide variety of sources, often repurposing waste products (1,2,15,16). Biochar is the stable carbon-rich by-product of the pyrolytic processing of plant and animal biomass in a zero or low-oxygen environment (17–19). It has the potential application as a promising adsorbent for the elimination of a variety of pollutants in both soil and aqueous environments due to its favourable adsorption properties, which are dependent on a variety of factors including the conditions of the pyrolysis process and original feedstock (16,20–23). Compared to current water treatment methods, biochar presents a potentially more sustainable approach as it is a low-cost and renewable adsorbent made using readily available biomaterials and can be optimized for specific adsorbates (20,24,25). Biochars also have minimal effect on the original properties of water whereas other methods such as chlorination and boiling generate carcinogenic by-products and increase concentrations of compounds such as metals (20).

Biochar has been reported to be well suited to remove aromatic-based contaminants, due to its large surface area and porosity, abundant surface oxygen-containing functional groups and

aromatic surface structure (2,18,26,27). Previous studies have investigated biochar's potential in adsorptive removal of pesticides, pharmaceuticals, polychlorinated biphenyls, steroid hormones, and dyes (16,18,26–29). The mechanisms for the adsorption of aromatics on biochar have not been fully characterized and the mechanisms may depend on both the chemical and physical properties of the biochar. Biochar also has the subsequent problem of separation of the adsorbent from the aqueous media after adsorption and filtration limiting the large-scale application (30). This can further lead to the possible desorption of the adsorbed pollutants, leading to secondary pollution (30). Biochar also offers the benefit of biomass conversion which provides a method of recycling common waste products, as it enables the transformation of organic residues into valuable products and renewable energy sources. The conversion of lignocellulosic biomasses such as woods, grasses, straws, husks etc. have all been found to be successful biomasses to produce valuable and effective adsorbents for various compounds (31–34).

1.2 Introduction to Pyrolysis

Pyrolysis is a complex, multi-step process by which organic matter is thermally decomposed between 200-800°C which provides the energy required to break down the feedstock's chemical structure (35). The gaseous by-products include hydrogen, carbon dioxide, carbon monoxide, and methane, while the overall process also produces oil, and char, in different proportions depending on process conditions and feedstock type (36). Overall, pyrolysis is composed of two mechanisms – primary and secondary (37). The primary mechanism involves the breaking of chemical bonds of the polymeric cellulose and hemicellulose that comprises the feedstock and releases volatile compounds, which undergo further reactions as part of the secondary mechanism (38). The initial phase of thermal decomposition results in the creation of benzene rings that combine to form the solid char residue with organic matter continuing to decompose up to 800°C (39). Because this organic matter is composed of long polymeric chains, decomposition results in depolymerization of these long chains into monomers releasing water, incondensable gas, condensable vapours, and other volatile compounds during the primary mechanism (37). The latter is released at a much higher rate during the initial phase of pyrolysis, from 250–300°C (37). The final stage of the primary mechanism creates small-chain organic compounds and incondensable gases due to the association of covalent bonds within the monomers (38,40). Whereas in the secondary mechanism, unstable compounds either crack or

recombine to restructure (37). During cracking, these compounds break down and form molecules with low molecular weights, while during recombination volatile compounds combine to form inert or volatile compounds with high molecular weights. Moisture content also plays a large role in the pyrolysis process, as a high amount of moisture will yield mostly liquid by-products including oils mixed with condensed water from pyrolysis, while a low moisture content will generate a product with more ash content and less oil (41). Pyrolysis can also be done either fast or slow, depending on the heating rate which can drastically affect the pyrolytic products.

The final products of pyrolysis include solid residual products, known as biochar, as well as liquids known as pyrolysis oil or bio-oil, and tar. The yield of these products depends on the type of material treated, as well as the pyrolysis conditions such as temperature, heating rate, residence time, pressure, feed particle size and type of reactor (42). For purposes requiring greater bio-oil than biochar, shorter residence times are needed in high-temperature pyrolysis, whereas slower pyrolysis yields greater char content (42). Rapid or fast pyrolysis maximizes the production of high-quality liquid oil that has the potential to be upgraded to hydrocarbons in petrol and diesel (37). During fast pyrolysis, organic matter is thermally treated in the absence of oxygen at about 600–650 °C at high heating rates of up to 1000 °C/s (37,43). This causes the organic matter to decompose rapidly, producing mostly vapours and aerosols, with small amounts of gas and coal. This method can produce large yields of high-quality fuel oil that can be used as energy sources for industrial applications in engines, turbines, and boilers (37).

Slow pyrolysis is a pyrolysis technique where lignocellulosic biomass is pyrolyzed in continuous or batch systems, which slowly heat the organic matter in an anaerobic environment at temperatures greater than 400 °C, with heating rates ranging between 5 to 7 °C/min, and 20 to 100 °C/min (35). The maximum residence time under these conditions ranges from minutes to hours during which volatile organic compounds undergo cracking and recombining to produce char and other fractional liquids as seen in secondary pyrolytic reactions (37). This combination of low heating rates, low temperature, and high residence times results in a greater yield of high-quality char, while minimizing the production of liquid and gaseous products (37,41).

Pyrolysis may also be carried out under different pressures and gases. In practice, pyrolysis is most commonly done at atmospheric pressure as creating a vacuum or high pressure drastically increases the cost of process equipment (42). Operation under high pressures results

in generally greater yields of biochar and gases, while lower pressure or vacuum results in increased production of liquid products (42). The use of inert gas such as N₂ as the pyrolytic gas is most common for facilitating thermal degradation, however, the use of reactive pyrolysis atmospheres such as CO₂ are also used. In this case there is a noted decrease in the solid yield of the biochar product, with a greater yield of liquid products in particular acetic acid indicating that the CO₂ was in fact reacting with either the biomass char or volatile products (44). While the yield of the biochar product decreases with the use of CO₂ flow gas, the surface area and adsorptive properties of the char may increase as a result of the increased reaction between the char and the gas for the pyrolysis process, which may be fluidized or fixed-bed reactors as shown schematically in **Figure 1.1**, where both possess exterior heating pyrolysis reactors transfer heat from the exterior surface to the interior of the metal and the main difference being in the continued mixing of the biomass in the fluidized bed as opposed to a stagnant bed for the fixed reactor (44). The main methods for heat transfer occur due to gas-solid heat transfer using convection and solid-solid heat transfer using conduction, where a fluidized bed provides greater conduction and thus heat transfer between solids (45,46). The constant motion of the bed further results in agitation and friction between chars can increase the physical eroding of the carbon layer increasing surface area (45,46). This thesis employs the use of fixed bed pyrolysis, as depicted in **Figure 1.1a** using slow pyrolysis to optimize the production of biochar in order to study the subsequent adsorptive properties towards aqueous aromatic compounds.

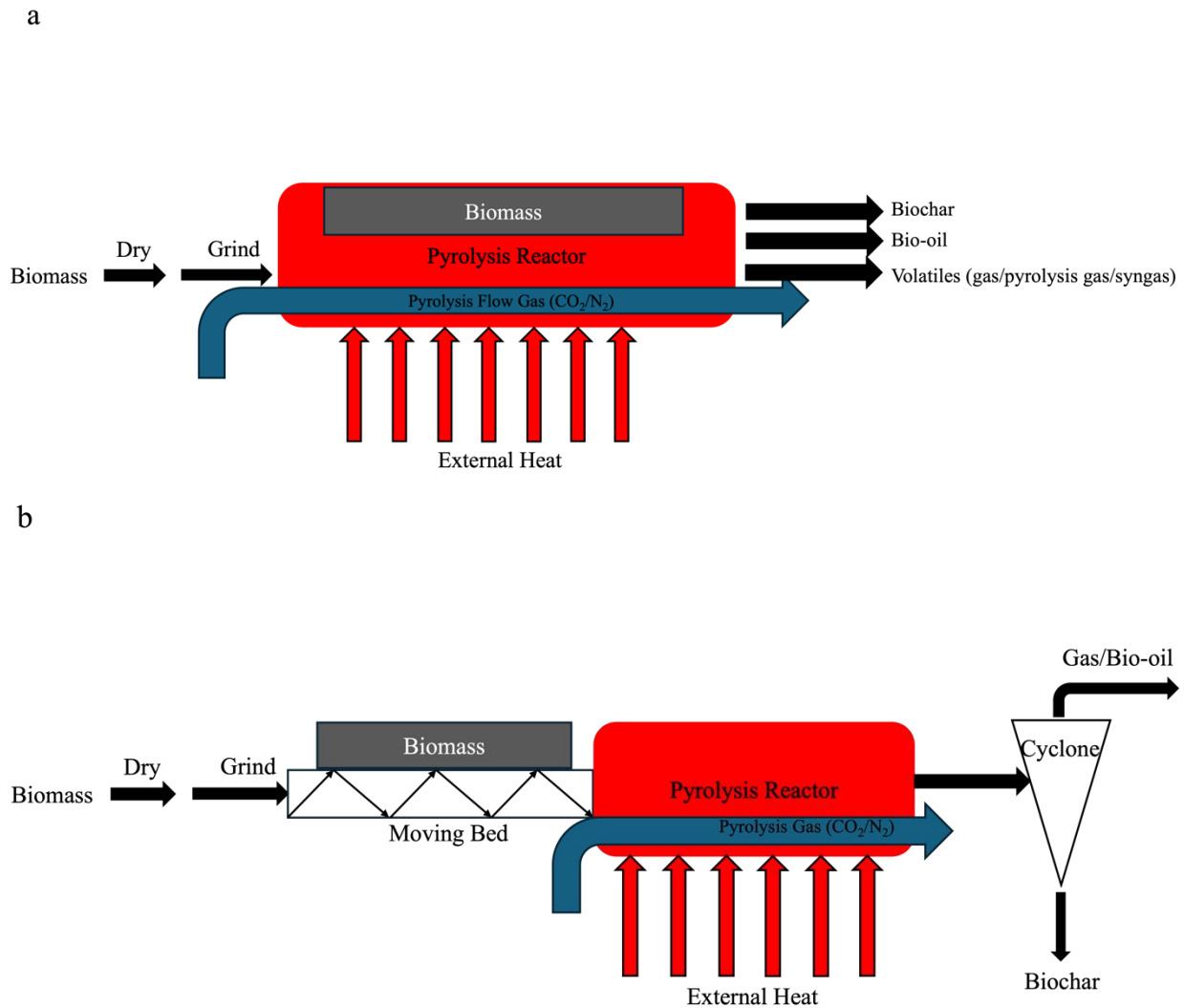


Figure 1.1 Schematic diagram of pyrolysis in a) fixed bed and b) fluidized bed reactors

1.3 Biochar Characterization Methods

This section will describe the various techniques to qualitatively and quantitatively investigate these characteristics. There are currently many different characterization methods used to identify the physical characteristics of biochar, including the surface area, porosity and pore distribution measured by nitrogen adsorption and desorption, surface functional groups often measured using FTIR spectroscopy, elemental composition measured using elemental analysis, and thermal stability using thermogravimetric analysis.

1.3.1 BET Surface Area Analysis

The surface areas and pore volumes of carbonaceous materials are critical properties in many environmental processes given the significant role that they can play in adsorption. The Brunauer-Emmett-Teller (BET) equation was originally developed to predict monolayer coverage of non-porous materials from measured multilayer physisorption of N_2 (47). Adsorption is defined as the adhesion of atoms or molecules of gas to a surface where the amount adsorbed depends on the exposed surface, however, also depends on the temperature, gas pressure and strength of interaction between the gas and solid (48). In BET surface area analysis, nitrogen is usually used as the adsorbate gas due to its availability in high purity and its strong interaction with most solids (48). However, besides N_2 , CO_2 is additionally used to characterize porous materials since N_2 is kinetically unable to access pores less than 0.5 nm, and CO_2 facilitates monolayer adsorption and avoids the volume-filling effects commonly observed when using N_2 , due to the larger quadrupole moment of CO_2 (49). Because the interaction between gaseous and solid phases is usually weak, the surface is cooled using liquid N_2 in order for the adsorption amounts to be detected (48). Known amounts of nitrogen gas are then released stepwise into the sample cell while relative pressures less than atmospheric pressure are achieved by creating conditions of partial vacuum (48). After the saturation pressure, no more adsorptions occur regardless of any further increase in pressure. After the adsorption layers are formed, the sample is removed from the nitrogen atmosphere and heated to cause the adsorbed nitrogen to be released from the material and quantified (48). The data collected is displayed in the form of a BET isotherm, which plots the amount of gas adsorbed as a function of the relative pressure. There are five types of adsorption isotherms possible (48,50).

Type I isotherms, seen in **Figure 1.2**, are pseudo-Langmuir isotherms and are obtained when $P/P_0 < 1$ and $c > 1$ in the BET equation (1), and depict monolayer adsorption. This occurs when the average pore diameter of the material is less than 2nm, resulting in monolayer adsorption pyrolysis Temperature on Biochar RM Composite(48).

A type II isotherm, such as in **Figure 1.2**, is obtained when $c > 1$ in the BET equation (1). At very low pressures, the micropores fill with nitrogen gas. In describing pore sizes, the notation of Dubinin is commonly adopted where micropores are defined as pores with a diameter of less than 2 nm, mesopores have diameters in the range 2-30 nm, and macropores are those pores with diameters larger than 30 nm (51). At the knee, monolayer formation is beginning, and

multilayer formation occurs at medium pressure. At the higher pressures, capillary condensation occurs.

A type III isotherm is obtained when the $c < 1$ and shows the formation of a multilayer. Because there is no asymptote in the curve, no monolayer is formed, and BET is not applicable.

Type IV isotherms occur when capillary condensation occurs. Gases condense in the tiny capillary pores of the solid at pressures below the saturation pressure of the gas. At the lower pressure regions, it shows the formation of a monolayer followed by a formation of multilayers. BET surface area characterization of mesoporous materials, which are materials with pore diameters between 2 - 50 nm, gives this type of isotherm.

Type V isotherms are very similar to type IV isotherms and are not applicable to BET.

$$\frac{P/P_0}{V(1-\frac{P}{P_0})} = \frac{1}{V_m C} + \frac{C-1}{C} * \frac{P/P_0}{V_0} \quad (1)$$

The BET equation, (1), uses the information from the isotherm to determine the surface area of the sample, where V is the volume adsorbed at pressure P and absolute temperature T ; P_0 is the vapour pressure of the gas at temperature T . V_m is the volume of gas adsorbed when the adsorbent surface is covered with a unimolecular layer and is termed the monolayer (51). The constant C is mathematically related to the heat of adsorption. If the function $((\frac{P}{P_0})/V(1 - P/P_0))$ is plotted against P/P_0 , a straight line should result, the slope and intercept of which give the values of V_m and C , respectively (51).

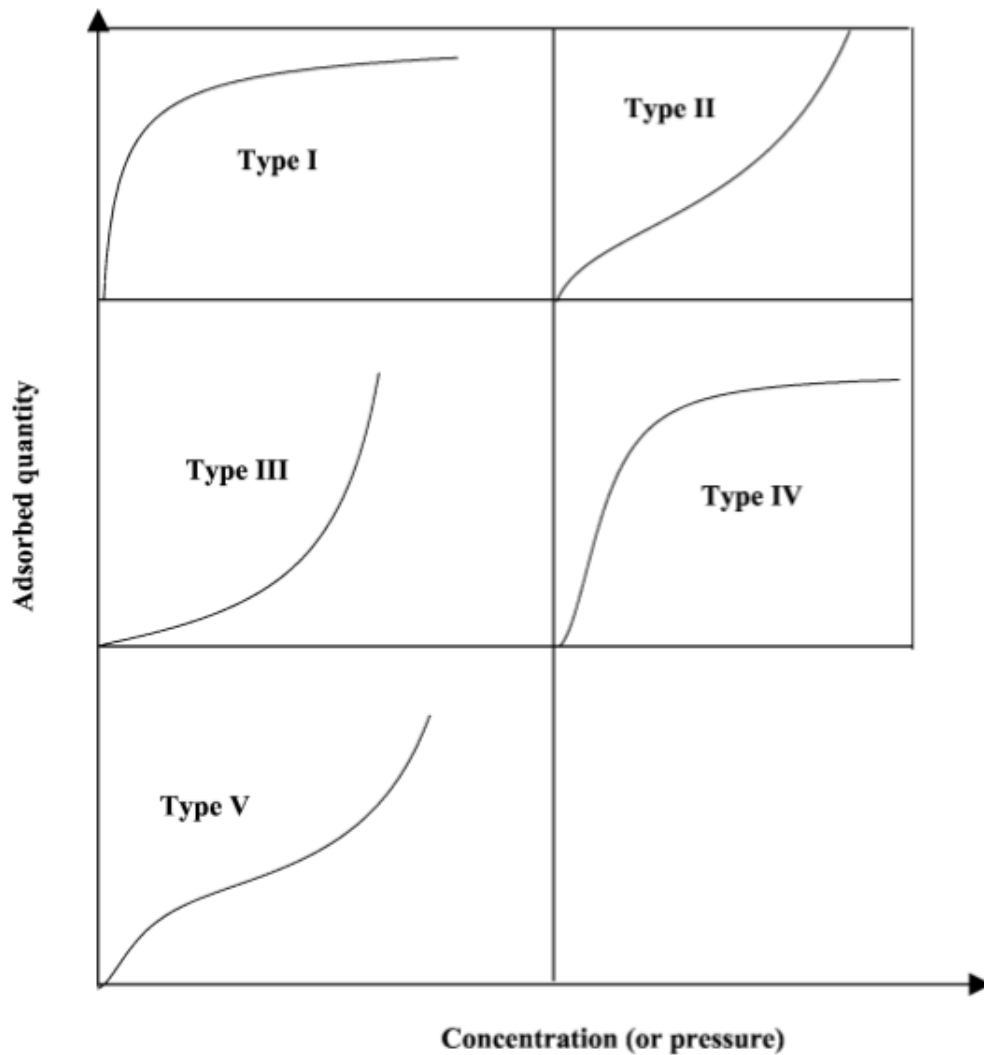


Figure 1.2 Adsorption isotherms for classification of BET isotherm results of concentration plotted against amount of adsorbate gas adsorbed by the sample

The BET method of calculating the surface area does come with some limitations, including needing the relative pressures lower than 0.3, otherwise there is the onset of capillary condensation, and at relative pressures that are higher than 0.025, to prevent only monolayer formation (48). Furthermore, when the BET equation is plotted, the graph should be of linear with a positive slope, otherwise the BET method was insufficient in obtaining the surface area. The monolayer capacity, X_m , can be calculated with using equation (3), and once X_m is determined, the total surface area, S , can be calculated with the equation (4), where L_{av} is

Avogadro's number, A_m is the cross sectional area of the adsorbate and equals 0.162 nm^2 for an adsorbed nitrogen molecule, and M_v is the molar volume, equal to 22414 mL (48).

$$X_m = \frac{1}{s+i} = \frac{C-1}{C_s} \quad (3)$$

$$S = \frac{X_m L_{av} A_m}{M_v} \quad (4)$$

Single point BET can also be used by setting the intercept to 0 and ignoring the value of C . The data point at the relative pressure of 0.3 will match up the best with a multipoint BET (48). Single point BET can be used over the more accurate multipoint BET to determine the appropriate relative pressure range for multi-point BET (48). The Surface area measurements taken in this thesis, were all calculated using multi-point BET using a Nova 2000e Surface Area and Pore Size Analyzer (Quantachrome Instrument, Florida, US).

1.3.2 Attenuated Total Reflectance (ATR)-FTIR Spectroscopy

Fourier-Transform Infrared (FTIR) spectroscopy is used for structural analysis and characterization of functional groups present on biochar surfaces. Structural analysis is performed using FTIR for this thesis using Platinum[®] attenuated total reflectance (Pt-ATR) attachment equipped with a diamond crystal in the main box of a Bruker Tensor II spectrometer. Infrared spectroscopy probes the molecular vibrations and biochar surface functional groups can be associated with characteristic infrared absorption bands, which correspond to the fundamental vibrations of the functional (52). A normal mode of vibration is infrared active (i.e., it absorbs the incident infrared light) if there is a change in the dipole moment of the molecule during the course of the vibration (52). All vibrations which are symmetrical with respect to the center are infrared inactive, in contrast, the asymmetric vibrations of all molecules are detected (52). Strong IR absorptions are observed for groups with a permanent dipole (i.e., for polar bonds). As such, the carbonyl groups, hydroxyl groups, asymmetric C-O-C stretches, and asymmetric aromatic carbon stretches are most commonly observed in FTIR spectra of biochar samples (53–56).

The stretching vibrations can be modelled using the harmonic oscillator model in which a chemical bond is represented by two-point masses linked by a spring (52). The bond strength is analogous to the spring constant, k , and the point masses (m_1 and m_2) model the masses of the atoms or chemical groups involved in the bond. The oscillation frequency m is given by the equation (5)

$$v = \left(\frac{1}{2\pi c}\right) \sqrt{\left(\frac{k(m_1+m_2)}{m_1 m_2}\right)} \quad (5)$$

The vibration frequency, m , thus depends on the bond strength, meaning that the frequencies are very sensitive to the electrostatic effects surrounding the bond (52). For example, the involvement of one of the atoms in a hydrogen bond will induce a weakening of the bond strength, and thus a frequency downshift of the stretching mode of the chemical group, which can give an insight into the types of interaction happening between adsorbents and the biochar surface functional groups.

A significant limitation of FTIR spectroscopy, especially for biochar, is that transmission spectroscopy does not work on a solid and opaque sample such as biochar. This issue is overcome using attenuated total reflectance (ATR) as a sampling technique in conjunction with IR spectroscopy, enabling the sample to be examined directly in either a solid or liquid state with little to no preparation. In ATR sampling, a beam of infrared light is passed through an ATR crystal, usually made from a material with a very high refraction index such as diamond, the infrared (IR) light travels through a crystal before being totally internally reflected at least once at the crystal-sample interface and travelling to the detector (57). Different materials can be used as ATR crystals; however, the main properties are selected so that the refractive index of the crystal as well as its chemical stability in different pH ranges are high enough such that total refraction may occur allowing for the production of an evanescent wave (46). During the internal reflection, the evanescent wave that is created penetrates into the sample and is absorbed depending on the molecular vibrations of the sample, as shown schematically in **Figure 1.3** (57). The penetration depth, d_p , of the evanescent wave into the sample, usually between 0.5 and 2 mm, is defined by the refractive index difference between the sample and the ATR crystal given by equation (6) where λ is the wavelength of light and n_1 and n_2 are the indices of refraction for the ATR crystal and the medium to be probe, and θ is the angle of incidence (57,58). The number of reflections is determined by the length of the ATR crystal and the angle of incidence, while the signal-to-noise ratio depends on the number of reflections (58). The IR beam then leaves the crystal at the opposite side of the crystal as it enters and is analyzed by the FTIR spectrometer (58).

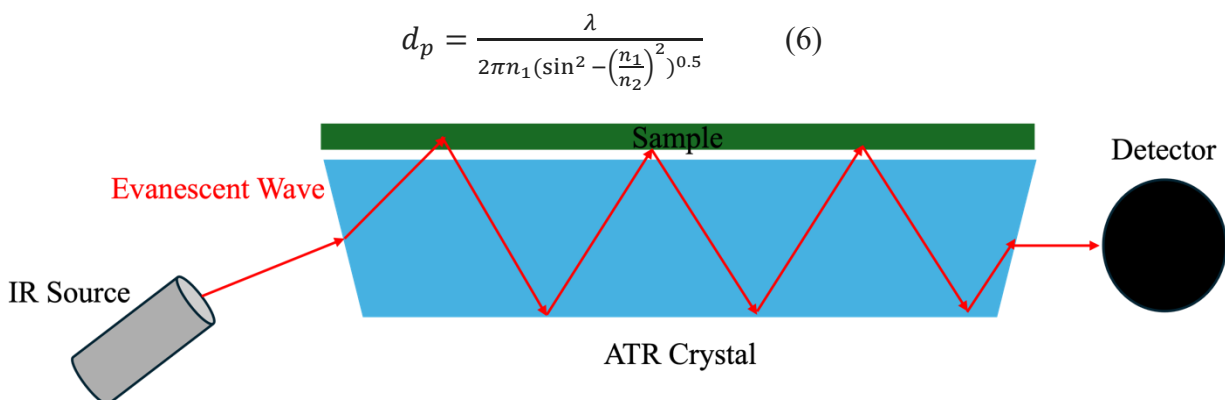


Figure 1.3 Illustration of evanescent wave in ATR crystal penetrating into sample for adsorption in ATR-FTIR spectroscopy (57)

1.3.3 Proximate and CHNS-O Elemental Analysis

Proximate analysis was originally developed for analysis of wood charcoal (59). More recently, however, this method has been utilized for assessing the quality of biochar to determine basic characteristic information including moisture, volatile matter (VM), fixed carbon (FC) and ash content (59). Ash content is related to the liming value and inorganic element content of biochar while VM and FC have been used to estimate the labile and recalcitrant biochar fractions, respectively (59,60). Proximate analysis determines moisture content as the percent mass loss on heating air-dry samples to 105°C in an air atmosphere, VM as percent mass lost between 105°C and 950°C, and percent ash as mass remaining after combustion at 750°C for 6 h (59).

CHNS elemental analysis involves the introduction of an accurately weighted sample into a high-temperature furnace (around 1000°C) where an inert high-purity gas is passed through, illustrated in **Figure 1.4**. Once the sample is placed into the reaction vessel by the autosampler, oxygen is then injected along with the inert carrier gas (He) in order to cause a flash-combustion of the sample, where the exothermic combustion of the tin sample capsule brings the temperature in the furnace above 1800°C (61). In the combustion process, carbon is converted to carbon dioxide; hydrogen to water; nitrogen to nitrogen gas/ oxides of nitrogen and sulphur to sulphur dioxide (61). If other elements such as chlorine are present, they will also be converted to combustion products, such as hydrogen chloride (61). The combustion products are swept out of the combustion chamber by an inert carrier gas such as helium and passed over heated (about 600°C) high-purity copper at the base of the combustion chamber or in a separate furnace. (61) The function of this copper is to act as a reducing agent in order to remove any oxygen not

consumed in the initial combustion and to convert any oxides of nitrogen to nitrogen gas which are then passed through the absorbent traps in order to leave only carbon dioxide, water, nitrogen and sulphur dioxide (61). This allows for the accurate detection of carbon, hydrogen, nitrogen and sulfur respectively, where the oxygen content is then determined based on subtraction of these values from the known initial mass of the sample. Detection of the gases can be carried out in a variety of ways including (i) gas chromatography (GC) separation followed by quantification using thermal conductivity detection (ii) a partial separation followed by thermal conductivity detection (CHN but not S), (iii) a series of separate infrared and thermal conductivity cells for detection of individual compounds (61). The analysis in this thesis was done using Neytech Vulcan D-550 muffle oven and elemental analysis of carbon, hydrogen, nitrogen, and sulfur was undertaken using model Thermo Flash EA 1112 series CHNS analyzer (Thermo Fisher Scientific, USA).

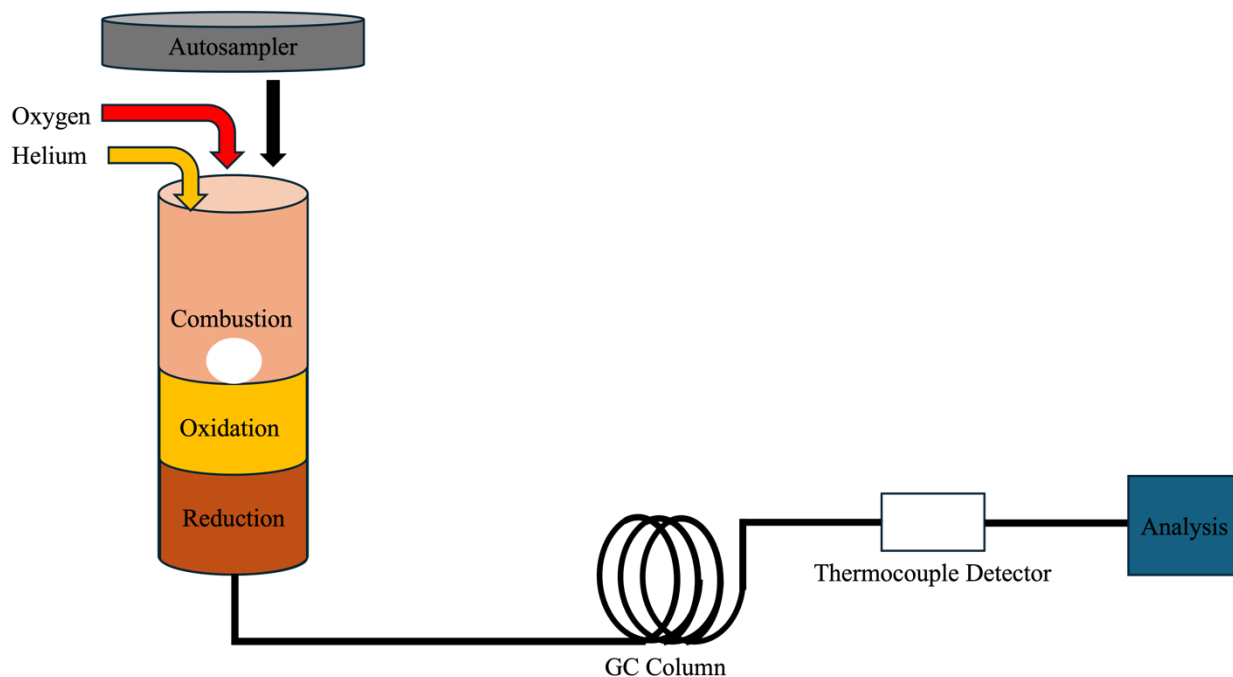


Figure 1.4 Block diagram of instrumentation for elemental CHNS-O analysis (61)

1.3.4 Scanning Electron Microscope (SEM) – Energy Dispersive X-Ray (EDX) Spectroscopy

Scanning electron microscopy (SEM) differs from optical microscopy as it uses electrons rather than light to observe an object (62). SEM is different than traditional microscopy as it uses electron emission rather than light, which allows for it to reach a magnification of 300 000X

compared to 400-1000 times the original sizes that is achievable with optical microscopy (62). Energy Dispersive X-ray Spectroscopy (EDX) works together with SEM to provide qualitative and semi-quantitative information of the elemental composition of the sample (62). Similar to light microscopes, SEM utilizes electrons as an analogue to light, following the scheme shown in **Figure 1.5**. SEMs produce an image by first aiming electrons produced from an electron source, usually by heating tungsten or solid-state hexaboride filaments and directing them towards the sample (63). The electron beam will diverge after passing through the anode plate from the emission source, after which the condenser lens, converges the electron beam to around 5 nm and collimates into a relatively parallel stream (63). A magnetic lens generally consists of two rotationally symmetric iron pole pieces in which there is a copper winding providing a magnetic field which further aids in focussing the electron beam (63).. The position of the focal point can then be controlled by adjusting the condenser lens current. For modern electron microscopes, a second condenser lens is often used to provide additional control of the electron beam (63). The images are then formed by collecting the released electrons on a cathode ray tube (CRT). The depth of the interaction of the electrons with the sample depends on the composition of the solid specimen, the energy of the incident electron beam, and the incident angle (63). Two kinds of scattering processes, the elastic and the inelastic process, are considered. The electrons retain all of their energy after an elastic interaction, and elastic scattering results in the production of back-scattered electrons when they travel back to the specimen surface and escape into the vacuum (63). On the other hand, electrons lose energy in the inelastic scattering process, and they excite electrons in the specimen lattice (63). When these low-energy electrons, generally with energy less than 50 eV, escape to the vacuum, they are termed “secondary electrons” and can be excited throughout the interaction volume; however, only those near the specimen surface can escape into the vacuum for their low (63). Both the backscattered electrons and secondary electrons can be collected by the detector to produce an image, where the more electrons the detector is able to interact with generates a higher quality image.

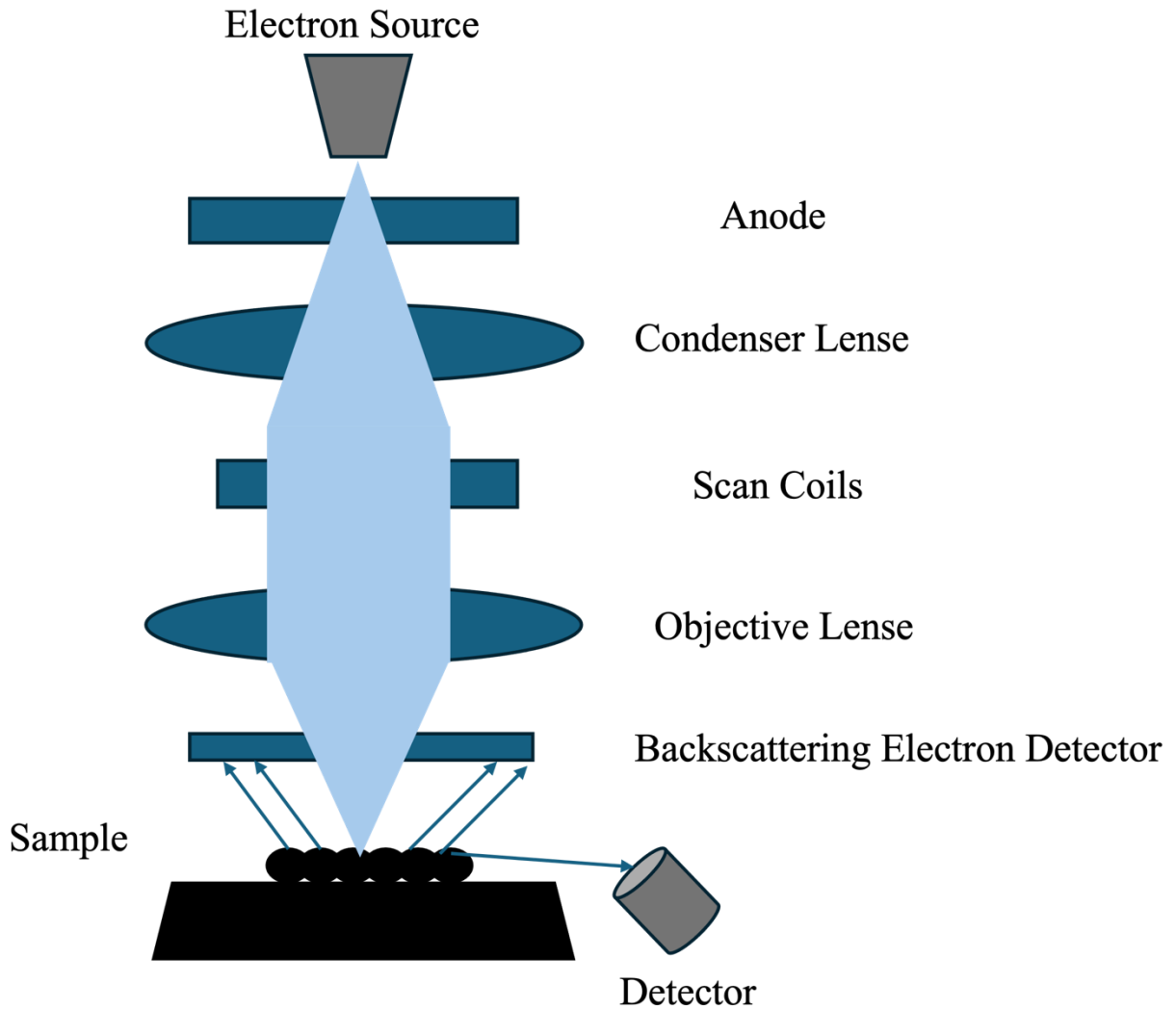


Figure 1.5 Schematic for the principal design of scanning electron microscope (62)

EDX is a technique that allows for elemental and chemical characterization of a specimen. When the electron beam penetrates the sample, X-rays are generated which are measured via the detector to determine the elemental composition (62). In order for this to occur, a beam of electrons is focused on the sample, where the ground state electrons are excited thus ejecting it from its' shell and leaving behind an electron hole (64). The electron-hole is then filled by a valence electron, releasing energy in the form of a photon, which occurs in SEM-EDX as x-ray photons which are particular to specific elements (62) Heinrich illustrated that the intensity of the incoming photons to the detector is correlated with the quantity of the determined element (62). This is shown in **Figure 1.6**, where the K-shell electrons are shown to be excited, thereby emitting characteristic x-rays which are termed as “K-lines” while those emitted from L and M

shells are referred to as “L Lines” and “M Lines” respectively (65). Therefore, when an element is heavier, x-rays produced from EDX are also found to be higher, meaning that incident electrons of higher energy are required (65). The analysis done in this thesis was done using a Hitachi SU3500 Scanning Electron Microscope combined with an Oxford AZtec X-Max50 SDD energy dispersive X-ray (EDX) detector.

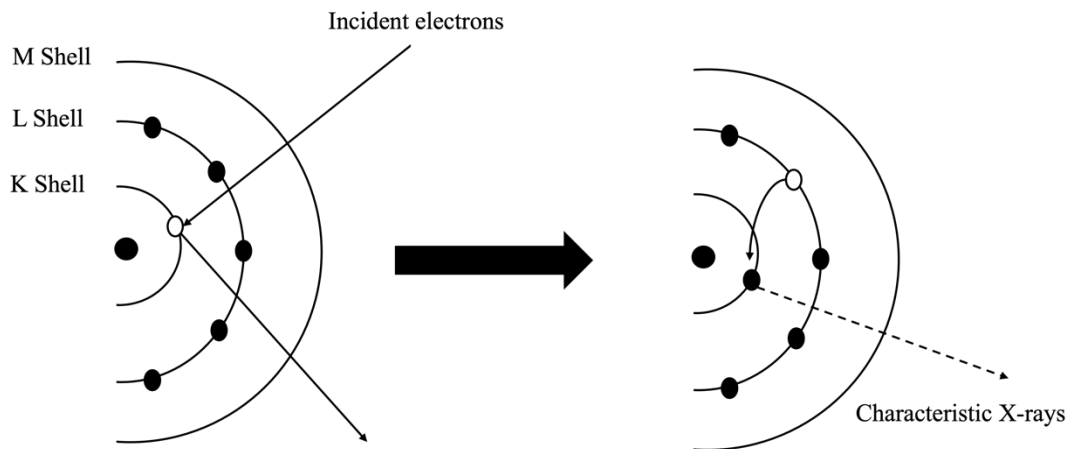


Figure 1.6 Schematic of principle for x-rays produced from electron guns in energy dispersive x-ray spectroscopy (65)

1.3.5 Thermogravimetric Analysis

Given that pyrolysis is defined as the thermochemical decomposition of biomass at high temperature, under the flow of either an inert or catalytic gas, understanding the effects of the biomass in these conditions is essential to understanding the mechanisms of the pyrolysis process (66). Thermogravimetric analysis (TGA), whose instrumentation is given by the block diagram in **Figure 1.7**, is a process whereby a sample is heated up to a desired temperature under the flow of a gas and the mass is measured throughout (67). Many samples undergo reactions that evolve gaseous byproducts, as in pyrolysis, which are removed and the changes in the remaining mass are able to give insight into the reactions that are occurring (67). This can yield valuable information on the composition of the biomass, and how that may affect the pyrolysis process, and the resultant product. The differential thermogravimetric analysis (DTG) is determined by taking the first derivative of the TGA plot, the mass loss vs the temperature, and more easily depicts the changes in the mass throughout the pyrolysis of the sample. The TGA for this thesis was performed using a Mettler Toledo TGA2.

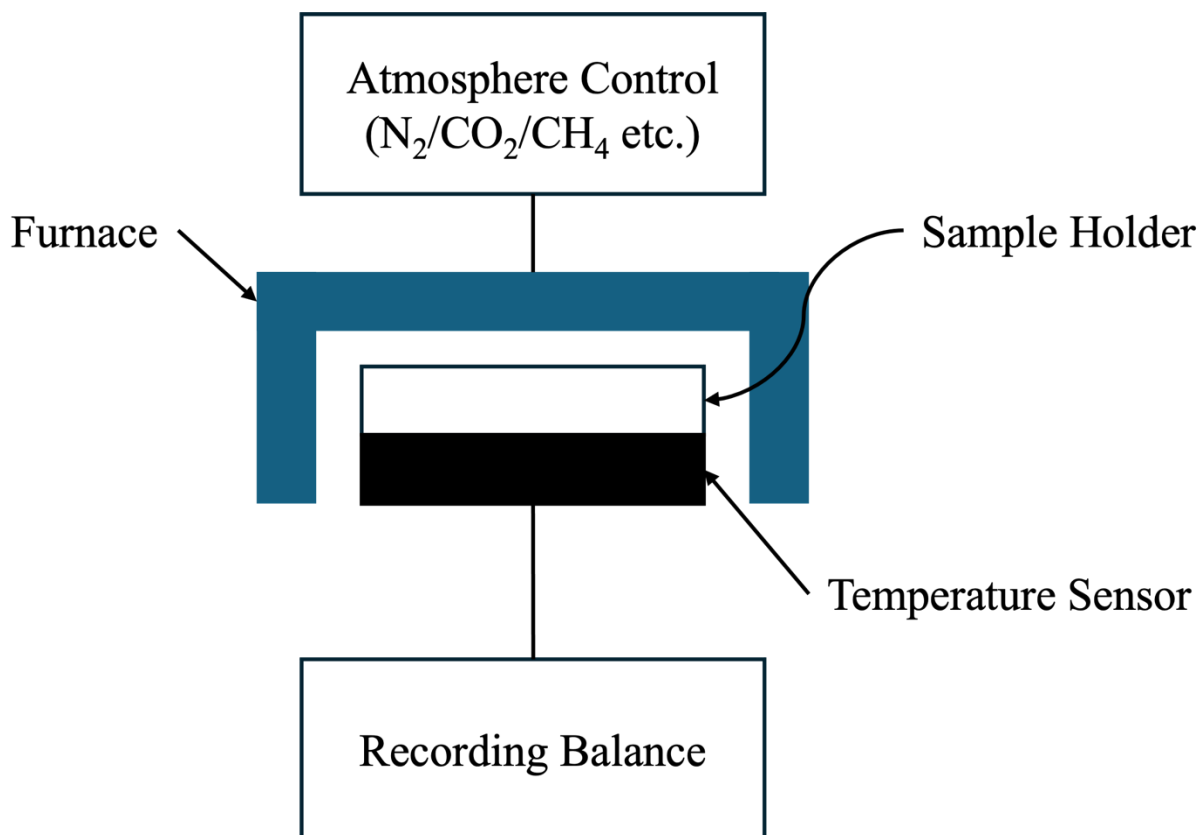


Figure 1.7 Block Diagram of instrumentation of thermogravimetric analysis (67)

1.4 Motivation and Objectives

This work aims to gain an understanding of the adsorption mechanisms that biochar has towards aromatic compounds in water, beginning with the development of a method for the investigation of adsorption mechanisms. The motivation for this is to find the underlying physical characteristics that have the largest effect on the adsorption of these aqueous compounds. Investigating the various adsorption mechanisms for organic compounds that are adsorbed using biochars produced from different pyrolysis conditions and post-treatments such as oxidation will allow for insight into how these processes affect the adsorption mechanisms as well. This will allow biochars to be engineered and designed to optimize their adsorption capacities, as well as possibly achieve specific adsorption of target compounds over others. The benefit of targeting specific adsorbates would be the possibility of re-use of previously inaccessible compounds, for example, the extraction of phenol can be recycled as it is a valuable product in pharmaceutical synthesis. Furthermore, real-world applications of adsorbents for environmental remediation will involve the adsorption of compounds in complex mixtures, complicating the possible adsorption mechanisms that are taking place. Research on the

adsorption of competing compounds in complex solutions is lacking in the literature, this work fills that gap by exploring how the determined adsorption mechanisms of biochar by be affected in these settings. Finally, one of the major problems for adsorption is the removal of the adsorbent from the body of water after adsorption has taken place. This work further investigates methods to ameliorate this issue, creating a value-added magnetic product.

1.5 Thesis Outline

Chapter 1 discusses the background of biochar, explaining how it is produced via pyrolysis and how it can be used to address different environmental issues. Within this, the process of pyrolysis is explained and how it allows for biomass to be thermochemically reduced to biochar. The missing understanding of how different physical properties of biochar can affect the specific adsorption mechanisms between biochar and intended organic compounds when used for adsorption in wastewater, is also explored and aids in reinforcing the objective of the thesis, of gaining a solid understanding of biochar's adsorption mechanisms towards organic compounds and the physical properties responsible.

Chapter 2 focuses on the development of a method in order to investigate adsorption mechanisms towards organic compounds, specifically aromatic compounds. This method tests the adsorption capacities of four test compounds, each with specific moieties that restrict the possible adsorption mechanisms by which they can be adsorbed, thus differences in their adsorptions allow for insight into the relative strength of adsorption mechanisms. This method is then used in order to investigate the properties of biochar that are responsible for strengthening certain mechanisms relative to others. This is done by observing changes in adsorption trends for biochars produced under different pyrolysis conditions whose effects on physical properties are well known. These pyrolysis conditions include inert or catalytic flow gas, pyrolysis temperature, and biomass and biomass composition. The results revealed that the oxygen-containing groups played one of the most significant roles in the adsorption mechanisms, where carbonyl groups increased π - π EDA interactions and hydroxyl groups strengthened both π - π EDA interactions and electrostatic interactions. This is further investigated in the following chapter.

Chapter 3 investigates the effect that common post-treatment methods have on the adsorption mechanisms of organic compounds in order to evaluate the effect of hydroxyl and carbonyl

groups have on π - π EDA interactions. HNO_3 post-treatment was used in order to evaluate the effect of both mineral ash content and hydroxyl groups on electrostatic interactions. The former was found to be negligible while the latter had a greater effect. Oxidation using H_2O_2 treatment added mainly hydroxyl groups, while KOH treatment increased aromaticity and carbonyl groups. The H_2O_2 post-treatment increased both electrostatic and EDA interactions with compounds containing EWGs, supporting the same correlation that was found in the previous chapter. KOH treatment also showed an increase in π - π EDA interactions, especially with compounds containing EDGs, further supporting these findings as well.

Given that there is now a more established understanding of the properties of biochar and how they affect the adsorption mechanism for compounds, biochar adsorption mechanisms are able to be generalized into 5 types depending on the strength of the π - π EDA interactions and whether they favour compounds with EDGs or EWGs, as well as if there are stronger electrostatic interactions. These five types of biochars are evaluated for how their adsorption mechanisms are altered in solution with multiple competing compounds in Chapter 4, which showed that they are altered differently depending on the most dominant adsorption mechanisms of the biochar.

Chapter 5 investigates the co-pyrolysis of biomass and red mud, an iron oxide-rich bioproduct of the alumina processing industry, as a possible solution to difficulties in the recovery of biochar after it is used as an adsorbent. The combination of biomass and iron oxide in pyrolysis was found to produce a magnetic adsorbent as the volatile gasses of the biomasses act as reducing agents for the iron oxide, reducing the iron to its magnetic form. This allows for ease of separation of the adsorbent after adsorption. This was found to be successful with both woody and non-woody biomasses, under various post-treatments and without the adsorption mechanisms of the biochar being significantly altered. It was also found that very little red mud was needed to make the product magnetic, with the optimal ratio being a 9:1 biomass to red mud before pyrolysis.

Finally, the conclusions will be presented in Chapter 6 beginning with a summary and conclusion and ending with suggestions for future work.

1.6 References

1. Qu, J.; Meng, Q.; Peng, W.; Shi, J.; Dong, Z.; Li, Z.; et al. Application of functionalized biochar for adsorption of organic pollutants from environmental media: Synthesis strategies, removal mechanisms and outlook. *Journal of Cleaner Production*. Elsevier Ltd October 15, 2023. doi:10.1016/j.jclepro.2023.138690.
2. Luo, Z.; Yao, B.; Yang, X.; Wang, L.; Xu, Z.; Yan, X.; et al. Novel insights into the adsorption of organic contaminants by biochar: A review. *Chemosphere* **2022**, 287. doi:10.1016/j.chemosphere.2021.132113.
3. Yu, F.; Bai, X.; Liang, M.; Ma, J. Recent progress on metal-organic framework-derived porous carbon and its composite for pollutant adsorption from liquid phase. *Chemical Engineering Journal*. Elsevier B.V. February 1, 2021. doi:10.1016/j.cej.2020.126960.
4. Tang, R.; Gong, D.; Deng, Y.; Xiong, S.; Zheng, J.; Li, L.; et al. π - π stacking derived from graphene-like biochar/g-C₃N₄ with tunable band structure for photocatalytic antibiotics degradation via peroxydisulfate activation. *Journal of Hazardous Materials* **2022**, 423. doi:10.1016/j.jhazmat.2021.126944.
5. Zhou, Q.; Li, R.; Li, T.; Zhou, R.; Hou, Z.; Zhang, X. Interactions among microorganisms functionally active for electron transfer and pollutant degradation in natural environments. *Eco-Environment and Health*. Elsevier B.V. March 1, 2023, pp 3–15. doi:10.1016/j.eehl.2023.01.002.
6. Qu, J.; Zhang, B.; Tong, H.; Liu, Y.; Wang, S.; Wei, S.; et al. High-efficiency decontamination of Pb(II) and tetracycline in contaminated water using ball-milled magnetic bone derived biochar. *Journal of Cleaner Production* **2023**, 385. doi:10.1016/j.jclepro.2022.135683.
7. Tang, Y.; Li, Y.; Zhan, L.; Wu, D.; Zhang, S.; Pang, R.; et al. Removal of emerging contaminants (bisphenol A and antibiotics) from kitchen wastewater by alkali-modified biochar. *Science of the Total Environment* **2022**, 805. doi:10.1016/j.scitotenv.2021.150158.
8. Huo, S.; Gao, W.; Zhou, P.; Deng, Z.; Han, Z.; Cui, X.; et al. Magnetic porous carbon composites for rapid and highly efficient degradation of organic pollutants in water. *Advanced Powder Materials* **2022**, 1(3). doi:10.1016/j.apmate.2022.01.001.
9. Gupta, M.; Savla, N.; Pandit, C.; Pandit, S.; Gupta, P. K.; Pant, M.; et al. Use of biomass-derived biochar in wastewater treatment and power production: A promising solution for a sustainable environment. *Science of the Total Environment*. Elsevier B.V. June 15, 2022. doi:10.1016/j.scitotenv.2022.153892.

10. Yao, B.; Luo, Z.; Zhi, D.; Hou, D.; Luo, L.; Du, S.; et al. Current progress in degradation and removal methods of polybrominated diphenyl ethers from water and soil: A review. *Journal of Hazardous Materials* **2021**, *403*. doi:10.1016/j.jhazmat.2020.123674.
11. Yaashikaa, P. R.; Senthil Kumar, P.; Varjani, S. J.; Saravanan, A. Advances in production and application of biochar from lignocellulosic feedstocks for remediation of environmental pollutants. *Bioresource Technology*. Elsevier Ltd November 1, 2019. doi:10.1016/j.biortech.2019.122030.
12. Cheng, N.; Wang, B.; Wu, P.; Lee, X.; Xing, Y.; Chen, M.; et al. Adsorption of emerging contaminants from water and wastewater by modified biochar: A review. *Environmental Pollution*. Elsevier Ltd March 15, 2021. doi:10.1016/j.envpol.2021.116448.
13. Qiu, B.; Tao, X.; Wang, H.; Li, W.; Ding, X.; Chu, H. Biochar as a low-cost adsorbent for aqueous heavy metal removal: A review. *Journal of Analytical and Applied Pyrolysis*. Elsevier B.V. May 1, 2021. doi:10.1016/j.jaap.2021.105081.
14. Jiang, B.; Lin, Y.; Mbog, J. C. Biochar derived from swine manure digestate and applied on the removals of heavy metals and antibiotics. *Bioresource Technology* **2018**, *270*, 603–611. doi:10.1016/j.biortech.2018.08.022.
15. Dai, Y.; Liu, Y.; Wang, Y.; Fang, W.; Chen, Y.; Sui, Y. A Practice of Conservation Tillage in the Mollisol Region in Heilongjiang Province of China: A Mini Review. *Polish Journal of Environmental Studies*. HARD Publishing Company 2023, pp 1479–1489. doi:10.15244/pjoes/156473.
16. Ai, T.; Jiang, X.; Liu, Q.; Lv, L.; Wu, H. Daptomycin adsorption on magnetic ultra-fine wood-based biochars from water: Kinetics, isotherms, and mechanism studies. *Bioresource Technology* **2019**, *273*, 8–15. doi:10.1016/j.biortech.2018.10.039.
17. Gai, X.; Wang, H.; Liu, J.; Zhai, L.; Liu, S.; Ren, T.; et al. Effects of feedstock and pyrolysis temperature on biochar adsorption of ammonium and nitrate. *PLoS ONE* **2014**, *9*(12). doi:10.1371/journal.pone.0113888.
18. Ahmed, M. J.; Hameed, B. H. Adsorption behavior of salicylic acid on biochar as derived from the thermal pyrolysis of barley straws. *Journal of Cleaner Production* **2018**, *195*, 1162–1169. doi:10.1016/j.jclepro.2018.05.257.

19. Sewu, D. D.; Boakye, P.; Jung, H.; Woo, S. H. Synergistic dye adsorption by biochar from co-pyrolysis of spent mushroom substrate and *Saccharina japonica*. *Bioresource Technology* **2017**, *244*, 1142–1149. doi:10.1016/j.biortech.2017.08.103.
20. Gwenzi, W.; Chaukura, N.; Noubactep, C.; Mukome, F. N. D. Biochar-based water treatment systems as a potential low-cost and sustainable technology for clean water provision. *Journal of Environmental Management*. Academic Press July 15, 2017, pp 732–749. doi:10.1016/j.jenvman.2017.03.087.
21. Mohan, D.; Sarswat, A.; Ok, Y. S.; Pittman, C. U. Organic and inorganic contaminants removal from water with biochar, a renewable, low cost and sustainable adsorbent - A critical review. *Bioresource Technology* **2014**, *160*, 191–202. doi:10.1016/j.biortech.2014.01.120.
22. He, M.; Xiong, X.; Wang, L.; Hou, D.; Bolan, N. S.; Ok, Y. S.; et al. A critical review on performance indicators for evaluating soil biota and soil health of biochar-amended soils. *Journal of Hazardous Materials* **2021**, *414*. doi:10.1016/j.jhazmat.2021.125378.
23. Yang, Z.; Fang, Z.; Zheng, L.; Cheng, W.; Tsang, P. E.; Fang, J.; et al. Remediation of lead contaminated soil by biochar-supported nano-hydroxyapatite. *Ecotoxicology and Environmental Safety* **2016**, *132*, 224–230. doi:10.1016/j.ecoenv.2016.06.008.
24. Yahiaoui, I.; Aissani-Benissad, F.; Fourcade, F.; Amrane, A. Removal of tetracycline hydrochloride from water based on direct anodic oxidation (Pb/PbO₂ electrode) coupled to activated sludge culture. *Chemical Engineering Journal* **2013**, *221*, 418–425. doi:10.1016/j.cej.2013.01.091.
25. Brinzila, C. I.; Pacheco, M. J.; Ciriaco, L.; Ciobanu, R. C.; Lopes, A. Electrodegradation of tetracycline on BDD anode. *Chemical Engineering Journal* **2012**, *209*, 54–61. doi:10.1016/j.cej.2012.07.112.
26. Zhang, X.; Wang, H.; He, L.; Lu, K.; Sarmah, A.; Li, J.; et al. Using biochar for remediation of soils contaminated with heavy metals and organic pollutants. *Environmental Science and Pollution Research* **2013**, *20*(12), 8472–8483. doi:10.1007/s11356-013-1659-0.
27. Liu, G.; Sheng, H.; Fu, Y.; Song, Y.; Redmile-Gordon, M.; Qiao, Y.; et al. Extracellular polymeric substances (EPS) modulate adsorption isotherms between biochar and 2,2',4,4'-tetrabromodiphenyl ether. *Chemosphere* **2019**, *214*, 176–183. doi:10.1016/j.chemosphere.2018.09.081.

28. Varjani, S.; Kumar, G.; Rene, E. R. Developments in biochar application for pesticide remediation: Current knowledge and future research directions. *Journal of Environmental Management* **2019**, *232*, 505–513. doi:10.1016/j.jenvman.2018.11.043.
29. Shen, J.; Huang, G.; An, C.; Zhao, S.; Rosendahl, S. Immobilization of tetrabromobisphenol A by pinecone-derived biochars at solid-liquid interface: Synchrotron-assisted analysis and role of inorganic fertilizer ions. *Chemical Engineering Journal* **2017**, *321*, 346–357. doi:10.1016/j.cej.2017.03.138.
30. Yi, Y.; Huang, Z.; Lu, B.; Xian, J.; Tsang, E. P.; Cheng, W.; et al. Magnetic biochar for environmental remediation: A review. *Bioresource Technology*. Elsevier Ltd February 1, 2020. doi:10.1016/j.biortech.2019.122468.
31. Nie, F.; Guan, K.; Zou, C.; Xu, Z.; Liu, Z. Synthesis of magnetic rice husk biochar and its application in the adsorption of Ni(II) from aqueous solutions. *Biomass Conversion and Biorefinery* **2023**. doi:10.1007/s13399-023-04032-z.
32. Thuan, D. Van; Chu, T. T. H.; Thanh, H. D. T.; Le, M. V.; Ngo, H. L.; Le, C. L.; et al. Adsorption and photodegradation of micropollutant in wastewater by photocatalyst TiO₂/rice husk biochar. *Environmental Research* **2023**, *236*. doi:10.1016/j.envres.2023.116789.
33. Burachevskaya, M.; Minkina, T.; Bauer, T.; Lobzenko, I.; Fedorenko, A.; Mazarji, M.; et al. Fabrication of biochar derived from different types of feedstocks as an efficient adsorbent for soil heavy metal removal. *Scientific Reports* **2023**, *13*(1). doi:10.1038/s41598-023-27638-9.
34. Shrivastava, P.; Kumar, A.; Tekasakul, P.; Lam, S. S.; Palamanit, A. Comparative investigation of yield and quality of bio-oil and biochar from pyrolysis of woody and non-woody biomasses. *Energies* **2021**, *14*(4). doi:10.3390/en14041092.
35. Chen, W. H.; Farooq, W.; Shahbaz, M.; Naqvi, S. R.; Ali, I.; Al-Ansari, T.; et al. Current status of biohydrogen production from lignocellulosic biomass, technical challenges and commercial potential through pyrolysis process. *Energy*. Elsevier Ltd July 1, 2021. doi:10.1016/j.energy.2021.120433.
36. Uddin, M. N.; Techato, K.; Taweekun, J.; Rahman, M. M.; Rasul, M. G.; Mahlia, T. M. I.; et al. An overview of recent developments in biomass pyrolysis technologies. *Energies*. MDPI AG November 1, 2018. doi:10.3390/en11113115.
37. Al-Rumaihi, A.; Shahbaz, M.; Mckay, G.; Mackey, H.; Al-Ansari, T. A review of pyrolysis technologies and feedstock: A blending approach for plastic and biomass towards optimum

- biochar yield. *Renewable and Sustainable Energy Reviews*. Elsevier Ltd October 1, 2022. doi:10.1016/j.rser.2022.112715.
38. Van de Velden, M.; Baeyens, J.; Brems, A.; Janssens, B.; Dewil, R. Fundamentals, kinetics and endothermicity of the biomass pyrolysis reaction. *Renewable Energy* **2010**, *35*(1), 232–242. doi:10.1016/j.renene.2009.04.019.
39. Mcgrath, T. E.; Chan, W. G.; Hajaligol, M. R. *Low Temperature Mechanism for the Formation of Polycyclic Aromatic Hydrocarbons from the Pyrolysis of Cellulose*; 2003; Vol. 66. <www.elsevier.com/locate/jaap>.
40. Hosoya, T.; Kawamoto, H.; Saka, S. Pyrolysis behaviors of wood and its constituent polymers at gasification temperature. *Journal of Analytical and Applied Pyrolysis* **2007**, *78*(2), 328–336. doi:10.1016/j.jaap.2006.08.008.
41. Bridgwater, A. V; Meier, D.; Radlein, D. *An Overview of Fast Pyrolysis of Biomass*. <www.elsevier.nl/locate/orggeochem>.
42. Al-Haj Ibrahim, H. Introductory Chapter: Pyrolysis. In *Recent Advances in Pyrolysis*; IntechOpen, 2020. doi:10.5772/intechopen.90366.
43. Ahmad, J.; Patuzzi, F.; Rashid, U.; Shahabz, M.; Ngamcharussrivichai, C.; Baratieri, M. Exploring untapped effect of process conditions on biochar characteristics and applications. *Environmental Technology and Innovation*. Elsevier B.V. February 1, 2021. doi:10.1016/j.eti.2020.101310.
44. Guizani, C.; Javier, F.; Sanz, E.; Salvador, S.; Guizani, C.; Escudero Sanz, F. J.; et al. Effects of CO₂ on biomass fast pyrolysis : reaction rate, gas yields and char reactive properties Effects of CO₂ on biomass fast pyrolysis: Reaction rate, gas yields and char reactive properties. *Fuel* **2014**, *116*, 310–320. doi:10.1016/j.fuel.2013.07.101i.
45. Bridgwater, A. V; Meier, D.; Radlein, D. *An Overview of Fast Pyrolysis of Biomass*. <www.elsevier.nl/locate/orggeochem>.
46. Sembiring, K. C.; Rinaldi, N.; Simanungkalit, S. P. Bio-oil from Fast Pyrolysis of Empty Fruit Bunch at Various Temperature. In *Energy Procedia*; Elsevier Ltd, 2015; Vol. 65, pp 162–169. doi:10.1016/j.egypro.2015.01.052.
47. Brunauer, S.; Emmett, P. H.; Teller, E. *Adsorption of Gases in Multimolecular Layers*; 1938. <https://pubs.acs.org/sharingguidelines>.

48. Hwang, N.; Barron, A. R. *OpenStax-CNX Module: M38278 1 BET Surface Area Analysis of Nanoparticles * This Work Is Produced by OpenStax-CNX and Licensed under the Creative Commons Attribution License 3.0* †. <<http://cnx.org/content/m38278/1.1/>>.
49. Sigmund, G.; Hüffer, T.; Hofmann, T.; Kah, M. Biochar total surface area and total pore volume determined by N₂ and CO₂ physisorption are strongly influenced by degassing temperature. *Science of the Total Environment* **2017**, *580*, 770–775. doi:10.1016/j.scitotenv.2016.12.023.
50. Khalfaoui, M.; Knani, S.; Hachicha, M. A.; Lamine, A. Ben. New theoretical expressions for the five adsorption type isotherms classified by BET based on statistical physics treatment. *Journal of Colloid and Interface Science* **2003**, *263*(2), 350–356. doi:10.1016/S0021-9797(03)00139-5.
51. Dollimore, D.; Spooner, P.; Turner, A. *Review Paper THE BET METHOD OF ANALYSIS OF GAS ADSORPTION DATA AND ITS RELEVANCE TO THE CALCULATION OF SURFACE AREAS*; Elsevier Sequoia S.A, 1976; Vol. 4.
52. Berthomieu, C.; Hienerwadel, R. Fourier transform infrared (FTIR) spectroscopy. *Photosynthesis Research*. September 2009, pp 157–170. doi:10.1007/s11120-009-9439-x.
53. Tan, X. F.; Zhu, S. S.; Wang, R. P.; Chen, Y. Di; Show, P. L.; Zhang, F. F.; et al. Role of biochar surface characteristics in the adsorption of aromatic compounds: Pore structure and functional groups. *Chinese Chemical Letters*. Elsevier B.V. October 1, 2021, pp 2939–2946. doi:10.1016/j.ccllet.2021.04.059.
54. Fan, Q.; Sun, J.; Chu, L.; Cui, L.; Quan, G.; Yan, J.; et al. Effects of chemical oxidation on surface oxygen-containing functional groups and adsorption behavior of biochar. *Chemosphere* **2018**, *207*, 33–40. doi:10.1016/j.chemosphere.2018.05.044.
55. Yang, X.; Wan, Y.; Zheng, Y.; He, F.; Yu, Z.; Huang, J.; et al. Surface functional groups of carbon-based adsorbents and their roles in the removal of heavy metals from aqueous solutions: A critical review. *Chemical Engineering Journal*. Elsevier B.V. June 15, 2019, pp 608–621. doi:10.1016/j.cej.2019.02.119.
56. Yang, X.; Wan, Y.; Zheng, Y.; He, F.; Yu, Z.; Huang, J.; et al. Surface functional groups of carbon-based adsorbents and their roles in the removal of heavy metals from aqueous solutions: A critical review. *Chemical Engineering Journal*. Elsevier B.V. June 15, 2019, pp 608–621. doi:10.1016/j.cej.2019.02.119.

57. Ramer, G.; Lendl, B. Attenuated Total Reflection Fourier Transform Infrared Spectroscopy . In *Encyclopedia of Analytical Chemistry*; Wiley, 2013. doi:10.1002/9780470027318.a9287.
58. Bieberle-Hütter, A.; Bronneberg, A. C.; George, K.; Van De Sanden, M. C. M. Operando attenuated total reflection Fourier-transform infrared (ATR-FTIR) spectroscopy for water splitting. *Journal of Physics D: Applied Physics*. IOP Publishing Ltd April 1, 2021. doi:10.1088/1361-6463/abd435.
59. Aller, D.; Bakshi, S.; Laird, D. A. Modified method for proximate analysis of biochars. *Journal of Analytical and Applied Pyrolysis* **2017**, *124*, 335–342. doi:10.1016/j.jaap.2017.01.012.
60. Archontoulis, S. V.; Huber, I.; Miguez, F. E.; Thorburn, P. J.; Rogovska, N.; Laird, D. A. A model for mechanistic and system assessments of biochar effects on soils and crops and trade-offs. *GCB Bioenergy* **2016**, *8*(6), 1028–1045. doi:10.1111/gcbb.12314.
61. CHNS Elemental Analysers. **2008**.
62. Mohammed, A.; Abdullah, A. *SCANNING ELECTRON MICROSCOPY (SEM): A REVIEW*.
63. Zhou, W.; Apkarian, R. P.; Lin Wang, Z.; Joy, D. *Fundamentals of Scanning Electron Microscopy*.
64. Kosasih, F. U.; Cacovich, S.; Divitini, G.; Ducati, C. Nanometric Chemical Analysis of Beam-Sensitive Materials: A Case Study of STEM-EDX on Perovskite Solar Cells. *Small Methods* **2021**, *5*(2). doi:10.1002/smt.202000835.
65. *MODULE II ENERGY DISPERSIVE ANALYSIS OF X-RAYS (EDAX)*.
66. Proximate analysis procedure.
67. Klasson, K. T. Biochar characterization and a method for estimating biochar quality from proximate analysis results. *Biomass and Bioenergy* **2017**, *96*, 50–58. doi:10.1016/j.biombioe.2016.10.011.

Chapter 2

2 Method for the Investigation of Biochar Adsorption Mechanisms for Aqueous Aromatic Organic Compounds

2.1 Statement of Authorship

The contents and some of the data of the following chapter have been submitted to be published in the Journal of Biomass and Bioenergy. This includes the adsorption results and physical characterization of the Douglas fir-derived biochars. The author of this thesis was responsible for a majority of the work herein, including experimental design and execution including biochar characterization, adsorption experimentation, data processing and analysis, as well as the writing of the manuscript and participating in the editing and review of the manuscript along with supervisors Dr. Yeung, Dr. Berruti and Dr. Klinghoffer.

2.2 Chapter Abstract

Biochar has been proven to be a successful adsorbent for organic compounds in water however, understanding the adsorption mechanisms through which this occurs has remained vague due to a lack of methods to investigate specific mechanisms (1–5). The purpose of this study was to develop a procedure to identify the mechanisms that are responsible for the adsorption of aqueous aromatic compounds by biochars. This would make it possible to determine which pollutants different biochars are best suited for removing, as well as develop a better understanding of what biochar characteristics are more favourable for the adsorption of certain pollutants in water. A series of adsorption experiments were performed using the four test compounds, ibuprofen (IBU), acetaminophen (ACT), methyl orange (MO), and methyl blue (MB) as representative organic pollutants under various pH values for four woody (RC, DF, PW, and HL) and four non-woody (RH, MC, PH, and SG) biomasses pyrolyzed under different pyrolysis temperatures and flow gases, N₂ and CO₂. This was done by comparing the relative adsorption of the compounds as well as considering their differences in adsorption capacities with increasing pH. Biochars produced under CO₂ flow gas, at higher pyrolysis temperature and with woody biomasses exhibited the greatest adsorption capacities for aromatic compounds due to greater surface area and aromaticity resulting in strong π - π interactions. In contrast, biochars produced with non-woody biomasses and at lower pyrolysis temperatures had more oxygen-containing functional groups and therefore stronger electrostatic interactions.

2.3 Introduction

The quality and availability of freshwater are decreasing due to the contamination of natural water resources by harmful pollutants including nitrogen and phosphorous-containing compounds, heavy metal ions and bioactive pharmaceuticals (6). The major sources of water contamination are agricultural activities, industrialization, and simply pollution from the general public as a result of population growth (7). Dissolved organic compounds in water pose a threat to the environment as well as human and ecological health, as they mimic and antagonize natural hormones, hinder metabolic processes, occupy hormone receptors and cause reproductive developmental problems when consumed by human and aquatic species leading to long-term adverse consequences on various ecosystems (8). These compounds include pharmaceuticals, personal care products, surfactants, and pesticides and are most often a result of municipal

wastewater discharge, as these compounds are not completely removed during treatment (9). Given how ubiquitous these compounds are in everyday life, sufficient and effective methods for their removal from water sources are essential.

Biochar is the stable carbon-rich by-product of the pyrolytic processing of plant and animal biomass in a zero or low-oxygen environment (2,10). It has the potential application as a promising adsorbent for the elimination of a variety of pollutants in both soil and aqueous environments due to its favourable adsorption properties, which are dependent on a variety of factors including the conditions of the pyrolysis process and original feedstock (2). Compared to current water treatment methods, biochar presents a potentially more sustainable approach as it is a low-cost and renewable adsorbent made using readily available biomaterials and can be optimized for specific adsorbates (11–14). Pharmaceutical compounds are often treated with methods such as oxidation, enzymatic, photocatalytic and photo electrocatalytic degradation and biodegradation by activated sludge, however, these methods are often not effective (8). Adsorption onto activated carbon is a method used to remove both organic pollutants as well as heavy metals from water sources, however, these are often derived from non-renewable fossil fuels and can range from \$2,000-\$7,000 (3,8). Thus, the use of biochar, which is an adsorbent produced from waste products, offers a promising solution for cost-effective and sustainable adsorbent.

Another prevailing issue with current activated carbon adsorbents is that because of the heterogeneous nature of the surface, there remains some uncertainty surrounding its adsorption mechanisms. This limits the design of treatment systems as it is difficult to predict the adsorption capacity when the adsorption mechanisms remain unclear and are based solely on empirical observations. Thus, the development of a systematic procedure to experimentally define the adsorption mechanisms between certain pollutants and carbon surfaces would allow for a comprehensive analysis and subsequent optimization of biochars with characteristics that are better suited to the clean-up of commonly found environmental pollutants. In the report by Rivera-Utrilla and co-workers, biochars of varying physical and chemical surface properties were used to identify individual properties that are best suited for the adsorption of specific compounds. It was concluded that the main variables affecting the adsorption onto carbon surfaces are: (i) the surface area, pore size and pore distribution (ii) the surface chemistry of the adsorbent, as determined by the surface functional groups and (iii) the pH of the solution (3).

Aggarwal et al. explained biochar adsorption through two major mechanisms: electrostatic and π -interactions (π stacking, π -H bonding, π - π electron donor-acceptor interactions) (1). Electrostatic interactions have been hypothesized as a key mechanism resulting from acidic oxygen surface groups on biochar being ionized in aqueous solution to produce hydrogen ions (1). The role of oxygenated functional groups was additionally highlighted when, upon removal of carboxylic groups from activated carbon via thermal treatment, a decrease in cation adsorption was observed (15). The same trend was seen for positively charged ammonia which showed higher sorption by more polar biochar, which was attributed to electrostatic interactions with the negatively charged oxygen-containing groups on the surface (16). This was confirmed through the effects of the pH of the solution; as pH increases, the concentration of negatively charged sites increases due to the deprotonation of oxygen-containing surface functional groups (carboxylic acid, lactones, and phenolics) (16). The significance of electrostatic interactions has often been attributed to the general trend that has been observed for increased adsorption of organic compounds at lower solution pH. The charge of the organic pollutants is dependent on the acid or base dissociation constants (pKa or pKb) of the ionizable groups of the pollutant molecules, as well as the pH of the solution; for example, the interaction with negatively charged biochar is seen to be greatest when compounds are positive or neutral and weakest when negative. Many authors have noticed the greater adsorption affinity of biochar when the pH of the reaction solution falls below the pKa of the adsorbent (2,17). Essanhow et al. looked into the adsorption of both ibuprofen and salicylic acid by pine wood biochar at increasing pH and found that both adsorbates are seen to have greater removal at more acidic pH (17). They noted that at higher pH, specifically pH greater than the pKa of the adsorbates, both ibuprofen and salicylic decreased in adsorption which was attributed to an increase in electrostatic repulsion from the negatively charged biochar and the compounds (17). When the pH is equal to the pKa, there is 50% ionization of the adsorbate, and as the pH surpasses the pKa the ionization ratio of the adsorbate ions increases exponentially (17). Thus, the decrease in adsorption as the pH increased further supports evidence of electrostatic interactions between adsorbates and biochar playing a large role in the adsorption capacity. As a result, the surface charge of biochar is also an extremely important property in terms of the adsorption of ionic molecules due to coulombic interactions. Biochar often bears electrical charge deficits due to acidic oxygen-containing functional groups on its surface, such as hydroxyl and carboxylic groups, which contribute to its typically negative charge and alkalinity (18–21).

Other researchers reported that, in addition to electrostatic interactions, π - π interactions, including π - π electron donor-acceptor (EDA) interactions, π -H bonding and π stacking, have been found to play a large role in adsorption (2,22). Biochar pyrolyzed at a high temperature often has a high micro-porosity and consists mainly of polyaromatic carbons which enhances the adsorption of organic compounds, while higher proportions of aliphatic carbons and functional groups are typical of biochars pyrolyzed at lower temperatures (2,4,23). The aromaticity of biochar increases hydrophobicity, contributing to even greater adsorption of organic compounds in aqueous solution (2,24,25). The higher the polarity of biochar, the higher the adsorption affinity toward polar compounds, while greater aromaticity increases the adsorption of aromatic compounds and may lead to induced electrostatic interaction such as π - π interaction, π -stacking, and London dispersion forces (2,24). In addition, the adsorption capacity was positively correlated with polar functional groups, as well oxygen-containing functional groups allow for H-bonding interactions for adsorbents (H-bonding donor) and chemicals (H-bonding acceptor) (2,24). Conversely, the H-bonding donor groups on the biochars allow for π -H bonding interactions with the aromatic rings of organic compounds under acidic conditions (2,22). Given this prevalence of π - π EDA interactions in the adsorption capacity of biochar, surface aromaticity and polarity of biochar are two very important factors when considering organic adsorption. However, how the functional groups affect adsorption mechanisms has yet to be explicitly demonstrated.

Though both electrostatic and π -interactions play a large role in the adsorption of various pollutants from water, it can be challenging to identify when these mechanisms are occurring, and which is most influential. Studies on biochar in the literature often include adsorption data of representative pharmaceutical compounds and dyes, however only to the extent of proving that adsorption of these specific compounds is possible. While electrostatic and π - π interactions are proposed to be responsible for adsorption, there remains little evidence to prove this, or to indicate which is the major mechanism. This makes it difficult to determine which biochar is best suited for which environment.

This study aimed to develop a procedure to characterize the specific physical and chemical interactions through which various biochars adsorb pharmaceutical compounds, specifically electrostatic and π -interactions. The possible significant adsorption mechanisms for aqueous organic compounds are schematically depicted in **Figure 2.1** are: 1) coulombic/electrostatic attraction/repulsion between charged sites on the adsorbent and adsorbate, 2) π - π electron donor-

acceptor (EDA) interactions between electron-rich π -systems and electron-deficient π -systems, and 3) π - π stacking (6,24). Four organic compounds, ibuprofen (IBU), acetaminophen (ACT), methyl orange (MO), and methylene blue (MB), were chosen as test compounds to investigate these adsorption mechanisms. These chemicals were chosen as model contaminant compounds due to their representative characteristics, including electron-donating and withdrawing groups and ionic moieties, which vary depending on the pH of the solution.

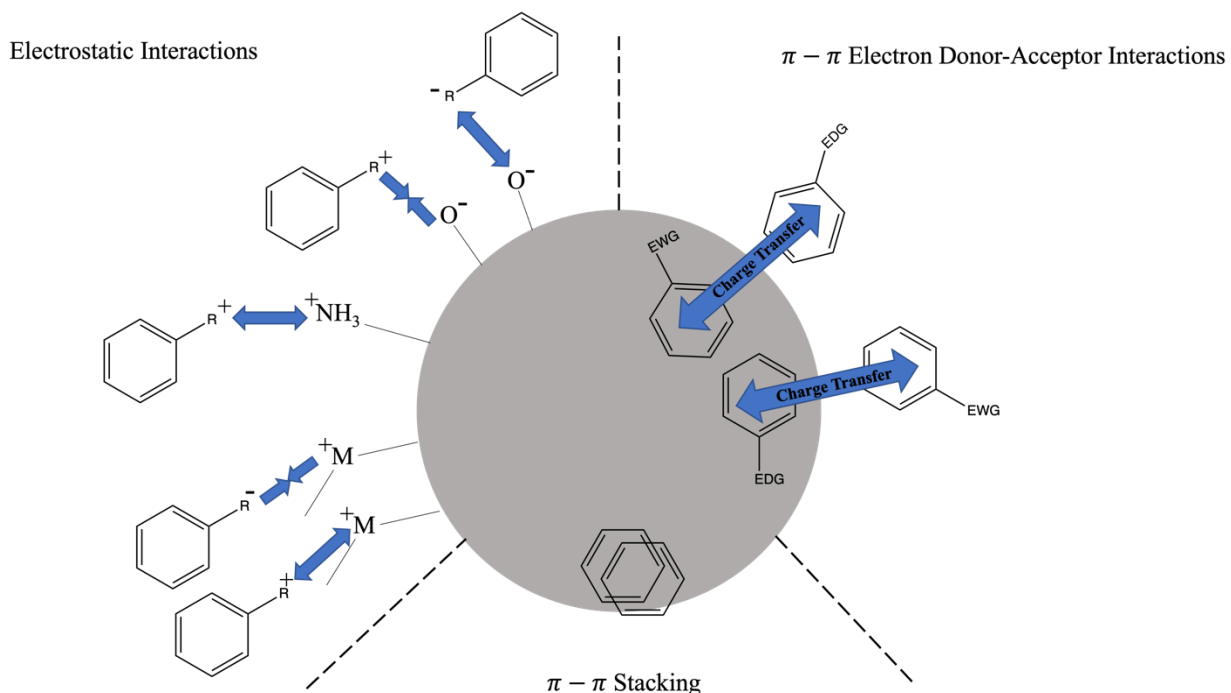


Figure 2.1 Schematic illustration of biochar adsorption mechanisms towards aromatic compounds in water

2.4 Materials and Methods

2.4.1 Materials

Two types of common woody biomasses were used: pinewood (PW), Douglas fir (DF), and red cedar (RC) chips were collected from a local furniture manufacturer in London, Ontario, Canada. As well as four non-woody biomasses, switch grass (SG), miscanthus (MC), and phragmites (PH), which were collected from near London, Ontario, Canada. Before the pyrolysis, the biomasses were pulverized using a blade grinder mill (VM 0197, Vitamix, USA) and sieved to the particle size range of 0.3-0.6 mm using standard test sieves (W.S. Tyler, USA).

The compressed N₂ and CO₂ gases were purchased from Praxair Canada Inc.

Methylene blue (MB), methyl orange (MO), ibuprofen (IBU), and acetaminophen (ACT) used as adsorbates were purchased from Sigma Aldrich, Canada.

2.4.2 Procedure for Pyrolysis

All biomasses were pyrolyzed using a tube furnace at 10°C/min until 500°C or 800°C and held for 3 hours with a flow gas rate of 2 mL/min. CO₂ flow gas was used for all of the biochars, while N₂ was used for PH and RC at 800°C. Each of the biochars was prepared separately, and after pyrolysis were washed with DI water and dried at 105°C overnight.

2.4.3 Methodology for Investigation of Biochar Adsorption Mechanisms for Aqueous Aromatic Compounds

The structures of the four test compounds ibuprofen (IBU), acetaminophen (ACT), methyl orange (MO), and methylene blue (MB) under acidic and basic conditions are shown in **Figure 2.2** while the properties of the compounds are summarized in **Table 2.1**. IBU is a weak carboxylic acid with a pKa of 4.5 (26). Since it is only weakly electron withdrawing at pH > pKa, it is mainly adsorbed via π - π stacking, electrostatic interaction between the aromatic groups of the biochar within the composite and the adsorbate compound (27). All of the compounds investigated were found to be active in the UV-visible spectrum, making them well-suited for UV spectroscopy for the determination of their concentrations in solution. As well, molecules were chosen such that their structures, sizes and molar masses do not vary significantly (within 150-300 g/mol) in order for their adsorption capacities in mg adsorbate per mg adsorbent could be accurately compared.

Table 2.1 Physical characteristics of aromatic compounds used as adsorbates for investigation of adsorption mechanisms of biochar

Compound	Abbreviation	pKa	Molar Mass (g/mol)	Size (nm)	Wavelength of Max. UV-Vis Absorbance Peak (nm)
-----------------	---------------------	------------	---------------------------	------------------	---

Ibuprofen	IBU	4.5(90)	151.2	~1nm x 0.6nm(91)	220
Acetaminophen	ACT	9.3(92)	206.3	~1nm x 0.6nm(91)	243
Methyl Orange	MO	4.5(93)	327.3	~1.7nm x 0.8nm(94)	464
Methylene Blue	MB	3.8(95)	319.9	~1.7nm x 0.8nm(96)	668

The pKa of ACT is 9.3, when the pH surpasses the pKa, its' structure loses a phenolic proton resulting in a negatively charged product (35). The decrease in adsorption after pH 8 can then be explained through electrostatic repulsion from the many negatively charged surface sites originating from oxygenated functional groups, or metal oxides on the surface. ACT has a neutral charge under acidic conditions with electron-donating groups (EDGs), while MO in similar conditions is a zwitterionic compound at pH < pKa of 4.5 and has an electron-withdrawing group (EWG) of sulfonyl (36). Because MO is zwitterionic when the pH is 4.5 or below, any electrostatic attraction or repulsion forces it may experience in these conditions from one charge will be balanced by the other opposing charge. Any adsorption of MO at low pH would thus be mainly due to EDA interactions with the deactivated ring. EDA interactions with EDGs and EWGs can then be determined from the differences in adsorption capacity between ACT and MO at low pH. ACT has a neutral charge below neutral pH with electron-donating groups, while MO is a neutral (zwitterionic) compound with only an EWG when the solution pH is lower than its pKa of 4.5(31).

The MO adsorption curves can further be used to evaluate the influence of the π - π EDA interactions in comparison to electrostatic interactions. After deprotonation of the amine, which takes place after the pH surpasses 4.5, MO gains an electron-donating group and an activated aromatic ring (36). Consequently, MO can then undergo EDA interactions with adsorbates with both EWG and EDGs but would also experience electrostatic repulsion. As the pH increases, so does the amount of negatively charged sites on the surface of the adsorbent, as oxygen-

containing functional groups are deprotonated. This results in a decrease in adsorption of MO due to electrostatic repulsion to the negatively charged aromatic amine group, but also an increase due to EDA interactions with both aromatic rings. Whether the adsorption will increase, or decrease would be dependent on which mechanism is stronger.

Lastly, the relative strength of the electrostatic interactions can be determined by the adsorption capacity of MB in comparison to the other compounds. Since MB is a positively charged dye with a +2 charge at $\text{pH} < \text{pK}_a$ of 3.8 and a +1 charge at $\text{pH} > \text{pK}_a$, MB is a cationic dye that remains positively charged regardless of the pH of the solution. As the pH increases the biochar surface typically becomes negatively charged and the electrostatic interactions with MB would then be proportional to its adsorption (37). MB and ACT are both comprised of an activated aromatic ring due to electron-donating groups. However, only MB is positively charged at the pH range we studied, while ACT is electrostatically neutral below pH 9 or anionic at above pH 9. This means that an equal adsorption capacity for both compounds under acidic conditions would indicate that MB is adsorbed due to π - π EDA interactions over electrostatic.

Current research into biochar adsorption often states that the physical properties, such as surface area, surface functionality, mineral/ash content, etc. of the adsorbent strongly influence the adsorption of organic compounds, however, there remains little investigation of the specific adsorption mechanisms and how large a role these properties play in them. Specifically, the oxygen-containing functional groups originated from the pyrolysis of the lignocellulosic biomass predominantly comprised of carboxylic, lactonic, and phenolic groups (38,39). These functional groups can be responsible for electrostatic interactions via the negatively charged sites that arise upon deprotonation, as well as π -interactions (π - π stacking, π - π EDA interactions, and $\text{H}\pi$ interactions) as there are often substituents on the polyaromatic surface. While the pH of the solution influences the electrostatic interactions, π interactions are independent.

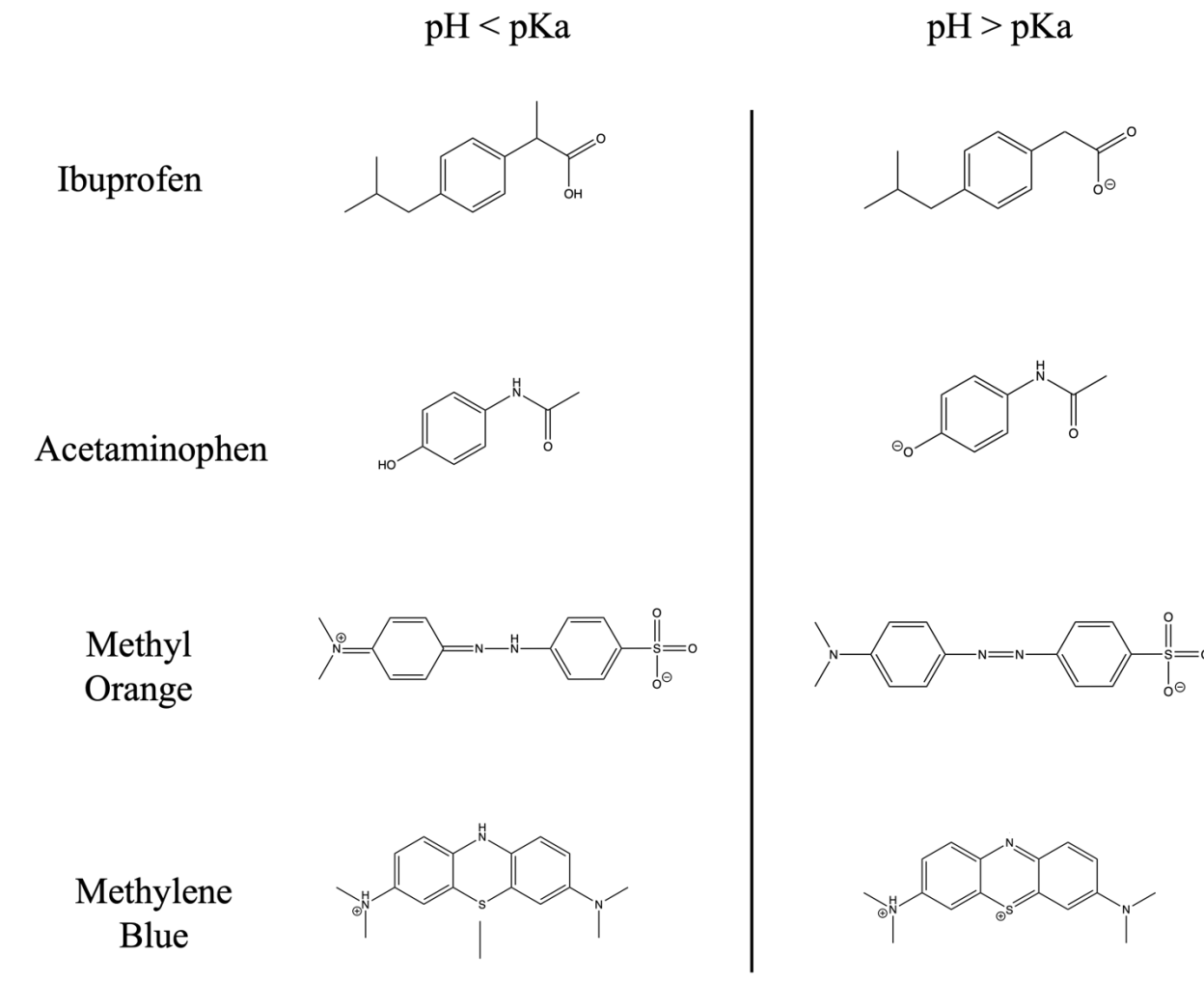


Figure 2.2 Structure of a) ibuprofen (IBU), b) acetaminophen (ACT), c) methyl orange (MO), and d) methylene blue (MB) at pH below and above individual pKa values (28,30,31,33)

2.4.4 Adsorption Experiments

The mechanisms for adsorption were determined by placing 0.1 g of each adsorbent sample in a 20.0 mL test tube containing 15 mL solution of 1 mM H₃PO₄ and 25 ppm of the test compound at the desired pH. Adsorption experiments were carried out at relative pH values of 2, 6, 8, and 11. The H₃PO₄ acted as a pH buffer, and the pH was adjusted using NaOH. Samples were agitated for 1 hour at 25 °C and filtered through Whatman No. 1 filter paper. The pH of the filtrate was determined after filtering using a pH meter (Thermo Scientific, Orion Star). The concentration of adsorbate remaining in the filtrate was determined at their λ_{max} using a UV-visible spectrophotometer (Thermo Scientific, Evolution 220). Samples were analyzed in

triplicate, and their average absorbances were used. The adsorption capacity was defined as the amount of chemically adsorbed on the unit mass of the tested adsorbent (mg/g). A preliminary adsorption test is done for each adsorbent tested using 100 ppm of ACT as the standard test solution. Beginning with 25 mg of adsorbent, the mass is increased, and the adsorption capacity is measured after 1 hour. The ratio the of mass of adsorbent to the concentration that gives an adsorption capacity of zero and below complete adsorption is used for the preceding tests.

2.4.5 Biochar Characterization Methods

2.4.5.1 Proximate and CHNS-O Elemental Analysis

The proximate analysis of the biomass samples was performed following the ASTM standard (ASTM D1762-84) using a Neytech Vulcan D-550 muffle oven. Elemental analysis of carbon, hydrogen, nitrogen, and sulphur is undertaken using the model Thermo Flash EA 1112 series CHNS analyzer (Thermo Fisher Scientific, USA). Samples are combusted at 900 °C under helium with a known amount of oxygen. The oxygen content in the sample is calculated by mass difference. The results were measured in triplicates with the averages being reported with standard deviations.

2.4.5.2 ATR-FTIR Spectroscopy

The surface organic functional groups present in the samples were detected using Fourier transform infrared spectroscopy (FT-IR) using a Platinum[®] attenuated total reflectance (Pt-ATR) attachment equipped with a diamond crystal in the main box of a Bruker Tensor II spectrometer. During the analysis, the sample in powder form was scanned within the range of 400-4000 cm⁻¹ at a resolution of 4 cm⁻¹ under transmittance mode and 32 accumulations for each spectrum.

2.4.5.3 BET Surface Analysis

Samples were tested for Brunauer-Emmett-Teller (BET) with Nova 2000e Surface Area and Pore Size Analyzer (Quantachrome Instrument, Florida, US). The physisorption measurements were performed via N₂ adsorption-desorption experiments at 77.35 K. Samples were degassed at 105°C for 1 hour to remove moisture, then the temperature was increased to 300°C and maintained for at least 3 hours before analysis.

2.4.5.4 SEM-EDX Spectroscopy

The samples were analyzed by SEM-EDX using a Hitachi SU3500 Scanning Electron Microscope (SEM) combined with an Oxford AZtec X-Max50 SDD energy dispersive X-ray (EDX) detector. EDX is a semi-quantitative technique that can detect all elements with a minimum detection limit of approximately 0.5 wt%. EDX spectra from individual particles were analyzed using a vector-based algorithm to determine the relative abundance of 10 elements: carbon (C), sodium (Na), magnesium (Mg), aluminum (Al), silicon (Si), potassium (K), calcium (Ca), titanium (Ti), oxygen (O), and iron (Fe). A 10 kV accelerating voltage was used for these analyses. The samples were coated with a thin layer of gold to minimize charging effects.

2.4.5.5 Thermogravimetric Analysis

Thermogravimetric analysis of samples was performed using a TG-Analyzer (Mettler Toledo TGA 2). About 5 mg of samples were heated from room temperature to 800°C under N₂ and CO₂ separately with a heating rate of 10°C/min.

2.5 Results and Discussion

2.5.1 Effect of N₂ and CO₂ Pyrolysis Flow Gas on Adsorption Mechanisms of Biochars for Aromatic Compounds

To investigate the effects of pyrolysis gas atmosphere, RC and PH were both pyrolyzed at 500°C and 800°C under N₂ and CO₂ flow gases. The thermogravimetric analysis of both RC and PH biomasses investigated in this section, under CO₂ and N₂ gas, are presented in **Figure 2.3**. According to the data in the TGA curves in **Figure 2.3**, there is a slightly greater weight loss found when using CO₂ gas than the inert N₂ gas for the RC and PH biomasses. This is determined given the greater decrease in weight% in the TGA curves, and shift of the DTG curves, which was found to be greater for the PH biomass than RC biomass (40). The PH biomass was therefore found to decompose at a greater rate than the RC biomass under CO₂ gas. The most significant difference between the biomasses is the peak around 300°C in the DTG of the PH biomass that is not observed in the RC biomass and the more pronounced peak around 450°C in the RC DTG curve. These peaks are representative of the decomposition of hemicellulose and cellulose respectively, where woody biomasses such as RC are higher in cellulose content than hemicellulose-like non-woody biomasses including PH. The peak around

300°C in the DTG curve for PH was also shown to be less intense under CO₂, suggesting that the decomposition of hemicellulose may be less favourable under this pyrolytic gas. The specific decomposition mechanisms of lignocellulosic biomass and their effect on the resultant biochar properties and adsorption are explained in greater depth in section 2.4.3. Despite the differences seen between the biomasses, all sequences for pyrolysis are still present in the DTG results under either gas for both RC and PH, with a slightly greater mass loss under CO₂. Thus, the sequence of reactions is not changed significantly due to flow gas, but rather an increase in pyrolysis reaction rate which can still have great effects on increasing specific surface area and aromaticity, both of which are essential in a strong adsorbent. Surface functional groups may also be affected by the pyrolysis gas, as is explored in the preceding sections.

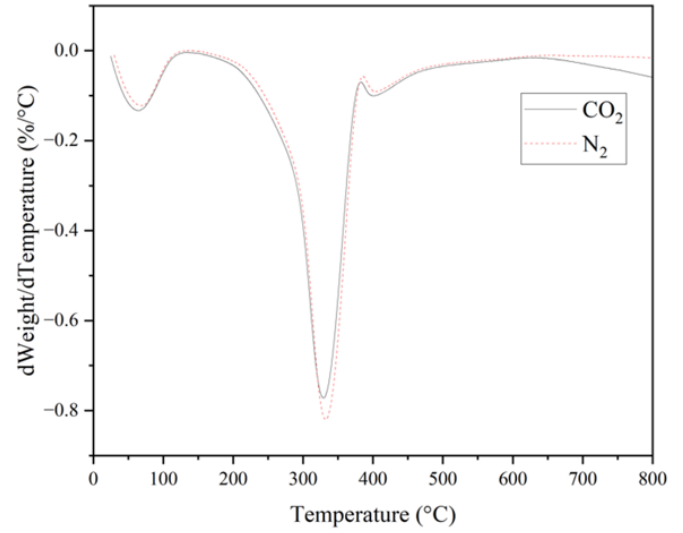
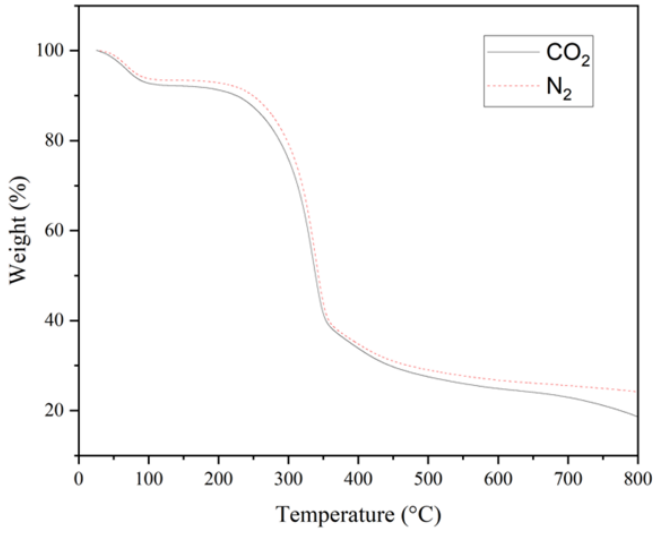
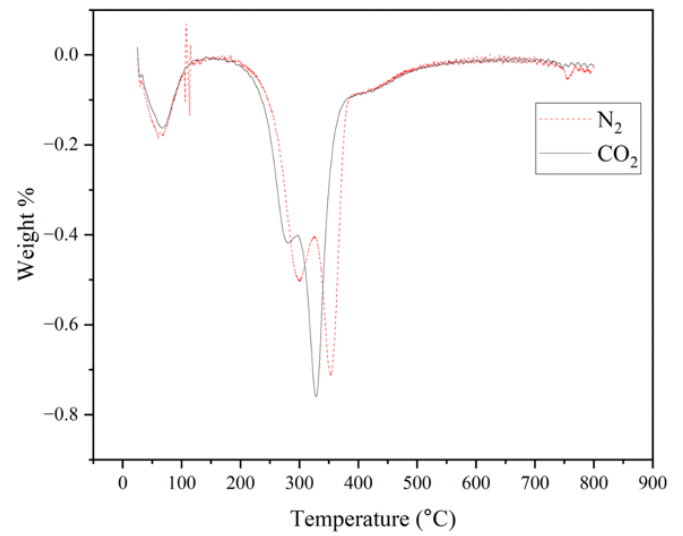
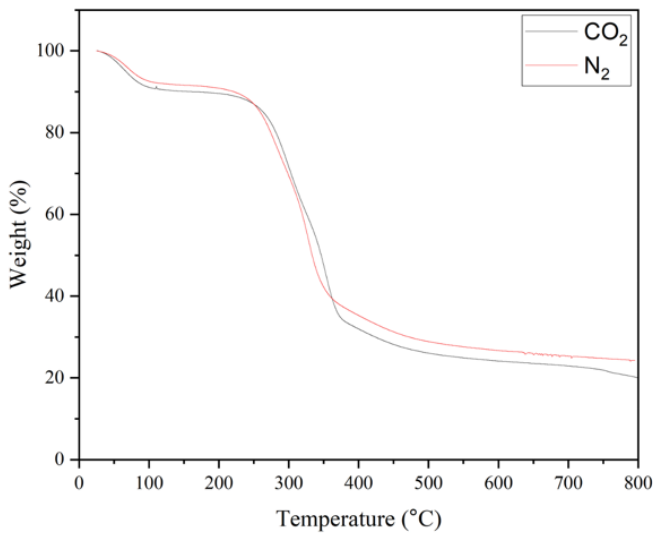
a**b**

Figure 2.3 TGA and DTG curves of a) RC and b) PH biomasses pyrolyzed under 2L/min CO₂ and N₂ pyrolytic gases

Nitrogen is expected to be inert while CO₂ can interact with the biomass and produced volatiles. Their adsorption mechanisms were then investigated using the proposed method. These biomasses were chosen given that they are two of the most common sources for biomass, however, they differ in their composition which can have large effects on the surface of the

resultant biochar and the adsorptive properties. Woody biomasses such as RC contain higher cellulose, and lower ash and hemicellulose content compared to non-woody/ herbaceous crops, and agricultural waste such as phragmites reeds (40). The physical and elemental analysis of the biomasses and biochars produced, (RC800-CO₂, RC800-N₂, PH800-CO₂, and PH800-N₂) are reported in **Table 2.1**. The BET results show that the use of CO₂ in pyrolysis yields a biochar with a greater surface area than when using N₂, regardless of the pyrolysis temperature. This is seen to have a greater effect in the RC800-N₂ and RC800-CO₂ biochars, where there is an increase of 67.2 m²/g to 448 m²/g. These results are in accordance with what has been seen in the literature, the surface area of biochar made under a CO₂ environment is greater and with a more developed pore structure than that from the N₂ environment (41,42). The SEM images, along with the EDX spectra in **Figure 2.4** show that the morphology of the biochars is much more intact and less broken down for RC800-N₂ and PH800-N₂ compared to RC800-CO₂ and PH800-CO₂ making the surface of the CO₂ produced biochars rougher and more porous and better suited for adsorption. Furthermore, the EDX spectra reveal that there is slightly higher oxygen content for the RC800-CO₂ and PH800-CO₂ biochars along with a higher ash content visualized by the light spots in the SEM images.

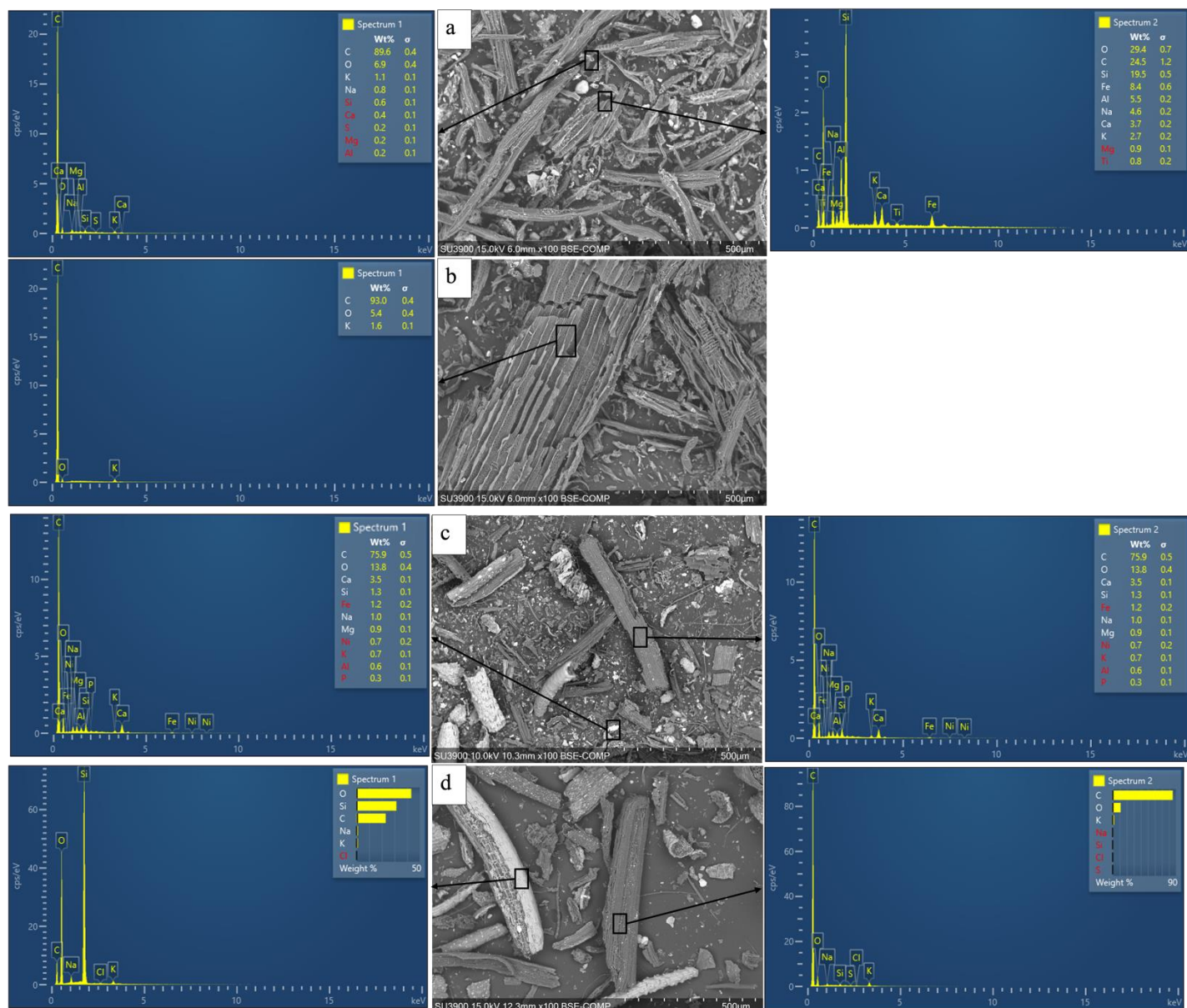


Figure 2.4 100X Magnification SEM images and EDX spectra of a) RC800-CO₂, b) RC800-N₂, c) PH800-CO₂, and d) PH800-N₂

The surface functional groups on the biochars were determined using ATR-FTIR spectrometry, whose results are reported in **Figure 2.5**. The biochars produced with the CO₂ gas showed distinct peaks around 1500 cm⁻¹ and 1000 cm⁻¹ for both the RC and PH biochars, which are representative of aromatic C=C and an asymmetric C-O-C stretch respectively. The RC800 biochar also showed a small peak around 1720 cm⁻¹, corresponding to a C=O stretch. The biochars produced using N₂ showed FTIR spectra that adsorbed in the same regions the peaks were seen for the CO₂ biochars, however, the peaks were broader with one large one seen for

both biomasses around 1000 cm⁻¹ and another at 1700 cm⁻¹, corresponding to C-O-C and C=O stretches respectively. Notably, there is a lack of aromatic peaks for the biochars produced with the inert gas. The results of the elemental analysis also corroborated the greater oxygen functional groups given that the C/O ratio was much higher for both RC800-N₂ and PH800-N₂ further indicating that there were fewer oxygen-containing functional groups on the surface of the biochars produced with the inert gas. These properties can have large effects on the adsorption mechanisms, explaining the differences in adsorption seen for the different biochars.

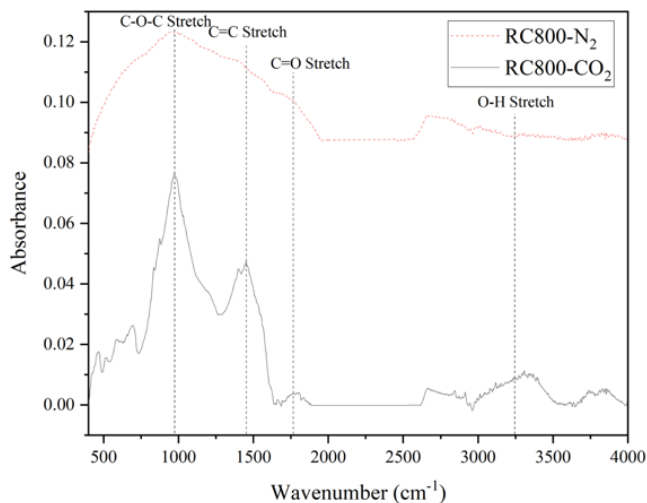
Table 2.2 Proximate and elemental analysis, and textural properties of biochars

Biochar	Proximate analysis (wt%)				Elemental analysis						BET analysis		
	Moisture	Volatile matter	Ash	Fixed carbon	C	H	N	O*	C/O	H/C	Surface area (m ² /g)	Average pore volume (cm ³ /g)	Average pore diameter (nm)
RC800-N ₂	3.23 ± 0.03	42.5 ± 1.2	17.3 ± 2.0	37.0 ± 3.2	74.3 ± 2.5	2.87 ± 2.2	0 ± 0.01	10.8 ± 4.7	6.64 ± 0.7	0.038 ± 0.003	67.2	0.046	2.76
PH800-N ₂	5.26 ± 0.1	35.5 ± 2.6	19.5 ± 0.3	39.7 ± 2.5	68.1 ± 2.4	0 ± 0.1	0.828 ± 0.3	10.0 ± 2.2	7.00 ± 0.2	0 ± 0.001	40.0	0.044	0.435
RC800-CO ₂	1.26 ± 0.1	44.6 ± 2.6	36.3 ± 1.2	17.9 ± 1.5	54.3 ± 0.9	0.98 ± 0.3	0.32 ± 0.15	8.1 ± 0.8	6.70 ± 0.01	0.018 ± 0.002	448	0.30	0.268
PH800-CO ₂	7.37 ± 0.1	68.5 ± 1.5	24.0 ± 1.3	0.15 ± 1.5	59.4 ± 1.5	0.86 ± 0.4	1.51 ± 0.9	14.2 ± 0.9	4.19 ± 0.05	0.011 ± 0.006	204	0.11	2.19

DF800- CO2	2.68	56.9	34.0	6.34	57.2	1.00	0.69	7.07	11.5	0.017	461	0.29	0.248
	±	±	±	±	±	±	±	±	±	±			
	1.2	1.5	3.1	1.4	3.8	0.2	0.04	3.8	0.2	0.003			
MC800 -CO2	4.01	78.2	16.7	1.13	61.9	1.23	1.03	19.2	3.23	0.020	369	0.20	2.19
	±	±	±	±	±	±	±	±	±	±			
	0.8	1.6	2.1	0.9	2.5	0.2	0.02	2.1	0.3	0.003			
RC500- CO2	3.43	48.2	10.9	37.5	59.0	4.41	0.42	25.3	2.45	0.075	394	0.90	2.65
	±	±	±	±	±	±	±	±	±	±			
	0.07	1.3	1.1	0.4	5.8	0.2	0.09	3.9	0.3	0.008			
PH500- CO2	2.61	48.6	18.3	30.4	73.9	1.63	1.47	3.58	20.7	0.022	5	0.060	4.44
	±	±	±	±	±	±	±	±	±	±			
	0.05	1.5	1.5	0.09	5.6	0.2	0.2	4.8	3.3	0.003			
DF500- CO2	2.93	29.5	8.48	59.1	77.2	2.92	0.57	10.8	7.16	0.038	103	0.050	1.91
	±	±	±	±	±	±	±	±	±	±			
	0.1	1.4	0.6	5.5	0.6	0.2	0.1	0.6	0.1	0.000			
MC500 -CO2	2.30	12.2	8.84	76.6	63.1	1.12	0.64	29.4	2.04	0.024	64	0.055	3.42
	±	±	±	±	±	±	±	±	±	±			
	0.2	1.9	0.5	1.2	5.8	0.3	0.1	6.1	0.4	0.005			

* Measured by difference (Total mass-C-H-N-Ash=O)

a



b

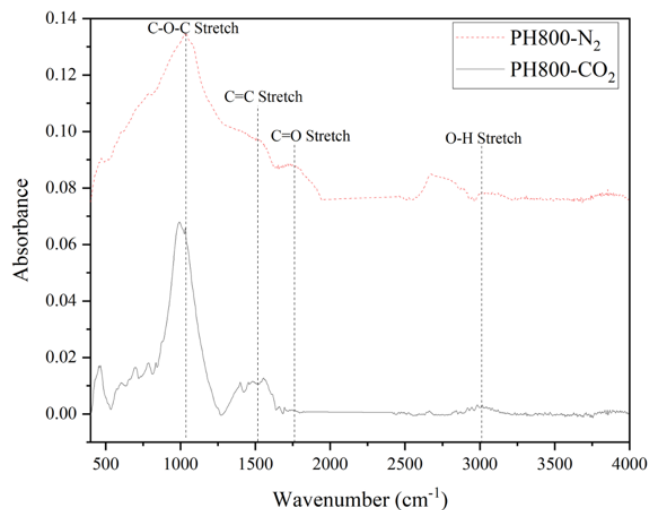


Figure 2.5 ATR-FTIR spectra of a) RC and b) PH derived biochars pyrolyzed at 800°C under CO₂ and N₂ pyrolytic gases

The adsorption characteristics of the four test compounds, IBU, ACT, MO, and MB, by the biochars produced under the inert and catalytic gas, are shown in **Figure 2.6**, while their structures at different pH values are given in **Figure 2.2**. Given the lower adsorption of IBU, ACT, and MO using biochar produced under N₂, it is evident that the better-performing adsorbent was the biochar pyrolyzed using CO₂ flow gas. This suggests that lower aromaticity, as seen for the biochars produced under the inert gas, would result in lower π - π stacking and EDA interactions. The adsorption capacities for MB are, however, similar and relatively constant regardless of whether the biochar was produced using CO₂ or N₂. The structure of MB, shown in **Figure 2.2**, has at least one positively charged group under any pH conditions, allowing for strong electrostatic interactions between MB and the negatively charged sites on the biochar surface (43). These groups are shown in the 2500 to 3000 cm⁻¹ signal in the FTIR, corresponding to the O-H stretch. In **Figure 2.5** there are strong peaks representing these hydroxyl O-H stretches for all the biochars except for RC800-N₂, whose MB adsorption is noticeably lower than RC800-CO₂. This then indicates that hydroxyl surface groups are the main biochar property that is responsible for electrostatic interactions, which when paired with a non-aromatic biochar

result in solely strong electrostatic interactions. The adsorption trends for all of the test compounds vary between the biomass and temperature of the pyrolysis, implying that the biomass played a role in the adsorption mechanisms. This is investigated further in later sections.

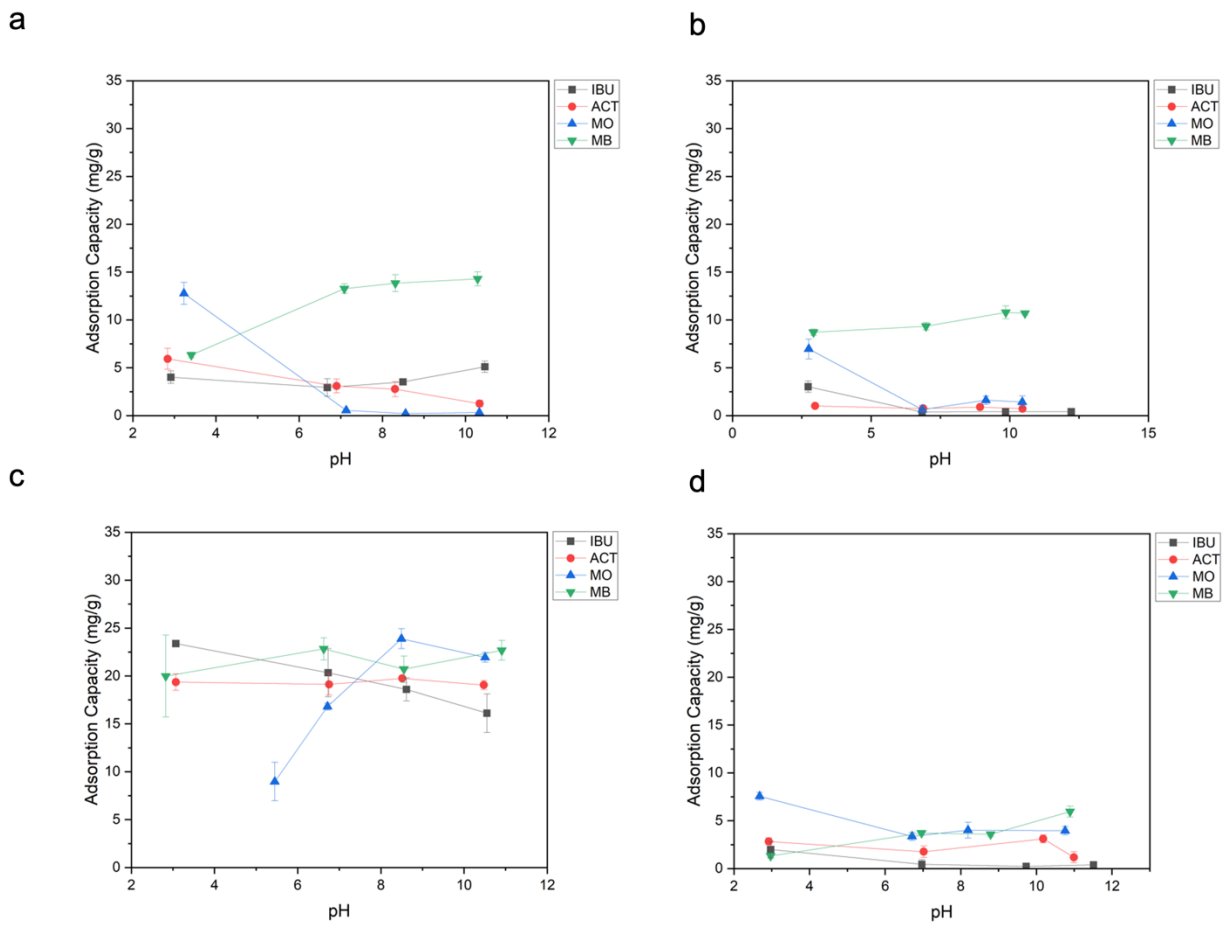


Figure 2.6 Adsorption capacities of IBU, ACT, MO, and MB with increasing pH for a) PH800-CO₂, b) PH800-N₂, c) RC800-CO₂, and d) RC800-N₂ where adsorption was performed using 50ppm of compounds and 50 mg of biochar in 15mL solutions

2.5.2 Effect of Pyrolysis Temperature on Adsorption Mechanisms of Woody and Non-Woody Biochar for Aromatic Compounds

To investigate the effect of the pyrolysis temperature on adsorption mechanisms, woody biomasses (RC, and DF) and non-woody biomasses (MC, and PH) were pyrolyzed at a ramp rate of 10°C /min to a temperature of 500°C and 800°C under CO₂. CO₂ was used as a flow gas due to superior performance compared to N₂. **Table 2.1** shows the physical and elemental results for the biochars. For both biomasses, the surface area and aromaticity were found to increase at higher

pyrolysis temperatures, while both having lower oxygen content. The adsorption mechanisms for these biochars were then investigated the uptake of aromatic compounds is presented in **Figure 2.7**. There was significantly lower overall adsorption of all of the test compounds for the biochars produced at 500°C compared to those produced at 800°C. This can be attributed to the surface area of the biochars, which is seen to be greater at higher temperatures, ranging from 204 m²/g to 461 m²/g and particularly for the woody-derived biochars. RC800-CO₂ and DF800-CO₂ had surface areas of 448 and 461 m²/g, compared to PH800-CO₂, and MC500-CO₂ whose surface areas were 204 and 369 m²/g respectively. The biochars pyrolyzed to 500°C had surface areas that ranged from only 5-394 m²/g. Notably, the average pore diameter is relatively larger for the biochars pyrolyzed to 500°C than 800°C, which appears to not have any significant effect on adsorption. Also, the pore diameter of the woody biochars is smaller pore sizes than the non-woody biochars at either pyrolysis temperature while still having greater maximum adsorption capacities. This means that there was an inverse correlation between the surface area and porosity, though the adsorption was found to increase only with greater surface area. The difference in surface morphology can be further visualized in the SEM images and EDX spectra depicted in **Figure 2.8**, where the biochar produced at a higher temperature had a more broken-down structure piece and precipitated metallic white particles, compared to the 500°C biochar. These imperfections in the 800°C biochar increase porosity and allow for greater surface area and therefore adsorption. The white particles, made of various metal oxides according to the corresponding EDX spectra, are due to the precipitation of metals out of the biochars at higher temperatures and do not contribute to the adsorption, as they are no longer being a part of the carbon structure.

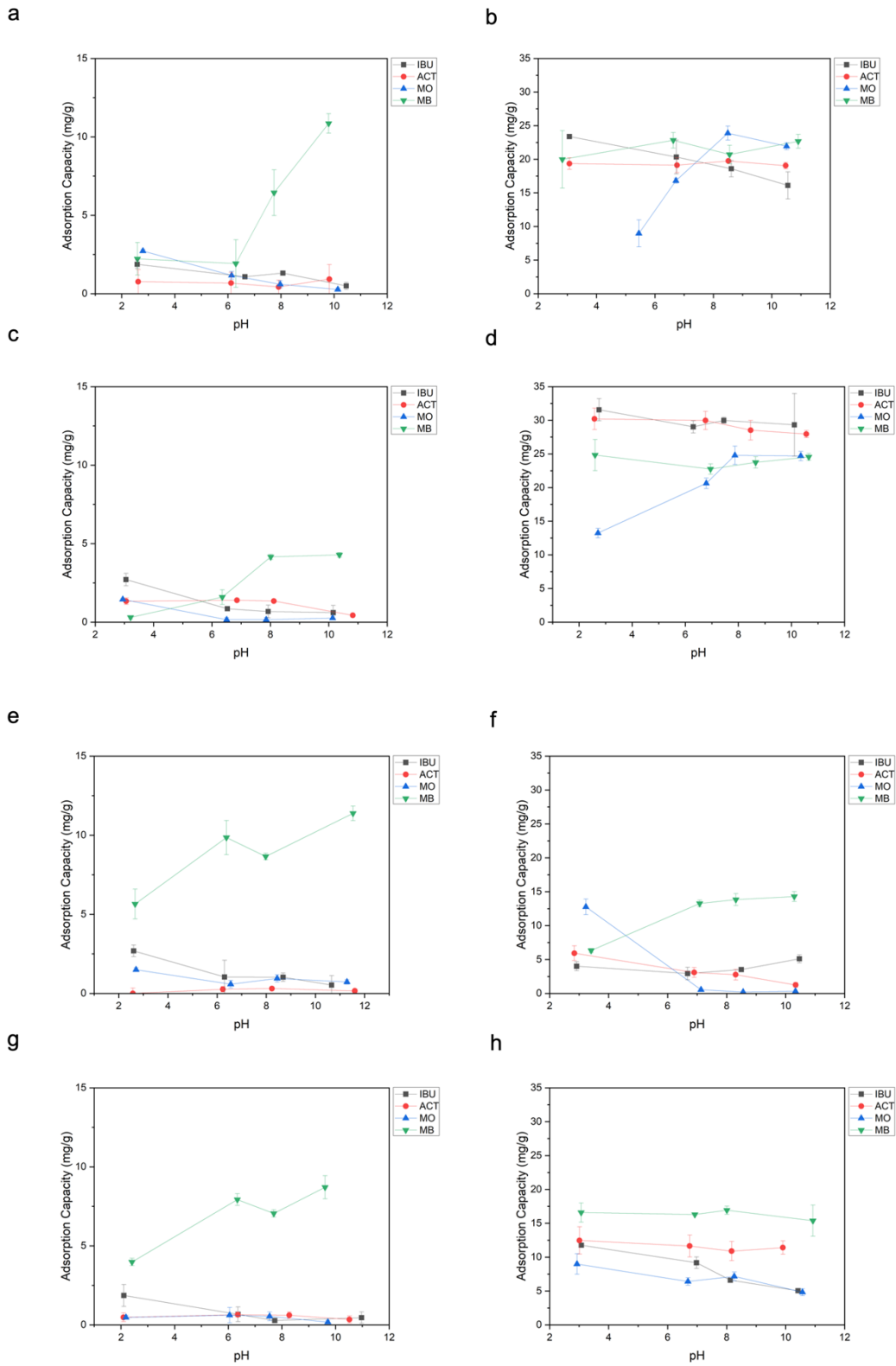
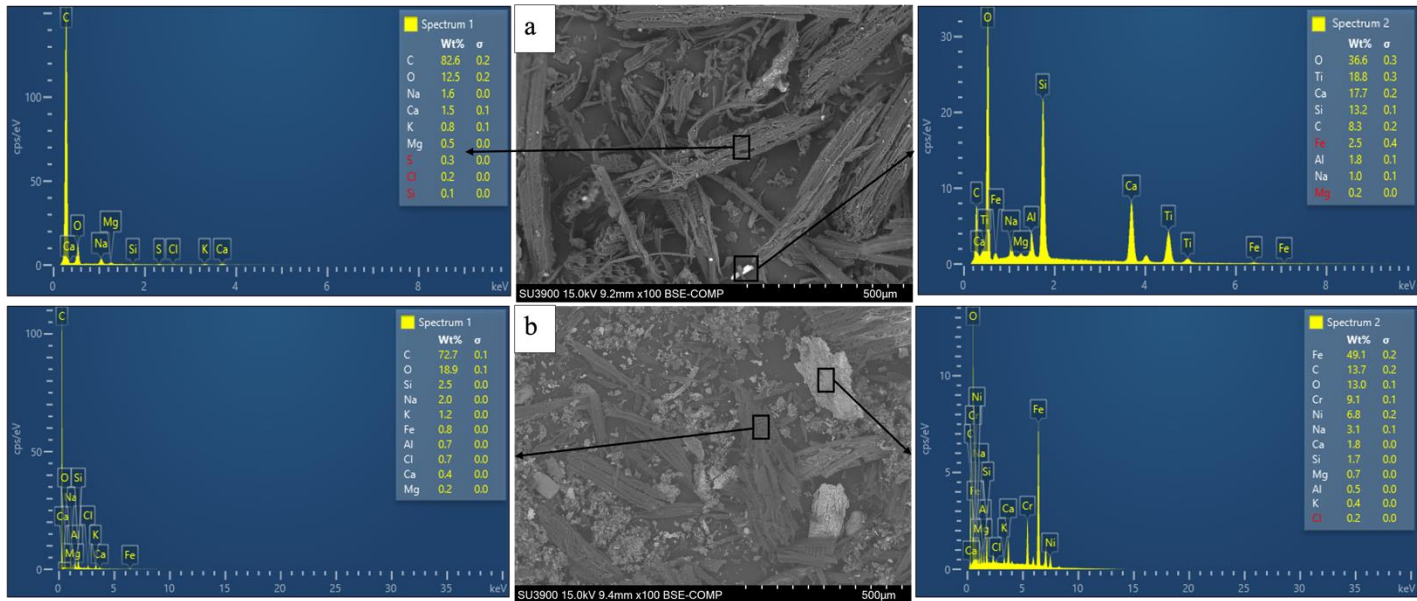
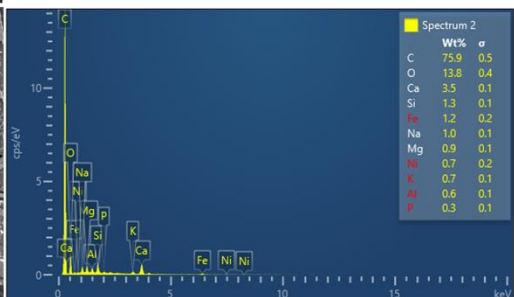
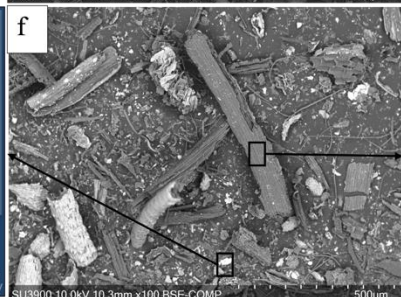
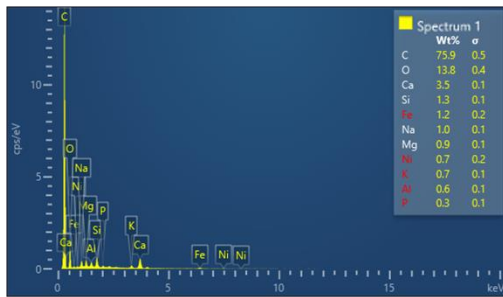
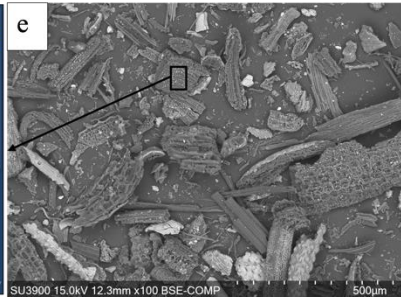
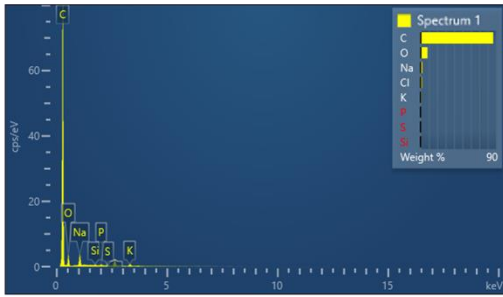
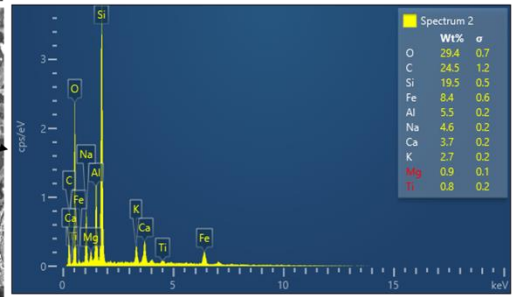
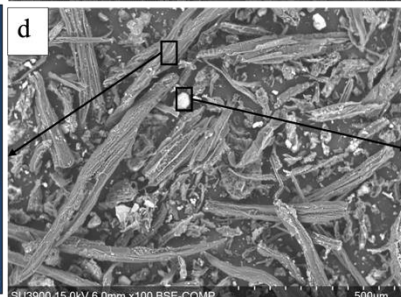
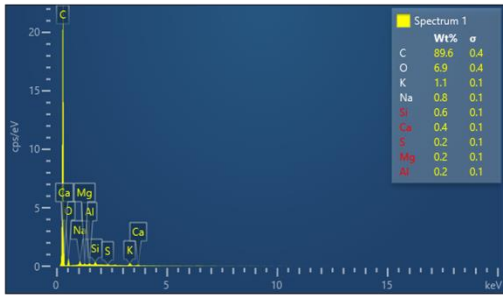
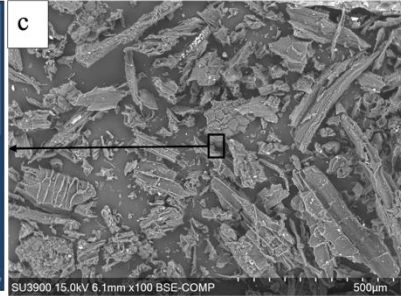
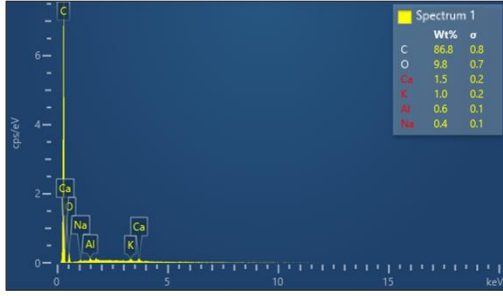


Figure 2.7 Adsorption capacities of IBU, ACT, MO, and MB with increasing pH for a) RC500-CO₂, b) RC800-CO₂, c) DF500-CO₂, d) DF800-CO₂, e) PH500-CO₂, f) PH800-CO₂, g) MC500-

CO₂, and g) MC800-CO₂ where adsorption was performed using 50 ppm of compounds and 50 mg of compounds and 50mg of biochar in 15 mL solutions





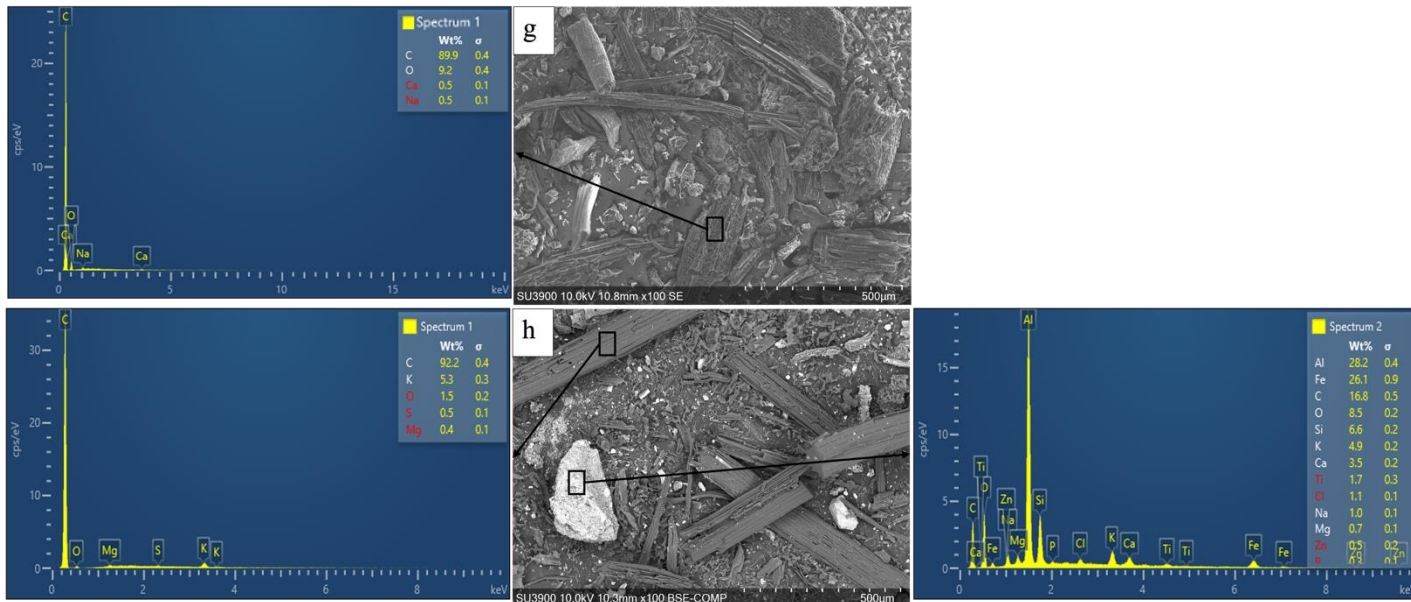


Figure 2.8 100X SEM images and EDX spectra of a) RC500-CO₂, b) RC800-CO₂, c) DF500-CO₂, d) DF800-CO₂, e) PH500-CO₂, f) PH800-CO₂, g) MC500-CO₂, and h) MC800-CO₂

Looking at the adsorption capacities for the woody and non-woody biochars produced at 500°C in **Figure 2.7a-d**, the adsorption capacities for MB are the only compound to be adsorbed. The biochars produced at this temperature are found to have lower aromaticity and greater oxygen functional groups, evidenced by the FTIR spectra seen in **Figure 2.9**, with the broadband around 3000 cm⁻¹ and sharp 1550 cm⁻¹ in all of the biochars produced at 500°C for the O-H stretch and C-O stretch respectively. The low H/C and high C/O ratios for the MC and PH chars compared to the RC and DF biochars also help to confirm the presence of oxygen-containing surface groups. These groups would act as negatively charged surface sites, contributing to stronger electrostatic interactions compared to π -interactions. Therefore, biochars pyrolyzed at lower temperatures within a CO₂ atmosphere, the oxygen groups formed on the surface will be in the form of hydroxyl groups which should increase electrostatic interactions.

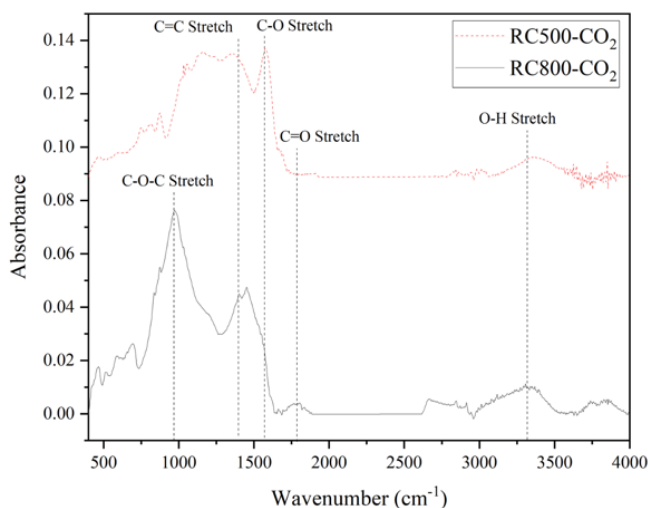
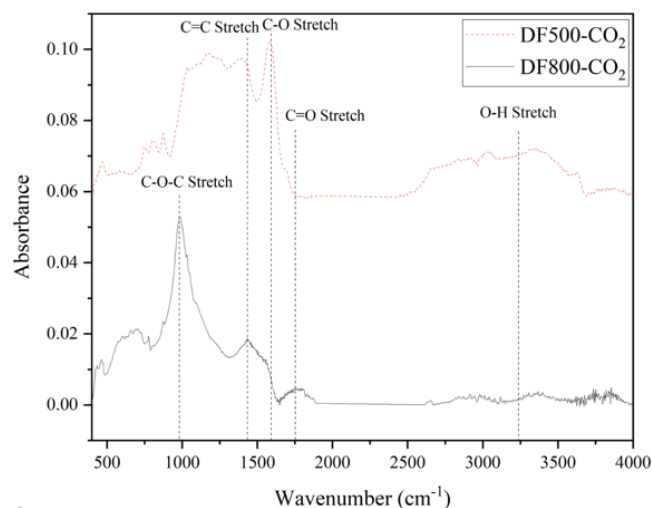
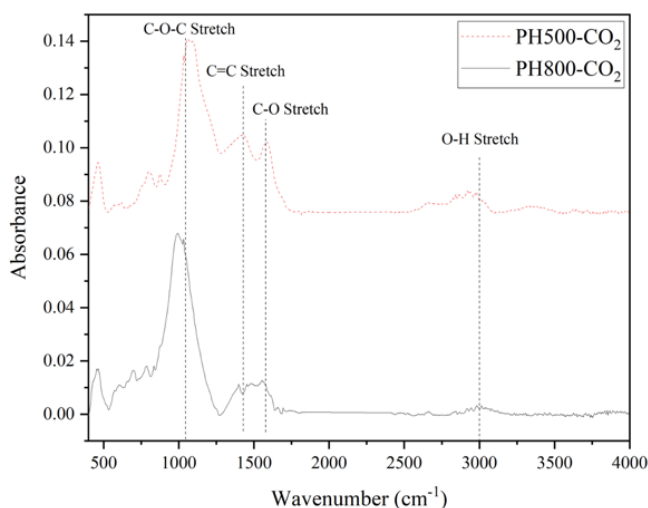
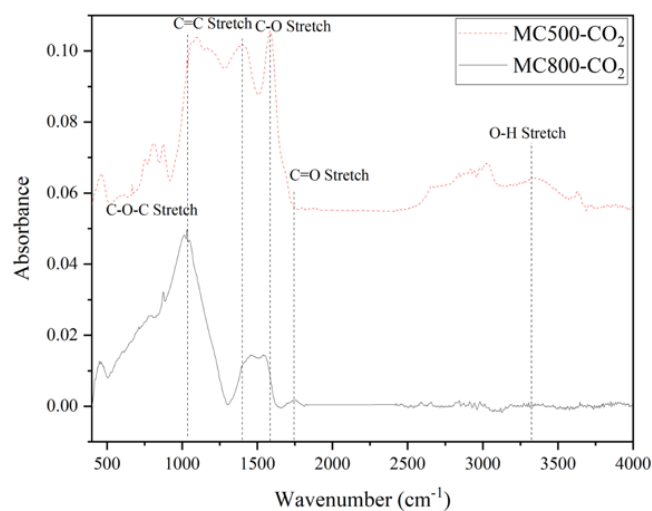
a**b****c****d**

Figure 2.9 ATR-FTIR spectra of a) RC500-CO₂, b) RC800-CO₂, c) DF500-CO₂, d) DF800-CO₂, e) PH500-CO₂, f) PH800-CO₂, g) MC500-CO₂, and h) MC800-CO₂

The RC500-CO₂ and DF500-CO₂ biochars exhibited a higher adsorption capacity for MB compared to the other test compounds in **Figure 2.7a-b**, suggesting strong electrostatic interactions and weaker π -interactions. This may be a result of lower aromaticity, and greater oxygen functional groups, namely hydroxyl (OH) groups, acting as negatively charged surface sites. This is confirmed by the FTIR spectra seen in **Figure 2.9**, with the broad bands at 3000 cm⁻¹ and sharp peak at 1550 cm⁻¹ corresponding to an O-H and C-O stretch respectively.

Interestingly, these peaks are not seen for the biochars produced at 800°C. This suggests that when biochar is pyrolyzed at a lower temperature with CO₂ flow gas, the oxygen groups will be in the form of hydroxyl groups which increase electrostatic interactions. The high C/O ratios also help to confirm the presence of oxygen-containing surface groups.

When pyrolyzed at higher temperatures, the biochars are found to have fewer hydroxyl groups, while also having a greater aromaticity, and more carbonyl groups (C=O) on the surface. This is evidenced by the small and broad peak around 1700 cm⁻¹ in the FTIR spectra in **Figure 2.9**. Since carbonyl groups are unable to be deprotonated and become negatively charged, they do not contribute to electrostatic interactions. Instead, they often act as EWGs when substituted to surface aromatics, due to resonance effects. This, coupled with the greater aromaticity (low H/C ratio) seen for the woody biochars pyrolyzed at 800°C compared to 500°C, is most likely responsible for the adsorption capacity for ACT, MO (under basic conditions) and IBU compared to MO (under acidic conditions). The carbonyl functional groups increase π - π EDA interactions specifically with compounds with EDGs such as ACT. The structure of MO, shown in **Figure 2.2**, has an electron-withdrawing sulfonyl group and is zwitterionic (neutral) under acidic conditions, once pH surpasses pKa of 4.5, and the structure changes and gains both (43) EDG and a negative charge (31). **Figure 2.7a-b** shows the adsorption capacity of RC800-CO₂ and DF800-CO₂ increasing with pH despite becoming negatively charged, which would result in a decrease in adsorption if electrostatic interactions were dominant, such as was seen for the adsorption trend of MO for PH800-CO₂. The low adsorption capacity for MB for DF800-CO₂ further indicates that the electrostatic interactions are not very strong compared to the π - π interactions. While MB has donating groups like ACT, the positively charged sulphide group is strongly electron-withdrawing due to inductive effects which act to overpower the weaker electron-donating resonance effects of the amide substituents.

The adsorption trends for MO by the PH800-CO₂ and MC800-CO₂ biochars were found to decrease under basic conditions, directly opposing the trends seen for the RC and DF biochars pyrolyzed at the same temperature. There was found to be a greater oxygen content for the non-woody biochars however, there were not found to be any carbonyl stretches on the FTIR spectra for the MC and PH-derived biochars pyrolyzed at either temperature. Instead, these biochars were shown to have O-H stretches in the 3000 cm⁻¹ region, and C-O-C stretches in the 100 cm⁻¹ regions. The aromatic peaks at 1600 cm⁻¹ were found to decrease with pyrolysis temperature,

though were not found to have a significant effect on adsorption mechanisms. These hydroxyl groups contribute to negatively charged surface sites, and thus the strong electrostatic interactions that were observed, while also acting as EDGs and increasing π - π EDA interactions with compounds with EWG such as MO. These adsorption differences seen between the different biomasses may be due to the different lignin compositions of the biomasses, with woody biomasses such as the softwoods used in this study being found to have higher lignin and cellulose content compared to the non-woody biomasses such as MC and PH which have a greater hemicellulose composition (40,44). The effect of the biomass on the adsorption mechanisms of the resultant biochars is explored in the next section.

2.5.3 Effect of Biomass on Adsorption Mechanisms of Biochar for Aromatic Compounds

The biomass and its composition have a large effect on the physical properties of the biochar that is produced, due to the difference in composition of lignin, cellulose, hemicellulose, and mineral content. The effect of the biomass composition on the adsorption mechanisms has yet to be explicitly shown, so to investigate the effect that the biomass had on the surface properties of the adsorption mechanisms, three biomasses were chosen as models for woody and non-woody biomasses. PW was used along with RC and DF for softwood biomasses, while SG was used along with the previously used MC and PH biomasses. Each of the biochars was pyrolyzed under the most favourable conditions determined from the previous sections, 800°C under CO₂ flow gas and the adsorption tests of the biochars were investigated and then presented in **Figure 2.10**.

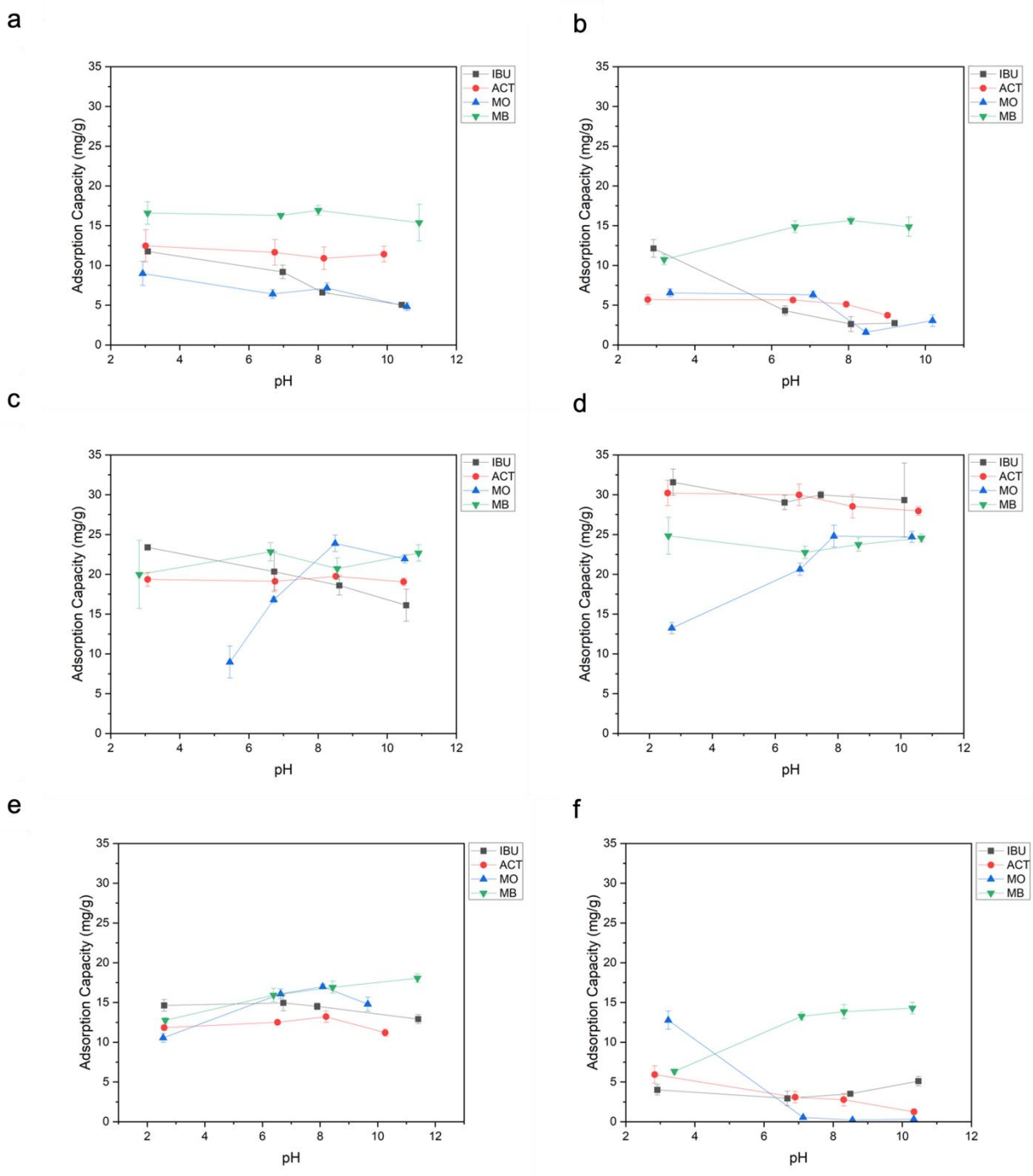


Figure 2.10 Adsorption capacities of IBU, ACT, MO, and MB with increasing pH for a) MC800-CO₂, b) SG800-CO₂, c) RC800-CO₂, d) DF800-CO₂, e) PW800-CO₂, and f) PH800-CO₂ where adsorption was performed using 50ppm of compounds and 50 mg of biochar in 15mL solutions

Aromaticity was not found to correlate with any adsorption mechanisms between the biomasses pyrolyzed at 800°C. This may be because the aromaticity was quite high and did not

vary significantly with the different biomasses; **Table 2.1** shows that the H/C ratio only ranges between 0.011-0.020, with the most aromatic being PH800-CO₂. **Table 2.1** also shows that the oxygen content for the non-woody biochars is roughly twice as great as the woody biochars. The FTIR spectra in **Figure 2.11** showed that all of the biochars have a peak in the range of 1100 cm⁻¹ and 1700 cm⁻¹, characteristic of a C-O-C stretch and aromatic C=C stretch respectively. Despite having lower oxygen content, the DF, RC, and PW were found to have a small broad peak at 1700 cm⁻¹, corresponding to a carbonyl stretch. This means that while the non-woody biochars had greater oxygen content, these oxygen groups were in the form of ether and hydroxyl groups, and the woody-derived biochars had less overall oxygen content but more carbonyl surface groups. Because carbonyl groups are not negatively charged sites like hydroxyl groups, biochars with more hydroxyl groups will be more likely to have electrostatic interactions as a dominant mechanism for adsorption. This is what was found when looking at the adsorption trends in **Figure 2.10**. The IBU adsorption for the RC800-CO₂, DF800-CO₂, and PW800-CO₂ biochars are shown to decrease slightly with pH compared to the PH800-CO₂, MC800-CO₂, and SG800-CO₂ biochars which saw a decrease in adsorption over the same pH range. This is indicative of there being stronger electrostatic interactions for the non-woody derived biochars, as greater electrostatic repulsion would explain the lower adsorption of the anionic IBU. This is corroborated by the adsorption of MB, which due to its being cationic, is absorbed at higher capacity when electrostatic interactions are stronger, as was also seen for these biochars. MB adsorption is also seen to be strong for the woody-derived biochars as well, though the stronger adsorption of the other test compounds indicates that this is most likely due to π - π EDA interactions.

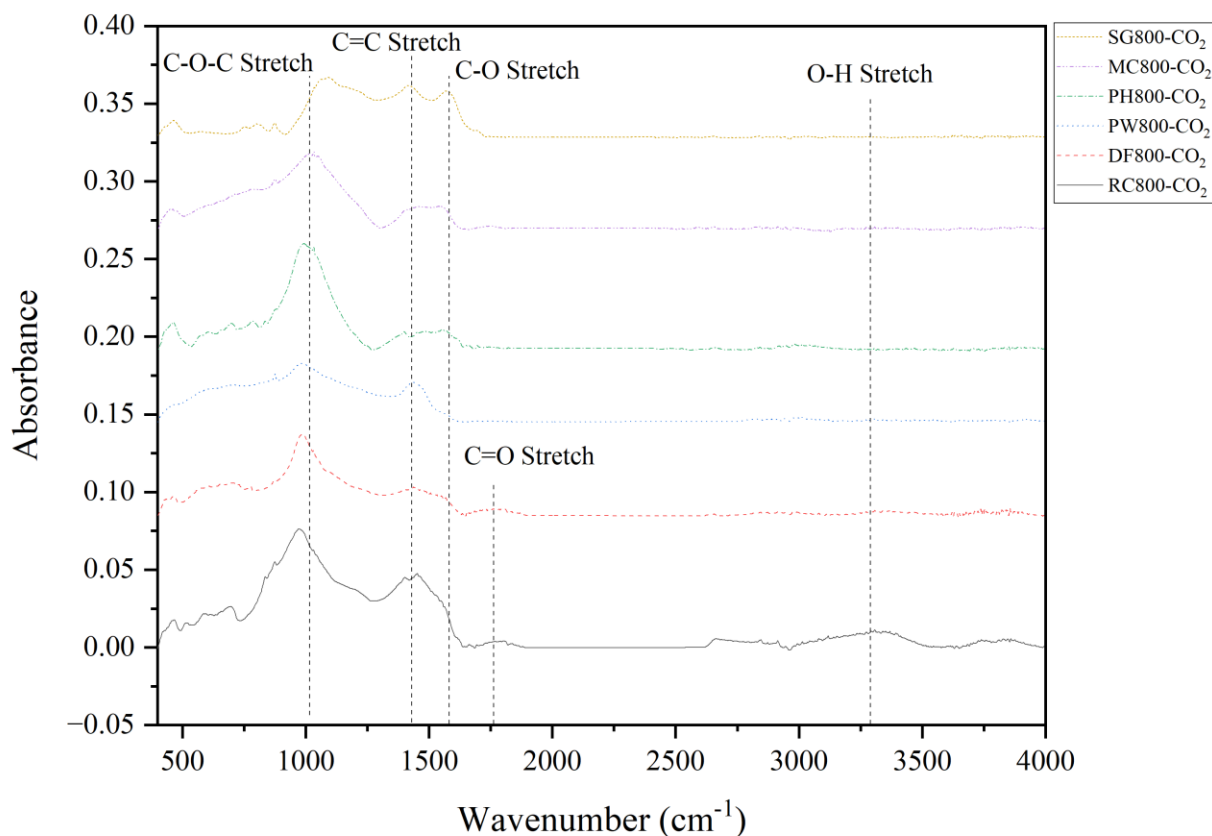


Figure 2.11 ATR-FTIR spectra of RC800-CO₂, DF800-CO₂, PW800-CO₂, PH800-CO₂, MC800-CO₂, and SG800-CO₂

Since hydroxyl and ether groups are EDGs, and carbonyl groups are electron-withdrawing, RC800-CO₂, DF800-CO₂, and PW800-CO₂ biochars are expected to have a stronger affinity to adsorb compounds with EDGs and lower adsorption for those with EWGs (45). In **Figure 2.10**, the adsorption of MO increases with pH for the woody biochars while it decreases for non-woody. As the pH of the solution rises, the structure of MO becomes negatively charged and gains an aromatic ring along with an EDGs. If the adsorption of MO is greater at a higher pH, the π - π EDA interactions with both of MO's aromatic rings must be a stronger mechanism for adsorption than electrostatics, otherwise, there would have been a decrease in adsorption. This is the case for the RC800-CO₂, DF800-CO₂, and PW800-CO₂ biochars, while the opposite is seen for the PH800-CO₂, MC800-CO₂, and SG800-CO₂ biochars. The adsorption trends for ACT also help to confirm that π - π EDA interactions are the dominant adsorption mechanism for woody biochars, as it shows strong adsorption of ACT whose structure has two donating hydroxyl and

amide groups. This is in contrast to the relatively low adsorption of ACT by PH800-CO₂, MC800-CO₂, and SG800-CO₂ biochars.

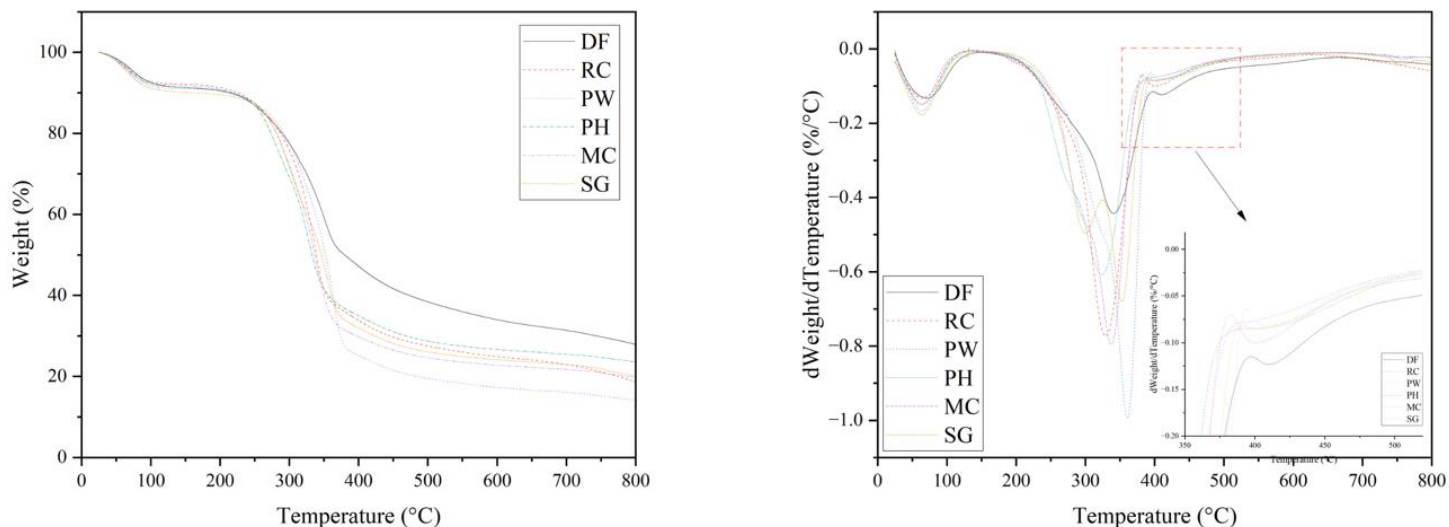
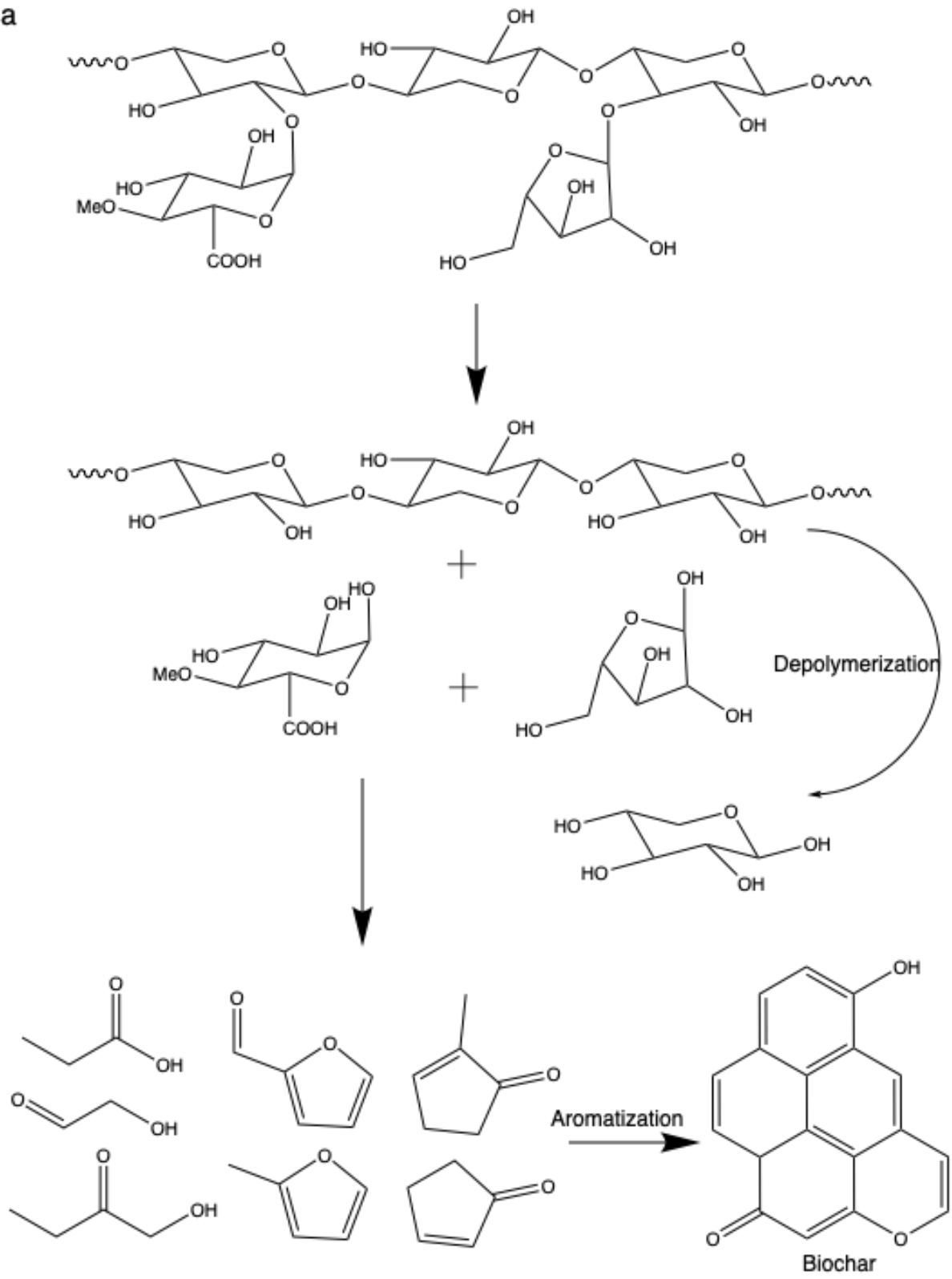


Figure 2.12 TGA and DTG curves of RC, DF, PW, PH, MC, and PH biomasses pyrolyzed under 2L/min of CO₂

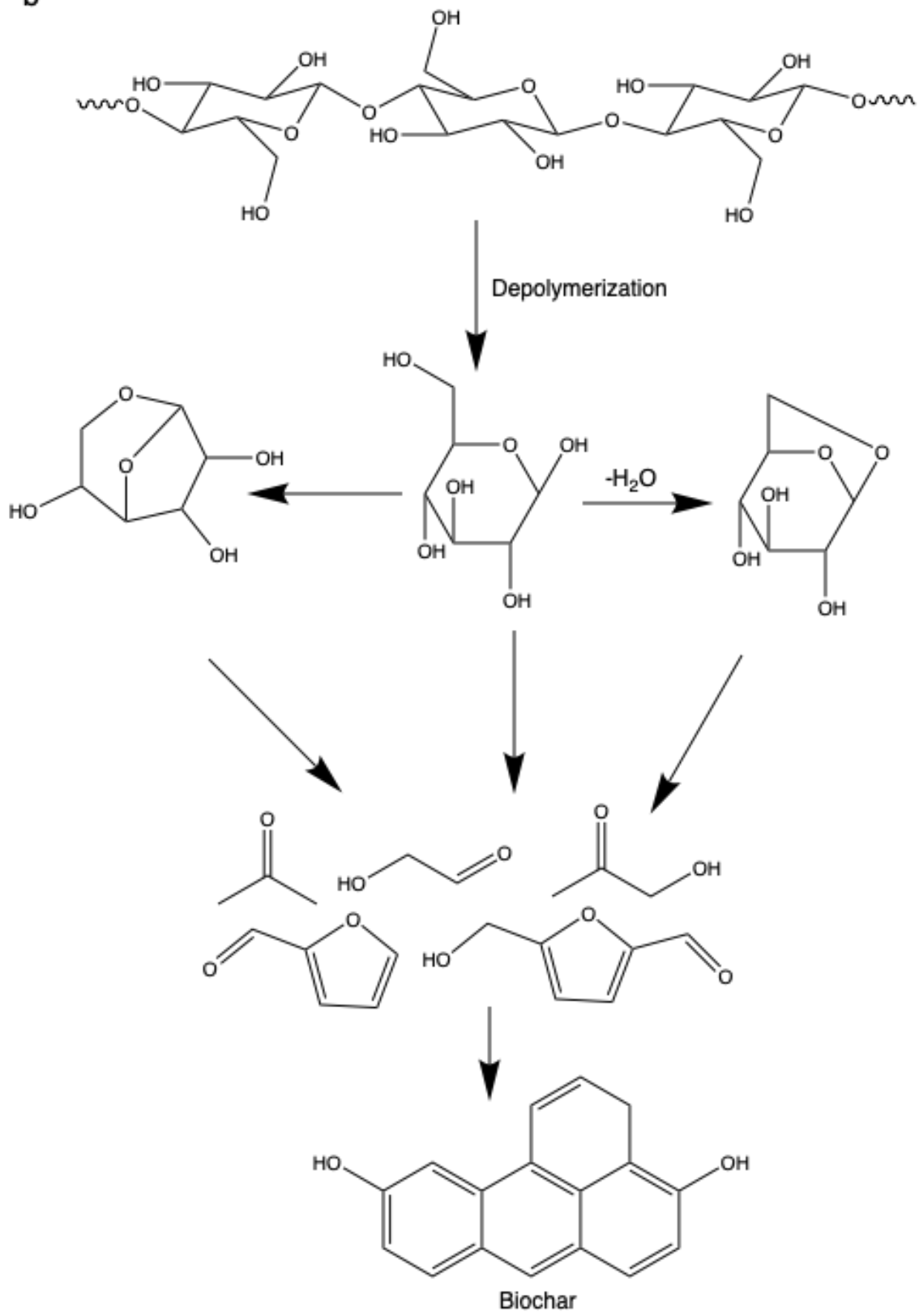
The thermogravimetric analysis of all of the biomasses investigated in this section under CO₂ is presented in **Figure 2.12**. The DTG results show three distinct peaks, representative of the sequence of pyrolysis beginning just below 300 °C, where there is first evaporation of water (46). The mechanisms for the decomposition of lignocellulosic biomass are proposed to be followed by the depolymerization of cellulose, and hemicellulose into polysaccharides and the decomposition of lignin (46,47). Hemicellulose is composed of short-chain heteropolysaccharides and has an amorphous branched structure, with an average polymerization degree of 200 (48). The proposed depolymerization of hemicellulose, as depicted in the first step of reactions in **Figure 2.13a**, is characteristically found to be broken into two segments, a slightly slower reaction where the more unstable heteropolysaccharide side chain breaks off occurring between 223°C and 250°C (48). Then, a faster depolymerization reaction followed by aromatization happens between 250°C and 333°C (48). The thermogravimetric analysis of all of the biomasses investigated in this section is presented in **Figure 2.12**. There are either two or three drops of weight % during the pyrolysis, more clearly represented as peaks in the DTG plot.

The first peak below 300°C is due primarily to the evaporation of water. This peak varies slightly on the biomass used, though is still clearly seen regardless of biomass composition. Interestingly, only the PH, MC, and SG biomasses have the double peak with a smaller peak or shoulder below 300°C, characteristic of the first pyrolytic reaction for hemicellulose (48,49). The woody biomasses do not show a peak in this region, instead only having a single strong peak between 325°C to 375°C, which is more representative of a greater cellulose content.

a



b



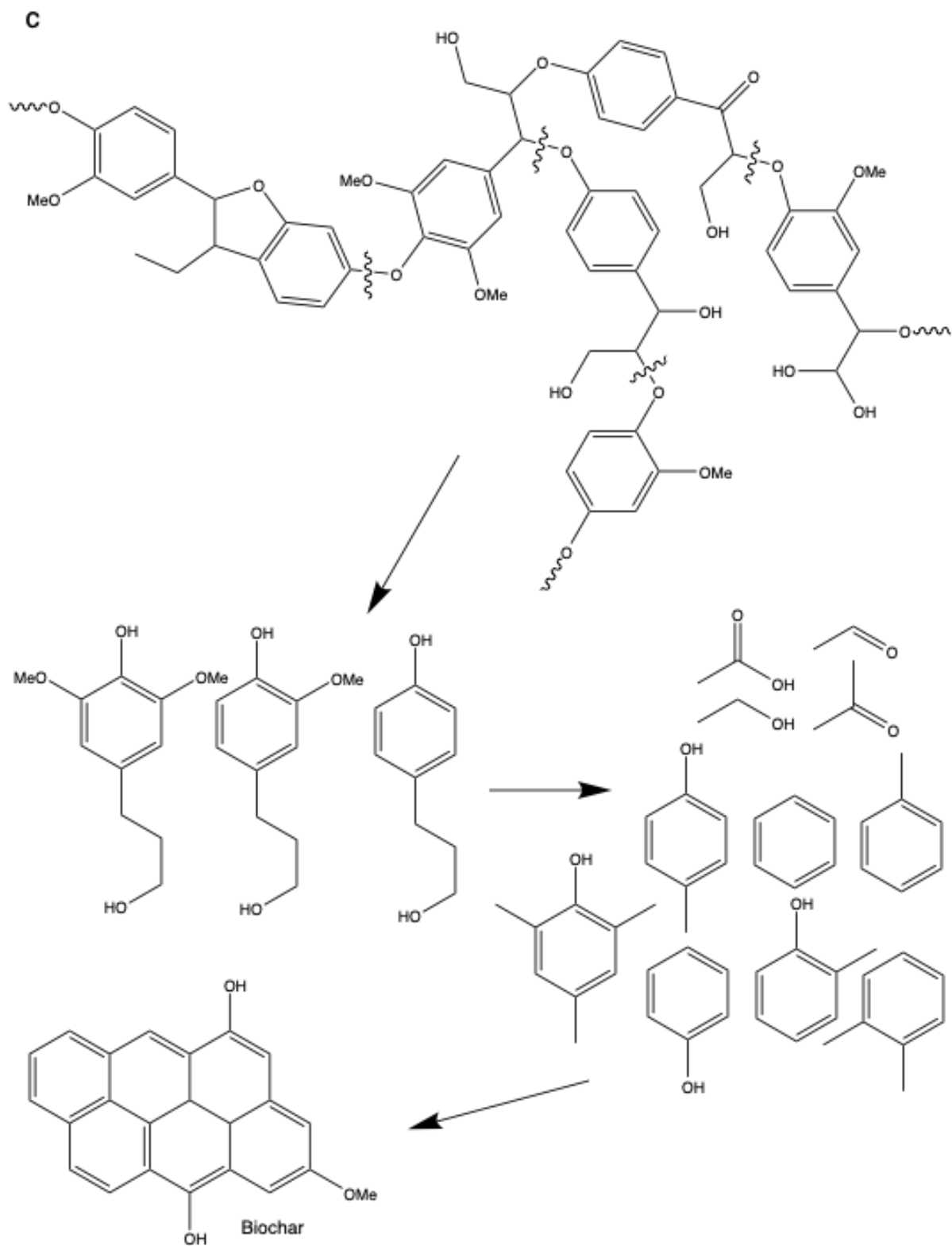


Figure 2.13 Pyrolytic decomposition mechanisms of a) hemicellulose, b) cellulose and c) lignin

Cellulose is a long linear macromolecule with a polymerization degree in the range of 7000-10 000, as opposed to hemicellulose which has a degree of polymerization of around 200 (48). Due to it having fewer side chains, cellulose has a more crystalline structure relative to hemicellulose and therefore has a slightly higher thermal stability (48). The dominant decomposition reaction for cellulose is proposed to be the breakage of the β -1, 4-glycosidic bond, shown in **Figure 2.13b**, leading to a simpler pyrolysis reaction, seen by a sharp peak in the DTG plot around 327°C to 370°C (47). When temperatures exceed 500°C, it is thought that deoxygenation reactions including decarboxylation result in the removal of oxygen-containing functional groups and the formation of benzene ring structures (47). Between the temperatures of 600°C and 800°C, dehydrogenation, demethylation, and other reactions occur to alter the aromatic ring structure into a macromolecular carbon structure (47). The composition of softwood biomasses has been reported to be between 40-50 wt% cellulose, 25-35 wt% hemicellulose, 16-33 wt% lignin, and 0.5-1 wt% ash (44). While herbaceous crops, and agricultural waste such as phragmites reeds have a lower cellulose content at around 30 wt%, and a much greater ash and hemicellulose content being around 7.5 wt% and 60 wt% respectively (40).

Lastly, lignin is a large polymer with a tridimensional phenylpropane structure, shown in **Figure 2.13**, making the structure more stable than cellulose or hemicellulose and consequently having an even greater thermal stability, decomposing at even higher temperatures around 312°C to 461°C (48). As shown in **Figure 2.13c**, the oxygen bridge bonds connecting the phenylpropane units and side chains are the weakest, and thus the first to break, forming benzene rings that readily react with other molecules to generate more stable macromolecules (50). With increasing temperature, more fused ring structures are formed, giving the biochar its largely aromatic structure (50). Lignin is also reported to have the smallest dweight/dtemperautre maximum comparatively to the other two biomasses (48). The last peak of the DTG plot in **Figure 2.12** shows a characteristically larger peak for the RC, DF, and PW biomasses, while the PH, MC, and SG biomasses had a smoother curve in this region corresponding to the decomposition of lignin, indicating a lower lignin content contributing to the surface properties of the char.

Therefore, since none of the biochars investigated in this section were found to significantly differ in their aromaticity from the elemental analysis results presented in **Table 2.1**, the varying compositions of cellulose, hemicellulose, and lignin are most influential on the surface functional groups, directly impacting the adsorption mechanisms of the resultant biochar towards aromatic compounds. The woody-derived biochars, including RC, DF, and PW all showed lower oxygen content than their non-woody counterparts PH, MC, and SG, however, were found to have more carbonyl groups, which were found to greatly increase π - π EDA interactions. This may be due to the greater lignin and cellulose relative to hemicellulose composition. This suggests that the decomposition of cellulose and lignin are to result in carbonyl groups. The non-woody biomasses produced biochars with stronger electrostatic interactions relative to π - π EDA interactions which is attributed to the presence of hydroxyl functional groups acting as negatively charged sites and EDGs, where the greater the number of groups, the relatively greater the electrostatic interactions. This therefore may be due to the greater hemicellulose content found in these biomasses, which produce chars with greater surface hydroxyl groups.

2.6 Conclusions

The proposed procedure in this study has shown promising results that allow for the interpretation of the adsorption mechanisms taking place between the biochar and organic compounds. In using the four test compounds as representative organic pollutants, the role of electrostatic and π - π interactions were able to be concluded on biochars produced by four woody (RC, DF, PW, and HL) and four non-woody (RH, MC, PH, and SG) biomasses under different pyrolysis temperatures and flow gases, N₂ and CO₂. This procedure proposes to be able to indicate what compounds biochars are best suited towards due to physical characteristics. Using this procedure, strong π - π interactions were found for biochars that had high aromaticity, while a large number of oxygen-containing functional groups had strong electrostatic integrations due to negative sites. These results helped to support the efficacy of this test procedure, while the results also alluded to the importance of oxygen-containing groups towards π - π EDA interactions. While biochars that were found to have mainly hydroxyl functional groups showed good adsorption of aromatic compounds with EWGs, biochars with carbonyl groups were found to have greater adsorption capacities for aromatic compounds with EDGs. Furthermore, it was found that there is a point where if too many negatively charged oxygen sites

are present relative to aromatic groups, the electrostatic interactions will dominate over π - π EDA and stacking interactions. After evaluating the composition of the biomasses, it was also found that the hemicellulose content contributed to greater hydroxyl groups, while greater cellulose and lignin content of the woody biochars produced chars with greater carbonyl groups. This procedure offers a novel method to evaluate these interactions and was able to be used to classify the adsorption mechanisms of the biochars produced under various pyrolysis conditions, summarized in the following **Table 2.2**. The large impact of the oxygen-containing functional groups on the surface of the biochar on the adsorption mechanisms towards aromatic compounds suggests that oxidative surface modification will have a significant impact on the adsorption properties of the biochar. To investigate this further, post-treatments to increase oxygen-containing functional groups were performed and presented in the following chapter.

Table 2.3 Summary of biochar adsorption mechanisms, physical characteristics and pyrolysis

Adsorption Mechanisms		Physical Properties	Pyrolysis Conditions		
Strong	Weak		Biomass	Pyrolysis Temp. (°C)	Pyrolysis Gas
<ul style="list-style-type: none"> π-π 	<ul style="list-style-type: none"> Electrostatic EDA with EWG 	<ul style="list-style-type: none"> High aromaticity 	Woody	>600	CO ₂
<ul style="list-style-type: none"> π-π Electrostatic 	<ul style="list-style-type: none"> EDA with EDG 	<ul style="list-style-type: none"> High aromaticity O-H groups 	Non-Woody	>600	CO ₂
<ul style="list-style-type: none"> Electrostatic EDA with EWG 	<ul style="list-style-type: none"> π-π EDA with EDG 	<ul style="list-style-type: none"> High aromaticity Ether + O-H groups 	Woody	<600	CO ₂
<ul style="list-style-type: none"> Electrostatic 	<ul style="list-style-type: none"> π-π 	<ul style="list-style-type: none"> O-H groups Low aromaticity 	Non-Woody	Any	N ₂
			Non-Woody	<600	CO ₂

	<ul style="list-style-type: none"> EDA with EWG and EDG 		Woody	<600	N ₂
<ul style="list-style-type: none"> Electrostatic EDA with EDG 	<ul style="list-style-type: none"> π-π 	<ul style="list-style-type: none"> High aromaticity C=O groups Low O-H groups 	Woody	>600	N ₂

2.7 References

1. Aggarwal, D.; Goyal, M.; Bansal, R. C. *Adsorption of Chromium by Activated Carbon from Aqueous Solution*; 1999; Vol. 37.
2. Jung, C.; Park, J.; Lim, K. H.; Park, S.; Heo, J.; Her, N.; et al. Adsorption of selected endocrine disrupting compounds and pharmaceuticals on activated biochars. *Journal of Hazardous Materials* **2013**, *263*, 702–710. doi:10.1016/j.jhazmat.2013.10.033.
3. Rivera-Utrilla, J.; Sánchez-Polo, M. Adsorption of Cr(III) on ozonised activated carbon. Importance of $C\pi$ - Cation interactions. *Water Research* **2003**, *37*(14), 3335–3340. doi:10.1016/S0043-1354(03)00177-5.
4. Vikrant, K.; Kim, K. H.; Peng, W.; Ge, S.; Sik Ok, Y. Adsorption performance of standard biochar materials against volatile organic compounds in air: A case study using benzene and methyl ethyl ketone. *Chemical Engineering Journal* **2020**, *387*. doi:10.1016/j.cej.2019.123943.
5. çaglar, E.; Donar, Y. O.; Sinag, A.; Biro Gul, I.; Bilge, S.; Aydincak, K.; et al. Adsorption of anionic and cationic dyes on biochars, produced by hydrothermal carbonization of waste biomass: Effect of surface functionalization and ionic strength. *Turkish Journal of Chemistry* **2018**, *42*(1), 86–99. doi:10.3906/kim-1704-12.
6. Zhang, C.; Zeng, G.; Huang, D.; Lai, C.; Chen, M.; Cheng, M.; et al. Biochar for environmental management: Mitigating greenhouse gas emissions, contaminant treatment, and potential negative impacts. *Chemical Engineering Journal*. Elsevier B.V. October 1, 2019, pp 902–922. doi:10.1016/j.cej.2019.05.139.
7. Ali, I. Water treatment by adsorption columns: Evaluation at ground level. *Separation and Purification Reviews* **2014**, *43*(3), 175–205. doi:10.1080/15422119.2012.748671.
8. Kolpin, D. W.; Furlong, E. T.; Meyer, M. T.; Thurman, E. M.; Zaugg, S. D.; Barber, L. B.; et al. Pharmaceuticals, hormones, and other organic wastewater contaminants in U.S. streams, 1999-2000: A national reconnaissance. *Environmental Science and Technology* **2002**, *36*(6), 1202–1211. doi:10.1021/es011055j.
9. Ternes, T. A.; Stumpf, M.; Mueller, J.; Haberer, K.; Wilken, R.-D.; Servos, M. *Behavior and Occurrence of Estrogens in Municipal Sewage Treatment Plants I. Investigations in Germany, Canada and Brazil*; 1999; Vol. 225.

10. Ahmad, M.; Rajapaksha, A. U.; Lim, J. E.; Zhang, M.; Bolan, N.; Mohan, D.; et al. Biochar as a sorbent for contaminant management in soil and water: A review. *Chemosphere*. Elsevier Ltd 2014, pp 19–33. doi:10.1016/j.chemosphere.2013.10.071.
11. Yahiaoui, I.; Aissani-Benissad, F.; Fourcade, F.; Amrane, A. Removal of tetracycline hydrochloride from water based on direct anodic oxidation (Pb/PbO₂ electrode) coupled to activated sludge culture. *Chemical Engineering Journal* **2013**, *221*, 418–425. doi:10.1016/j.cej.2013.01.091.
12. Brinzila, C. I.; Pacheco, M. J.; Ciríaco, L.; Ciobanu, R. C.; Lopes, A. Electrodegradation of tetracycline on BDD anode. *Chemical Engineering Journal* **2012**, *209*, 54–61. doi:10.1016/j.cej.2012.07.112.
13. Gómez-Pacheco, C. V.; Sánchez-Polo, M.; Rivera-Utrilla, J.; López-Peñalver, J. Tetracycline removal from waters by integrated technologies based on ozonation and biodegradation. *Chemical Engineering Journal* **2011**, *178*, 115–121. doi:10.1016/j.cej.2011.10.023.
14. Gwenzi, W.; Chaukura, N.; Noubactep, C.; Mukome, F. N. D. Biochar-based water treatment systems as a potential low-cost and sustainable technology for clean water provision. *Journal of Environmental Management*. Academic Press July 15, 2017, pp 732–749. doi:10.1016/j.jenvman.2017.03.087.
15. Bautista-Toledo, I.; Rivera-Utrilla, J.; Ferro-Garcia, M. A.; Moreno-Castilla, C. *INFLUENCE OF THE OXYGEN SURFACE COMPLEXES OF ACTIVATED CARBONS ON THE ADSORPTION OF CHROMIUM IONS FROM AQUEOUS SOLUTIONS: EFFECT OF SODIUM CHLORIDE AND HUMIC ACID*; 1994; Vol. 32.
16. Fidel, R. B.; Laird, D. A.; Spokas, K. A. Sorption of ammonium and nitrate to biochars is electrostatic and pH-dependent. *Scientific Reports* **2018**, *8*(1). doi:10.1038/s41598-018-35534-w.
17. Essandoh, M.; Kunwar, B.; Pittman, C. U.; Mohan, D.; Mlsna, T. Sorptive removal of salicylic acid and ibuprofen from aqueous solutions using pine wood fast pyrolysis biochar. *Chemical Engineering Journal* **2015**, *265*, 219–227. doi:10.1016/j.cej.2014.12.006.
18. Mukherjee, A.; Zimmerman, A. R.; Harris, W. Surface chemistry variations among a series of laboratory-produced biochars. *Geoderma* **2011**, *163*(3–4), 247–255. doi:10.1016/j.geoderma.2011.04.021.

19. Gai, X.; Wang, H.; Liu, J.; Zhai, L.; Liu, S.; Ren, T.; et al. Effects of feedstock and pyrolysis temperature on biochar adsorption of ammonium and nitrate. *PLoS ONE* **2014**, *9*(12). doi:10.1371/journal.pone.0113888.
20. Rajapaksha, A. U.; Vithanage, M.; Ahmad, M.; Seo, D. C.; Cho, J. S.; Lee, S. E.; et al. Enhanced sulfamethazine removal by steam-activated invasive plant-derived biochar. *Journal of Hazardous Materials* **2015**, *290*, 43–50. doi:10.1016/j.jhazmat.2015.02.046.
21. Blanco-Canqui, H. Biochar and Soil Physical Properties. *Soil Science Society of America Journal* **2017**, *81*(4), 687–711. doi:10.2136/sssaj2017.01.0017.
22. Zhu, D.; Hyun, S.; Pignatello, J. J.; Lee, L. S. Evidence for π - π electron donor-acceptor interactions between π -donor aromatic compounds and π -acceptor sites in soil organic matter through pH effects on sorption. *Environmental Science and Technology* **2004**, *38*(16), 4361–4368. doi:10.1021/es035379e.
23. Yuan, H.; Lu, T.; Huang, H.; Zhao, D.; Kobayashi, N.; Chen, Y. Influence of pyrolysis temperature on physical and chemical properties of biochar made from sewage sludge. *Journal of Analytical and Applied Pyrolysis* **2015**, *112*, 284–289. doi:10.1016/j.jaap.2015.01.010.
24. Zhang, X.; Gao, B.; Zheng, Y.; Hu, X.; Creamer, A. E.; Annable, M. D.; et al. Biochar for volatile organic compound (VOC) removal: Sorption performance and governing mechanisms. *Bioresource Technology* **2017**, *245*, 606–614. doi:10.1016/j.biortech.2017.09.025.
25. Kang, S.; Xing, B. Phenanthrene sorption to sequentially extracted soil humic acids and humins. *Environmental Science and Technology* **2005**, *39*(1), 134–140. doi:10.1021/es0490828.
26. Domańska, U.; Pobudkowska, A.; Pelczarska, A.; Gierycz, P. pKa and solubility of drugs in water, ethanol, and 1-octanol. In *Journal of Physical Chemistry B*; American Chemical Society, 2009; Vol. 113, pp 8941–8947. doi:10.1021/jp900468w.
27. Tang, R.; Gong, D.; Deng, Y.; Xiong, S.; Zheng, J.; Li, L.; et al. π - π stacking derived from graphene-like biochar/g-C₃N₄ with tunable band structure for photocatalytic antibiotics degradation via peroxymonosulfate activation. *Journal of Hazardous Materials* **2022**, *423*. doi:10.1016/j.jhazmat.2021.126944.
28. Domańska, U.; Pobudkowska, A.; Pelczarska, A.; Gierycz, P. pKa and solubility of drugs in water, ethanol, and 1-octanol. In *Journal of Physical Chemistry B*; American Chemical Society, 2009; Vol. 113, pp 8941–8947. doi:10.1021/jp900468w.

29. Gonzalez, G.; Sagarzazu, A.; Zoltan, T. Influence of Microstructure in Drug Release Behavior of Silica Nanocapsules. *Journal of Drug Delivery* **2013**, *2013*, 1–8. doi:10.1155/2013/803585.
30. Lorphensri, O.; Intravijit, J.; Sabatini, D. A.; Kibbey, T. C. G.; Osathaphan, K.; Saiwan, C. Sorption of acetaminophen, 17 α -ethynyl estradiol, nalidixic acid, and norfloxacin to silica, alumina, and a hydrophobic medium. *Water Research* **2006**, *40*(7), 1481–1491. doi:10.1016/j.watres.2006.02.003.
31. de Oliveira, H. P. Determination of pKa of dyes by electrical impedance spectroscopy. *Microchemical Journal* **2008**, *88*(1), 32–37. doi:10.1016/j.microc.2007.09.002.
32. Wu, L.; Liu, X.; Lv, G.; Zhu, R.; Tian, L.; Liu, M.; et al. Study on the adsorption properties of methyl orange by natural one-dimensional nano-mineral materials with different structures. *Scientific Reports* **2021**, *11*(1). doi:10.1038/s41598-021-90235-1.
33. Jiaqi, Z.; Yimin, D.; Danyang, L.; Shengyun, W.; Liling, Z.; Yi, Z. Synthesis of carboxyl-functionalized magnetic nanoparticle for the removal of methylene blue. *Colloids and Surfaces A: Physicochemical and Engineering Aspects* **2019**, *572*, 58–66. doi:10.1016/j.colsurfa.2019.03.095.
34. Arias, M.; López, E.; Nunez, A.; Rubinos, D.; Soto, B.; Barral, M. T.; et al. *ADSORPTION OF METHYLENE BLUE BY RED MUD, AN OXIDE-RICH BYPRODUCT OF BAUXITE REFINING*.
35. Lorphensri, O.; Intravijit, J.; Sabatini, D. A.; Kibbey, T. C. G.; Osathaphan, K.; Saiwan, C. Sorption of acetaminophen, 17 α -ethynyl estradiol, nalidixic acid, and norfloxacin to silica, alumina, and a hydrophobic medium. *Water Research* **2006**, *40*(7), 1481–1491. doi:10.1016/j.watres.2006.02.003.
36. de Oliveira, H. P. Determination of pKa of dyes by electrical impedance spectroscopy. *Microchemical Journal* **2008**, *88*(1), 32–37. doi:10.1016/j.microc.2007.09.002.
37. Jiaqi, Z.; Yimin, D.; Danyang, L.; Shengyun, W.; Liling, Z.; Yi, Z. Synthesis of carboxyl-functionalized magnetic nanoparticle for the removal of methylene blue. *Colloids and Surfaces A: Physicochemical and Engineering Aspects* **2019**, *572*, 58–66. doi:10.1016/j.colsurfa.2019.03.095.
38. çaglar, E.; Donar, Y. O.; Sinag, A.; Biro Gul, I.; Bilge, S.; Aydinçak, K.; et al. Adsorption of anionic and cationic dyes on biochars, produced by hydrothermal carbonization of waste

- biomass: Effect of surface functionalization and ionic strength. *Turkish Journal of Chemistry* **2018**, *42*(1), 86–99. doi:10.3906/kim-1704-12.
39. Parsa, M.; Nourani, M.; Baghdadi, M.; Hosseinzadeh, M.; Pejman, M. Biochars derived from marine macroalgae as a mesoporous by-product of hydrothermal liquefaction process: Characterization and application in wastewater treatment. *Journal of Water Process Engineering* **2019**, *32*. doi:10.1016/j.jwpe.2019.100942.
40. Dolores Gómez-Sánchez, M.; Sánchez, R.; Espinosa, E.; Rosal, A.; Rodríguez, A. Production of Cellulosic Pulp from Reed (*Phragmites australis*) to Produce Paper and Paperboard. *Bioprocess Engineering* **2017**, *1*(3), 65–68. doi:10.11648/j.be.20170103.11.
41. Guizani, C.; Escudero Sanz, F. J.; Salvador, S. Effects of CO₂ on biomass fast pyrolysis: Reaction rate, gas yields and char reactive properties. *Fuel* **2014**, *116*, 310–320. doi:10.1016/j.fuel.2013.07.101.
42. Aljaziri, J.; Gautam, R.; Alturkistani, S.; Fiene, G. M.; Tester, M.; Sarathy, S. M. On the effects of CO₂ atmosphere in the pyrolysis of *Salicornia bigelovii*. *Bioresource Technology Reports* **2022**, *17*. doi:10.1016/j.biteb.2022.100950.
43. Jiaqi, Z.; Yimin, D.; Danyang, L.; Shengyun, W.; Liling, Z.; Yi, Z. Synthesis of carboxyl-functionalized magnetic nanoparticle for the removal of methylene blue. *Colloids and Surfaces A: Physicochemical and Engineering Aspects* **2019**, *572*, 58–66. doi:10.1016/j.colsurfa.2019.03.095.
44. Pasangulapati, V.; Ramachandriya, K. D.; Kumar, A.; Wilkins, M. R.; Jones, C. L.; Huhnke, R. L. Effects of cellulose, hemicellulose and lignin on thermochemical conversion characteristics of the selected biomass. *Bioresource Technology* **2012**, *114*, 663–669. doi:10.1016/j.biortech.2012.03.036.
45. Hou, R.; Jin, L.; Yin, B. Synthesis and electron donating property of novel porphyrazines containing tetrathiacrown ether-linked tetrathiafulvalene moieties. *Inorganic Chemistry Communications* **2009**, *12*(8), 739–743. doi:10.1016/j.inoche.2009.05.036.
46. Parthasarathy, P.; Zuhara, S.; Al-Ansari, T.; McKay, G. A review on catalytic CO₂ pyrolysis of organic wastes to high-value products. *Fuel* **2023**, *335*. doi:10.1016/j.fuel.2022.127073.
47. Chen, D.; Cen, K.; Zhuang, X.; Gan, Z.; Zhou, J.; Zhang, Y.; et al. Insight into biomass pyrolysis mechanism based on cellulose, hemicellulose, and lignin: Evolution of volatiles and

kinetics, elucidation of reaction pathways, and characterization of gas, biochar and bio-oil.

Combustion and Flame **2022**, 242. doi:10.1016/j.combustflame.2022.112142.

48. Chen, D.; Cen, K.; Zhuang, X.; Gan, Z.; Zhou, J.; Zhang, Y.; et al. Insight into biomass pyrolysis mechanism based on cellulose, hemicellulose, and lignin: Evolution of volatiles and kinetics, elucidation of reaction pathways, and characterization of gas, biochar and bio-oil.

Combustion and Flame **2022**, 242. doi:10.1016/j.combustflame.2022.112142.

49. Lu, X.; Gu, X. A review on lignin pyrolysis: pyrolytic behavior, mechanism, and relevant upgrading for improving process efficiency. *Biotechnology for Biofuels and Bioproducts*.

BioMed Central Ltd December 1, 2022. doi:10.1186/s13068-022-02203-0.

50. Lu, X.; Gu, X. A review on lignin pyrolysis: pyrolytic behavior, mechanism, and relevant upgrading for improving process efficiency. *Biotechnology for Biofuels and Bioproducts*.

BioMed Central Ltd December 1, 2022. doi:10.1186/s13068-022-02203-0.

Chapter 3

3 Investigation of Effect of Physical Properties on Adsorption Mechanisms for Aqueous Organic Compounds by Biochar after Oxidative Post-Treatments using HNO₃, H₂O₂, and KOH

3.1 Statement of Authorship

The contents and some of the data of the following chapter have been submitted to be published in the Journal of Biomass and Bioenergy. This includes the adsorption results and physical characterization of the Douglas fir-derived biochars. The author of this thesis was responsible for a majority of the work herein, including experimental design and execution including biochar characterization, adsorption experimentation, data processing and analysis, as well as the writing of the manuscript and participating in the editing and review of the manuscript along with supervisors Dr. Yeung, Dr. Berruti and Dr. Klinghoffer.

3.3 Chapter Abstract

A potential application of biochars produced by pyrolysis of lignocellulosic feedstocks is as sustainable adsorbent materials for the removal of organic compounds in water, such as pharmaceuticals and dyes. The impact of biochar's physical characteristics on the adsorption mechanisms of organic aromatic compounds in the water is investigated using, Douglas fir and red cedar-derived biochars produced and treated under different conditions. CO₂ was used as pyrolysis flow gas, producing biochars with greater oxygen-containing functional groups and higher aromaticity compared to those produced under N₂ leading to greater adsorption. The pyrolysis temperature was varied between 500 and 800 °C and the resultant biochars showed greater adsorption for organic compounds when pyrolyzed at higher temperatures, attributed to greater aromaticity and surface area. The effect of different oxygen-containing groups, mainly on π - π interactions was explored by characterizing the biochar surface after three different post-pyrolysis treatments (HNO₃, H₂O₂, and KOH) and comparing the effects on the adsorption mechanisms for test compounds (ibuprofen, acetaminophen, methyl orange, and methylene blue). The results showed that increasing aromaticity and electron-donating groups, such as hydroxyl functional groups, increased π - π electron donor-acceptor interactions with compounds containing electron-withdrawing groups. The presence of electron-withdrawing carbonyl groups resulted in an increase in adsorption towards compounds with electron-donating groups.

3.4 Introduction

Water sources are facing enormous threats due to increasing contamination from a wide range of organic and aromatic pollutants raising concerns about public health (1–3). With the continuous expansion of industrial development, larger quantities of aromatic compounds are discharged into ecological surroundings due to either the lack of treatment or insufficient removal during treatments (4,5). These compounds can include antibiotics (6), dyes (7), hormones, petroleum hydrocarbons, and persistent organic matter (8) which can have highly detrimental effects on human and animal health and the whole ecosystem. Organic compounds such as dyes or antibiotics can damage the immune systems of aquatic organisms and cause human cell abnormalities due to poor biodegradability and high carcinogenicity (1,9,10). To counter this, many wastewater treatment techniques such as adsorption, photocatalytic

degradation, and advanced oxidation processes have been studied; however, adsorption is considered the most economical and effective (1,11). Among different adsorbents, biochar has recently been the focus of many publications for removing organic and aromatic compounds as it can be produced from a wide variety of sources, often repurposing waste products (1,2,12,13). Biochar has specifically been reported to be well suited to remove aromatic-based contaminants, due to its large surface area and porosity, abundant surface oxygen-containing functional groups and aromatic surface structure (2,14–16). Previous studies have investigated biochar's potential in adsorptive removal of pesticides, pharmaceuticals, polychlorinated biphenyls, steroid hormones, and dyes (13–18). The mechanisms for the adsorption of aromatics on biochar have not been fully characterized and the mechanisms may depend on the chemical and physical properties of the biochar. While the effect of pyrolysis conditions and post-treatment procedures on biochar's physical characteristics are studied extensively in the literature, their impact on adsorption mechanisms has not been reported.

Pyrolysis temperature can significantly alter the surface structure and physical properties, namely surface functional groups, of the resultant biochar (19). As the pyrolysis temperature increases, surface area and porosity increase, and functional groups gradually emerge between 100°C and 500°C and begin to volatilize at 600°C (20,21). Since the types of functional groups directly affect the adsorptive properties of biochar, investigating the effect of pyrolysis temperature on adsorption mechanisms is essential to enable the design of effective adsorbents. EDA interactions are recognized as an important type of noncovalent specific interaction involving the biochar's aromatic π -system since its oxygen-containing functional groups often exhibit electron donating or withdrawing behaviour (22,23).

Surface oxidation has been investigated in the recent literature, as it can promote the formation of functional groups on the surface and expand the surface area and pore size of the biochar (24,25). Nitric acid (HNO₃), potassium hydroxide (KOH), and hydrogen peroxide (H₂O₂) are commonly used to promote oxidation of the surface (24–26). Oxidation could have a large effect on many of the mechanisms responsible for the adsorption of organics, including electrostatic interaction, as well as π - π EDA interactions (27,28). Biochar often contains various oxygen groups, such as hydroxyl and carbonyl groups (29,30). Hydroxyl groups act as electron-donating groups, while carbonyl groups have the opposite electron-withdrawing effects, altering the adsorption mechanisms of the biochar (31).

Typically, the surface structural properties of biochars, such as surface functional groups, surface area, and pore volume/size, are correlated with the adsorption performance of aromatics without any detail regarding the specificity of the mechanisms responsible (31,32). This is because the corresponding mechanisms of biochar surface functional groups are usually complex and difficult to determine. Considering surface area, porosity, ash and mineral content, hydrophobicity, aromaticity and the many possible surface functional groups that all contribute to different adsorption mechanisms of biochars, it is difficult to determine which characteristic plays a role in which mechanisms and to what extent. This gap in the literature was addressed by comparing not only the various different properties of biochars prepared under different conditions and observing how these changes specifically effect adsorption of organic compounds, oxygen-containing functional groups were found to have the greatest influence on the adsorption mechanisms, specifically π - π electron donor-acceptor (EDA) interactions. Thus, oxidative post treatments including HNO₃, H₂O₂, and KOH chemical activation were used to mechanically add hydroxyl, and carbonyl groups, along with increasing aromaticity, in order to determine how these different groups influence the EDA interactions. This was done by comparing the adsorption characteristics of four test compounds (ibuprofen (IBU), acetaminophen (ACT), methyl orange (MO), and methylene blue (MB)) utilizing biochars produced from softwood (Douglas fir) biomass under different pyrolysis temperatures and post-surface modifications of the surface functionalities and determining the appropriate mechanism.

3.5 Materials and Methods

3.5.1 Materials

Two types of common woody biomasses were used: Red Cedar (RC), and Douglas fir (DF), which were collected from a local furniture manufacturer in London, Ontario, Canada. As well two non-woody biomasses, miscanthus (MC), and phragmites (PH) were also used which were collected near London, Ontario, Canada. Before the pyrolysis, the biomasses were pulverized using a blade grinder mill (VM 0197, Vitamix, USA) and sieved to the particle size range of 0.3-0.6 mm using standard test sieves (W.S. Tyler, USA).

The compressed N₂ and CO₂ gases were purchased from Praxair Canada Inc.

Methylene blue (MB), methyl orange (MO), ibuprofen (IBU), and acetaminophen (ACT) used as adsorbates were purchased from Sigma Aldrich, Canada.

3.5.2 Biochar Preparation and Post-Treatment Procedures

All biomasses were pyrolyzed in a tube furnace by heating at 10°C/min until 500°C or 800°C and held for 3 hours with a gas flow rate of 2 mL/min. If the flowing gas used was N₂, the biochars were referred to as DF/RC500-N₂ (for pyrolysis temperature 500°C) and DF/RC800-N₂ (for pyrolysis temperature 800°C) and if they were made using CO₂ as the flowing gas they were referred to as DF/RC500-CO₂ and DF8/RC00-CO₂.

3.5.3 HNO₃ Post Treatment

The method for the acid-treated biochars is based on the method by Ngyuen et al (33), 1 g of RC500-CO₂, DF500-CO₂, PH500-CO₂, and MC500-CO₂ were separately placed in 50 mL of 30wt% HNO₃ and left to mix at room temperature for 4 hours. The biochars were then washed with DI-water and then dried overnight at 105°C. The modified samples were referred to as RC500-CO₂-HNO₃, DF500-CO₂-HNO₃, PH500-CO₂-HNO₃, and MC500-CO₂-HNO₃.

3.5.4 H₂O₂ Post-Treatment

H₂O₂ post-treatment was based on a method that was proposed by Huff et al. (34), where treatment of RC800-CO₂, RC500-CO₂, DF800-CO₂, and DF500-CO₂ biochars was done by separately mixing 1g of each biochar with 50 mL of 9.8 M H₂O₂ at room temperature for 1 hour before being filtered through Whatman filter paper No. 1 and being washed with DI-water. The oxidized biochar is then dried at 105°C overnight and referred to as RC800-CO₂-H₂O₂, RC500-CO₂-H₂O₂, DF800-CO₂-H₂O₂, and DF500-CO₂-H₂O₂.

3.5.5 KOH Post-Treatment

KOH treatment, based on the procedure proposed by Lu et al. (35), where the RC800-CO₂, RC500-CO₂, DF800-CO₂, and DF500-CO₂ biochars were all separately placed in 100 mL of 5M KOH and left to mix for 1 hour at room temperature before being filtered through Whatman No.1 filter paper, washed with DI-water, and dried overnight at 105°C. The biochar was then activated in a tube furnace at 700°C with a ramp rate of 10°C/min for 1 hour under 2 mL/min flow of N₂. After activation, the biochars were then washed again with DI water and dried overnight at

105°C. The post-treated biochar is then referred to as RC800-CO₂-KOH, RC500-CO₂-KOH, DF800-CO₂-KOH, and DF500-CO₂-KOH.

3.5.6 Biochar Characterization Methods

3.5.6.1 Proximate and elemental analysis

The proximate analysis of the biomass samples was performed following the ASTM standard (ASTM D1762-84) using a Neytech Vulcan D-550 muffle oven. Elemental analysis of carbon, hydrogen, nitrogen, and sulphur was carried out using the model Thermo Flash EA 1112 series CHNS analyzer (Thermo Fisher Scientific, USA). Samples were combusted at 900 °C under helium with a known amount of oxygen. The oxygen content in the sample is calculated by mass difference. The elemental analysis for the RM-containing products was performed using inductively coupled plasma–mass spectrometry (ICP-MS) using an Agilent 1260 infinity HPLC connected directly to an Agilent 7700 series ICP-MS. The results were measured in triplicates with the averages being reported with standard deviations.

3.5.6.2 ATR-FTIR spectroscopy

The surface organic functional groups present in the samples were detected using Fourier Transform Infrared spectroscopy (FT-IR) using a Platinum[®] attenuated total reflectance (Pt-ATR) attachment equipped with a diamond crystal in the main box of a Bruker Tensor II spectrometer. During the analysis, the sample in powder form was scanned within the range of 400-4000 cm⁻¹ at a resolution of 4 cm⁻¹ under transmittance mode and 32 accumulations for each spectrum.

3.5.6.3 BET Surface Analysis

Samples were tested for Brunauer-Emmett-Teller (BET) with Nova 2000e Surface Area and Pore Size Analyzer (Quantachrome Instrument, Florida, US). The physisorption measurements were performed via N₂ adsorption-desorption experiments at 77.35 K. Samples were degassed at 105°C for 1 hour to remove moisture, then the temperature was increased to 300°C and maintained for at least 3 hours before each analysis.

3.5.6.4 SEM-EDX Spectroscopy

The samples were analyzed by SEM-EDX using a Hitachi SU3500 Scanning Electron Microscope (SEM) combined with an Oxford AZtec X-Max50 SDD energy dispersive X-ray (EDX) detector. EDX is a semi-quantitative technique that can detect all elements with a

minimum detection limit of approximately 0.5 wt%. EDX spectra from individual particles were analyzed using a vector-based algorithm to determine the relative abundance of 10 elements: carbon (C), sodium (Na), magnesium (Mg), aluminum (Al), silicon (Si), potassium (K), calcium (Ca), titanium (Ti), oxygen (O), and iron (Fe). A 10 kV accelerating voltage was used for these analyses. The samples were coated with a thin layer of gold to minimize charging effects.

3.5.7 Test for Adsorption Mechanisms

The adsorption mechanisms were investigated by placing 25 mg of each adsorbent sample in a 20.0 mL test tube containing a 15 mL solution of 3 mM H₃PO₄ and 100 ppm of the test compound at the desired pH. Adsorption experiments were carried out at relative pH values of 2, 6, 8, and 11. The pH was controlled with a phosphate buffer, prepared with 3 mM H₃PO₄, and the pH was adjusted by adding NaOH. Samples were agitated for 1 hour at 25 °C and filtered through Whatman No. 1 filter paper. The pH of the filtrate was determined after filtering using a pH meter (Thermo Scientific, Orion Star). The concentration of adsorbate remaining in the filtrate was determined at 220, 243, 464, and 668 nm for IBU, ACT, MO, and MB, respectively, using a UV-visible spectrophotometer (Thermo Scientific, Evolution 220). Samples were analyzed in triplicates, and their average absorbances were recorded. The adsorption capacity was defined as the amount of chemically adsorbed on the unit mass of the tested adsorbent (mg/g).

3.6 Results and Discussion

The physical properties of the biochars tested in this chapter, including surface area, proximate and elemental analysis, were performed in triplicate samples and presented in **Table 3.1**.

Table 3.1 Proximate and elemental analysis, and textural properties of biochars

Biochar	Proximate analysis (wt%)				Elemental analysis						BET analysis		
	Moisture	Volatile matter	Ash	Fixed carbon	C	H	N	O**	C/O	H/C	Surface area (m ² /g)	Average pore volume (cm ³ /g)	Average pore diameter (nm)
RC800-CO ₂	1.26 ±	44.6 ±	36.3 ±	17.9 ±	54.3 ±	0.98 ±	0.32 ±	8.1 ±	6.70 ±	0.018 ±	448	0.30	0.268

	0.1	2.6	1.2	1.5	0.9	0.3	0.15	0.8	0.01	0.002			
DF800- CO ₂	2.68	56.9	34.0	6.34	57.2	1.00	0.69	7.07	11.5	0.017	461	0.29	0.248
	±	±	±	±	±	±	±	±	±	±			
	1.2	1.5	3.1	1.4	3.8	0.2	0.04	3.8	0.2	0.003			
RC500- CO ₂	3.43	48.2	10.9	37.5	59.0	4.41	0.42	25.3	2.45	0.075	394	0.90	2.65
	±	±	±	±	±	±	±	±	±	±			
	0.07	1.3	1.1	0.4	5.8	0.2	0.09	3.9	0.3	0.008			
DF500- CO ₂	2.93	29.5	8.48	59.1	77.2	2.92	0.57	10.8	7.16	0.038	103	0.050	1.91
	±	±	±	±	±	±	±	±	±	±			
	0.1	1.4	0.6	5.5	0.6	0.2	0.1	0.6	0.1	0.0004			
RC500- CO ₂ - HNO ₃	6.63	50.8	5.04	37.6	49.6	3.39	1.45	40.0	1.27	0.068	429	0.030	0.28
	±	±	±	±	±	±	±	±	±	±			
	1.1	0.1	0.1	0.05	0.9	0.3	0.3	1.0	0.05	0.003			
DF500- CO ₂ - HNO ₃	6.26	36.9	3.24	53.6	62.3	1.58	2.06	31.6	1.96	0.025	112	0.086	3.06
	±	±	±	±	±	±	±	±	±	±			
	0.1	0.1	0.06	0.1	0.8	0.2	0.3	1.2	0.07	0.003			
PH500- CO ₂ - HNO ₃	6.29	55.3	12.1	26.4	57.9	1.36	6.64	22.5	2.59	0.024	33	0.017	0.021
	±	±	±	±	±	±	±	±	±	±			
	0.1	0.2	0.09	0.09	0.5	0.1	1.2	0.5	0.03	0.003			
MC500- CO ₂ - HNO ₃	6.81	65.1	3.63	24.5	95.3	1.56	1.43	6.43	13.55	0.016	22	0.015	0
	±	±	±	±	±	±	±	±	±	±			
	0.09	0.1	0.08	0.03	5.7	0.2	0.2	1.9	0.02	0.0003			

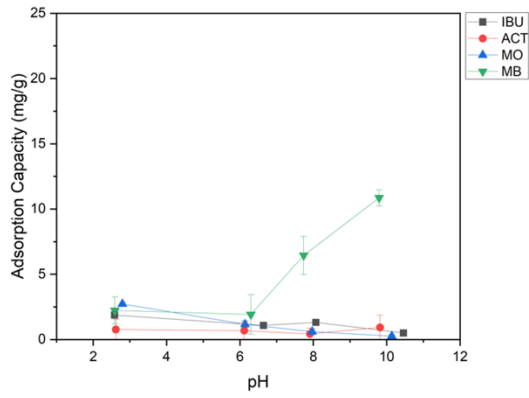
RC800- CO ₂ - H ₂ O ₂	6.42 ± 0.3	34.1 ± 2.1	12.6 ± 0.6	46.9 ± 1.8	73.7 ± 1.3	1.14 ± 0.07	1.30 ± 0.3	11.3 ± 1.1	6.54 ± 0.2	0.015 ± 0.00009	708	0.45	2.56
DF800- CO ₂ - H ₂ O ₂	7.45 ± 0.4	37.5 ± 1.5	20.1 ± 0.7	35.0 ± 1.6	64.7 ± 0.8	1.85 ± 0.2	1.28 ± 0.1	12.1 ± 0.9	5.39 ± 0.06	0.029 ± 0.003	676	0.40	2.37
RC500- CO ₂ - H ₂ O ₂	4.04 ± 0.1	56.0 ± 1.0	4.19 ± 0.09	35.8 ± 0.9	65.4 ± 0.5	2.12 ± 0.4	0.20 ± 0.2	28.4 ± 0.8	2.30 ± 0.05	0.012 ± 0.006	36	0.90	3.97
DF500 CO ₂ - H ₂ O ₂	1.17 ± 0.09	51.4 ± 0.9	5.68 ± 0.1	41.7 ± 1.1	65.4 ± 0.4	2.12 ± 0.2	0.20 ± 0.09	17.8 ± 0.3	4.11 ± 0.05	0.012 ± 0.003	20	0.91	11.5
RC800- CO ₂ - KOH	6.21 ± 0.5	47.8 ± 0.9	10.7 ± 1.5	35.3 ± 2.0	25.4 ± 1.7	0.30 ± 0.3	3.95 ± 1.8	59.7 ± 6.6	0.36 ± 0.04	0.122 ± 0.01	602	0.41	2.51
DF800- CO ₂ - KOH	5.73 ± 0.6	49.9 ± 1.0	13.4 ± 0.8	40.0 ± 1.9	65.0 ± 0.7	0.01 ± 0.001	0.05 ± 0.08	21.5 ± 0.8	1.86 ± 0.05	0.00015 ± 0.00001	606	0.36	2.35
RC500- CO ₂ - KOH	4.76 ± 0.5	41.3 ± 0.9	1.41 ± 1.2	52.5 ± 1.7	83.5 ± 0.8	1.25 ± 0.1	0*** ± 0.001	13.9 ± 0.02	5.46 ± 0.2	0.015 ± 0.002	828	0.48	2.31
DF500 CO ₂ - KOH	5.21 ± 0.4	39.3 ± 1.5	2.89 ± 2.0	12.5 ± 2.5	80.3 ± 2.9	1.23 ± 0.3	0.01 ± 0.01	15.6 ± 1.7	5.15 ± 1.8	0.015 ± 0.006	395	0.22	2.18

*Measured by difference (Total mass-C-H-N-Ash=O)

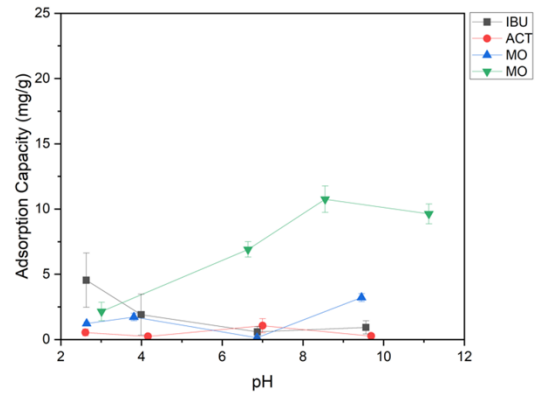
3.6.1 Effect of HNO₃ Post Treatment on Adsorption Mechanisms

The use of nitric acid for biochar post-treatment has become more common because it has been found to remove a significant amount of the mineral ash content and increase the oxygen content, both of which can improve the adsorption capacities (36,37). Thus, to understand the effect that ash content and oxygen groups can play on the adsorption mechanisms of organic compounds, RC500-CO₂, and DF500-CO₂ were treated with HNO₃, and the adsorption mechanisms were compared to those observed before treatment in **Figure 3.1**. After treatment with nitric acid, the ash content reduced from 10.1% to 5.04% and 8.48% to 3.24% for RC and DF biochars respectively, as shown in **Table 3.1**. While there is an increase in adsorption of MB at high pH after acid treatment, corresponding to an increase in electrostatic interactions, this is most likely not due to the removal of the ash content but rather to an increase in hydroxyl functional groups on the surface. This is because there is also a small increase seen for ACT, IBU and MO at any pH, after acid treatments, despite them all being anionic compounds under these conditions. Since the mineral content of the biochar creates positively charged sites within the biochar, the decrease in ash content does not correlate with the increase in the adsorption of these compounds. Hydroxyl groups, on the other hand, can contribute to electrostatic interactions as they can become deprotonated, and can also increase π - π EDA interactions which could explain the increase in adsorption capacities for the anionic compounds. This is consistent with the FTIR results reported in **Figure 3.2** where there is an increase in the broad peak at 3000 cm⁻¹ (O-H stretch) and large peaks around 1700 cm⁻¹ (C-O stretch).

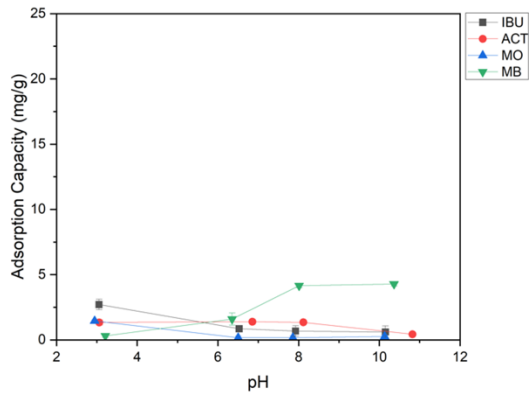
a



b



c



d

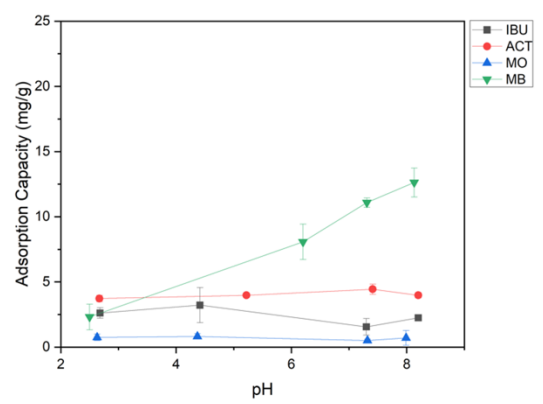


Figure 3.1 Adsorption capacities of IBU, ACT, MO, and MB with increasing pH for a) RC500-CO₂, b) RC500-CO₂-HNO₃, c) DF500-CO₂, and d) DF500-CO₂-HNO₃

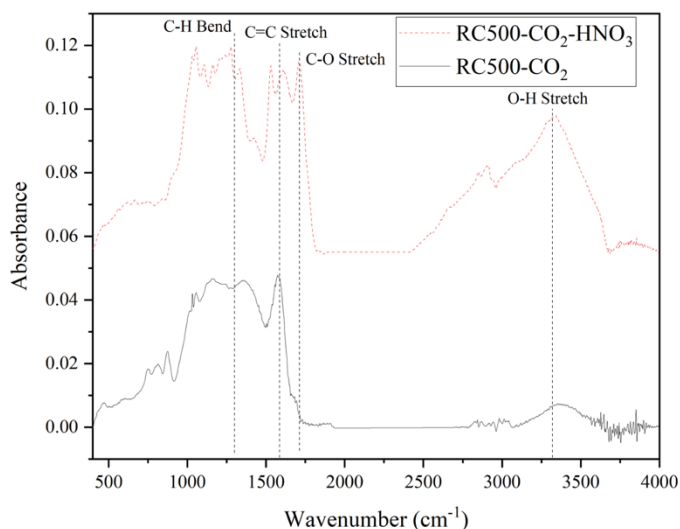
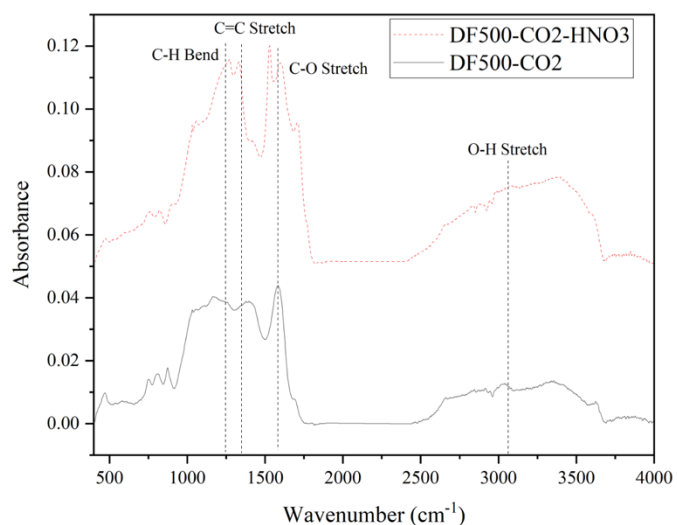
a**b**

Figure 3.2 ATR-FTIR spectra of a) RC500-CO₂, b) RC500-CO₂-HNO₃, c) DF500-CO₂, and d) DF500-CO₂-HNO₃

Thus, while the reduction of ash content by HNO₃ post-treatment was found not to have any significant effect in decreasing electrostatic interactions, this post-treatment method also added hydroxyl groups to the biochar surface which had the effect of increasing electrostatic interactions, and consequently, the adsorption of cationic compounds such as MB increased.

3.6.2 Effect of H₂O₂ Post Treatment on Adsorption Mechanisms

Post-treatment of biochar using H₂O₂ oxidation has been found to oxidize the surface, specifically through the addition of the hydroxyl functional groups on the surface (38). This has the effect of increasing the amount of negatively charged sites on the biochar surface and thus, increasing electrostatic interactions. However, the effect of hydroxyl groups may also affect π - π EDA interactions which has not been thoroughly investigated in the literature. Hydroxyl groups, when substituted to aromatic rings, have electron-donating properties due to inductive effects. To investigate the extent of the effect of additional hydroxyl groups on π - π EDA interactions, RC800-CO₂ and DF800-CO₂ biochars were treated with H₂O₂. These biochars were chosen due to their strong π - π EDA interactions, evidenced in the previous section. Hydroxyl addition was confirmed to have succeeded given the higher oxygen content shown for the post-treated biochars, presented in **Table 3.1**. Looking at the FTIR spectra for the RC800-CO₂, RC500-CO₂,

DF500-CO₂, and DF800-CO₂ compared to after H₂O₂ treatment in **Figure 3.3**, there is a noticeably larger O-H and C-O stretches visualized by the peaks at the 3000 cm⁻¹, and 1500 cm⁻¹ after treatment for each of the biochars produced at both pyrolysis temperatures. Interestingly, the results show that the surface area of the biochars that were pyrolyzed at 500°C decreased after oxidation, while the RC800-CO₂ and DF800-CO₂ saw an increase in surface area to 708 and 461 m²/g respectively. This is consistent with literature results, which reported the surface area increases more for biochars produced at higher pyrolysis temperatures (39,40). The lower oxygen content, such as for the DF800-CO₂ biochar, leaves more carbon for the H₂O₂ to react with and break down resulting in a larger porosity and greater surface area (39). The decrease in surface area after oxidation of the RC500-CO₂-H₂O₂ and DF500-CO₂-H₂O₂ is most likely due to the collapse and filling of pores as the carbon surface is broken down as it reacts. This is seen to be an even more significant breakdown than was seen by increasing the pyrolysis temperature. The SEM images and EDX spectra in **Figure 3.4** show that there is little change in the biochar's physical structure after oxidation for any of the biochars, with the biochar comprising relatively equal-sized particles before and after.

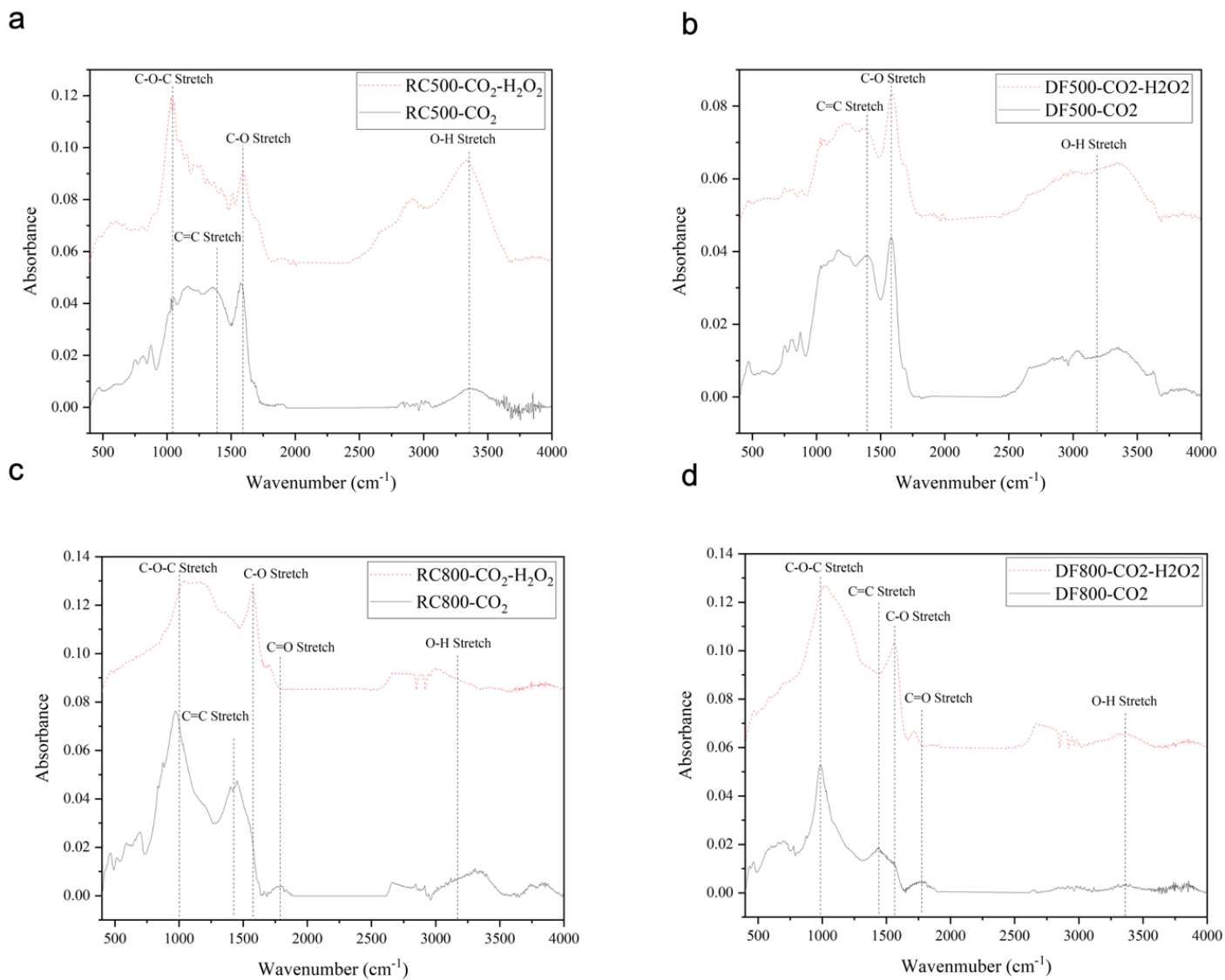
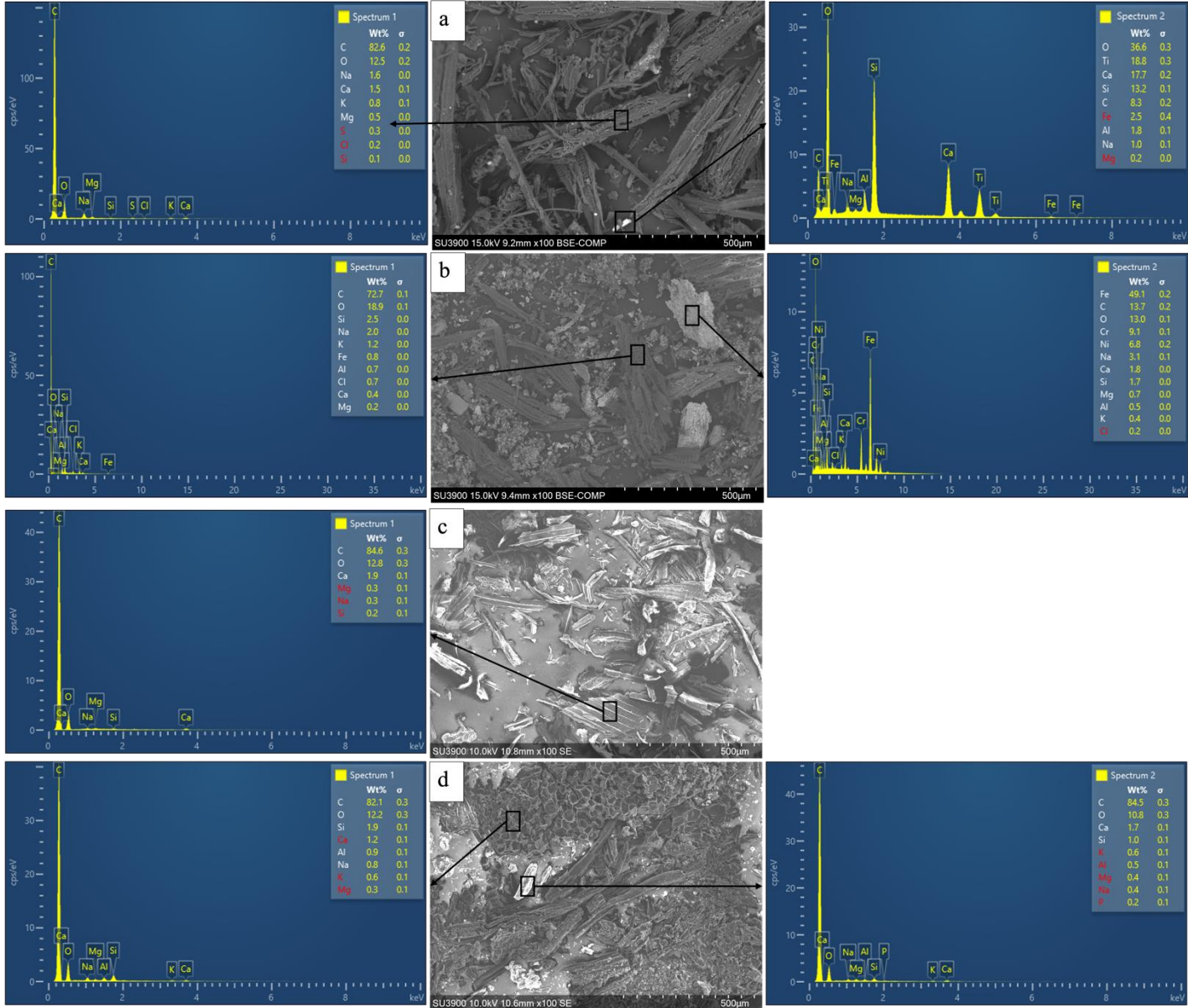


Figure 3.3 ATR-FTIR spectra of a) RC500-CO₂ and RC500-CO₂-H₂O₂, b) DF500-CO₂ and DF500-CO₂-H₂O₂, c) RC800-CO₂ and RC800-CO₂-H₂O₂, and d) DF800-CO₂, and DF800-CO₂-H₂O₂



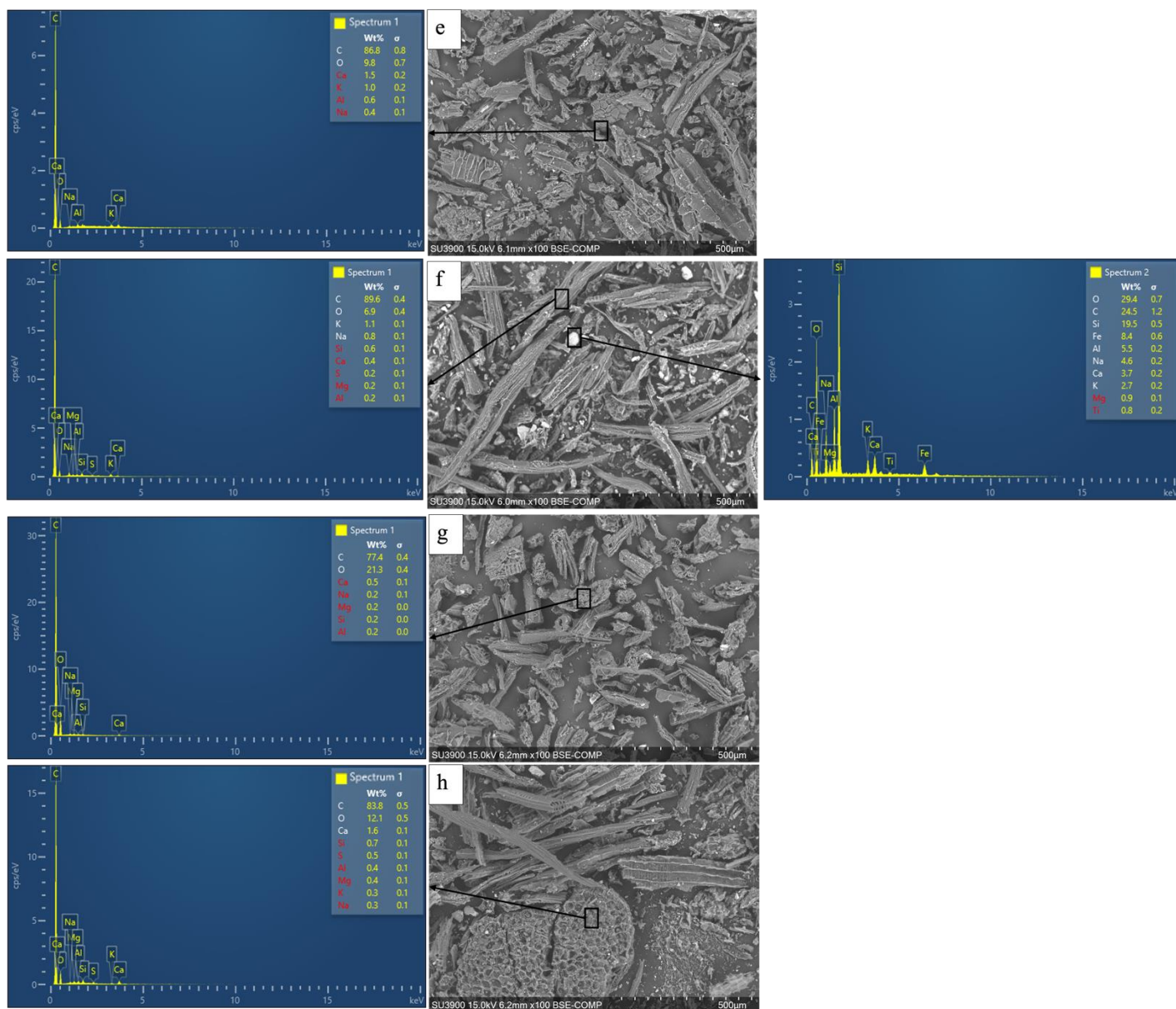
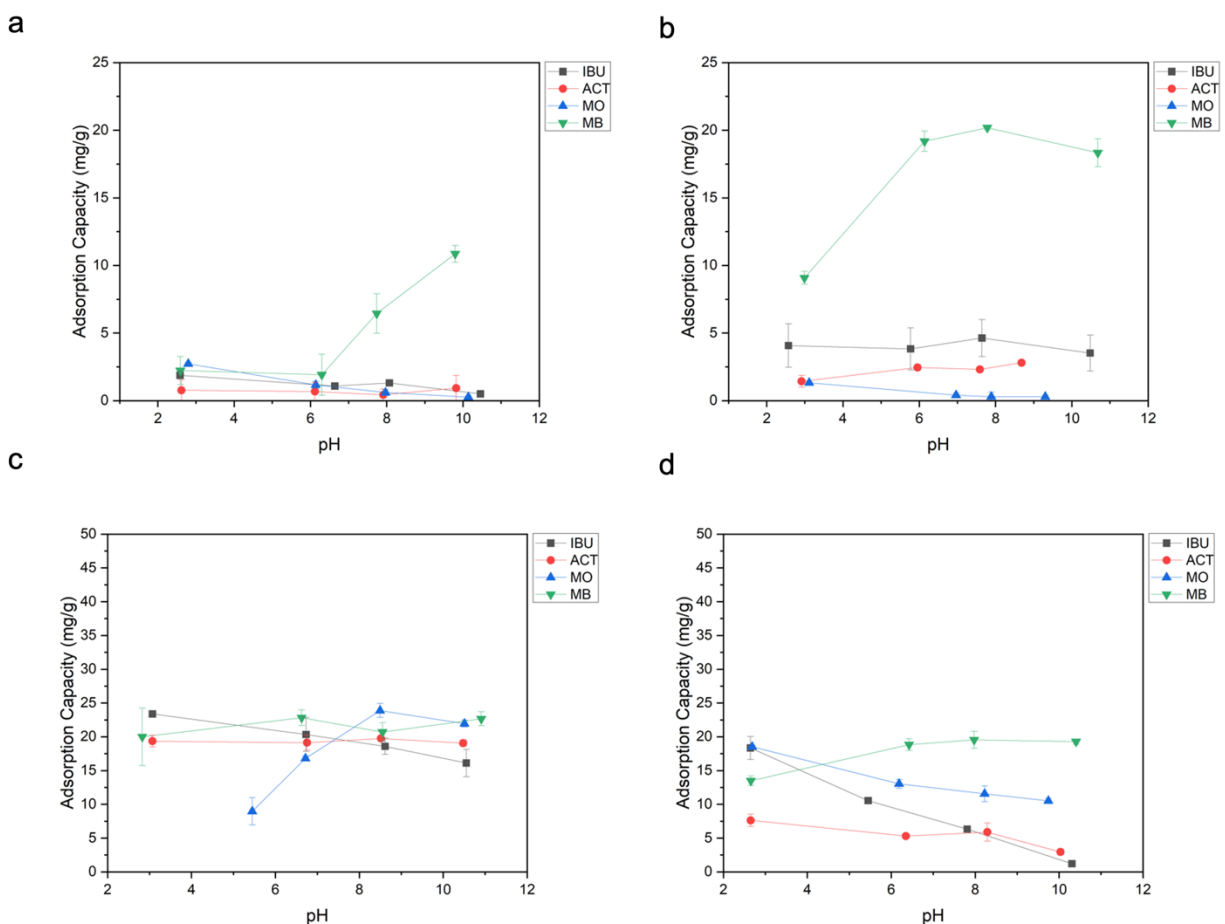


Figure 3.4 100X SEM images and EDX spectra of a) RC500-CO₂, b) RC800-CO₂, c) RC500-CO₂-H₂O₂, d) RC800-CO₂-H₂O₂, e) DF500-CO₂, f) DF800-CO₂, g) DF500-CO₂-H₂O₂, h) DF800-CO₂-H₂O₂

The adsorption results for the biochars before and after oxidation treatment are shown in **Figure 3.5**, where it is clear that there is a drastic difference in the adsorption trends of the test compounds after post-treatment for both biochars, with the order of adsorption capacities for the test compounds being nearly reversed after treatment. Both the DF and RC-derived biochars had high adsorption capacities for ACT, IBU and MO under basic conditions and had the lowest adsorption capacity for MB. After H₂O₂ treatment, both RC500-CO₂-H₂O₂, RC800-CO₂-H₂O₂, DF500-CO₂-H₂O₂, and DF800-CO₂-H₂O₂ exhibited a decrease in adsorption capacity of all test

compounds except for MB, with RC500-CO₂-H₂O₂ and DF500-CO₂-H₂O₂ only showing an increase in adsorption under basic conditions. High MB adsorption indicates that there is a strong electrostatic interaction, and the observed increase in adsorption indicates that the added hydroxyl groups do increase electrostatic interactions due to the addition of negatively charged sites. Hydroxyl groups will also become more deprotonated at higher pH, which explains the trend in increasing adsorption with pH for MB and decreasing adsorption for IBU and MO for RC800-CO₂-H₂O₂ and DF800-CO₂-H₂O₂.



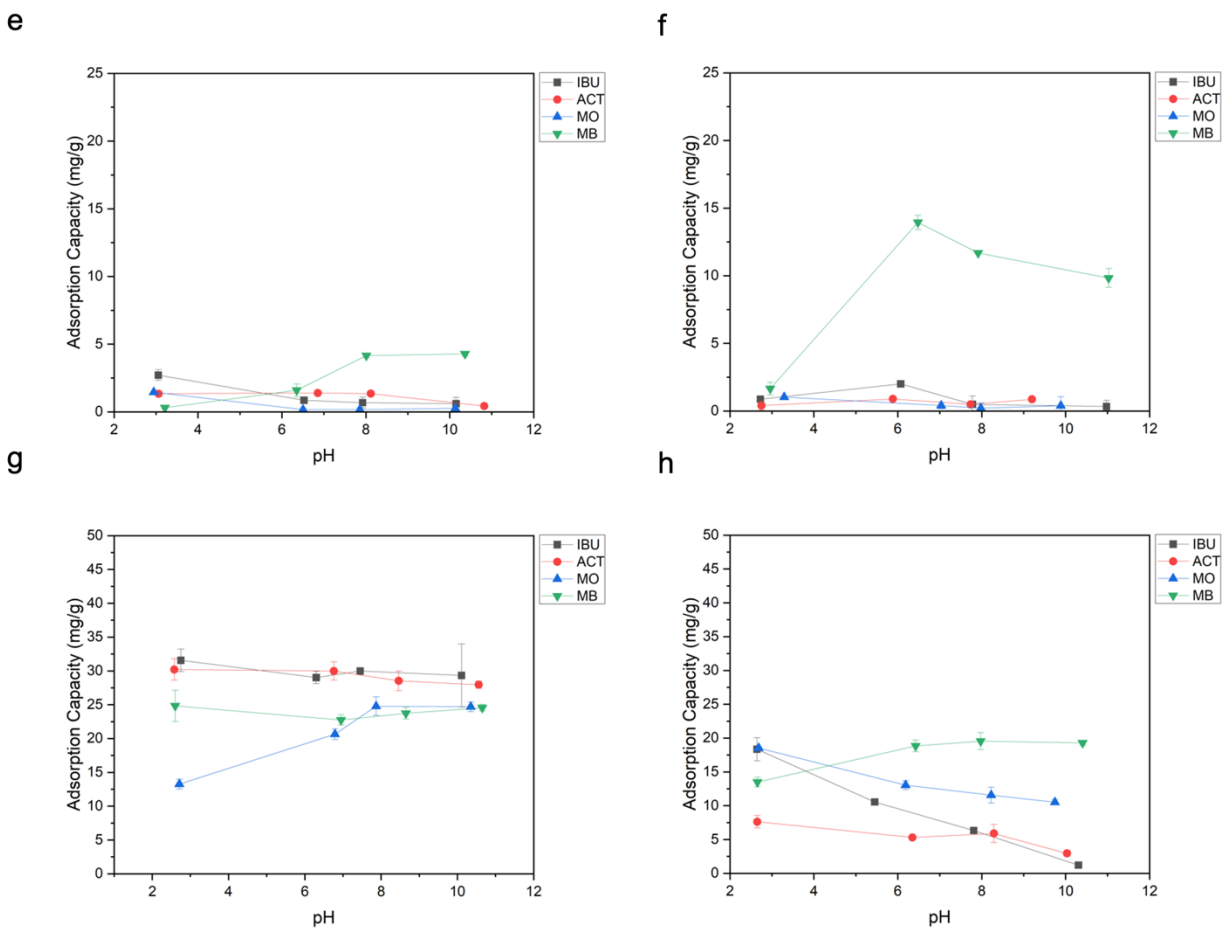


Figure 3.5 Adsorption capacities of IBU, ACT, MO, and MB with increasing pH for a) RC500-CO₂, b) RC500-CO₂-H₂O₂, c) RC800-CO₂, d) RC800-CO₂-H₂O₂, e) DF500-CO₂, f) DF500-CO₂-H₂O₂, g) DF800-CO₂, and h) DF800-CO₂-H₂O₂ where adsorption was performed using 50ppm of compounds and 50 mg of biochar in 15mL solutions

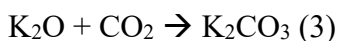
As well, the broad peak in the FTIR spectra in **Figure 3.3**, around 1700 cm⁻¹ corresponding to the C=O stretch, decreases after treatment suggesting that there is a decrease in carbonyl functional groups while hydroxyl groups increase. This means that the surface electron donating groups (OH) increased, while the electron-withdrawing groups (C=O) decreased, thus strengthening EDA interactions with compounds with EWGs. After oxidation, the woody biochar's adsorption of MO decreased with increasing pH, while the opposite was observed before H₂O₂ treatment. As explained earlier, this is due to electrostatic interactions which then overpower the π - π EDA interactions responsible for the high adsorption capacity of MO that was seen for the untreated biochars. It is important to note that for the RC800-CO₂ and DF800-CO₂, the overall π - π interactions did not decrease as the adsorption for IBU, whose structure

contains neither electron donating nor withdrawing groups, was absorbed in a similar amount by the non-treated biochars under acidic conditions. This is because IBU is neutral at acidic pH, and there able to undergo π - π stacking in the presence of hydroxyl groups or not. On the other hand, ACT was seen to have lower adsorption compared to IBU for the post-treated biochar at low pH, as opposed to equal adsorption capacities before treatment. This indicates that the increased presence of hydroxyl groups hindered the π - π EDA interactions while not affecting π - π stacking interactions. Since there is a decrease in aromaticity shown by the increase in the H/C ratio and loss of aromatic C=C stretching peak in the FTIR spectra, it is implied that the oxygen functional groups play a larger role in π -interactions than aromaticity.

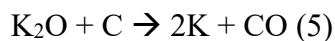
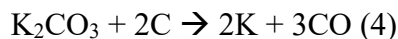
To see the effect of oxidation on biochars that have a dominant electrostatic adsorption mechanism, the RC500-CO₂, and DF500-CO₂ biochars were also treated with H₂O₂. The adsorption results are shown in **Figure 3.5** where the electrostatic interactions increase, given the significantly higher adsorption capacities of MB after post-treatment. The adsorption capacities of IBU, ACT and MO do not increase after treatment, indicating that this biochar did not see an increase in π - π EDA interactions like the biochars produced at higher temperatures. This is attributed to low aromaticity, while electrostatic interactions are due to greater hydroxyl groups.

3.6.3 Effect of KOH Post Treatment on Adsorption Mechanisms

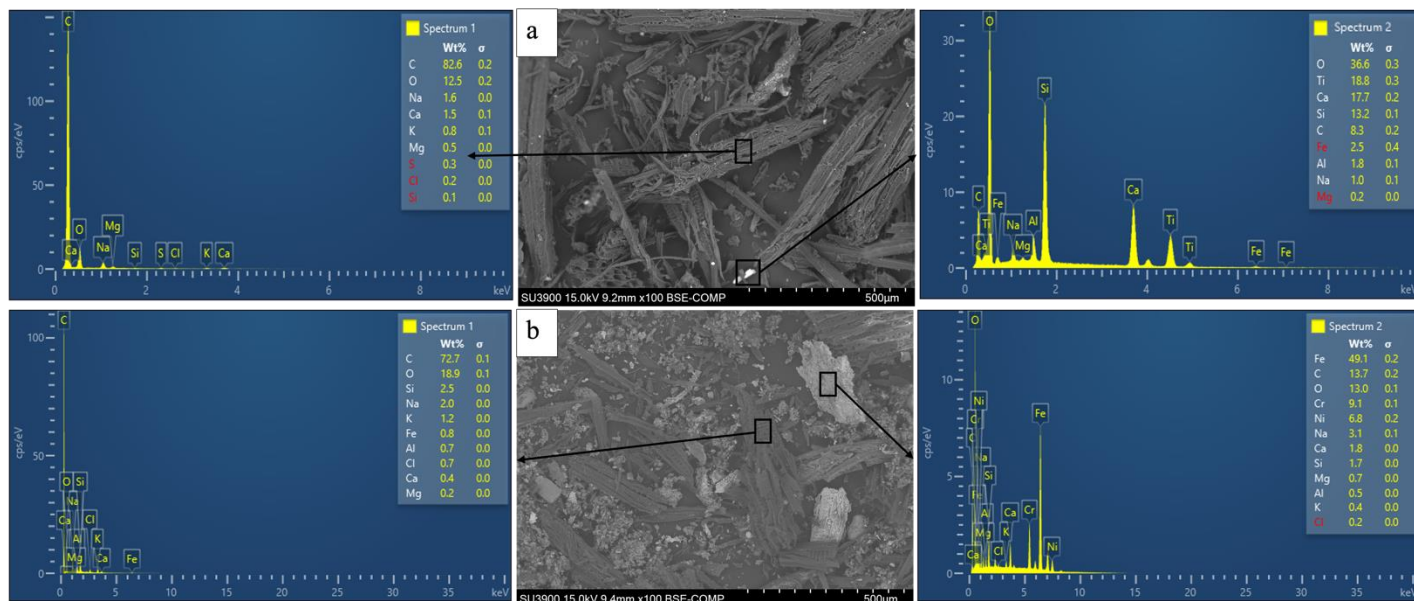
KOH chemical activation is a common post-treatment method used to increase the surface area of biochar to improve its adsorption capacity for compounds such as metals or organic compounds (41–43). The chemical activation mechanism first involves the reaction of KOH with the carbon surface of the biochar at 760°C, shown in equation (1), where K₂CO₃ and K₂O are produced along with H₂ gas (44). KOH also breaks down following the reaction displayed in equation (2), while the K₂O produced by these reactions reacts with CO₂ to produce K₂CO₃ as shown in equation (3) (44).

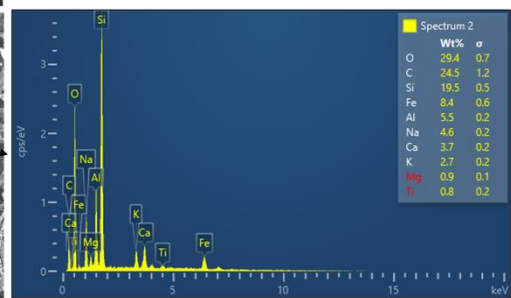
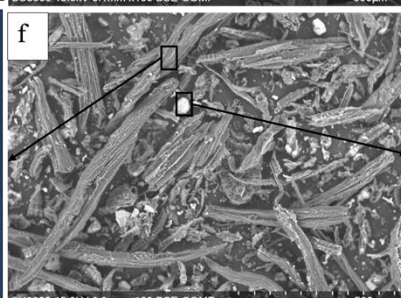
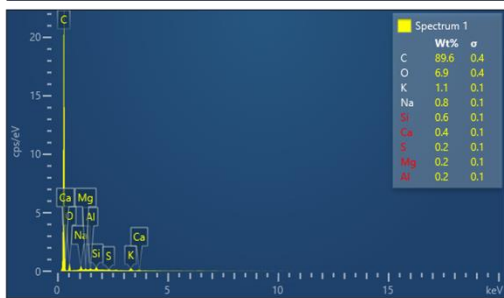
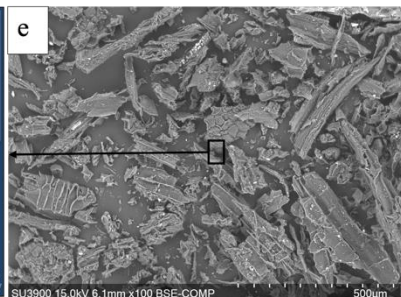
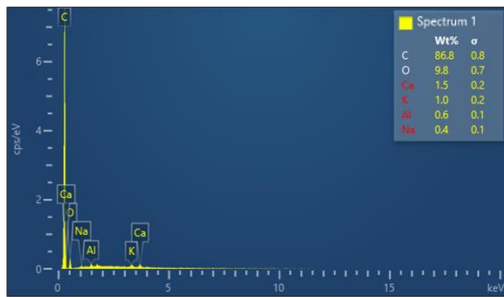
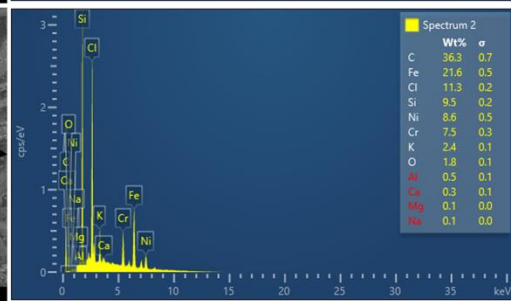
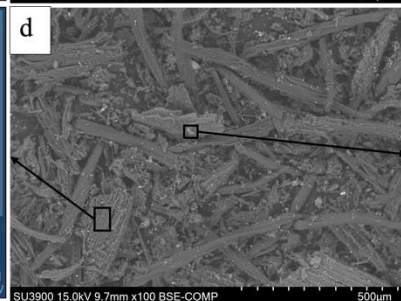
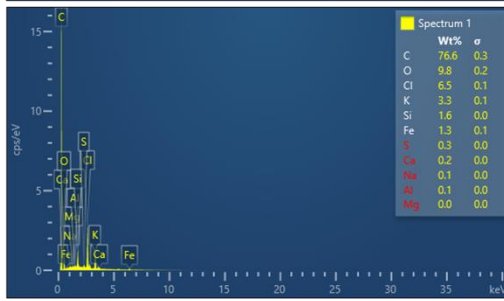
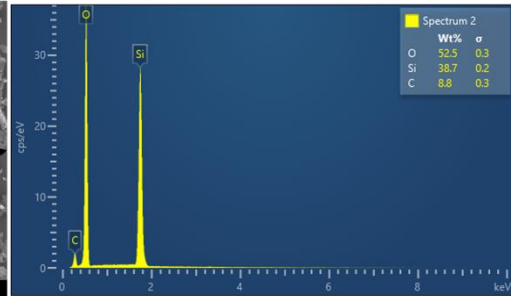
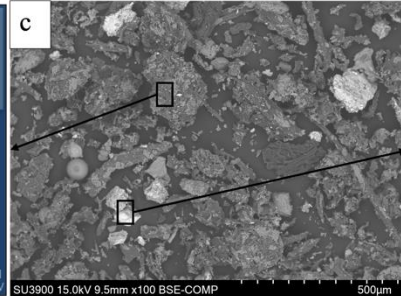
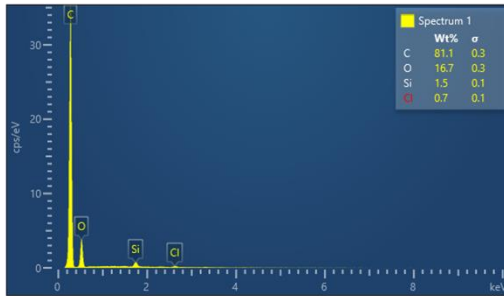


The K_2CO_3 and K_2O then further react with the carbon surface following equations (4) and (5), breaking down the carbon structure and increasing surface area and porosity (44,45).



The remaining metallic K left on the biochar structure is then washed off with DI water after activation (44). Lu et al. reported that the surface O-containing groups of the biochar play a key role in the chemical activation process as they can react with KOH during the activation process and should therefore be considered in terms of adsorption mechanisms. (46). To investigate the effect of this surface modification on the adsorption mechanisms for organic compounds, the RC and DF biochars pyrolyzed at both 500°C and 800°C were activated using KOH, and the physical characteristics are presented in **Table 3.1**. As expected, the surface area of the biochars increased significantly after activation, as did the pore diameter of the RC800-CO₂-KOH and DF800-CO₂-KOH. The SEM images and EDX spectra in **Figure 3.6** show that while the KOH activation had the effect of increasing surface area and porosity, for all biochars it was not found to significantly affect the physical characteristics, with the RC500-CO₂-KOH and DF500-CO₂-KOH biochars being made up of relatively larger particle sizes around 200µm in size compared to RC800-CO₂-KOH and DF800-CO₂-KOH biochars around 50 µm, as before post-treatment.





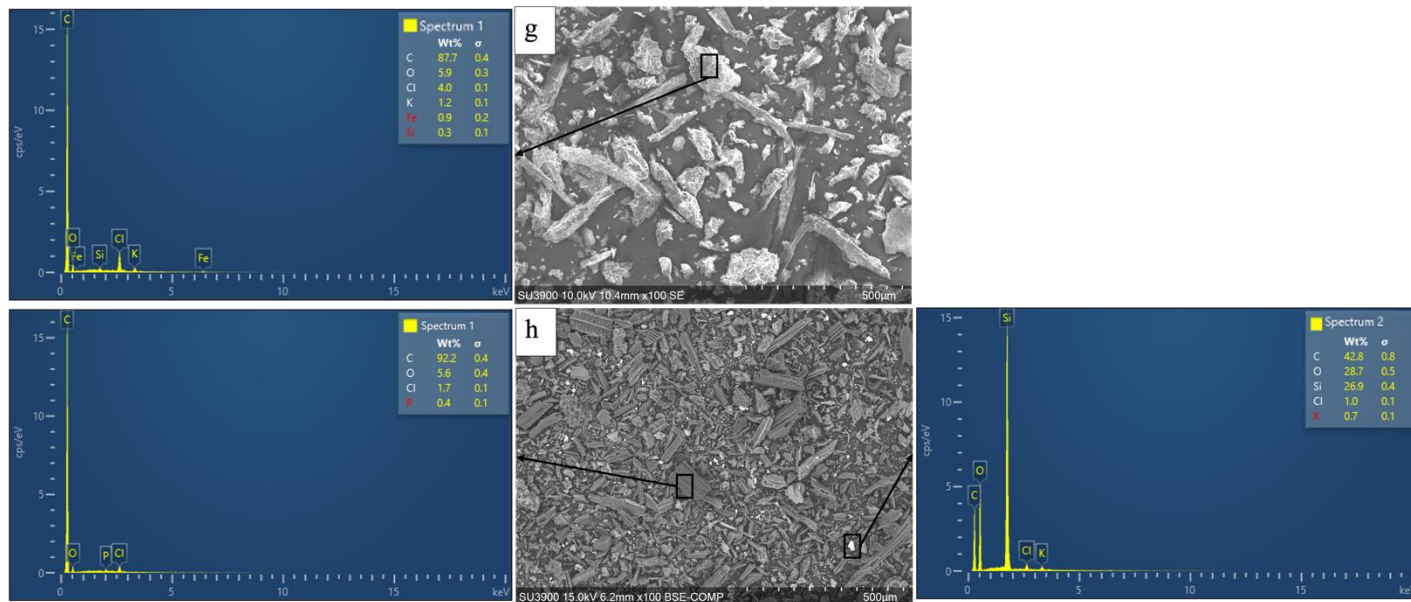


Figure 3.6 100X SEM images of a) RC500-CO₂, b) RC800-CO₂, c) RC500-CO₂-KOH d) RC800-CO₂-KOH, e) DF500-CO₂, f) DF800-CO₂, g) DF500-CO₂-KOH, h) DF800-CO₂-KOH

The oxygen content was also found to have increased after KOH treatment for both RC and DF-derived biochars at both pyrolysis temperatures. Looking at the FTIR spectra in **Figure 3.7**, it can be seen that the RC500-CO₂-KOH and DF500-CO₂-KOH biochars have a very broad peak around 1000 cm⁻¹, a smaller shoulder peak at 1500 cm⁻¹ corresponding to aromatic C=C, and C-O stretches respectively. In comparison, the spectra for the pre-activated RC500- CO₂ and DF500- CO₂ biochars had stronger aromatic C-O and O-H stretching absorbance peaks. This is indicative of a loss of surface hydroxyl groups. However, a peak was observed around 1700 cm⁻¹ which is representative of a carbonyl stretch (C=O). The RC800-CO₂-KOH and DF800-CO₂-KOH biochars both showed the same peaks as before activation, having lower intensity O-H, aromatic C=C and C-O-C stretches and a stronger C=O stretch around 1700 cm⁻¹. Therefore, KOH activation was found to increase surface porosity, aromaticity, and oxygen functionality, specifically increasing the number of carbonyl functional groups while decreasing hydroxyl groups. This allows for the investigation into the effects of carbonyl functional groups on the adsorption mechanisms of biochars towards aromatic compounds.

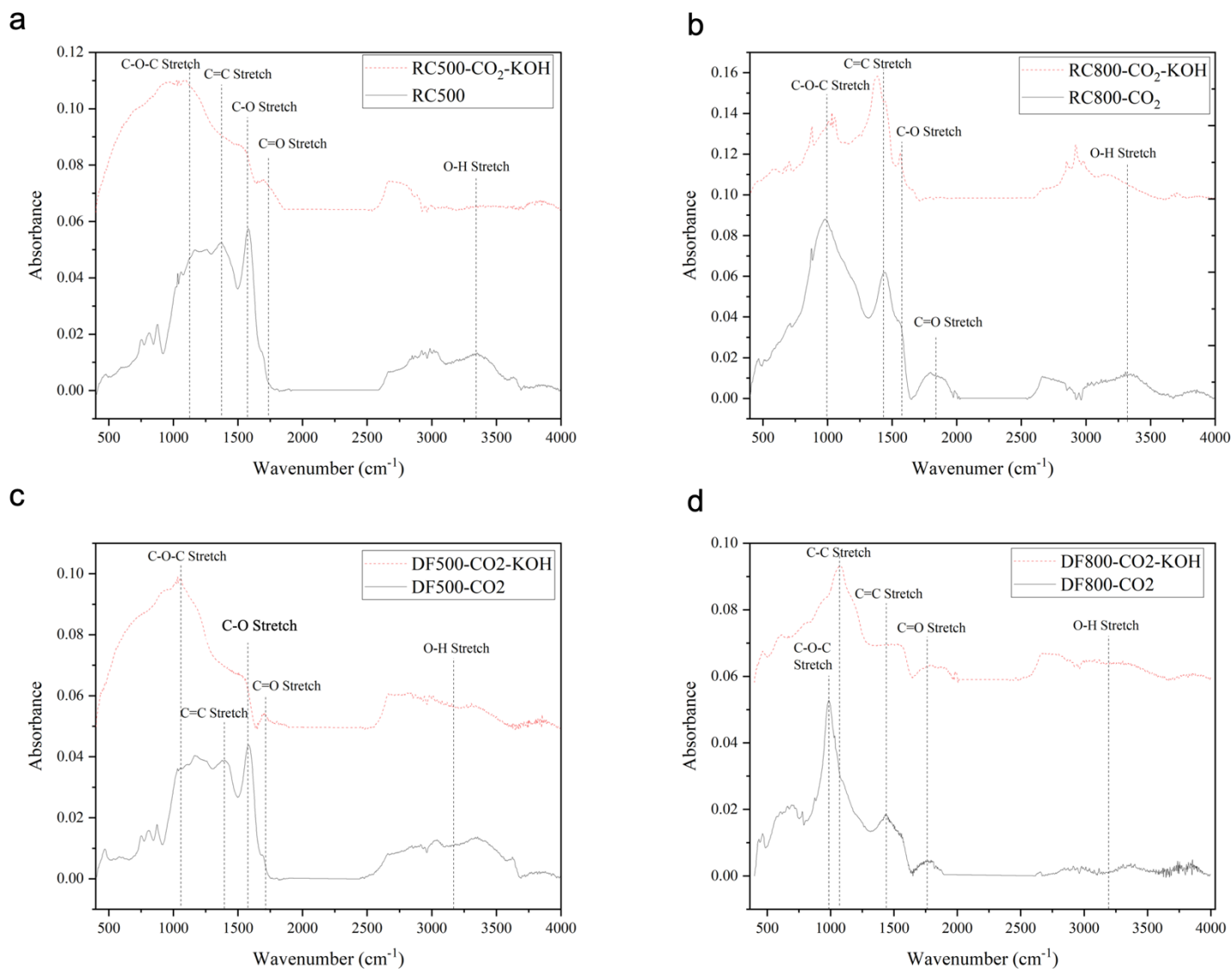


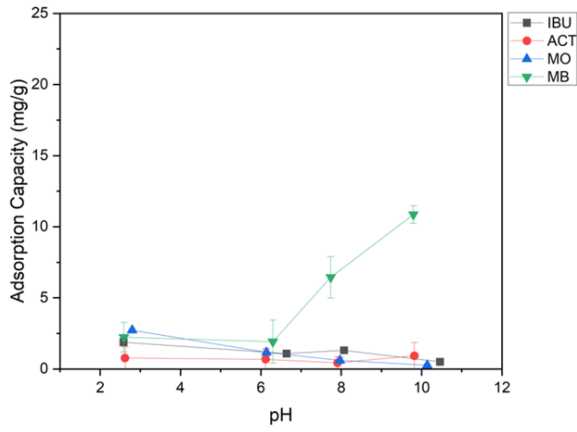
Figure 3.7 ATR-FTIR spectra of) RC500–CO₂ and RC500–CO₂–KOH, and b) RC800–CO₂, and RC800–CO₂–KOH, c) DF500–CO₂ and DF500–CO₂–KOH, and d) DF800–CO₂, and DF800–CO₂–KOH

KOH activation of the 500 and 800 biochars was able to compare the effect of carbonyl functional groups on the adsorption mechanisms for aromatic compounds, specifically for π - π EDA interactions. Both the RC800-CO₂ and DF800-CO₂ biochars became aromatic with carbonyl and hydroxyl functional groups after treatment, with the biochar pyrolyzed at lower temperature having slightly less aromaticity according to H/C ratios determined through elemental analysis. The adsorption results, presented in **Figure 3.8**, show that after the RC800-CO₂ and DF800-CO₂ are activated, the relative adsorption capacities of the test compounds are

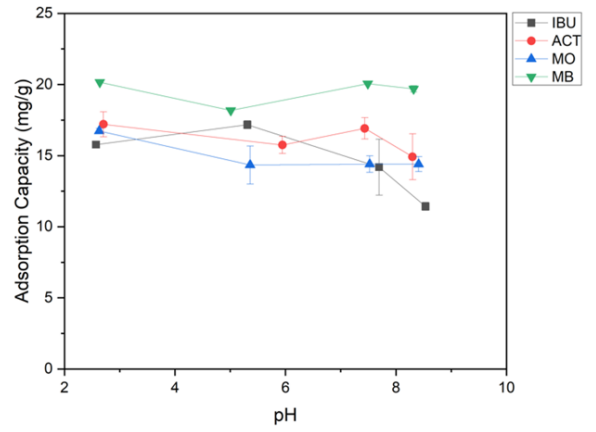
in the order of MB>MO>ACT>IBU, with the greatest difference in adsorption mechanisms before activation being the increase in adsorption of MO under acidic conditions. The lower adsorption of IBU indicates that the EDA interactions are relatively stronger, and the OH surface groups are most likely responsible for the increased adsorption of MO under these conditions. The pH effects of the adsorption of MO are also lost after activation, indicating that the π - π EDA interactions are stronger than the electrostatic repulsion between the MO and the negative sites of the biochar under basic conditions. MO is also adsorbed significantly more than IBU and ACT. Since both are aromatic compounds but neither contains electron-withdrawing groups (EWGs) like MO, it can be concluded that the increase in π - π EDA interactions is specific to compounds with EWGs. This is logical given the electron-donating properties of hydroxyl groups due to their inductive effects.

The RC500-CO₂-KOH and DF500-CO₂-KOH biochars had adsorption mechanisms similar to that of the DF800-CO₂ biochar, where there was high adsorption of all test compounds except for MO under low pH. The only difference for the KOH-treated biochars is that IBU was also seen to decrease in adsorption with pH. This is due to the electrostatic interactions repelling IBU as it becomes anionic, originating from the increase in oxygen groups and negatively charged surface sites after activation. However, MO is negatively charged under these conditions as well but has much higher adsorption, indicating that this must be due to EDA interactions as MO has both EWGs and EDGs. This therefore further confirms that the aromaticity and carbonyl groups that were found to increase after treatment, resulted in an increase in EDA interactions for biochar produced at either pyrolysis temperature.

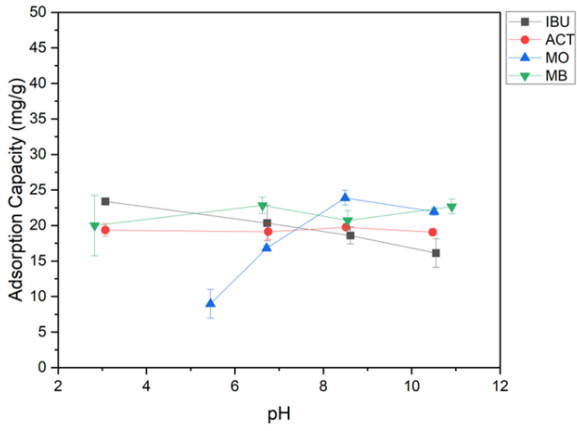
a



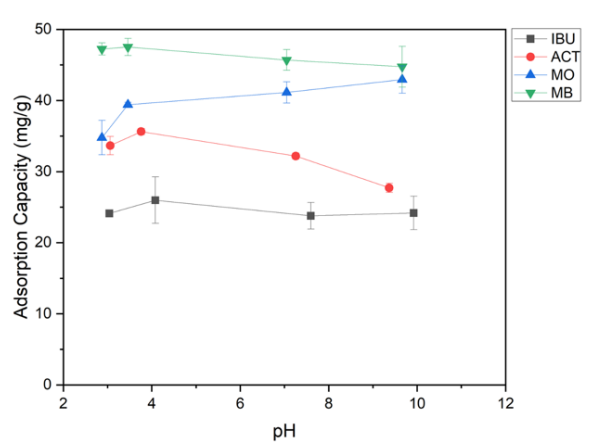
b



c



d



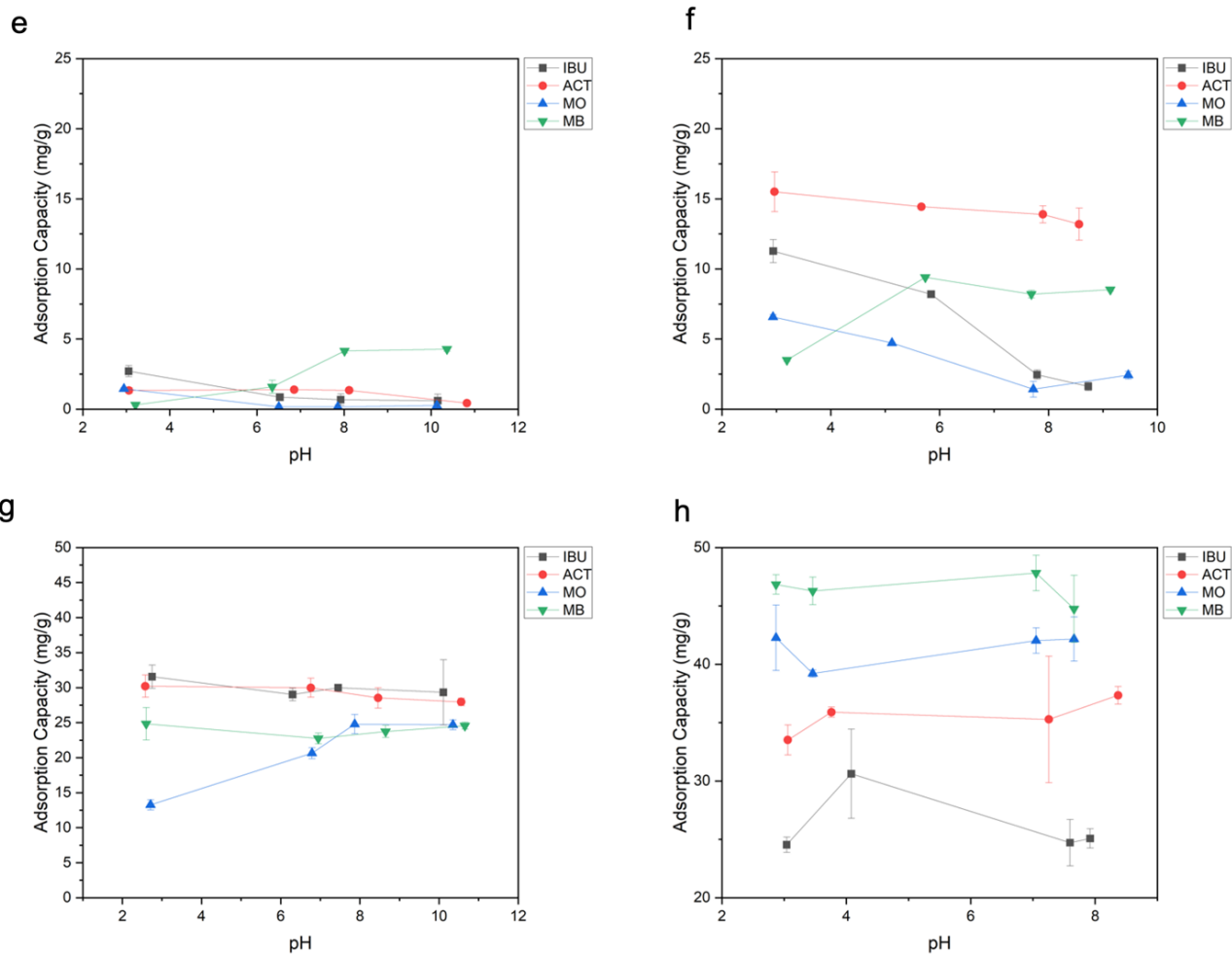


Figure 3.8 Adsorption capacities of IBU, ACT, MO, and MB with increasing pH for a) RC500-CO₂, b) RC500-CO₂-KOH c) RC800-CO₂, d) RC800-CO₂-KOH, e) DF500-CO₂, f) DF500-CO₂-KOH, g) DF800-CO₂, and h) DF800-CO₂-KOH where adsorption was performed using 50ppm of compounds and 50 mg of biochar in 15mL solutions

3.7 Conclusion

This study investigated the physical properties responsible for biochar's adsorption mechanisms towards aromatic organic compounds in water after three post-treatments, HNO₃, H₂O₂, and KOH, on different RC and DF biochars prepared under CO₂ at 800°C. The use of HNO₃ treatment introduced hydroxyl groups and decreased ash content, allowing for investigation of both properties' effects on electrostatic interactions. It was found that the adsorption mechanisms were not very dependent on the mineral content of the biochar but were influenced much more by the oxygen-containing functional groups. To further investigate the effect of hydroxyl groups, woody biochars RC500-CO₂, DF500-CO₂, RC800-CO₂, and DF800-

CO₂ were treated with H₂O₂ to increase aromaticity and OH surface groups. These tests showed that OH groups increased electrostatic interactions for all the biochars while increasing π - π EDA interactions with compounds with EWGs for the RC800-CO₂, and DF800-CO₂ biochars due to their greater aromaticity and electron-donating effects of the hydroxyl groups. The effect of carbonyl groups was investigated using chemical activation with KOH as a post-treatment, which increased C=O surface groups to the DF500-CO₂, and DF800-CO₂ biochars and increased the aromaticity of the DF500-CO₂. These results showed that increasing aromaticity had the effect of increasing the relative strength of the EDA interactions, and that carbonyl functional groups increased these interactions with compounds containing EDGs. Given this, in combination with the results presented in Chapter 2, biochar adsorption mechanisms of all of the biochars tested in this thesis, up to this point are summarized in **Table 3.2**. Because the main factors contributing to which adsorption mechanism the biochar will have toward the aromatic test compounds were the aromaticity, hydroxyl and carbonyl functional groups, there were found to only be five main combinations of these properties resulting in five main categories for biochar adsorption mechanisms. Knowing this, it will become important to understand how these different adsorption mechanisms behave in real-world settings, such as more complex mixtures of compounds that may compete for adsorption mechanisms. This is investigated further in the preceding chapter 4.

Table 3.2 Summary of biochar adsorption mechanisms, physical characteristics and pyrolysis conditions

Adsorption Mechanisms		Physical Properties	Pyrolysis Conditions			Post-Treatment
Strong	Weak		Biomass	Pyrolysis Temp. (°C)	Pyrolysis Gas	
<ul style="list-style-type: none"> π-π 	<ul style="list-style-type: none"> Electrostatic EDA with EWG 	<ul style="list-style-type: none"> High aromaticity 	Woody	>600	CO ₂	
			Non-woody	>600	CO ₂	KOH
<ul style="list-style-type: none"> π-π 			Non-Woody	>600	CO ₂	

<ul style="list-style-type: none"> • Electrostatic 	<ul style="list-style-type: none"> • EDA with EDG 	<ul style="list-style-type: none"> • High aromaticity • O-H groups 	Woody	>600	CO ₂	H ₂ O ₂
<ul style="list-style-type: none"> • Electrostatic • EDA with EWG 	<ul style="list-style-type: none"> • π-π • EDA with EDG 	<ul style="list-style-type: none"> • High aromaticity • Ether + O-H groups 	Woody	<600	CO ₂	
			Woody	>600	CO ₂	KOH
<ul style="list-style-type: none"> • Electrostatic 	<ul style="list-style-type: none"> • π-π • EDA with EWG and EDG 	<ul style="list-style-type: none"> • O-H groups • Low aromaticity 	Non-Woody	Any	N ₂	
			Non-Woody	<600	CO ₂	
			Any	<600	CO ₂	H ₂ O ₂
<ul style="list-style-type: none"> • Electrostatic • EDA with EDG 	<ul style="list-style-type: none"> • π-π 	<ul style="list-style-type: none"> • High aromaticity • C=O groups • Low O-H groups 	Woody	>600	N ₂	
			Woody	<600	CO ₂	KOH

3.8 References

1. Qu, J.; Meng, Q.; Peng, W.; Shi, J.; Dong, Z.; Li, Z.; et al. Application of functionalized biochar for adsorption of organic pollutants from environmental media: Synthesis strategies, removal mechanisms and outlook. *Journal of Cleaner Production*. Elsevier Ltd October 15, 2023. doi:10.1016/j.jclepro.2023.138690.
2. Luo, Z.; Yao, B.; Yang, X.; Wang, L.; Xu, Z.; Yan, X.; et al. Novel insights into the adsorption of organic contaminants by biochar: A review. *Chemosphere* **2022**, 287. doi:10.1016/j.chemosphere.2021.132113.
3. Yu, F.; Bai, X.; Liang, M.; Ma, J. Recent progress on metal-organic framework-derived porous carbon and its composite for pollutant adsorption from liquid phase. *Chemical Engineering Journal*. Elsevier B.V. February 1, 2021. doi:10.1016/j.cej.2020.126960.
4. Chen, Y. di; Lin, Y. C.; Ho, S. H.; Zhou, Y.; Ren, N. qi. Highly efficient adsorption of dyes by biochar derived from pigments-extracted macroalgae pyrolyzed at different temperature. *Bioresource Technology* **2018**, 259, 104–110. doi:10.1016/j.biortech.2018.02.094.
5. Redding, A. Z.; Burns, S. E.; Upson, R. T.; Anderson, E. F. Organoclay sorption of benzene as a function of total organic carbon content. *Journal of Colloid and Interface Science* **2002**, 250(1), 261–264. doi:10.1006/jcis.2001.8205.
6. Tang, Y.; Li, Y.; Zhan, L.; Wu, D.; Zhang, S.; Pang, R.; et al. Removal of emerging contaminants (bisphenol A and antibiotics) from kitchen wastewater by alkali-modified biochar. *Science of the Total Environment* **2022**, 805. doi:10.1016/j.scitotenv.2021.150158.
7. Zhou, Q.; Li, R.; Li, T.; Zhou, R.; Hou, Z.; Zhang, X. Interactions among microorganisms functionally active for electron transfer and pollutant degradation in natural environments. *Eco-Environment and Health*. Elsevier B.V. March 1, 2023, pp 3–15. doi:10.1016/j.eehl.2023.01.002.
8. Qu, J.; Zhang, B.; Tong, H.; Liu, Y.; Wang, S.; Wei, S.; et al. High-efficiency decontamination of Pb(II) and tetracycline in contaminated water using ball-milled magnetic bone derived biochar. *Journal of Cleaner Production* **2023**, 385. doi:10.1016/j.jclepro.2022.135683.
9. Huo, S.; Gao, W.; Zhou, P.; Deng, Z.; Han, Z.; Cui, X.; et al. Magnetic porous carbon composites for rapid and highly efficient degradation of organic pollutants in water. *Advanced Powder Materials* **2022**, 1(3). doi:10.1016/j.apmate.2022.01.001.

10. Gupta, M.; Savla, N.; Pandit, C.; Pandit, S.; Gupta, P. K.; Pant, M.; et al. Use of biomass-derived biochar in wastewater treatment and power production: A promising solution for a sustainable environment. *Science of the Total Environment*. Elsevier B.V. June 15, 2022. doi:10.1016/j.scitotenv.2022.153892.
11. Yao, B.; Luo, Z.; Zhi, D.; Hou, D.; Luo, L.; Du, S.; et al. Current progress in degradation and removal methods of polybrominated diphenyl ethers from water and soil: A review. *Journal of Hazardous Materials* **2021**, *403*. doi:10.1016/j.jhazmat.2020.123674.
12. Dai, Y.; Liu, Y.; Wang, Y.; Fang, W.; Chen, Y.; Sui, Y. A Practice of Conservation Tillage in the Mollisol Region in Heilongjiang Province of China: A Mini Review. *Polish Journal of Environmental Studies*. HARD Publishing Company 2023, pp 1479–1489. doi:10.15244/pjoes/156473.
13. Ai, T.; Jiang, X.; Liu, Q.; Lv, L.; Wu, H. Daptomycin adsorption on magnetic ultra-fine wood-based biochars from water: Kinetics, isotherms, and mechanism studies. *Bioresource Technology* **2019**, *273*, 8–15. doi:10.1016/j.biortech.2018.10.039.
14. Ahmed, M. J.; Hameed, B. H. Adsorption behavior of salicylic acid on biochar as derived from the thermal pyrolysis of barley straws. *Journal of Cleaner Production* **2018**, *195*, 1162–1169. doi:10.1016/j.jclepro.2018.05.257.
15. Zhang, X.; Wang, H.; He, L.; Lu, K.; Sarmah, A.; Li, J.; et al. Using biochar for remediation of soils contaminated with heavy metals and organic pollutants. *Environmental Science and Pollution Research* **2013**, *20*(12), 8472–8483. doi:10.1007/s11356-013-1659-0.
16. Liu, G.; Sheng, H.; Fu, Y.; Song, Y.; Redmile-Gordon, M.; Qiao, Y.; et al. Extracellular polymeric substances (EPS) modulate adsorption isotherms between biochar and 2,2',4,4'-tetrabromodiphenyl ether. *Chemosphere* **2019**, *214*, 176–183. doi:10.1016/j.chemosphere.2018.09.081.
17. Varjani, S.; Kumar, G.; Rene, E. R. Developments in biochar application for pesticide remediation: Current knowledge and future research directions. *Journal of Environmental Management* **2019**, *232*, 505–513. doi:10.1016/j.jenvman.2018.11.043.
18. Shen, J.; Huang, G.; An, C.; Zhao, S.; Rosendahl, S. Immobilization of tetrabromobisphenol A by pinecone-derived biochars at solid-liquid interface: Synchrotron-assisted analysis and role of inorganic fertilizer ions. *Chemical Engineering Journal* **2017**, *321*, 346–357. doi:10.1016/j.cej.2017.03.138.

19. Suliman, W.; Harsh, J. B.; Abu-Lail, N. I.; Fortuna, A. M.; Dallmeyer, I.; Garcia-Perez, M. Influence of feedstock source and pyrolysis temperature on biochar bulk and surface properties. *Biomass and Bioenergy* **2016**, *84*, 37–48. doi:10.1016/j.biombioe.2015.11.010.
20. Zhang, C.; Ho, S. H.; Chen, W. H.; Fu, Y.; Chang, J. S.; Bi, X. Oxidative torrefaction of biomass nutshells: Evaluations of energy efficiency as well as biochar transportation and storage. *Applied Energy* **2019**, *235*, 428–441. doi:10.1016/j.apenergy.2018.10.090.
21. O'Connor, D.; Peng, T.; Li, G.; Wang, S.; Duan, L.; Mulder, J.; et al. Sulfur-modified rice husk biochar: A green method for the remediation of mercury contaminated soil. *Science of the Total Environment* **2018**, *621*, 819–826. doi:10.1016/j.scitotenv.2017.11.213.
22. Kah, M.; Sigmund, G.; Xiao, F.; Hofmann, T. Sorption of ionizable and ionic organic compounds to biochar, activated carbon and other carbonaceous materials. *Water Research*. Elsevier Ltd 2017, pp 673–692. doi:10.1016/j.watres.2017.07.070.
23. Peng, H.; Pan, B.; Wu, M.; Liu, Y.; Zhang, D.; Xing, B. Adsorption of ofloxacin and norfloxacin on carbon nanotubes: Hydrophobicity- and structure-controlled process. *Journal of Hazardous Materials* **2012**, *233–234*, 89–96. doi:10.1016/j.jhazmat.2012.06.058.
24. Zhao, Z.; Zhou, W. Insight into interaction between biochar and soil minerals in changing biochar properties and adsorption capacities for sulfamethoxazole. *Environmental Pollution* **2019**, *245*, 208–217. doi:10.1016/j.envpol.2018.11.013.
25. Zheng, H.; Zhang, Q.; Liu, G.; Luo, X.; Li, F.; Zhang, Y.; et al. Characteristics and mechanisms of chlorpyrifos and chlorpyrifos-methyl adsorption onto biochars: Influence of deashing and low molecular weight organic acid (LMWOA) aging and co-existence. *Science of the Total Environment* **2019**, *657*, 953–962. doi:10.1016/j.scitotenv.2018.12.018.
26. Chunlan, L.; Shaoping, X.; Yixiong, G.; Shuqin, L.; Changhou, L. Effect of pre-carbonization of petroleum cokes on chemical activation process with KOH. *Carbon* **2005**, *43*(11), 2295–2301. doi:10.1016/j.carbon.2005.04.009.
27. Mohan, D.; Sarswat, A.; Ok, Y. S.; Pittman, C. U. Organic and inorganic contaminants removal from water with biochar, a renewable, low cost and sustainable adsorbent - A critical review. *Bioresour. Technol.* **2014**, *160*, 191–202. doi:10.1016/j.biortech.2014.01.120.
28. Pignatello, J. J.; Mitch, W. A.; Xu, W. Activity and Reactivity of Pyrogenic Carbonaceous Matter toward Organic Compounds. *Environmental Science and Technology* **2017**, *51*(16), 8893–8908. doi:10.1021/acs.est.7b01088.

29. Regkouzas, P.; Diamadopoulos, E. Adsorption of selected organic micro-pollutants on sewage sludge biochar. *Chemosphere* **2019**, *224*, 840–851. doi:10.1016/j.chemosphere.2019.02.165.
30. Li, Y.; Wang, Z.; Xie, X.; Zhu, J.; Li, R.; Qin, T. Removal of Norfloxacin from aqueous solution by clay-biochar composite prepared from potato stem and natural attapulgite. *Colloids and Surfaces A: Physicochemical and Engineering Aspects* **2017**, *514*, 126–136. doi:10.1016/j.colsurfa.2016.11.064.
31. Tan, X. F.; Zhu, S. S.; Wang, R. P.; Chen, Y. Di; Show, P. L.; Zhang, F. F.; et al. Role of biochar surface characteristics in the adsorption of aromatic compounds: Pore structure and functional groups. *Chinese Chemical Letters*. Elsevier B.V. October 1, 2021, pp 2939–2946. doi:10.1016/j.ccllet.2021.04.059.
32. Yang, X.; Wan, Y.; Zheng, Y.; He, F.; Yu, Z.; Huang, J.; et al. Surface functional groups of carbon-based adsorbents and their roles in the removal of heavy metals from aqueous solutions: A critical review. *Chemical Engineering Journal*. Elsevier B.V. June 15, 2019, pp 608–621. doi:10.1016/j.cej.2019.02.119.
33. Nguyen, D. H.; Tran, H. N.; Chao, H. P.; Lin, C. C. Effect of nitric acid oxidation on the surface of hydrochars to sorb methylene blue: An adsorption mechanism comparison. *Adsorption Science and Technology* **2019**, *37*(7–8), 607–622. doi:10.1177/0263617419867519.
34. Huff, M. D.; Lee, J. W. Biochar-surface oxygenation with hydrogen peroxide. *Journal of Environmental Management* **2016**, *165*, 17–21. doi:10.1016/j.jenvman.2015.08.046.
35. Lü, F.; Lu, X.; Li, S.; Zhang, H.; Shao, L.; He, P. Dozens-fold improvement of biochar redox properties by KOH activation. *Chemical Engineering Journal* **2022**, *429*. doi:10.1016/j.cej.2021.132203.
36. Nguyen, D. H.; Tran, H. N.; Chao, H. P.; Lin, C. C. Effect of nitric acid oxidation on the surface of hydrochars to sorb methylene blue: An adsorption mechanism comparison. *Adsorption Science and Technology* **2019**, *37*(7–8), 607–622. doi:10.1177/0263617419867519.
37. Domańska, U.; Pobudkowska, A.; Pelczarska, A.; Gierycz, P. pKa and solubility of drugs in water, ethanol, and 1-octanol. In *Journal of Physical Chemistry B*; American Chemical Society, 2009; Vol. 113, pp 8941–8947. doi:10.1021/jp900468w.
38. Zhang, Y.; Zheng, Y.; Yang, Y.; Huang, J.; Zimmerman, A. R.; Chen, H.; et al. Mechanisms and adsorption capacities of hydrogen peroxide modified ball milled biochar for the removal of

- methylene blue from aqueous solutions. *Bioresource Technology* **2021**, 337.
doi:10.1016/j.biortech.2021.125432.
39. Tan, Z.; Zhang, X.; Wang, L.; Gao, B.; Luo, J.; Fang, R.; et al. Sorption of tetracycline on H₂O₂-modified biochar derived from rape stalk. *Environmental Pollutants and Bioavailability* **2019**, 31(1), 198–207. doi:10.1080/26395940.2019.1607779.
40. Zuo, X. J.; Liu, Z.; Chen, M. D. Effect of H₂O₂ concentrations on copper removal using the modified hydrothermal biochar. *Bioresource Technology* **2016**, 207, 262–267.
doi:10.1016/j.biortech.2016.02.032.
41. Fan, Q.; Sun, J.; Chu, L.; Cui, L.; Quan, G.; Yan, J.; et al. Effects of chemical oxidation on surface oxygen-containing functional groups and adsorption behavior of biochar. *Chemosphere* **2018**, 207, 33–40. doi:10.1016/j.chemosphere.2018.05.044.
42. Kaser, N.; Augoustides, V.; Kolar, P.; Hall, S. G.; Vicente, B. Effect of Surface Modification by Oxygen-Enriched Chemicals on the Surface Properties of Pine Bark Biochars. *Processes* **2022**, 10(10). doi:10.3390/pr10102136.
43. Huang, H.; Tang, J.; Gao, K.; He, R.; Zhao, H.; Werner, D. Characterization of KOH modified biochars from different pyrolysis temperatures and enhanced adsorption of antibiotics. *RSC Advances* **2017**, 7(24), 14640–14648. doi:10.1039/c6ra27881g.
44. Li, P.; Wan, K.; Chen, H.; Zheng, F.; Zhang, Z.; Niu, B.; et al. Value-Added Products from Catalytic Pyrolysis of Lignocellulosic Biomass and Waste Plastics over Biochar-Based Catalyst: A State-of-the-Art Review. *Catalysts*. MDPI September 1, 2022. doi:10.3390/catal12091067.
45. Lu, X.; Gu, X. A review on lignin pyrolysis: pyrolytic behavior, mechanism, and relevant upgrading for improving process efficiency. *Biotechnology for Biofuels and Bioproducts*. BioMed Central Ltd December 1, 2022. doi:10.1186/s13068-022-02203-0.
46. Huang, H.; Tang, J.; Gao, K.; He, R.; Zhao, H.; Werner, D. Characterization of KOH modified biochars from different pyrolysis temperatures and enhanced adsorption of antibiotics. *RSC Advances* **2017**, 7(24), 14640–14648. doi:10.1039/c6ra27881g.

Chapter 4

4 Competitive Adsorption of Acetaminophen, Methyl Orange and Methylene Blue by Five Biochars with Different Adsorption Mechanisms

4.1 Statement of Authorship

The contents and some of the data of the following chapter have been submitted to be published in the journal, *Chemosphere*. The author of this thesis was responsible for a majority of the work herein, including experimental design and execution including biochar characterization, adsorption experimentation, data processing and analysis, as well as the writing of the manuscript and participating in the editing and review of the manuscript along with supervisors Dr. Yeung, Dr. Berruti and Dr. Klinghoffer.

4.3 Chapter Abstract

This study investigates the adsorption of methyl orange (MO), methylene blue (MB), and acetaminophen (ACT) using biochars produced from Douglas fir and Miscanthus at different temperatures and with different post-pyrolysis treatments that added surface functional groups. Compounds were adsorbed separately and in mixtures to examine the competitive nature of the adsorption of these compounds. MO is known to interact with MB and ACT, while MB and ACT are not likely to interact due to both having electron-donating groups. When comparing the biochar adsorption capacities for these compounds when alone and mixed, biochars with both hydroxyl and carbonyl surface functional groups had higher adsorption capacities for the tested compounds when they were in mixed solutions. Biochars with only hydroxyl groups exhibited competing adsorption mechanisms and poorer adsorption capacities of aromatic compounds in complex solutions. This provides an understanding of how competing adsorption mechanisms of aromatic compounds by biochars vary depending on the dominant adsorption mechanisms of the biochar, which will allow for more effective real-world applications for water purification in the future.

4.4 Introduction

Rising environmental and health concerns due to water contamination from organic pollutants due to industrial and agricultural wastes are driving research into sustainable methods of water treatment (1,2). Organic dyes, antibiotics, petroleum hydrocarbons, and persistent organic matter including various pharmaceuticals are all examples of common contaminants found in wastewater for which adsorption has proven to be the most effective and sustainable method for water treatment (2–5). There exist different adsorbents that have been investigated in the past including activated carbon, zeolite, silica gel, modified chitosan and carbon, however, biochar has the advantage of both economic feasibility and sustainability (6–10). Biochar is a low-cost carbonaceous by-product of the pyrolysis of waste biomass which has been utilized in a wide variety of applications including separation, carbon sequestration, energy storage/conversion and water filtration (1,10–13). Biochar is increasingly being considered for use in adsorption applications due to its unique physicochemical properties including high microporous volumes, high aromaticity, abundant surface oxygen-containing functional groups, huge specific surface area (SSA) as well as low cost (1,14–18). In particular, there has been a large amount of recent research into the adsorption of organic compounds by biochar (19–21).

However, many of the existing studies have only looked at the adsorption of individual organic species, while pollutants in the environment exist in the presence of other species (22,23).

Limiting adsorption studies only to individual compounds provides an incomplete understanding of the biochar's potential for the removal of organic compounds in a multispecies/multi-component system. The competitive adsorption under multispecies systems has received very little attention. This study provides insight into the sorption of organic compounds in multicomponent solutions, providing insights into how the adsorption mechanisms may differ under these complex circumstances. Some studies have been done on the competitive adsorption of metals, however, the competitive adsorption of complex mixtures of organic compounds remains sparse (24–26). Of the few studies, there were mainly antagonistic effects observed whereby compounds compete for adsorption sites. However, there is little investigation into the effects of intermolecular interactions between compounds, and how these are affected by the adsorption mechanisms of the biochar (27,28).

The adsorption mechanisms depend on the physical characteristics of the biochar which are impacted by the biomass properties and pyrolysis conditions (ex. temperature, flow gas, residence time) (19,29). To investigate the effect that different adsorption mechanisms may have on competitive adsorption, five biochars were investigated in this work with varying properties, which result in different adsorption mechanisms including π - π electron donor-acceptor (EDA) interactions and electrostatic interactions. These interactions and mechanisms have both been found to be influenced by the physical characteristics of the biochar including aromaticity and oxygen-containing functional groups. Methyl orange (MO), methylene blue (MB), and acetaminophen (ACT) were used as test organic compounds, where three competitive adsorption tests of each possible pairing were done for each of the five biochars. These compounds were chosen since they are common pollutants found in water sources, aromatic, and active within the UV-visible spectrum. Also, while MB and ACT have electron-donating groups, MO has electron-withdrawing groups allowing testing for situations where the compounds were likely to interact with one another, such as MB and MO, and when they would not such as for MB and ACT. The biochars chosen for investigation were chosen such that they each had different adsorption mechanisms and physical characteristics. Miscanthus-derived biochar at lower pyrolysis temperature was chosen because of its lower aromaticity and high hydroxyl groups, giving the biochar strong electrostatic interactions. Douglas Fir biochar pyrolyzed at higher temperatures

was also investigated, as well as the biochar after oxidative post-treatment with H₂O₂ and KOH to investigate the effect of the increased oxygen content these treatment methods have shown to give biochars (30,31).

4.5 Materials and Methods

4.5.1 Materials

Douglas fir (DF) biomass was supplied by a local furniture manufacturer in London, Ontario, Canada and miscanthus (MC) biomass was collected from near London, Ontario, Canada. Before the pyrolysis, the biomass was pulverized using a blade grinder mill and sieved to the particle size range of 0.3-0.6 mm using standard test sieves (W.S. Tyler, USA). The compressed CO₂ gas used for pyrolysis was purchased from Praxair Canada Inc. 85% Methylene blue (MB) (product #7220793), 85% methyl orange (MO) (product #1002790460), >98% ibuprofen (IBU) (product #102051532), and >98% acetaminophen (ACT) (product #1002893831) used as adsorbates were purchased from Sigma Aldrich, Canada.

4.5.2 Preparation of Biochars

DF and MC biomasses were pyrolyzed in a tube furnace by heating at 10°C/min until 500°C or 800°C and held for 3 hours under a carbon dioxide atmosphere with a gas flow rate of 2 NL/min. Four DF biochars were produced, one at 500°C which was then treated with KOH, and three at 800°C, one of which was treated with KOH, one with H₂O₂ and the other was not modified further and is referred to with the abbreviation for the biomass followed by the pyrolysis temperature and then the pyrolysis gas and post-treatment if applicable, i.e., DF800-CO₂. MC was only pyrolyzed at 500°C to produce a biochar referred to as MC500-CO₂.

4.5.3 H₂O₂ Post-Treatment

H₂O₂ post-treatment was based on the method by Huff et al. (127), where treatment of DF800-CO₂ biochar was done by mixing 1g of biochar with 50 mL of 9.8 M H₂O₂ at room temperature for 1 hour before filtering it through Whatman filter paper No. 1 and washing it with DI-water. The oxidized biochars were then dried at 105°C overnight and referred to as DF800-CO₂-H₂O₂.

4.5.4 KOH Post-Treatment

KOH treatment was based on the procedure proposed by Lu et al. (128), where 5 g of DF500-CO₂, and DF800-CO₂ biochars were each separately placed in 100 mL of 5M KOH and left to mix for 1 hour at room temperature before being filtered through Whatman No.1 filter paper, washed with DI-water, and dried overnight at 105°C. The biochars were then activated in a tube furnace at 700°C with a ramp rate of 10°C/min for 1 hour under 2 NL/min flow of N₂. After activation, the biochars were then washed again with DI water and dried overnight at 105°C. The post-treated biochars were then referred to as DF500-CO₂-KOH and DF800-CO₂-KOH.

4.5.5 Biochar Characterization Methods

4.5.5.1 CHNS-O Elemental Analysis

CHNS-O elemental analysis was done for all of the biomass samples and was performed following the ASTM standard (ASTM D1762-84) using a Netzsch Vulcan D-550 muffle oven. Elemental analysis of carbon, hydrogen, nitrogen, and sulphur was carried out using the model Thermo Flash EA 1112 series CHNS analyzer (Thermo Fisher Scientific, USA). Samples were combusted at 900 °C under helium with a known amount of oxygen. The oxygen content in the sample was calculated by mass difference. The results were measured in triplicates and presented as averages with standard deviations.

4.5.5.2 ATR-FTIR Spectroscopy

The surface organic functional groups present in the samples were detected using Fourier Transform InfraRed (FT-IR) spectroscopy using a Platinum[®] attenuated total reflectance (Pt-ATR) attachment equipped with a diamond crystal in the main box of a Bruker Tensor II spectrometer. During the analysis, the sample in powder form was scanned within the range of 400-4000 cm⁻¹ at a resolution of 4 cm⁻¹ under transmittance mode and 32 accumulations for each spectrum.

4.5.5.3 BET Surface Area

Samples were tested for Brunauer-Emmett-Teller (BET) surface area with a Nova 2000e Surface Area and Pore Size Analyzer (Quantachrome Instrument, Florida, US). The physisorption measurements were performed via N₂ adsorption-desorption experiments at 77.35

K. Samples were degassed at 105°C for 1 hour to remove moisture, then the temperature was increased to 300°C and maintained for at least 3 hours before each analysis.

4.5.6 Adsorption Mechanisms Tests

The adsorption mechanisms were investigated by placing 25 mg of each adsorbent biochar sample in a 20 mL test tube containing 15 mL of a 3 mM H₃PO₄ solution and 100 ppm of the test compound at the desired pH. Adsorption experiments were carried out at relative pH values of 2, 6, 8, and 11. The pH was controlled with a phosphate buffer, prepared with 3 mM H₃PO₄, and the pH was adjusted by adding NaOH. Samples were agitated for 1 hour at 25 °C and filtered through Whatman No. 1 filter paper. The pH of the filtrate was determined after filtering using a pH meter (Thermo Scientific, Orion Star). The concentration of adsorbate remaining in the filtrate was determined at 220, 243, 464, and 668 nm for IBU, ACT, MO, and MB, respectively, using a UV-visible spectrophotometer (Thermo Scientific, Evolution 220). Samples were analyzed in triplicates, and their average absorbances were recorded. The adsorption capacity was defined as the amount of chemical adsorbed per unit mass of the tested adsorbent (mg/g).

4.5.7 Competitive Adsorption Tests

The competitive adsorption mechanisms were investigated by placing 25 mg of adsorbent (biochar) in 20 mL test tubes containing 15 mL of a 3 mM H₃PO₄ solution containing 100 ppm of each of the two compounds without adjusting for pH so that the solution remains acidic as MO only has EWGs under these conditions. The performance under these conditions was compared to the adsorption of each compound individually at acidic pH. Adsorption tests were performed with the following mixtures for each biochar: MO and MB, MO and ACT, and ACT and MB. Samples were agitated for 1 hour at 25 °C and filtered through Whatman No. 1 filter paper. The pH of the filtrate was determined using a pH meter (Thermo Scientific, Orion Star). The concentration of adsorbate remaining in the filtrate was determined at 243, 464, and 668 nm for ACT, MO, and MB, respectively, using a UV-visible spectrophotometer (Thermo Scientific, Evolution 220). Samples were analyzed in triplicates, and their average absorbances were recorded. The adsorption capacity was defined as the amount of chemical adsorbed per unit mass of the tested adsorbent (mg/g).

4.6 Results and Discussion

4.6.1 Adsorption Mechanisms of Biochars

Previous studies have found that the characteristics that have the biggest impact on the adsorption mechanisms of aromatic contaminants are the aromaticity, and the oxygen functional groups (34–36). The aromaticity is often indicated by the H/C ratio, calculated by the elemental analysis. The oxygen functional groups, which can be characterized by FTIR spectroscopy, commonly consist of carbonyl groups that have electron-withdrawing effects or hydroxyl groups that have electron-donating effects. Hydroxyl groups are also the main moieties that give biochar its highly negative surface charge, acting as negatively charged sites upon deprotonation, while carbonyl groups are not able to significantly contribute to electrostatic interactions (37). This means that a greater number of hydroxyl groups will result in both greater electrostatic interactions and π - π EDA interactions with compounds containing EWGs. Conversely, a greater number of carbonyl groups relative to hydroxyl groups could mean that an increase in π - π EDA interactions with compounds with EWGs will also mean a decrease in electrostatic interactions. Table 1 shows the surface areas of the biochars produced. While surface area impacts the overall adsorption capacity, the adsorption mechanisms are more likely to be influenced by surface functionalities. Given these trends, five biochars were chosen to represent the various types of physical characteristics influential towards adsorption. MC500-CO₂ was chosen since it is a biochar with low aromaticity and a relatively higher amount of oxygen groups giving it very strong electrostatic interactions. DF800-CO₂ was chosen due to its high aromaticity but relatively lower oxygen content, while DF800-CO₂-KOH and DF500-CO₂-KOH were selected as they had similarly high aromaticities to DF800-CO₂, with mainly hydroxyl and carbonyl groups respectively. DF800-CO₂-H₂O₂ was also investigated due to its high aromaticity and strong electrostatic interactions that it was found to have due to a strong repulsion to MB with increasing pH. All of these biochars along with their adsorption mechanisms are presented in **Table 4.1**.

Table 4.1 Adsorption mechanisms, elemental composition and surface parameters of biochars

Biochar	Adsorption Mechanisms		Elemental Analysis (%mass)						BET SSA (m ² / g)	Average Pore Volume (cm ³ /g)	Average Pore Diameter (nm)
	Strong	Weak	C	H	N	O*	Ash	H/C			
DF500- CO ₂ - KOH	-Electrostatic -EDA with EDGs	- π - π stacking	80.3 ± 2.9	1.23 ± 0.3	0.01 ± 0.01	15.6 ± 1.7	2.89 ± 2.0	1.5*1 0 ⁻² ± 0.006	395	0.22	2.18
DF800- CO ₂	- π - π stacking	-Electrostatic -EDA with EWGs	57.2 ± 3.8	1.00 ± 0.2	0.69 ± 0.04	7.07 ± 3.8	34.0 ± 3. 1	1.7*1 0 ⁻² ± 0.003	461	0.29	0.248
DF800- CO ₂ - H ₂ O ₂	- π - π stacking -Electrostatic	-EDA with EDGs	64.7 ± 0.8	1.85 ± 0.2	1.28 ± 0.1	12.1 ± 0.9	20.1 ± 0.7	2.9*1 0 ⁻² ± 0.003	676	0.40	2.37
DF800- CO ₂ - KOH	-Electrostatic -EDA with EWGs	- π - π stacking -EDA with EDGs	65.0 ± 0.7	0.01 ± 0.00 1	0.05 ±0.0 8	21.5 ± 0.8	13.4 ±0.8	1.5*1 0 ⁻⁴ ± 0.000 01	606	0.36	2.35
MC500- CO ₂	-Electrostatic	- π - π stacking -EDA with	63.1 ± 5.8	1.12 ± 0.3	0.64 ± 0.1	29.4 ± 6.1	8.84 ± 0.5	2.4*1 0 ⁻² ± 0.005	64	0.055	3.42

* Measured by difference (Total mass-C-H-N-Ash=O)

DF800-CO₂ had very high aromaticity, evidenced by the low H/C ratio, (**Table 1**), which resulted in strong π - π interactions with the adsorbents. The carbonyl groups that were present on the surface (**Figure 4.1**) resulted in strong adsorption of compounds with EDGs. This is

evidenced by the higher adsorption of MO under basic conditions compared to acidic conditions, shown in **Figure 4.2a**. This is likely due to the carbonyl groups acting as EWGs which attract MO due to π - π EDA interactions and the fact that there are few hydroxyl groups to act as negatively charged sites to repel it. This explains the low electrostatic interactions; in the case of strong electrostatic interactions, MO would have had lower adsorption when anionic in basic pH

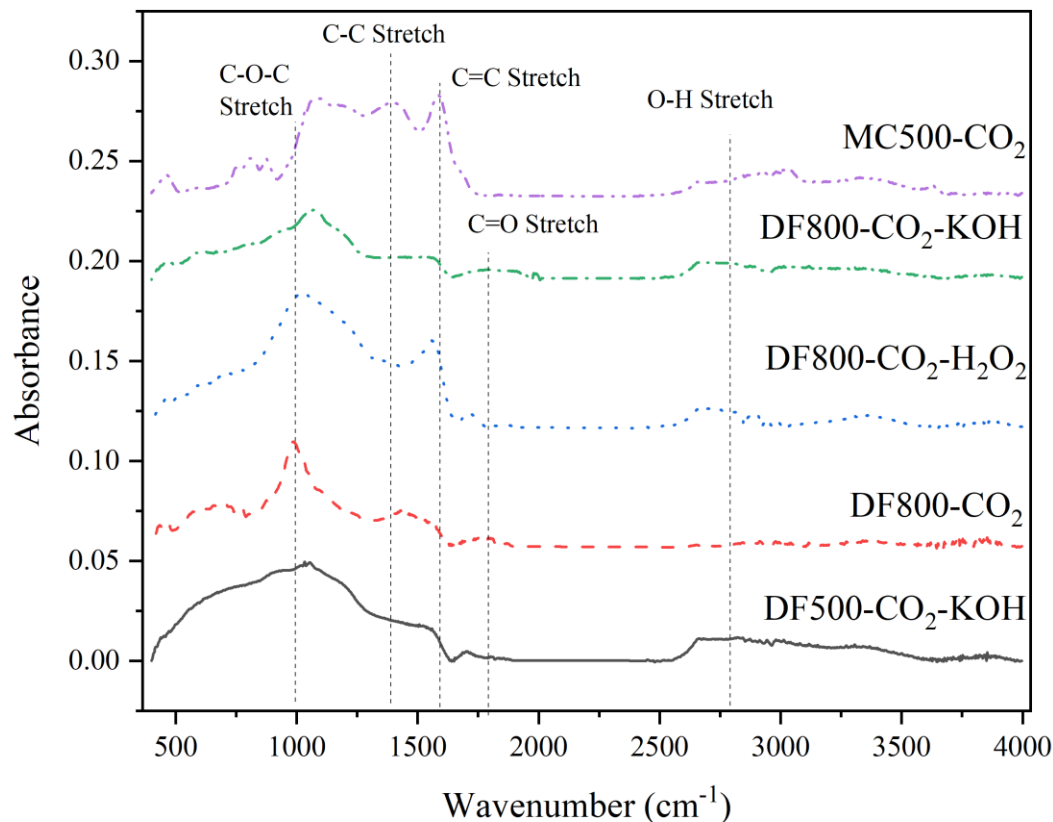


Figure 4.1 ATR-FTIR spectra of DF500-CO₂, DF800-CO₂, DF800-CO₂-H₂O₂, DF800-CO₂-KOH, and MC500-CO₂

Biochar produced at 500 °C with KOH post-treatment (DF500-CO₂-KOH) also has a similar high aromaticity and low H/C ratio and therefore π - π interactions. However, it was found to have a greater peak for O-H stretches while also having a distinct peak for a carbonyl C=O stretch in the FTIR spectrum presented in **Figure 4.1**. This suggests a larger amount of hydroxyl groups on the surface along with the carbonyl groups, giving the biochar slightly stronger electrostatic interactions while maintaining dominantly strong π - π EDA interactions with

compounds with EDGs such as ACT. As shown in Figure 2b, ACT had the highest adsorption of all the compounds tested with DF500-CO₂-KOH. Unlike DF800-CO₂, the presence of hydroxyl groups also increased electrostatic interactions, indicated by the decrease of IBU and increase of MB with increasing pH.

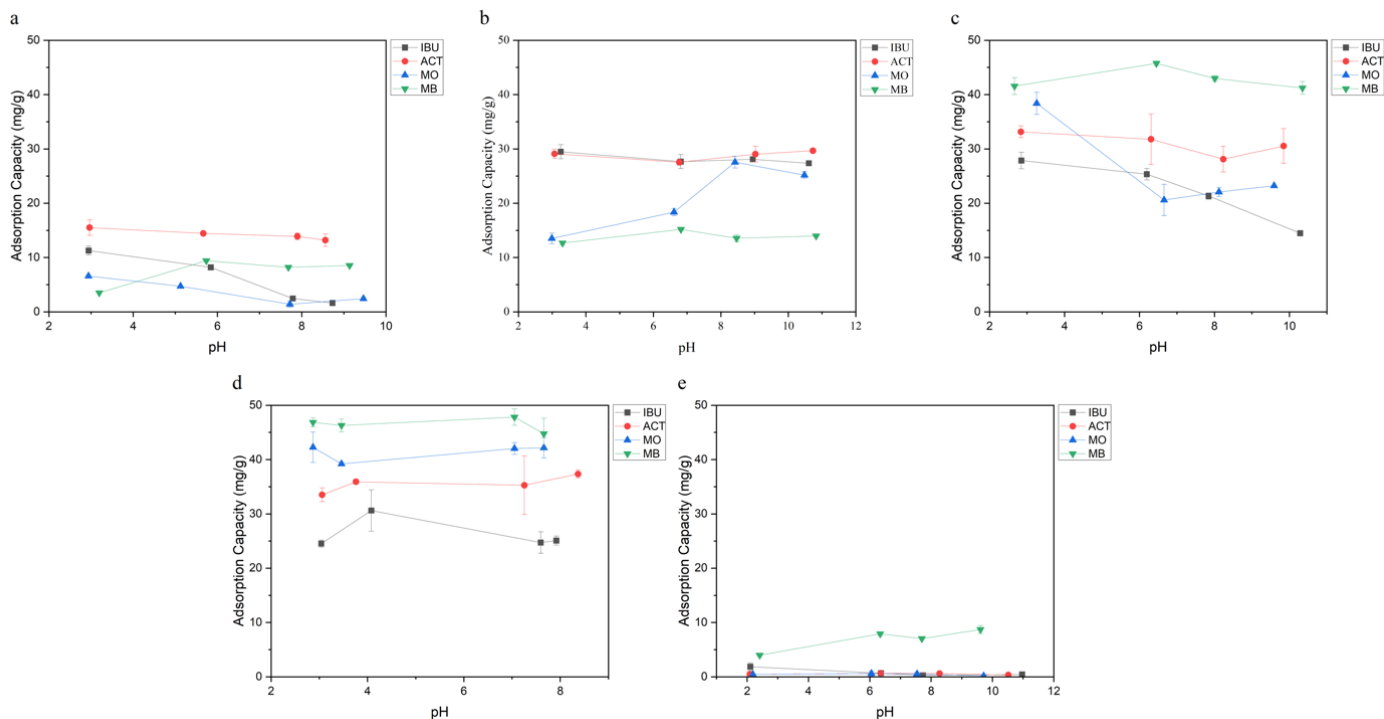


Figure 4.2 Adsorption capacities of IBU, ACT, MO, and MB with increasing pH for a) DF500-CO₂-KOH, b) DF800-CO₂, c) DF800-CO₂-H₂O₂, d) DF800-CO₂-KOH, and e) MC500-CO₂ where adsorption was performed using 50ppm of compounds and 50 mg of biochar in 15mL solutions

Biochar that was produced at 800 °C and treated with KOH (DF800-CO₂-KOH) had high aromaticity and contained primarily hydroxyl groups with no carbonyl groups observed in the FTIR spectrum (**Figure 4.1**). This biochar showed the highest adsorption capacities for MO and MB at low pH compared to IBU and ACT in **Figure 4.2c**. This is due to electrostatic interactions along with π - π EDA interactions with EWGs present in MO and MB.

After H₂O₂ treatment, the DF800-CO₂ biochar became more aromatic with slightly more oxygen groups, however fewer oxygen groups than KOH treatment or MC biochar. This is evidenced by the fact that the relatively high H/C ratio in **Table 4.1** for the DF800-CO₂-H₂O₂ and the second-lowest oxygen content at 12.1%. According to the results on the functionality of

the biochar in the FTIR spectrum in **Figure 4.1**, there is a strong peak correlating to the C-O-C stretch and another for the O-H stretch indicating that the oxygen content that is present in the biochar is made of hydroxyl and ether groups, both of which are EDGs. Looking at the adsorption results in **Figure 4.2c**, this biochar had high adsorption of MO at low pH which decreased significantly at higher pH and high adsorption of MB. This means there are strong π - π EDA interactions with compounds with EWGs such as MO, but more importantly, there are stronger electrostatic interactions which are responsible for the high adsorption of MB and the decreasing adsorption of MO.

Lastly, MC500-CO₂ had one of the lowest aromaticity of the biochars, and the greatest oxygen content, comprised mainly of ether and hydroxyl groups given the C-O-C and O-H stretches around 1000 and 3000 cm⁻¹ in the FTIR spectra in **Figure 4.1**. Thus, MC500-CO₂ showed significantly greater electrostatic interactions than π - π interactions, given that MB was the only compound that was significantly adsorbed, due to the electrostatic interaction between the negatively charged sites from the deprotonated hydroxyl groups on the biochar and the cationic moieties on the MB.

4.6.2 Competitive Adsorption of Methyl Orange and Methylene Blue

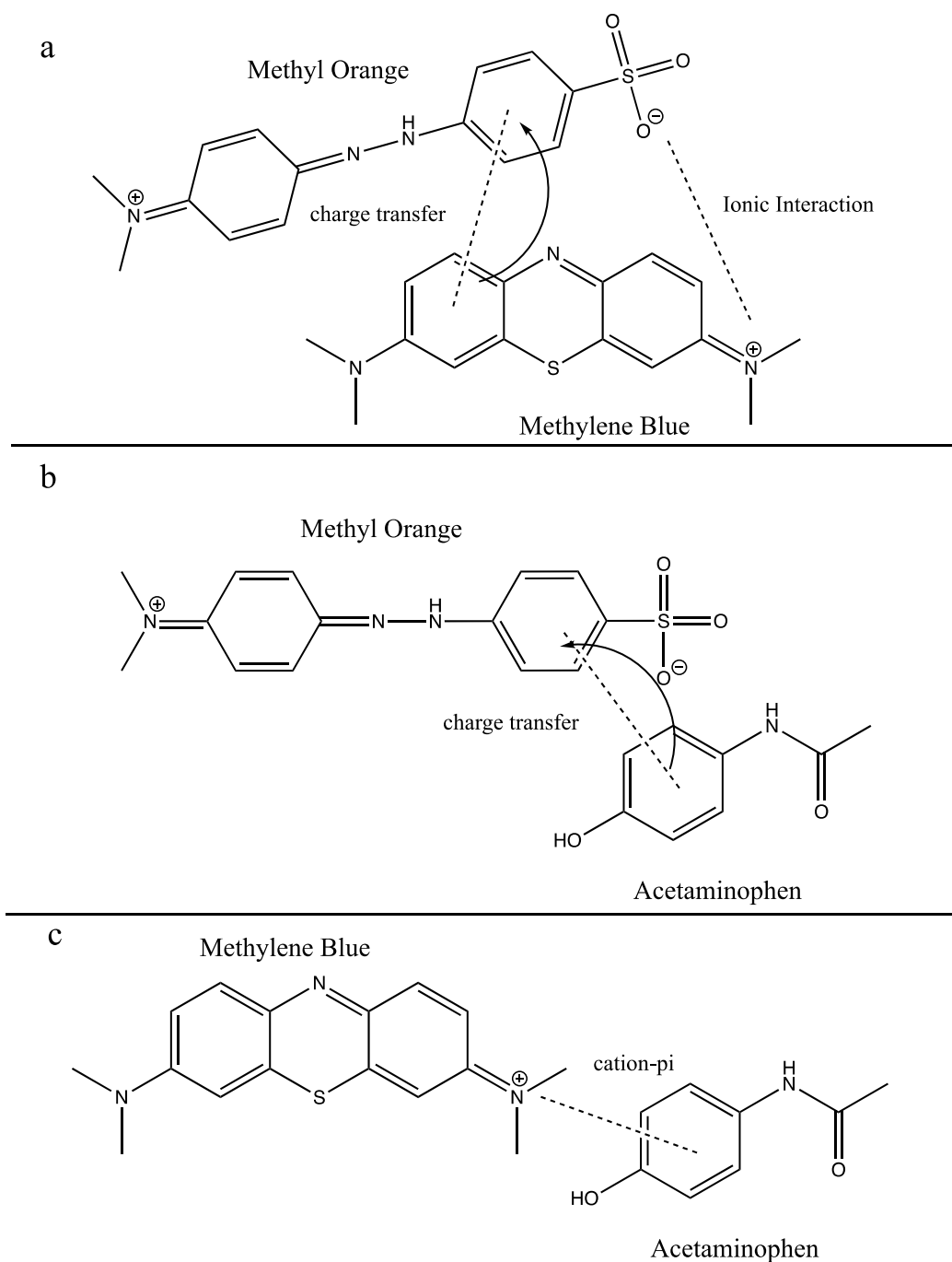


Figure 4.3 Schematic of possible intermolecular interactions between a) MO and MB, b) MO and ACT, and c) ACT and MB

The different biochar samples were used to adsorb MO and MB individually and in a mixture. The structures of MO and MB, schematically shown in **Figure 3a**, can help explain the behaviour observed. MB can undergo a charge transfer interaction with MO given the electron-

donating amine group bonded to the aromatic ring of the MB, and the electron-withdrawing sulphate group on the MO (38–41). MO is also able to electrostatically interact with MB through their ionic charges (42). The adsorption of MO and MB individually, and in a mixture are shown in **Figure 4** for all of the biochars investigated. DF500-CO₂-KOH and MC500-CO₂ biochars both showed an increase in the adsorption of MO and MB when in a mixture, indicating that the combination of these compounds results in a synergetic increase in adsorption. Multiple possibilities could explain this trend in adsorption. This could be due to a complex that is formed by the intermolecular interactions of MO and MB which has a stronger affinity towards the biochar than the compounds do individually. Another explanation may be that the mechanisms through which MO and MB are adsorbed are different, so they do not compete for adsorption sites. Thirdly, another possibility is that when MO is adsorbed via π - π EDA interactions, MB will then be attracted to the MO on the biochar surface. In the case of MC500-CO₂, MB would be adsorbed onto the surface first via electrostatic interactions and MO would then be attracted to the adsorbed MB since this biochar has shown stronger electrostatic interactions as previously stated. DF500-CO₂-KOH has strong electrostatic interactions and strong EDA interactions with compounds with EDGs and EWGs, while MC500-CO₂ has very strong electrostatic interactions and weak π - π interactions. MO was not adsorbed at all by MC500-CO₂, therefore the increase in adsorption of MB by adding MO is most likely due to the MB adsorbing first onto the surface of the biochar, thus providing sites for adsorption of MO. Once MO adsorbs to the surface, MB will be adsorbed further allowing for increased adsorption of both compounds. This would be less likely to happen when either compound is adsorbed alone as MB is more likely to interact with MO due to its withdrawing groups than itself, given that aromatic compounds are less likely to stack if they both have donating or both withdrawing groups.

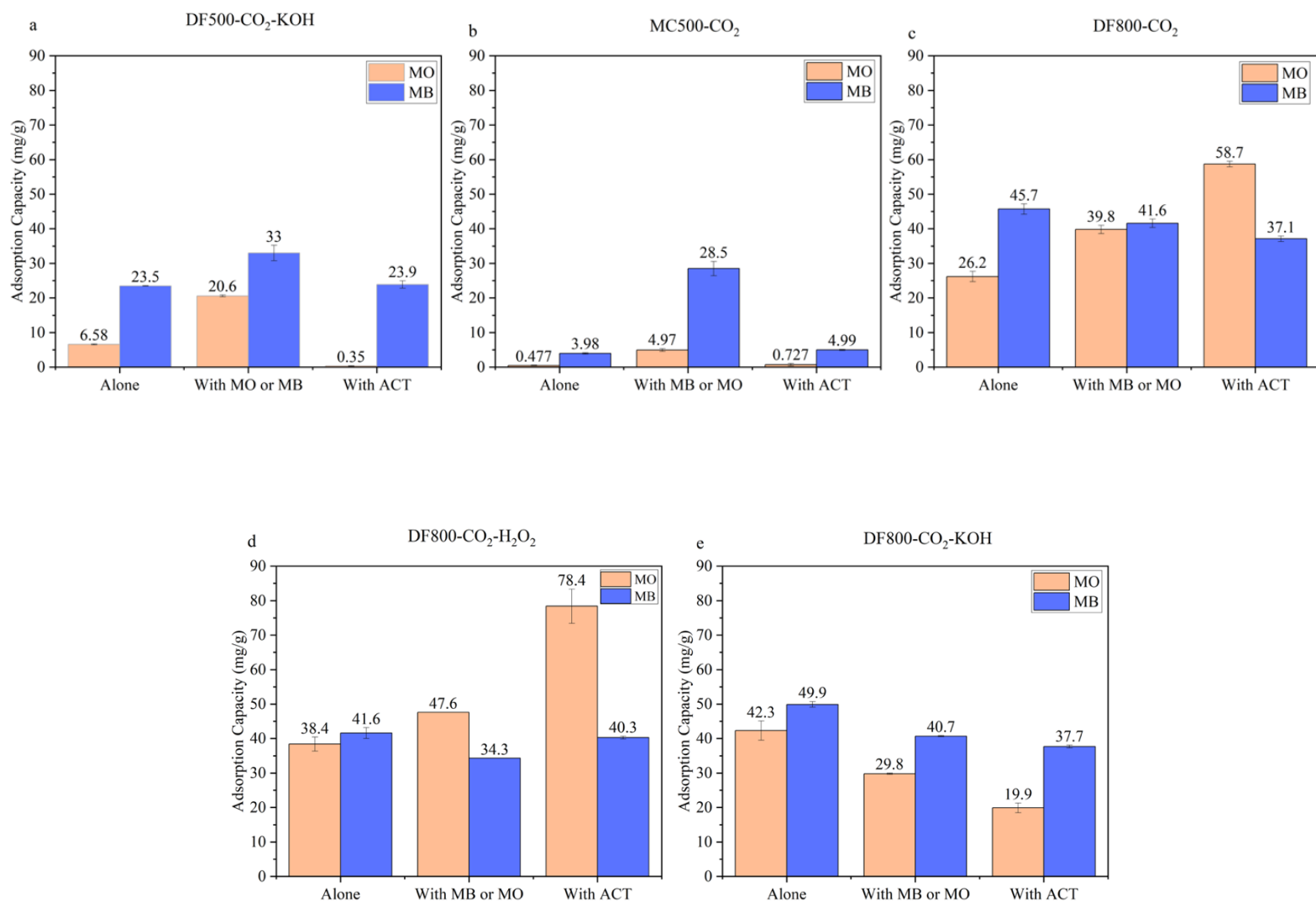


Figure 4.4 Adsorption Capacities of biochar in a solution containing MO, MB or mixtures of these compounds for biochars a) DF500-CO₂-KOH, b) MC500-CO₂, c) DF800-CO₂, d) DF800-CO₂-H₂O₂, and e) DF800-CO₂-KOH

For biochar produced at 800 °C with no post-treatment (DF800-CO₂), the adsorption of MO increased, and the adsorption of MB remained the same when they were combined as can be seen in **Figure 4.4c**. Given the strong π - π EDA interactions, especially with compounds with EDGs, and weak electrostatic interactions, this biochar has strong adsorption of MB through π - π EDA interactions. A proposed explanation for the increase in MO when combined with MB is that the MO is likely to interact with MB, which is well absorbed by the biochar. Thus, MO is adsorbed more when adsorbed in multispecies solution with MB, as they are likely to interact via intermolecular interactions. Since MB did not increase when adsorbed with MO, like what was

observed for DF500-CO₂-KOH and MC500-CO₂, DF800-CO₂ may adsorb the compounds via similar adsorption sites. If there is competition for adsorption sites, then MB will be adsorbed at a higher capacity as DF800-CO₂ has a higher affinity for this compound due to electrostatic interactions. Therefore, the adsorption capacity of MB would not change, however, the adsorption of MO will be increased by the presence of MB.

When biochar was treated with H₂O₂ (DF800-CO₂-H₂O₂) the resulting biochar had high aromaticity and contained hydroxyl functional groups only. The adsorption of MB in an MB/MO mixture was lower compared to MB only while the adsorption of MO increased slightly, as shown in **Figure 4.4d**. Due to hydroxyl surface groups, this biochar has strong electrostatic interactions and EDA interactions with compounds with EWGs. Therefore, there may be competition between adsorption sites, where MO is preferentially adsorbed as the π - π EDA interactions are stronger than electrostatic interactions. Since MB decreases in adsorption, however, this means that there is more competition for adsorption sites and fewer intermolecular interactions between compounds. The π - π EDA interactions observed for DF800-CO₂-H₂O₂ can then be said to be stronger than those of DF800-CO₂, as they are great enough that the compounds more favourably interact with the biochar than each other.

Biochar treated with KOH was used to adsorb MO and MB and the results are shown in **Figure 4.4e**. The adsorption of MO and MB alone when combined followed different trends compared to those of DF500-CO₂-KOH and MC500-CO₂. With KOH-treated biochar, the adsorption of MO and MB decreased when adsorbed together. This suggests that the MO and MB are adsorbed by the same sites, thus competing for adsorption. MO and MB are both able to interact with aromatic groups that have hydroxyl substituents; MO via π - π EDA interactions, and MB through electrostatic interactions. This would lead to competitive adsorption, explaining the decrease in adsorption that was observed. The FTIR spectrum of DF800-CO₂-KOH in **Figure 1** shows stretches that are characteristic of hydroxyl groups, further suggesting that π - π EDA and electrostatic interactions compete in this situation.

4.6.3 Competitive Adsorption Methyl Orange and Acetaminophen

ACT has both an amide and a hydroxyl group, both of which are electron-donating groups, making this compound likely to have stronger charge transfer interactions with MO, as seen in **Figure 4.3b** (43). ACT is also neutral at low pH, meaning that the complex formed by MO and

ACT would have a zero net charge, decreasing potential electrostatic interactions (38,41,43). The adsorption of MO and ACT individually and in binary mixtures was tested for the different biochars and presented in **Figure 4.5**. Looking at the adsorption capacity of MO by DF500-CO₂-KOH, shown in **Figure 4.5a**, when in a solution of equal parts ACT and MO, there was a significant decrease in adsorption of both MO and ACT. This would imply that ACT and MO interact more with one another than the biochar, which would result in both being poorly adsorbed by the biochar. This is the opposite result that was seen when MO was adsorbed with MB by this biochar as shown in the previous section. Given that the most significant difference between MB and ACT is the positive charge on MB, the complex formed from MO and MB is likely adsorbed by electrostatic interactions which are not able to adsorb the MO and ACT complex as it has a net neutral charge. The decrease in adsorption also indicates that there may be competition for adsorption sites, or the intermolecular interactions between MO and ACT cause a decrease in adsorption capacity relative to when the compounds are adsorbed separately. Since DF500-CO₂-KOH was shown to have strong π - π EDA interactions which would adsorb MO and ACT via different sites, a possible explanation would be that MO and ACT are more likely to undergo intermolecular charge transfer interactions between themselves than the π - π EDA interactions with the biochar. This interaction would be equally as likely for MO and MB, however since MB can be adsorbed by electrostatic unlike ACT, there was the opportunity for MO and MB to interact with both each other and the biochar thus increasing both their adsorption capacities.

The adsorption capacity of MO increased relative to when adsorbed alone when combined with ACT in the case of DF800-CO₂, while the adsorption capacity of ACT remained the same, as shown in **Figure 4.5c**. This is similar to the results for MO combined with MB for this biochar, except MO increases more when combined with ACT as opposed to with MB. This indicates that the MO adsorption capacity is higher when adsorbed with ACT as it can interact with ACT which has a stronger affinity towards adsorption than the MO. Also, since this is the same trend as was seen for MB, this implies that the adsorption mechanisms through which this occurs are not the electrostatic interactions but π - π EDA interactions, as this is the only interaction both ACT and MB can be adsorbed by. This is consistent as this was determined to be the strongest adsorption mechanism for this biochar.

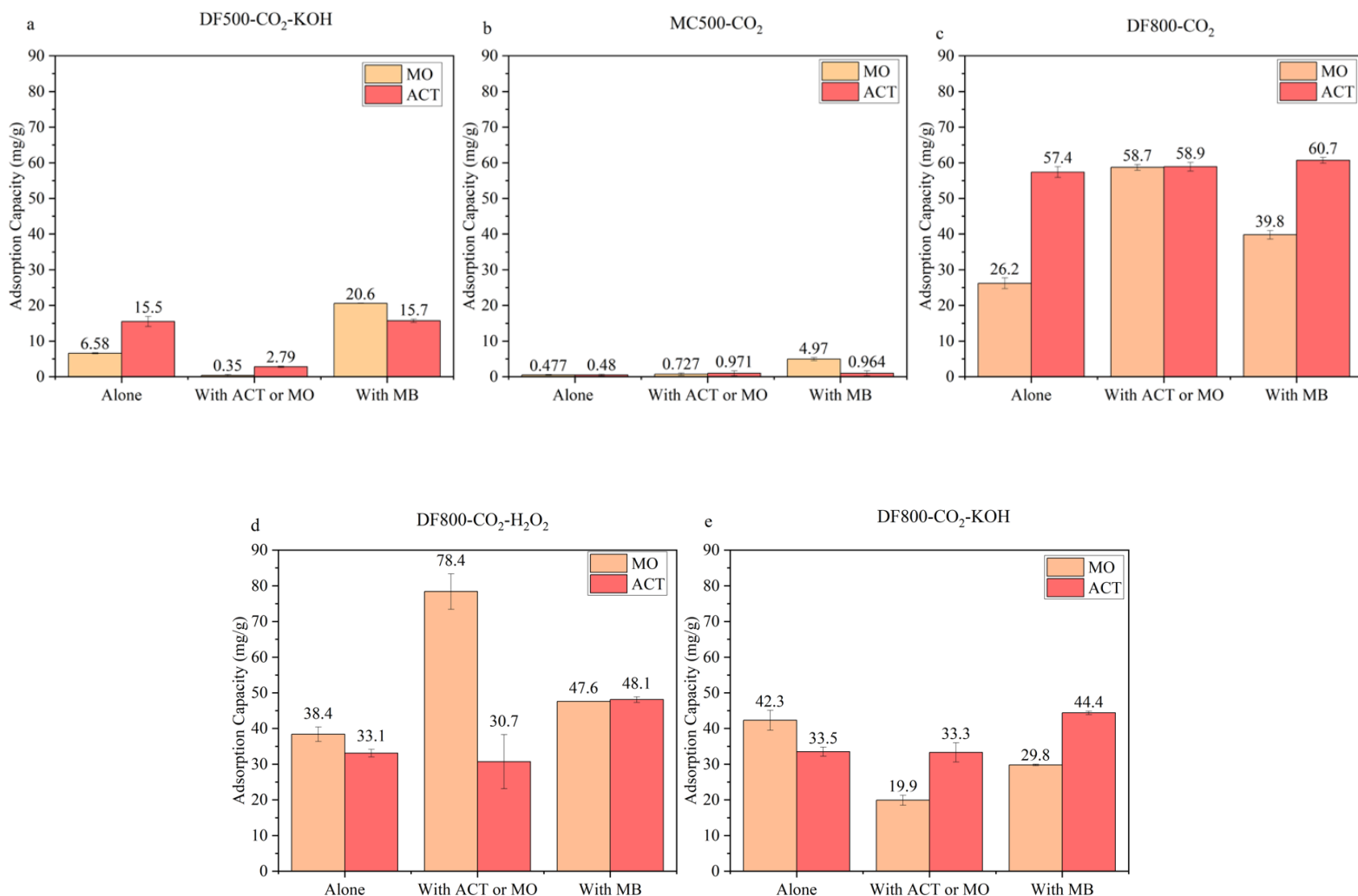


Figure 4.5 Adsorption Capacities of biochar in a solution containing MO, ACT or mixtures of these compounds for biochars a) DF500-CO₂-KOH, b) MC500-CO₂, c) DF800-CO₂, d) DF800-CO₂-H₂O₂, and e) DF800-CO₂-KOH

For the DF800-CO₂-H₂O₂, when adsorbing both MO and ACT together, resulted in relatively higher adsorption of MO while the adsorption of ACT remained the same as when adsorbed alone. **Figure 4.5d** shows that the adsorption capacity of MO increased more when combined with ACT than MB, and ACT was not seen to decrease in adsorption when combined with MO as MB did. Since ACT does not have a positive charge, it instead has stronger electron-donating groups and therefore the greater increase in adsorption of MO with ACT may be attributed to stronger π - π EDA interactions towards ACT compared to MB. ACT and MO can also be said to adsorb via different adsorption sites, while MB adsorbs at the same sites as MO and therefore

competes for adsorption. This is because ACT will be adsorbed at aromatic rings with electron-withdrawing carbonyl groups, while MO and MB will be adsorbed at aromatic groups with hydroxyl groups, due to both their negative charge and electron-donating character. This results in competition between MO and MB, but not MO and ACT.

The adsorption capacities for DF800-CO₂-KOH interestingly displayed the opposite trends with respect to those observed for DF800-CO₂-H₂O₂ and DF800-CO₂ were observed when adsorbing MO and ACT together. Looking at **Figure 4.5e**, the adsorption of MO decreased while the adsorption of ACT remained the same as when adsorbed separately. When MO was adsorbed with MB, both compounds' adsorption capacity decreased relative to when adsorbed separately, possibly due to competition for adsorption sites. When MO was adsorbed with ACT on the other hand, only the adsorption of MO decreased while ACT had no change in adsorption, suggesting that the ACT adsorption mechanisms are stronger than that of MO. There was less evidence for competition for adsorption sites than was seen for the DF800-CO₂-H₂O₂ and DF800-CO₂ biochars, where there was an increase in the adsorption of MO. DF800-CO₂-H₂O₂ and DF800-CO₂ have more carbonyl groups, according to FTIR spectra in **Figure 4.1**, which only contribute to π - π EDA interactions with compounds with EDGs, while DF800-CO₂-H₂O₂ was found to predominantly have hydroxyl groups that contribute to both electrostatic and π - π EDA interactions with compounds with EWGs. This would mean that the presence of carbonyl groups and hydroxyl groups allows for multiple adsorption mechanisms without competition, therefore increasing the adsorption capacities of the compounds since they can form intermolecular interactions with one another. However, the greater the number of hydroxyl groups relative to carbonyl groups, the more electrostatic and π - π EDA interactions with EWGs will compete. This could result in the decreasing adsorption of one or both compounds, depending on which adsorption mechanism is stronger.

Lastly, MC500-CO₂ showed no change in the adsorption of MO or ACT when combined, as seen in **Figure 4.5e**. This is most likely due to this biochar having no strong adsorption of either when adsorbed alone, the combination of the two did not affect adsorption.

4.6.4 Competitive Adsorption of Acetaminophen and Methylene Blue

The compounds MB and ACT both have electron-donating groups, as seen in **Figure 4.3c** and are less able to interact via a charge transfer interaction (39,43). There is however the

possibility of a weaker cation- π intermolecular interaction that can happen between ACT and the positively charged MB (44). The adsorption of ACT and MB was investigated both separately and in binary mixtures for each of the five biochars tested, as shown in **Figure 4.6**. When looking at the change in adsorption capacities of ACT and MB when adsorbing together, DF500-CO₂-KOH, MC500-CO₂, DF800-CO₂, and DF800-CO₂-KOH all showed no significant change in the adsorption of MB or ACT when adsorbed together, except for a small decrease in adsorption for both compounds. This may be due to MB and ACT not interacting very well, making it unlikely that either would increase the adsorption of the other. The compounds may compete for adsorption sites on the biochar instead, making their adsorption capacities decrease slightly if not remaining the same.

Figure 4.5d shows that the adsorption capacities of ACT by DF800-CO₂-H₂O₂ slightly increased when adsorbed with MB, which is well adsorbed given strong electrostatic interactions. This may be due to ACT and MB forming weak cation- π interactions, which would cause ACT to be adsorbed at a higher capacity with MB (44). This interaction is notably weaker since MB and ACT do not interact as strongly and was only found for DF800-CO₂-H₂O₂, which is the biochar with the greatest number of hydroxyl groups, reported in **Figure 4.1**, and strongest electrostatic interactions.

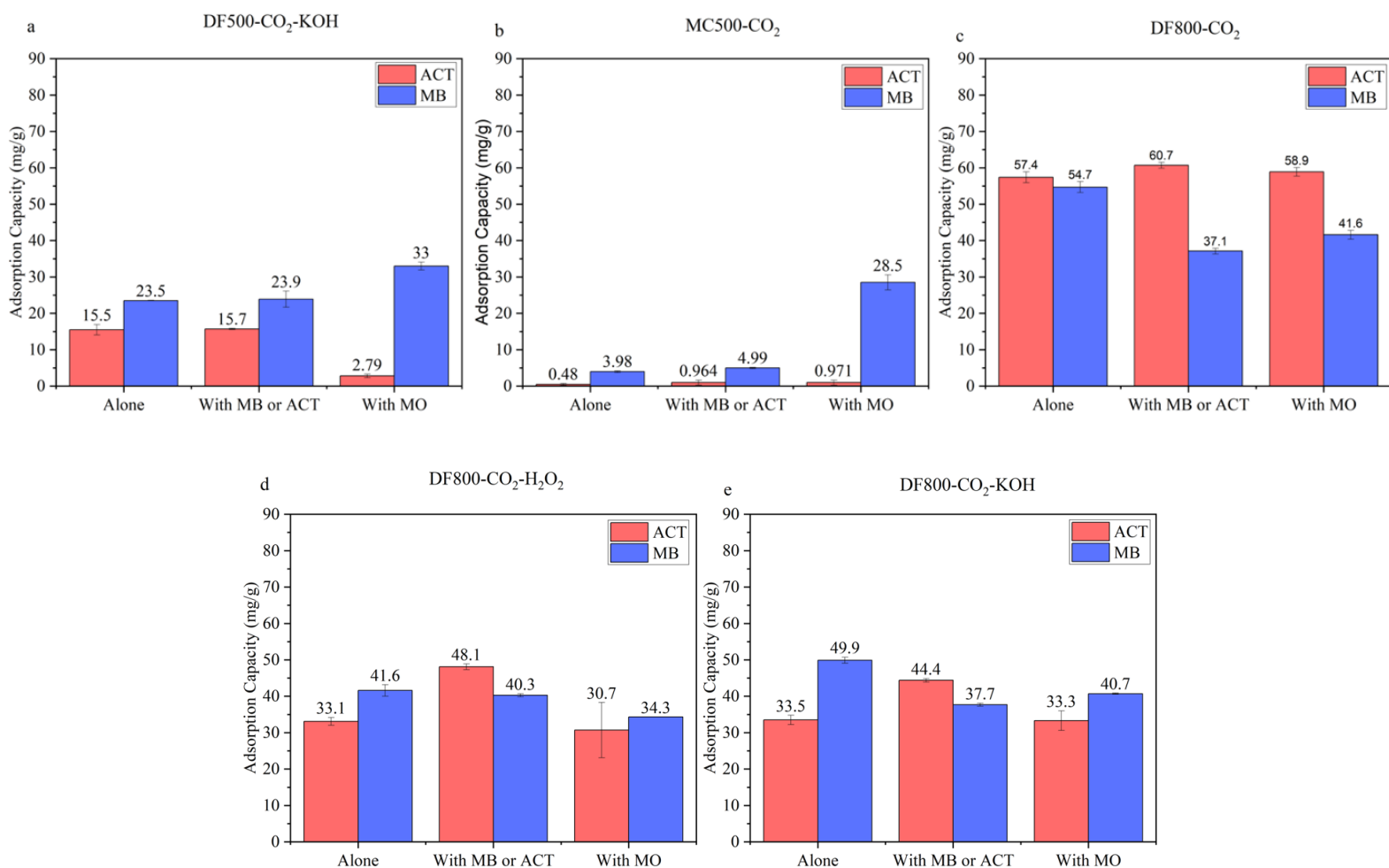


Figure 4.6 Adsorption Capacities of biochar in a solution containing MB, ACT or mixtures of these compounds for biochars a) DF500-CO₂-KOH, b) MC500-CO₂, c) DF800-CO₂, d) DF800-CO₂-H₂O₂, and e) DF800-CO₂-KOH

4.7 Conclusion

The adsorption of three aromatic compounds, MO, MB, and ACT, individually and in mixtures was explored using biochar with different properties, the results have been summarized in **Table 4.2**. In general, it was found that the biochars that contained different types of oxygen functional groups on the surface, i.e., both hydroxyl and carbonyl groups present in FTIR, had greater synergetic adsorption when adsorbing compounds in a mixture as there is less competition for adsorption sites. Biochars with only hydroxyl groups exhibited competing adsorption mechanisms and poorer adsorption capacities of aromatic compounds in complex solutions.

Table 4.2 Simplified summary of changes in adsorption capacities of aromatic adsorbates when adsorbed in solution with other aromatic compounds

Biochar	Adsorbate	Change in Adsorption in solution with		
		ACT	MO	MB
DF800-CO ₂	ACT	-	No change	No change
	MO	Increase	-	Increase
	MB	Decrease	Decrease	-
DF500-CO ₂ -KOH	ACT	-	Decrease	No change
	MO	Decrease	-	Increase
	MB	Increase	Increase	-
DF800-CO ₂ -H ₂ O ₂	ACT	-	No change	Increase
	MO	Increase	-	Increase
	MB	No change	Decrease	-
DF800-CO ₂ -KOH	ACT	-	No change	Increase
	MO	Decrease	-	Decrease
	MB	Decrease	Decrease	-
MC500-CO ₂	ACT	-	No change	No change
	MO	No change	-	Increase
	MB	No change	Increase	-

MO is known to be able to interact with MB both through a π - π charge transfer and ionic charge interactions and is the most likely pairing to increase adsorption when adsorbed together. Because of this, it is more likely that MO and MB can interact both with each other and the biochar. So long as the compounds do not compete for adsorption sites, the adsorption of both compounds should be greater when adsorbed together, as was seen for DF500-CO₂-KOH. In the case where there is competition for adsorption sites, there is lower adsorption of the compound with lesser attraction to the biochar, as was seen for DF800-CO₂, and DF800-CO₂-H₂O₂. However, if only one of the compounds is strongly adsorbed by the biochar and the other is not, it was found that the adsorption of the other compound increased relative to when adsorbed alone, as shown by the increased adsorption of MO for DF800-CO₂ and MC500-CO₂.

Both MO and ACT are also more likely to be adsorbed by π - π EDA interactions and not likely to compete for adsorption sites but are likely to interact with one another. DF800-CO₂ and DF800-CO₂-H₂O₂ saw increased adsorption of these compounds when adsorbed together, suggesting that the π - π EDA interactions between the compounds and the biochar must be stronger than the intermolecular interactions between MO and ACT.

Lastly, ACT and MB both have EDGs and are not likely to interact with one another as well as being likely to compete for adsorption sites. MB is also able to be adsorbed by electrostatic interactions however, this does not increase ACT when adsorbed together since there is not a strong enough electrostatic interaction for most biochars. DF800-CO₂-H₂O₂ and MC500-CO₂ were seen to be exceptions to this, where ACT increased when adsorbed with MB. This may be because this biochar allowed for weak cation- π intermolecular interactions between the compounds.

Overall, this work provides a greater understanding of how aromatic compounds may behave differently in terms of adsorption when interacting with one another, as well as the adsorbent surface. This is essential in designing adsorbents for real applications where a variety of common organic contaminants are meant to be adsorbed together. Further, these findings provide insight into how biochars may take advantage of intermolecular interactions to increase adsorption capacities compared to what may be found in laboratory settings.

4.8 References

1. Luo, Z.; Yao, B.; Yang, X.; Wang, L.; Xu, Z.; Yan, X.; et al. Novel insights into the adsorption of organic contaminants by biochar: A review. *Chemosphere* **2022**, *287*. doi:10.1016/j.chemosphere.2021.132113.
2. Qu, J.; Meng, Q.; Peng, W.; Shi, J.; Dong, Z.; Li, Z.; et al. Application of functionalized biochar for adsorption of organic pollutants from environmental media: Synthesis strategies, removal mechanisms and outlook. *Journal of Cleaner Production*. Elsevier Ltd October 15, 2023. doi:10.1016/j.jclepro.2023.138690.
3. Tang, Y.; Li, Y.; Zhan, L.; Wu, D.; Zhang, S.; Pang, R.; et al. Removal of emerging contaminants (bisphenol A and antibiotics) from kitchen wastewater by alkali-modified biochar. *Science of the Total Environment* **2022**, *805*. doi:10.1016/j.scitotenv.2021.150158.
4. Zhou, Y.; Lu, J.; Zhou, Y.; Liu, Y. Recent advances for dyes removal using novel adsorbents: A review. *Environmental Pollution*. Elsevier Ltd September 1, 2019, pp 352–365. doi:10.1016/j.envpol.2019.05.072.
5. Qu, J.; Liu, R.; Bi, X.; Li, Z.; Li, K.; Hu, Q.; et al. Remediation of atrazine contaminated soil by microwave activated persulfate system: Performance, mechanism and DFT calculation. *Journal of Cleaner Production* **2023**, *399*. doi:10.1016/j.jclepro.2023.136546.
6. Li, M.; Wei, D.; Liu, T.; Liu, Y.; Yan, L.; Wei, Q.; et al. EDTA functionalized magnetic biochar for Pb(II) removal: Adsorption performance, mechanism and SVM model prediction. *Separation and Purification Technology* **2019**, *227*. doi:10.1016/j.seppur.2019.115696.
7. Sinaei Nobandegani, M.; Yu, L.; Hedlund, J. Zeolite membrane process for industrial CO₂/CH₄ separation. *Chemical Engineering Journal* **2022**, *446*. doi:10.1016/j.cej.2022.137223.
8. Benvenuti, J.; Fisch, A.; Dos Santos, J. H. Z.; Gutterres, M. Silica-based adsorbent material with grape bagasse encapsulated by the sol-gel method for the adsorption of Basic Blue 41 dye. *Journal of Environmental Chemical Engineering* **2019**, *7*(5). doi:10.1016/j.jece.2019.103342.
9. Liu, Z.; Zhang, F. S.; Sasai, R. Arsenate removal from water using Fe₃O₄-loaded activated carbon prepared from waste biomass. *Chemical Engineering Journal* **2010**, *160*(1), 57–62. doi:10.1016/j.cej.2010.03.003.
10. Ai, T.; Jiang, X.; Liu, Q.; Lv, L.; Wu, H. Daptomycin adsorption on magnetic ultra-fine wood-based biochars from water: Kinetics, isotherms, and mechanism studies. *Bioresource Technology* **2019**, *273*, 8–15. doi:10.1016/j.biortech.2018.10.039.

11. Purakayastha, T. J.; Bera, T.; Bhaduri, D.; Sarkar, B.; Mandal, S.; Wade, P.; et al. A review on biochar modulated soil condition improvements and nutrient dynamics concerning crop yields: Pathways to climate change mitigation and global food security. *Chemosphere* **2019**, *227*, 345–365. doi:10.1016/j.chemosphere.2019.03.170.
12. He, M.; Xiong, X.; Wang, L.; Hou, D.; Bolan, N. S.; Ok, Y. S.; et al. A critical review on performance indicators for evaluating soil biota and soil health of biochar-amended soils. *Journal of Hazardous Materials* **2021**, *414*. doi:10.1016/j.jhazmat.2021.125378.
13. Gujre, N.; Soni, A.; Rangan, L.; Tsang, D. C. W.; Mitra, S. Sustainable improvement of soil health utilizing biochar and arbuscular mycorrhizal fungi: A review. *Environmental Pollution*. Elsevier Ltd January 1, 2021. doi:10.1016/j.envpol.2020.115549.
14. Liu, G.; Sheng, H.; Fu, Y.; Song, Y.; Redmile-Gordon, M.; Qiao, Y.; et al. Extracellular polymeric substances (EPS) modulate adsorption isotherms between biochar and 2,2',4,4'-tetrabromodiphenyl ether. *Chemosphere* **2019**, *214*, 176–183. doi:10.1016/j.chemosphere.2018.09.081.
15. Zhang, X.; Gao, B.; Zheng, Y.; Hu, X.; Creamer, A. E.; Annable, M. D.; et al. Biochar for volatile organic compound (VOC) removal: Sorption performance and governing mechanisms. *Bioresource Technology* **2017**, *245*, 606–614. doi:10.1016/j.biortech.2017.09.025.
16. Ahmed, M. J.; Hameed, B. H. Adsorption behavior of salicylic acid on biochar as derived from the thermal pyrolysis of barley straws. *Journal of Cleaner Production* **2018**, *195*, 1162–1169. doi:10.1016/j.jclepro.2018.05.257.
17. Varma, R. S. Biomass-Derived Renewable Carbonaceous Materials for Sustainable Chemical and Environmental Applications. *ACS Sustainable Chemistry and Engineering*. American Chemical Society April 1, 2019, pp 6458–6470. doi:10.1021/acssuschemeng.8b06550.
18. Moreira, M. T.; Noya, I.; Feijoo, G. The prospective use of biochar as adsorption matrix – A review from a lifecycle perspective. *Bioresource Technology*. Elsevier Ltd December 1, 2017, pp 135–141. doi:10.1016/j.biortech.2017.08.041.
19. Qiu, B.; Shao, Q.; Shi, J.; Yang, C.; Chu, H. Application of biochar for the adsorption of organic pollutants from wastewater: Modification strategies, mechanisms and challenges. *Separation and Purification Technology*. Elsevier B.V. November 1, 2022. doi:10.1016/j.seppur.2022.121925.

20. Stylianou, M.; Christou, A.; Michael, C.; Agapiou, A.; Papanastasiou, P.; Fatta-Kassinou, D. Adsorption and removal of seven antibiotic compounds present in water with the use of biochar derived from the pyrolysis of organic waste feedstocks. *Journal of Environmental Chemical Engineering* **2021**, *9*(5), 105868. doi:10.1016/j.jece.2021.105868.
21. Luo, Z.; Yao, B.; Yang, X.; Wang, L.; Xu, Z.; Yan, X.; et al. Novel insights into the adsorption of organic contaminants by biochar: A review. *Chemosphere* **2022**, *287*. doi:10.1016/j.chemosphere.2021.132113.
22. Peng, X.; Ou, W.; Wang, C.; Wang, Z.; Huang, Q.; Jin, J.; et al. Occurrence and ecological potential of pharmaceuticals and personal care products in groundwater and reservoirs in the vicinity of municipal landfills in China. *Science of the Total Environment* **2014**, *490*, 889–898. doi:10.1016/j.scitotenv.2014.05.068.
23. Jin, R.; Zhao, C.; Song, Y.; Qiu, X.; Li, C.; Zhao, Y. Competitive adsorption of sulfamethoxazole and bisphenol A on magnetic biochar: Mechanism and site energy distribution. *Environmental Pollution* **2023**, *329*. doi:10.1016/j.envpol.2023.121662.
24. Lee, H. S.; Shin, H. S. Competitive adsorption of heavy metals onto modified biochars: Comparison of biochar properties and modification methods. *Journal of Environmental Management* **2021**, *299*. doi:10.1016/j.jenvman.2021.113651.
25. Meng, Z.; Xu, T.; Huang, S.; Ge, H.; Mu, W.; Lin, Z. Effects of competitive adsorption with Ni(II) and Cu(II) on the adsorption of Cd(II) by modified biochar co-aged with acidic soil. *Chemosphere* **2022**, *293*. doi:10.1016/j.chemosphere.2022.133621.
26. Deng, Y.; Huang, S.; Dong, C.; Meng, Z.; Wang, X. Competitive adsorption behaviour and mechanisms of cadmium, nickel and ammonium from aqueous solution by fresh and ageing rice straw biochars. *Bioresource Technology* **2020**, *303*. doi:10.1016/j.biortech.2020.122853.
27. Martínez-Costa, J. I.; Leyva-Ramos, R.; Padilla-Ortega, E.; Aragón-Piña, A.; Carrales-Alvarado, D. H. Antagonistic, synergistic and non-interactive competitive sorption of sulfamethoxazole-trimethoprim and sulfamethoxazole-cadmium (ii) on a hybrid clay nanosorbent. *Science of the Total Environment* **2018**, *640–641*, 1241–1250. doi:10.1016/j.scitotenv.2018.05.399.
28. Reguyal, F.; Sarmah, A. K. Adsorption of sulfamethoxazole by magnetic biochar: Effects of pH, ionic strength, natural organic matter and 17 α -ethinylestradiol. *Science of the Total Environment* **2018**, *628–629*, 722–730. doi:10.1016/j.scitotenv.2018.01.323.

29. Liu, L.; Deng, G.; Shi, X. Adsorption characteristics and mechanism of p-nitrophenol by pine sawdust biochar samples produced at different pyrolysis temperatures. *Scientific Reports* **2020**, *10*(1). doi:10.1038/s41598-020-62059-y.
30. Tan, Z.; Zhang, X.; Wang, L.; Gao, B.; Luo, J.; Fang, R.; et al. Sorption of tetracycline on H₂O₂-modified biochar derived from rape stalk. *Environmental Pollutants and Bioavailability* **2019**, *31*(1), 198–207. doi:10.1080/26395940.2019.1607779.
31. Chen, W.; Gong, M.; Li, K.; Xia, M.; Chen, Z.; Xiao, H.; et al. Insight into KOH activation mechanism during biomass pyrolysis: Chemical reactions between O-containing groups and KOH. *Applied Energy* **2020**, *278*. doi:10.1016/j.apenergy.2020.115730.
32. Huff, M. D.; Lee, J. W. Biochar-surface oxygenation with hydrogen peroxide. *Journal of Environmental Management* **2016**, *165*, 17–21. doi:10.1016/j.jenvman.2015.08.046.
33. Lü, F.; Lu, X.; Li, S.; Zhang, H.; Shao, L.; He, P. Dozens-fold improvement of biochar redox properties by KOH activation. *Chemical Engineering Journal* **2022**, *429*. doi:10.1016/j.cej.2021.132203.
34. Chen, B.; Zhou, D.; Zhu, L. Transitional adsorption and partition of nonpolar and polar aromatic contaminants by biochars of pine needles with different pyrolytic temperatures. *Environmental Science and Technology* **2008**, *42*(14), 5137–5143. doi:10.1021/es8002684.
35. Xiao, X.; Chen, Z.; Chen, B. H/C atomic ratio as a smart linkage between pyrolytic temperatures, aromatic clusters and sorption properties of biochars derived from diverse precursory materials. *Scientific Reports* **2016**, *6*. doi:10.1038/srep22644.
36. Tan, X. F.; Zhu, S. S.; Wang, R. P.; Chen, Y. Di; Show, P. L.; Zhang, F. F.; et al. Role of biochar surface characteristics in the adsorption of aromatic compounds: Pore structure and functional groups. *Chinese Chemical Letters*. Elsevier B.V. October 1, 2021, pp 2939–2946. doi:10.1016/j.ccllet.2021.04.059.
37. Zhang, X.; Xiong, Y.; Wang, X.; Wen, Z.; Xu, X.; Cui, J.; et al. MgO-modified biochar by modifying hydroxyl and amino groups for selective phosphate removal: Insight into phosphate selectivity adsorption mechanism through experimental and theoretical. *Science of the Total Environment* **2024**, *918*. doi:10.1016/j.scitotenv.2024.170571.
38. Waghchaure, R. H.; Adole, V. A.; Jagdale, B. S. Photocatalytic degradation of methylene blue, rhodamine B, methyl orange and Eriochrome black T dyes by modified ZnO nanocatalysts:

- A concise review. *Inorganic Chemistry Communications*. Elsevier B.V. September 1, 2022. doi:10.1016/j.inoche.2022.109764.
39. Santoso, E.; Ediati, R.; Kusumawati, Y.; Bahruji, H.; Sulistiono, D. O.; Prasetyoko, D. Review on recent advances of carbon based adsorbent for methylene blue removal from waste water. *Materials Today Chemistry*. Elsevier Ltd June 1, 2020. doi:10.1016/j.mtchem.2019.100233.
40. Cheng, Y.; Wang, B.; Shen, J.; Yan, P.; Kang, J.; Wang, W.; et al. Preparation of novel N-doped biochar and its high adsorption capacity for atrazine based on π - π electron donor-acceptor interaction. *Journal of Hazardous Materials* **2022**, 432. doi:10.1016/j.jhazmat.2022.128757.
41. Chen, M.; Yan, Z.; Luan, J.; Sun, X.; Liu, W.; Ke, X. π - π electron-donor-acceptor (EDA) interaction enhancing adsorption of tetracycline on 3D PPY/CMC aerogels. *Chemical Engineering Journal* **2023**, 454. doi:10.1016/j.cej.2022.140300.
42. Pan, J.; Zhou, L.; Chen, H.; Liu, X.; Hong, C.; Chen, D.; et al. Mechanistically understanding adsorption of methyl orange, indigo carmine, and methylene blue onto ionic/nonionic polystyrene adsorbents. *Journal of Hazardous Materials* **2021**, 418. doi:10.1016/j.jhazmat.2021.126300.
43. Gupta, M.; Srivastava, A.; Srivastava, S. Molecular quantum mechanics of rapid oxidation of acetaminophen BY sodium periodate at alkaline pH. In *Materials Today: Proceedings*; Elsevier Ltd, 2021; Vol. 50, pp 1173–1180. doi:10.1016/j.matpr.2021.08.050.
44. Peiris, C.; Fernando, J. C.; Alwis, Y. V.; Priyantha, N.; Gunatilake, S. R. An insight into the sorptive interactions between aqueous contaminants and biochar. In *Sustainable Biochar for Water and Wastewater Treatment*; Elsevier, 2022; pp 643–666. doi:10.1016/B978-0-12-822225-6.00020-8.

Chapter 5

5 Production of Magnetic Biochar via Co-Pyrolysis with Red Mud and Investigation of Adsorption Mechanisms

5.1 Statement of Authorship

The contents and data of the following chapter have been published in the journals of Waste Management, Analytical and Applied Pyrolysis, and the Canadian journal of Chemical Engineering under a title of the references shown below. The author of this thesis was responsible for a majority of the work herein, including experimental design and execution biochar characterization, adsorption experimentation, data processing and analysis, as well as the writing of the manuscript and participating in the editing and review of the manuscript. The author also aided Dr. Kang in the initial preparation and synthesis of composites. Dr. Sarchami helped to perform some elemental analysis including CHNS-O and ICP analysis, and some of the pyrolysis and physical activation of samples were performed by Dr.Papari. Magnetic susceptibility tests were performed by Dr. Bartoli, Dr. Torsello, and Dr. Gerbaldo. Editing and revision was done with the help of supervisors Dr. Yeung, Dr. Berruti and Dr. Klinghoffer.

Loebsack, G.; Kang, K.; Yeung, K. K.-C.; Bartoli, M.; Berruti, F.; Klinghoffer, N. Magnetic Adsorbents from Co-Pyrolysis of Non-woody Biomass and Red Mud for Water Decontamination. *Can. J. Chem. Eng.* **2024**. doi:10.1002/cjce.25407.

Loebsack, G.; Kang, K.; Klinghoffer, N.; Yeung, K. K.-C.; Torsello, D.; Gerbaldo, R.; Berruti, F. Adsorption Mechanisms and Optimal Production of Magnetic Red Mud Biochar Composites from Soft Wood Biomass. *J. Anal. Appl. Pyrolysis.* **2023**, 106340, doi:10.1016/j.jaap.2023.106340

Kang, K*.; **Loebsack, G.;** Sarchami, T.; Klinghoffer, N.; Papari, S.; Yeung, K. K.-C.; Berruti, F. Production of a bio-magnetic adsorbent via co-pyrolysis of pine wood waste and red mud. *J. Waste Manag.* **2022**, 149, 124-133. doi:10.1016/j.wasman.2022.06.009.

5.2 Chapter Abstract

Red mud (RM), and woody and non-woody biomasses are all underutilized resources for renewable composite materials, which could be used in environmental decontamination processes. This study aims to investigate the efficacy of co-pyrolyzing Douglas fir, pine wood, red cedar, miscanthus, phragmites, and switch grass with RM to produce magnetic biochar composites. When pyrolyzed, RM is reduced to magnetic iron while biochar portion is responsible for the adsorption of organic compounds. Ibuprofen, acetaminophen, methyl orange, and methylene blue were used as test compounds to investigate the overall adsorptive capacity of the composite and to determine the possible adsorption mechanisms. This study reveals the impacts of pyrolysis temperatures of 500, 650, and 800 °C, biomass precursors, and H₂O₂ post-treatment on the physical and adsorptive properties of the resulting adsorbent. The optimum biomass-to-biochar ratio was also studied to determine the optimal magnetic and adsorptive properties of composites produced for miscanthus, pinewood and Douglas fir biomasses. The composite produced from a 1-1 mixture of RM and miscanthus showed the highest adsorption capacity of composites produced from the non-woody biomasses, with 13.8 and 8.34 mg/g of ibuprofen and acetaminophen adsorbed, respectively. This is attributed to its greater π -interactions as a result of lower surface oxygen sites. The overall best-performing magnetic adsorbent capable of adsorbing up to 32.8 mg/g of acetaminophen was able to be produced by co-pyrolyzing red mud and pine wood biomass at a 9:1 ratio.

5.3 Introduction

Rapid accumulation of waste biomass is an ever-growing global issue that calls for effective means of minimization, and more ideally, conversion into value-added products (1). Production of biochar through pyrolysis is an emerging sustainable treatment method suitable for upgrading biomass into value-added adsorbents (2). However, production of high-quality biochar adsorbent requires high temperatures and suffers from low yields (3). Moreover, the use of biochar adsorbent in open water sources is hampered by the difficulty of separation after adsorption and results in the risk of secondary pollution (4). Depending on the density and porosity, biochar or portions of biochar may float on water, causing difficulties in properly mixing to ensure effective mass transfer. As a result, it is highly desirable to develop the high-performing magnetic biochar which can be recovered easily after use

Red mud (RM) is an industrial waste generated from the alumina production process (5). Its production is estimated to be approximately 100 million tonnes per year worldwide (6). The high generation of RM has posed environmental problems due to its high alkalinity and significant accumulation occupying cultivated land (7). This has resulted in soil alkalization, groundwater pollution, as well as air pollution (8). Earlier studies have demonstrated that RM, containing Fe_2O_3 , Al_2O_3 , SiO_2 , TiO_2 , Na_2O , and CaO , could potentially become a novel feedstock for pyrolysis to produce an adsorbent for the removal of compounds, including heavy metal ions, dyes, phenolic pollutants, and inorganic anions (9–11).

Because of the availability of Fe in RM, co-pyrolyze RM with biomass to produce the magnetic adsorbent represents a novel and simplified approach (12). The transition of Fe_2O_3 to Fe_3O_4 is often observed when RM is co-pyrolyzed with lignin (13). The transition of iron species is caused by the reduction of Fe_2O_3 , which is promoted by electrons released by the thermal degradation of the biomass, and the reducing agent may be reductive gaseous products such as CO, H_2 , and some condensable hydrocarbons. According to Cho et al. (2019), the consecutive reduction of Fe_2O_3 occurs within the temperature range of 380 and 700 °C and can lead to the formation of the metallic Fe phase ($\text{Fe}_2\text{O}_3 \rightarrow \text{Fe}_3\text{O}_4 \rightarrow \text{FeO} \rightarrow \text{Fe}$) (14). As the iron oxide is reduced to metallic iron, it gains 4 unpaired electrons as opposed to two unpaired, giving the final product more paramagnetic properties than the non-pyrolyzed RM. Magnetic adsorbents are significantly more attractive for water purification than non-magnetic adsorbents as they can be separated easily with a magnetic field for regeneration and reuse (15). The current magnetic biochar synthesis methods include impregnation-pyrolysis, co-precipitation, reductive co-deposition, and hydrothermal carbonization (16). However, they are still under investigation due to the consumption of fine chemicals (e.g., transition metal salts, metal hydroxides), complicated operating procedures, and relatively high costs.

A study on the reaction mechanism is needed to understand how the simultaneous minimization of biomass and RM was achieved. It is reported that the magnetic adsorbents synthesized by this approach are effective in the removal of different metal species, including Pb (II) (12,17–19). However, the adsorption performance of organic compounds, such as pharmaceuticals and dyes, is rarely explored. The goal of this work is to study the properties and adsorption mechanisms of the composites produced by the co-pyrolysis of RM and different

biomasses: red cedar (RC), Douglas fir (DF), pine wood (PW), miscanthus (MC), switch grass (SG), and phragmites (PH), at different temperatures and after H₂O₂ post treatments. The effect of different types of lignocellulosic biomass on the adsorptive properties of four RM composites is investigated and the impact of aromaticity and surface functional groups on the adsorption mechanisms of the composites are explored using ibuprofen (IBU), acetaminophen (ACT), methyl orange (MO), and methylene blue (MB) as representative test molecules of adsorbate organic contaminant with different characteristics. Furthermore, the optimal conditions to produce RM-biomass composites are investigated to produce optimized adsorbents with magnetic properties.

5.4 Materials and Methods

5.4.1 Materials

Red mud (RM) was received from Alcan International Ltd., Canada in slurry form. The sample was dried in a muffle oven at 105 °C for 12 hours and then crushed into powder manually.

The pinewood (PW), Douglas fir (DF), and red cedar (RC) chips were collected from a local furniture manufacturer in London, Ontario, Canada. Before use, the PW, DF, HL, and RC were pulverized using a blade grinder mill (VM 0197, Vitamix, USA) and sieved to the particle size range of 0.3 to 0.6 mm measured using standard test sieves produced by W. Tyler, USA.

Four types of common non-woody biomass were used: switch grass (SG), miscanthus (MC), and phragmites (PH), which were collected from near London, Ontario, Canada. Before the co-pyrolysis, the biomasses were pulverized using a blade grinder mill (VM 0197, Vitamix, USA) and sieved to the particle size range of 0.3-0.6 mm using standard test sieves (W.S. Tyler, USA).

The compressed CO₂ gas was purchased from Praxair Canada Inc.

Methylene blue (MB) (product #7220793), 85% methyl orange (MO) (product #1002790460), >98% ibuprofen (IBU) (product #102051532), and >98% acetaminophen (ACT) (product #1002893831) used as adsorbates were purchased from Sigma Aldrich, Canada.

5.4.2 Co-Pyrolysis Procedure

All the bio-magnetic adsorbents were synthesized using the co-pyrolysis method. For each run, ~30 g of feedstock mixture was loaded into a split furnace (Lindberg STF55666C Blue M,

Thermo Scientific, USA) and pyrolyzed at 800 °C under a constant CO₂ flow rate of 500 mL/min. The mixture containing RM and biomass had a mass ratio of either 2:1, 1:1, 1:2, or 1:9. Following 30 min of CO₂ flow, the furnace temperature was elevated from ambient to 800 °C with a ramping rate of 10 °C/min, and the target temperature was held for 3 hours. Afterward, the CO₂ flow was kept on while the furnace was cooled down to ambient temperature before the biochar sample collection. The adsorbents are named “RM/Biomass-x/y”, where “x/y” indicates the mass ratio of RM to biomass loaded. As an example, “RM/SG-1/1” means that the adsorbent is prepared by the co-pyrolysis of a mixture containing a 1/1 mass ratio of RM and SG at 800 °C.

5.4.3 H₂O₂ Post Treatment

H₂O₂ post-treatment was based on the method by Huff et al. (20), where treatment of composite biochars was done by separately mixing 5g of each biochar with 25 mL of 9.8 M H₂O₂ at room temperature for 1 hour before being filtered through Whatman filter paper No. 1 and being washed with DI-water. The oxidized biochar is then dried at 105°C overnight.

5.4.4 Biochar Characterization Methods

5.4.4.1 BET Surface area

Samples were tested for Brunauer-Emmett-Teller (BET) with Nova 2000e Surface Area and Pore Size Analyzer (Quantachrome Instrument, Florida, US). The physisorption measurements were performed via N₂ adsorption-desorption experiments at 77.35 K. Samples were degassed at 105°C for 1 hour to remove moisture, then the temperature was increased to 300°C and maintained for at least 3 hours before analysis.

5.4.4.2 ATR-FTIR Spectroscopy

The surface organic functional groups present in the samples were detected using Fourier transform infrared spectroscopy (FT-IR) using a Platinum[®] attenuated total reflectance (Pt-ATR) attachment equipped with a diamond crystal in the main box of a Bruker Tensor II spectrometer. During the analysis, the sample in powder form was scanned within the range of 400-4000 cm⁻¹ at a resolution of 4 cm⁻¹ under transmittance mode and 32 accumulations for each spectrum.

5.4.4.3 SEM-EDX Spectroscopy

The samples were analyzed by SEM-EDX using a Hitachi SU3500 Scanning Electron Microscope (SEM) combined with an Oxford AZtec X-Max50 SDD energy dispersive X-ray

(EDX) detector. EDX is a semi-quantitative technique that can detect all elements with a minimum detection limit of approximately 0.5 wt%. EDX spectra from individual particles were analyzed using a vector-based algorithm to determine the relative abundance of 10 elements: carbon (C), sodium (Na), magnesium (Mg), aluminum (Al), silicon (Si), potassium (K), calcium (Ca), titanium (Ti), oxygen (O), and iron (Fe). A 10 kV accelerating voltage was used for these analyses. The samples were coated with a thin layer of gold to minimize charging effects.

5.4.4.4 CHNS-O, ICP and Proximate analysis

The proximate analysis of the biomass samples was performed following the ASTM standard (ASTM D1762-84) using a Neytech Vulcan D-550 muffle oven. Elemental analysis of carbon, hydrogen, nitrogen, and sulphur is undertaken using the model Thermo Flash EA 1112 series CHNS analyzer (Thermo Fisher Scientific, USA). Samples are combusted at 900 °C under helium with a known amount of oxygen. The oxygen content in the sample is calculated by mass difference. The elemental analysis for the RM-containing products was performed using inductively coupled plasma–mass spectrometry (ICP-MS) using an Agilent 1260 infinity HPLC connected directly to an Agilent 7700 series ICP-MS. The results were measured in triplicates and presented as averages with standard deviations.

5.4.5 Magnetic Susceptibility Tests

RM and biochar composites were dispersed into a polymeric matrix using ultrasonication with two components BFA diglycidyl resin purchased from CORES (Cores epoxy resin, LPL). The curing agent was a mix of primary dispersion amines and DMP-30 which promoted a two-step polymerization. The ultrasounds were pulsed with cycles of 20 seconds alternating with a pause of 10 seconds to allow better heat diffusion. After the addition of the curing agent, the mixture was further ultrasonicated for 2 min and left in the moulds for 16 h at room temperature. A final thermal curing was performed using a ventilated oven (I.S.C.O. Srl “The scientific manufacturer”) at 70 °C for 6 h. Magnetic properties were investigated with a DC magnetometer/AC susceptometer (Lakeshore 7225) equipped with an electromagnet at room temperature in quasi-static conditions. Magnetic hysteresis cycle measurements were performed on the composite samples up to 30 kA/m to estimate the main magnetic parameters of the materials (i.e., magnetic susceptibility, coercive force, and magnetic hysteresis loss calculated from the area of hysteresis loop). The mass magnetic susceptibility, χ_p , is computed as the slope of the low field first magnetization branch of the

hysteresis loop. The composite sample's weight was measured and the filler wt.% is known from the preparation, allowing the magnetic characterization of the filler alone, since the signal from the polymeric matrix is negligible.

5.4.6 Adsorption Mechanisms Tests

The mechanisms for adsorption were determined by placing 0.1 g of each adsorbent sample in a 20.0 mL test tube containing 15 mL solution of 1 mM H₃PO₄ and 50 ppm of the test compound at the desired pH. Adsorption experiments were carried out at relative pH values of 2, 6, 8, and 11. The pH was controlled with a phosphate buffer, prepared with 3 mM H₃PO₄, and the pH was adjusted by adding NaOH. Samples were agitated for 1 hour at 25 °C and filtered through Whatman No. 1 filter paper. The pH of the filtrate was determined after filtering using a pH meter (Thermo Scientific, Orion Star). The concentration of adsorbate remaining in the filtrate was determined at 220, 243, 464, and 668 nm for IBU, ACT, MO, and MB using a UV-visible spectrophotometer (Thermo Scientific, Evolution 220). Samples were analyzed in triplicates, and their average absorbances were reported. The adsorption capacity was defined as the amount of chemically adsorbed on the unit mass of the tested adsorbent (mg/g).

5.5 Results and Discussion

Before the synthesis of the adsorbents, it is important to understand the chemical compositions of the raw materials used. The chemical compositions of the RM and the four woody biomasses are provided in **Table 5.1**. As shown in the table, RM has a high Fe content of 33.28 wt%, therefore it is expected to be the major source of iron in the solid phase co-pyrolysis product, which will be the primary contributor to the magnetic properties. Non-woody showed a higher ash content (3.3-12.8 wt%) and lower carbon content (37.0-44.6 wt%), compared to the softwood biochars which had ash ranging from 0.41-3.11 wt % and carbon content from 42.97-46.11 wt%. For the application as adsorbents, having higher carbon content is desirable as after the co-pyrolysis, the bio-magnetic composite produced will only present biochar-like properties when there is sufficient carbon retained in the solid product (19).

Table 5.1 Elemental composition of red mud and biomasses

Elements	O	Fe	Al	Ti	Na	Si	C	Ca
Red Mud	35.75	33.28	10.73	6.55	5.05	4.31	3.01	1.12
(wt%)								
Biomass	Proximate analysis (wt%)				Elemental analysis (wt%)			
	Moisture	Volatile Matter	Ash	Fixed carbon	C	H	N	O**
Pine Wood	7.71	76.90	0.41	14.98	46.11	5.90	0.16	47.83
	±0.05	±0.9	±0.1	±1.0	±0.1	±0.1	±0.5	±0.5
Douglas Fir	10.78	63.93	2.27	33.80	46.00	5.49	0.38	48.12
	±0.05	±0.4	±0.01	±0.3	±0.1	±0.1	±0.5	±0.5
Red Cedar	8.81	75.52	1.10	23.37	42.97	0.397	1.06	40.77
	±0.05	±1.1	±0.1	±0.9	±0.1	±0.1	±0.5	±0.5
Switch Grass	9.2	75.4	3.3	21.2	39.4	5.1	1.1	54.4
	±0.4	±0.3	±0.3	±0.1	±0.1	±0.1	±0.5	±0.5
Miscanthus	8.4	71.9	5.5	22.6	44.1	5.9	0.7	49.3
	±0.5	±0.1	±0.3	±0.1	±0.1	±0.1	±0.5	±0.5
Phragmites	9.4	67.9	6.5	25.9	44.6	6.3	1.46	47.6
	±0.3	±0.3	±0.3	±0.3	±0.1	±0.1	±0.5	±0.5

5.5.1 Investigation of Physical Characteristics of Biochar RM Composite

After the co-pyrolysis, SEM-EDX characterizations were conducted to study the morphological properties of the adsorbents. As shown in **Figure 5.1**, the solid product out of the co-pyrolysis consists of different particles with non-uniform shapes and sizes. Some of the particles originate from the RM while others are derived mainly from the biomass particles in the

raw material mixture. Looking at the 400X magnification images, the particles are formed by the interaction of RM and the biomass. Specifically, the cylindrical particle in the center of **Figure 1b** for example, shows an open porous structure that is characteristic of biochar and cannot be produced by the pyrolysis of RM (22). On the surface and in the exposed pores of the base, the significantly smaller spherical particles which are the pyrolyzed RM particles can be found bonded to the surface. These particles appear to range from 50 to $>10\mu\text{m}$ while the larger biomass particles were in the range of 100-200 μm in length for all of the biomasses investigated.

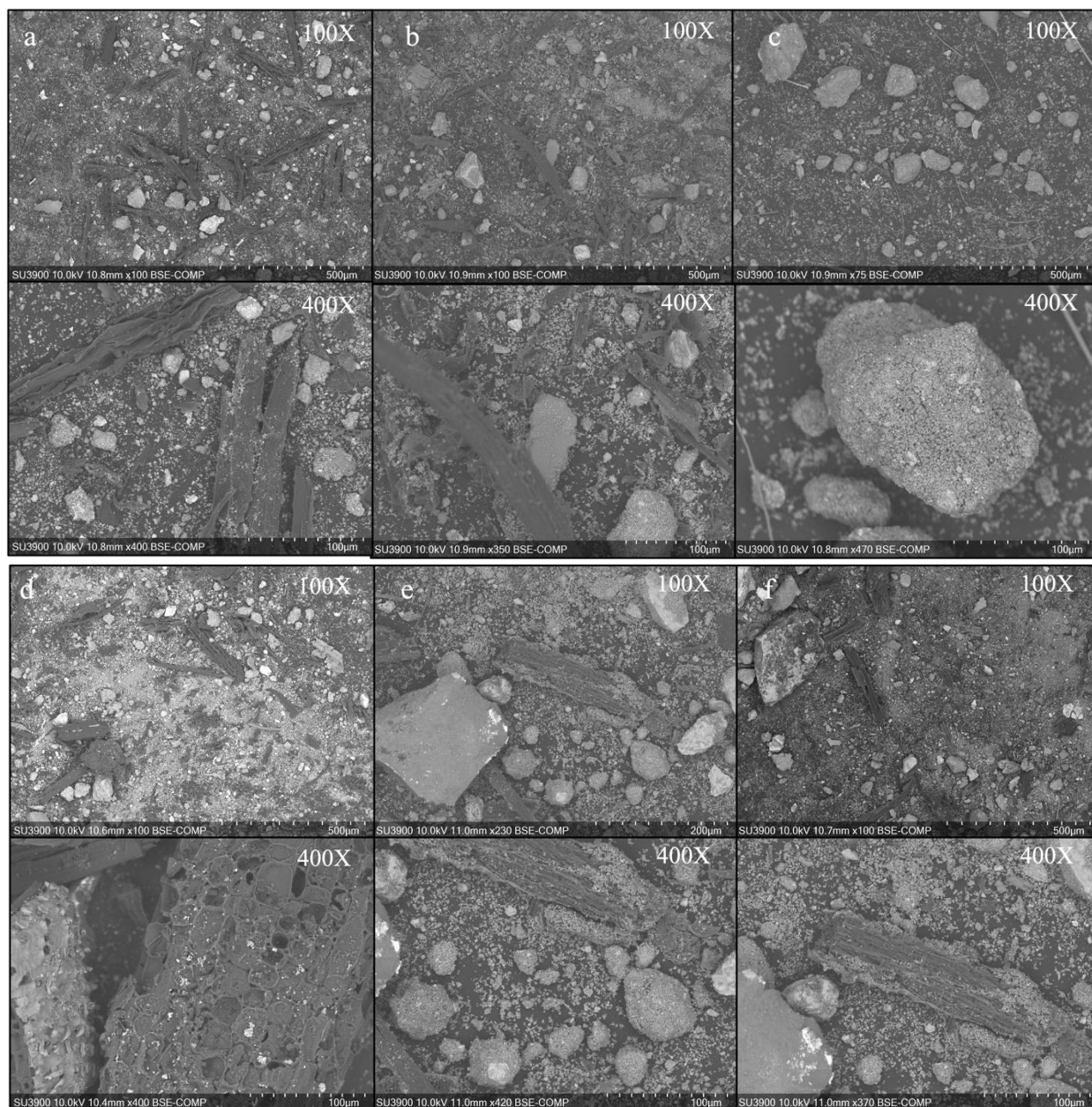


Figure 5.1 SEM images at 100X and 400X Magnification of a) RM/RC-1/1, b) RM/DF-1/1, c) RM/PW-1/1, d) RM/MC-1/1, e) RM/PH-1/1, and f) RM/SG-1/1

To further identify the elemental composition of the formed bio-magnetic adsorbents, EDX elemental analysis was performed at different spots and the results are provided in **Figure 5.1**. As shown in the figure on Spectrum 1 of **Figure 5.1a**, the most dominant elements are carbon and oxygen, accounting for 84.9 wt% and 10 wt%, respectively. This was consistent with all the other samples investigated as well. This suggests that the particles are mainly comprised of carbon similar to biochar, making it desirable for the adsorbent application as biochar normally exhibits high porosity and surface area, as well as different types of functional groups (23). Based on Spectrum 2 in **Figure 5.1a**, the most dominant elements, other than oxygen are Ca (18.3 wt%), Al (14.5 wt%), and Fe (13.1 wt%). Therefore, the small particles represented by Spectrum 2 result from the pyrolysis of RM, and the presence of Fe-containing species enables the particle to become magnetically separable, which is a benefit of bio-magnetic adsorbent. Specifically, conventional biochar might show excellent adsorption performance, but its low density increases the flow instability in water bodies and might cause difficulty in tracking and separation. In contrast, the bio-magnetic adsorbent could be separated using an external magnetic field, therefore preventing the risk of secondary pollution and easing the regeneration and reuse (24). The SEM images and the EDX spectra together show that the particles produced by co-pyrolysis can have different elemental compositions including biochar-like properties to promote the adsorption and magnetic properties to ease the separation from water after adsorption.

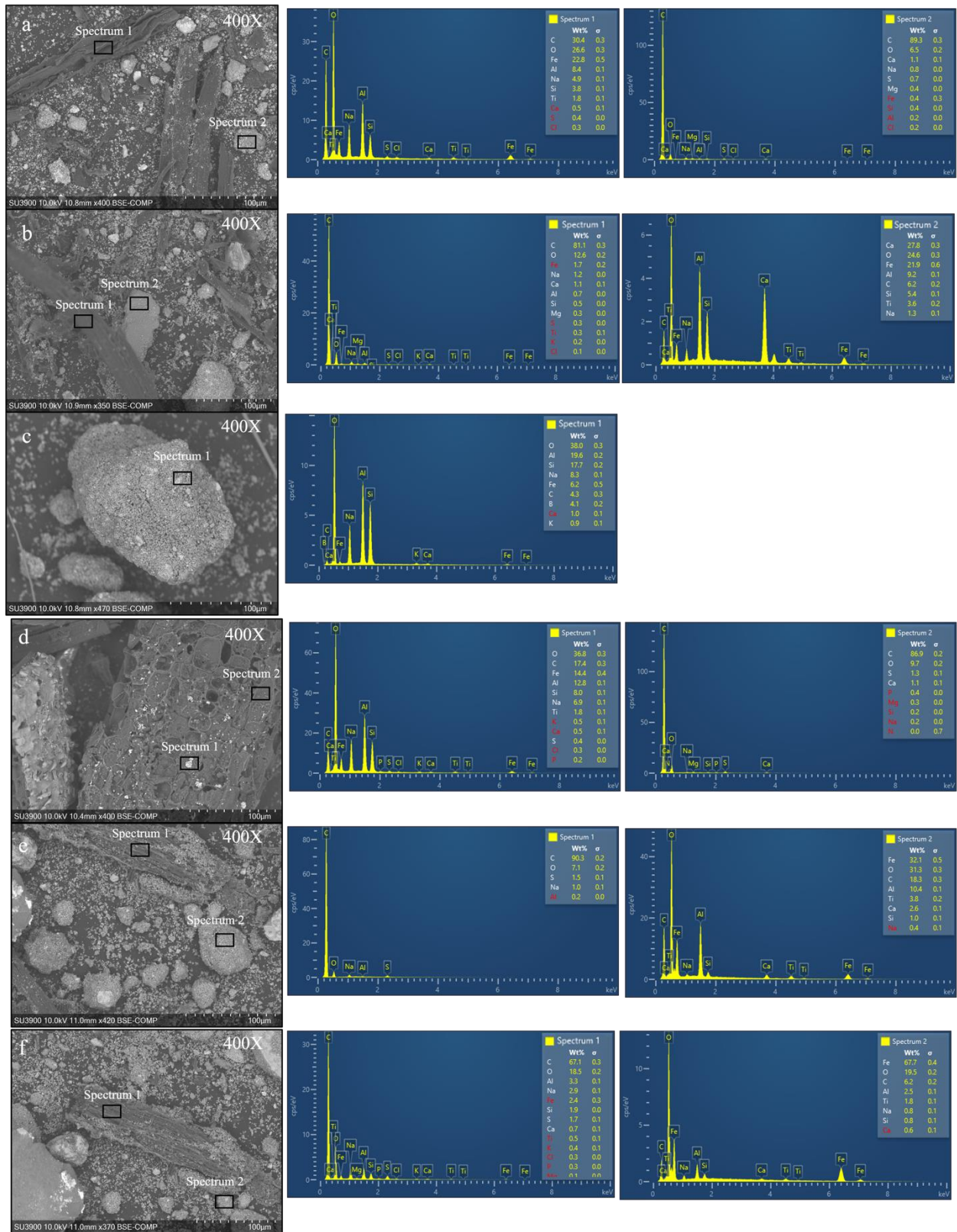


Figure 5.2 100X magnification SEM images and EDX spectra of a) RM/RC-1/1, b) RM/DF-1/1, c) RM/PW-1/1, d) RM/MC-1/1, e) RM/PH-1/1, and f) RM/SG-1/1

When looking at the adsorption capacity of composites and biochars reported in **Table 5.2**, the adsorption of all the organic compounds tested by RM and RM800 is 0 mg/g. There is a negative correlation between the ratio of RM to biochar and overall adsorptive capacity. In other words, the greater the mass of biomass in the feedstock, the greater the adsorption capacity of the pyrolytic product. This indicates that the biochar portion of the composite contributes entirely to the adsorptive character of the composite. The RM is then only added to provide magnetic properties to the final composite due to the presence of iron oxide in the RM particles. This is important to remember when investigating adsorption mechanisms, as it is only the biochar portion that significantly affects the adsorptive properties of the resulting final composite.

To determine whether the RM had any catalytic effect on the decomposition of the feedstock during pyrolysis, the yields of the pyrolytic products of the RM, feedstocks, and combined composites were investigated and are presented in **Table 5.2**. The theoretical yield was found to be within the variability of the experimental yields for all biomasses tested both woody and non-woody, thus confirming that there was no catalytic effect by the RM on the decomposition of the biomass. Therefore, it can be stated that, if the RM contributes only to the magnetic properties of the final product, the adsorption mechanisms of the biochar of biomass and the composite produced via co-pyrolysis with RM will be congruent. Thus, the following investigation on the effect of feedstock composition on the adsorption mechanisms applies to the behaviour of both the biochar and the corresponding RM composites.

Table 5.2 Yields, physical properties, and adsorption capacities of biochar and composite adsorbents

Sample Name	Yield (wt%)	Variability * (\pm wt%)	Theoretical yield (wt%)	Variability y* (\pm wt%)	Surface area (m ² /g)	Average pore volume (cm ³ /g)	Average pore diameter (nm)	Max. adsorption capacity of ACT (mg/g)
Raw RM	-	-	-	-	41.92	0.045	2.15	0
RM800	71.78	6.52	-	-	12	0.02	3.45	0
SG800	22.1	-	-	-	75.6	0.037	1.98	5.72
MC800	19.6	-	-	-	369	0.20	2.19	12.5
PH800	23.4	-	-	-	204	0.11	2.19	10.8

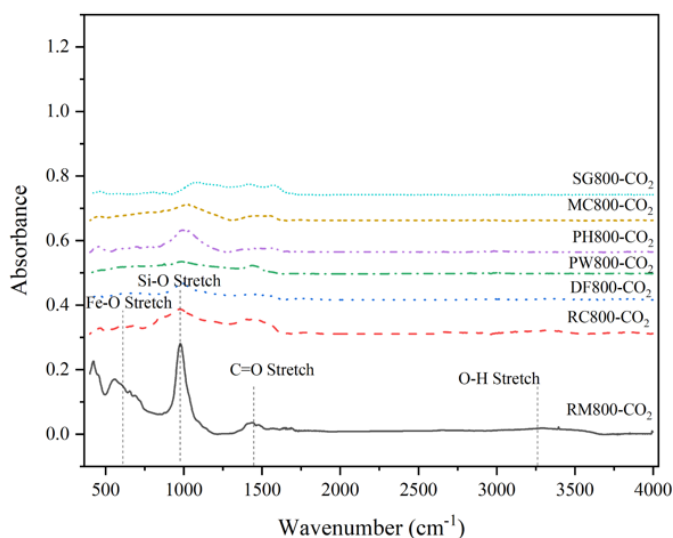
PW800	11.67	3.83	-	-	522	0.31	1.20	31.8
RC800	8.27	2.98	-	-	448	0.30	0.27	30.5
DF800	21.18	5.98	-	-	461	0.29	0.25	35.2
<hr/>								
1:1 RM:SG 800	47.04	-	-	-	49.0	0.044	3.56	4.03
1:1 RM:MC 800	43.40	-	-	-	67.4	0.054	3.22	10.7
1:1 RM:PH 800		-	-	-	62.6	0.050	3.86	4.79
1:1 RM:PW 800	54.13	-	41.73	7.56	54	0.054	2.00	6.81
1:1 RM:RC 800	47.86	-	40.03	7.17	106	0.083	0.16	10.2
1:1 RM:DF 800	45.45	-	46.48	8.85	105	0.084	0.16	9.49
<hr/>								
2:1 RM:MC 800	56.18	-	-	-	-	-	-	25.9
1:1 RM:MC 800	43.40	-	-	-	67.4	0.054	3.22	10.7
1:2 RM:MC 800	38.19	-	-	-	-	-	-	2.60
<hr/>								
2:1 RM:DF 800	56.88	-	62.39	8.85	-	-	-	6.16
1:1 RM:DF 800	45.45	-	62.96	8.85	105	0.084	0.16	9.49
1:2 RM:DF 800	36.16	-	55.28	8.85	-	-	-	13.4
<hr/>								
2:1 RM:PW 800	54.5	-	62.37	7.56	-	-	-	0.178
1:1 RM:PW 800	54.13	-	64.33	7.56	54	0.054	2	6.81
1:2 RM:PW 800	42.43	-	53.68	7.56	-	-	-	12.0
1:9 RM:PW 800	25.6	-	39.72	7.56	-	-	-	32.8
<hr/>								
1:1 RM:PW 500	57.70	-	-	-	72.5	0.058	1.60	-
1:1 RM:PW 650	47.04	-	-	-	103	0.074	1.43	-
1:1 RM:PW 800	54.13	-	64.33	7.56	54	0.054	2	6.81
<hr/>								
1:1 RM:PW 800- H ₂ O ₂	89.38	-	-	-	48.12	0.050	2.07	-

*Results reported based on 3 to 5 repeated preparation batches in the form of “average value ± standard deviation.”

The FT-IR spectra are plotted in **Figure 5.3**, the broad bands in the range of 3300 to 2900 cm⁻¹, which were present in the raw RM and biomass samples, disappeared for the spectra of all

composite adsorbents, suggesting the complete removal of surface -OH groups by dehydration. Other bands were observed at 1426-1423 cm^{-1} , and 972-969 cm^{-1} , 452-455 cm^{-1} on spectra of both RM and the adsorbents, which could be assigned to the stretching vibrations C=O, Si-O, and Fe-O groups (25). The intensities of the Si-O band decreased in the adsorbent due to the dissolution of silicate. The asymmetric and symmetric stretching vibration bands of (Al)O-H (3304 cm^{-1}) and AlO(OH) (3113 cm^{-1}) were observed on the raw RM (26), but not the adsorbents, indicating that they were destructed during the co-pyrolysis process. The FTIR spectra of the biochar without RM are significantly different than that of the composites as the RM portion absorbs so much of the incident light that little of the biochar portion is visible in the spectrum.

a



b

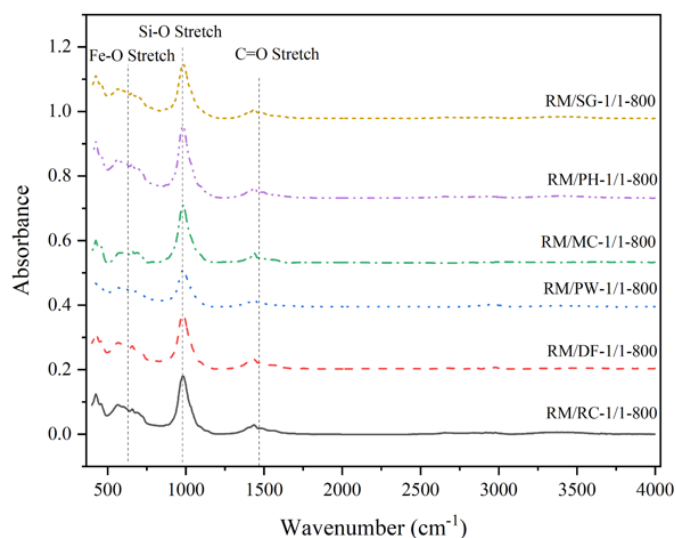


Figure 5.3 FTIR spectra of a) RC800-CO₂, DF800-CO₂, PW800-CO₂, MC800-CO₂, PH800-CO₂, and SG800-CO₂ and b) RM, and RM/biochar composites

5.5.2 Investigation on Effect of Pyrolysis Temperature on Biochar RM Composite

To study the influence of synthesis temperatures, a series of adsorbents were prepared at 550 °C, 650 °C, and 800 °C using RM and PW as the sample biomass. Importantly, it was found that only the composite produced at 800 °C maintained magnetic properties. Because of this, the 800 °C composites were the only composites investigated in further sections, though the properties of the 500 °C and 650 °C composites were investigated to understand the effects of

temperature on the production process. The mass yields and textural properties are given in **Table 5.2**. The yield results show that the yield of adsorbent decreased by ~10 wt% when the pyrolysis temperature increased from 500 to 650 °C; however, the drop of yield reduced to ~1.5 wt% when the temperature was further raised to 800 °C, which is supported by the results of TG/DTG analysis seen in **Figure 5.4**. Other than mass yield, the co-pyrolysis temperature also had significant impacts on the characteristics of the adsorbents.

On the other hand, the introduction of the biomass phase is expected to provide more surface area after the process. Interestingly, the surface area maximized at 102.78 m²/g at 650 °C then decreased to 54.23 m²/g at 800 °C. As the pore size indicates in **Table 5.2**, the prepared adsorbents showed an overall smaller average pore size than the RM. The fluctuations in total pore volume and average pore size with changing temperature could be explained by the pore enlargement and blockage of the pore mouth. Specifically, from 500 °C to 650 °C, the inner volumes of the pores increased while the pores decreased. This is possible because the thermal decomposition of the RM caused shrinkage of the metal oxides and silica, which increased the inner pore volume, whereas the average pore size decreased due to the blockage of the pore mouth caused by precipitation of condensed hydrocarbons on the adsorbent surface released by the de-volatilization of PW. When the temperature further increased from 650 °C to 800 °C, the decrease in the pore volume could be explained by their collapse, and the increase in average pore size could be the result of the pore collapse and the consumption of precipitated hydrocarbons during the reduction of the metals in the adsorbent. In addition, when reduced, the metals in the adsorbent, e.g., Fe, may become catalytically active and help to crack the precipitated hydrocarbons to increase the pore size (27).

The TGA profile in **Figure 5.4** also shows that RM is significantly more stable than any of the biomasses upon pyrolysis to 800 °C, shown by a low weight loss of 29.14 wt% for RM vs. 86.32 wt% for PW, for example. Therefore, after co-pyrolysis occurs at temperatures above 400 °C, the solid mass obtained for adsorption will mainly consist of the RM. **Figure 5.4** reveals that weight loss in both samples became negligible after 650 °C. For RM, the weight loss peaks occurring at 264 °C and 303 °C are due to the loss of absorbed H₂O and the removal of H₂O from Al(OH)₃ (28). The weight loss within the temperature range of 400–650 °C resulted from the release of CO₂ during the decomposition of CaCO₃ (29).

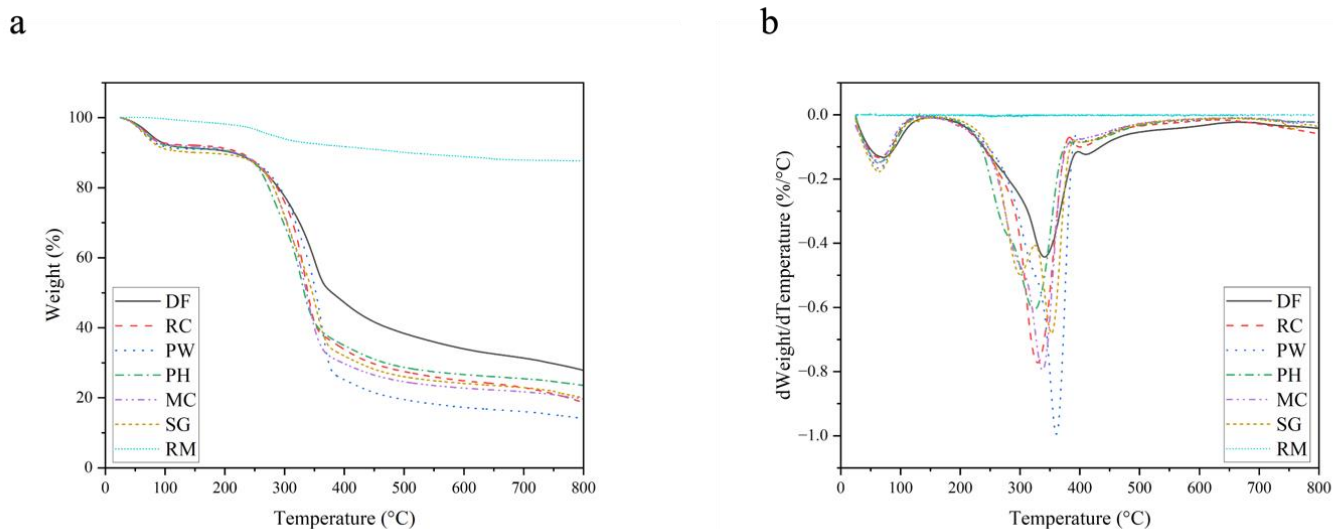


Figure 5.4 a) TGA and b) DTG curves for RM, RC, DF, PW, MC, PH, and SG up to 800 °C

To compare the influence of pyrolysis temperatures, adsorbent samples were prepared at 550 °C, 650 °C, and 800 °C. The mass yields textural properties and the elemental composition are given in **Table 5.2** where the yield of R-PW adsorbent was reported to be 47.04 wt% at 650°C, indicating that the co-pyrolysis at this temperature or higher could achieve the reduction of the mixture mass by more than 50 percent.

5.5.3 Investigation of Adsorption Properties of Biochar RM Composites

Figure 5.5 shows the adsorption capacities for ibuprofen (IBU), acetaminophen (ACT), methyl orange (MO), and methylene blue (MB) measured for four composites made from eight different types of softwood (DF, HL, PW, and RC) and non-woody biomasses (SG, RH, MC, and PH). To further study the adsorption mechanisms and to address whether adsorption is due to physical properties (surface area, pore size etc.) or surface chemistry (surface functional groups), more detailed characterizations of the bio-magnetic adsorbents were performed. **Table 5.2** shows the textural properties of the bio-magnetic composites. All of the adsorbent surface areas do not vary significantly, ranging from 47 m²/g (RM/RH-1/1) to 67 m²/g (RM/MC-1/1) for the non-woody derived composites, and around 100 m²/g for the woody derived composites. Their performance trends do not follow surface area trends, which suggests that the differences in adsorption were not due to differences in surface area but most likely due to chemical interactions on the surface.

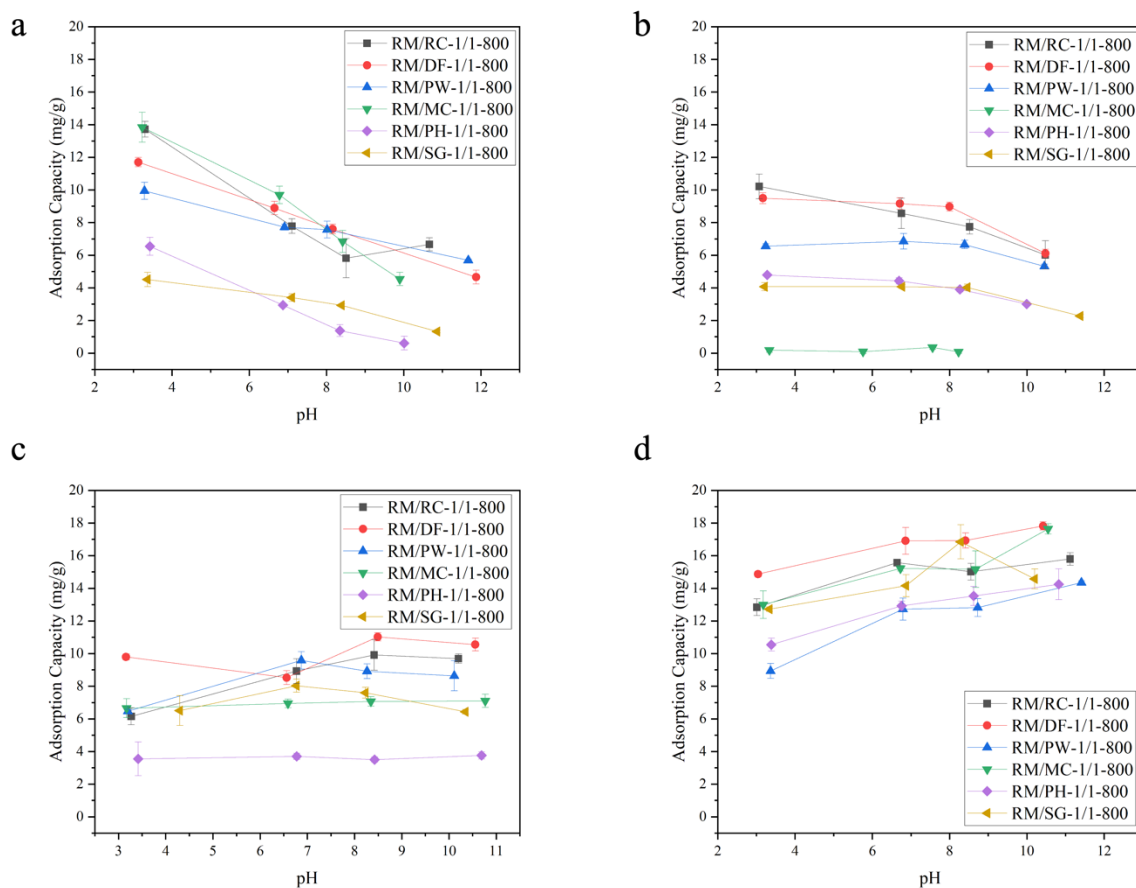


Figure 5.5 Adsorption capacities for RM/biochar composites of a) ibuprofen, b) acetaminophen, c) methyl orange, and d) methylene blue with increasing pH

Overall, the woody composites, when co-pyrolyzed with RM, resulted in the best-performing adsorbents, similar to their biochar counterparts, as woody biochars have previously been found to be superior adsorbents to non-woody biochars in previous chapters. For the composites produced from non-woody biomasses, RM/MC-1/1 showed significantly higher adsorption capacities of IBU and ACT than other non-woody biomasses and good adsorption capacities of MO and MB. This indicated that MC was the best candidate to produce bio-magnetic adsorbent. This overall higher adsorption for the woody composites was only seen for IBU and ACT, however, where IBU and ACT demonstrated gradually decreasing adsorption capacities as the pH increased. This is because both IBU and ACT become negatively charged at higher pH ($pK_a = 4.5$ and 9.3 respectively), thus repelling from the likewise negatively charged biochar surface groups (30).

The adsorption of MO tended to increase slightly with increasing pH for the woody composites, while there was little change in adsorption with pH for the non-woody composites, as well as lower overall adsorption. Since MO is likely to be adsorbed by π - π EDA interactions, the increase in adsorption despite the growing electrostatic repulsion as MO becomes negatively charged, indicates that this mechanism is most likely stronger than the electrostatic interactions. Since the adsorption of MO by the non-woody composites does not decrease with pH, this electrostatic interaction is not stronger than the EDA interactions for these composites. Thus, while the electrostatic interactions are greater than the π - π stacking interactions that are responsible for the adsorption of IBU, the π - π EDA interactions are stronger than the electrostatic interactions for all composites. Since this adsorption mechanism can only come from the highly aromatic biochar component, this means that biochar must contribute significantly to the overall adsorption mechanisms for the composites.

MB was found to be the best adsorbate adsorbed across all composites tested and produced from both woody and non-woody biomasses, pointing to strong electrostatic interactions as MB is positively charged. This was found to be a strong adsorption mechanism for all of the composites produced for each of the biomasses, woody or not, with the woody biomasses having slightly higher adsorption capacities overall due to higher surface areas presented in **Table 5.2**. Given that the metal content of the RM portion of the composite would contribute to positively charged sites, the higher adsorption of MB indicates that the RM does not significantly contribute to the adsorption mechanisms.

In comparing the adsorption mechanisms of the composites with the mechanisms of their biochar counterparts produced under the same conditions without the RM, shown in **Figure 5.6** by the adsorption capacities of the test compounds. These results revealed that the adsorption trends remained similar to the biochars alone, with the overall adsorption capacity decreasing. This means that the co-pyrolysis of biomass with RM can produce a magnetic adsorbent successfully, however the adsorption properties of the composite will be weaker. This is most likely because the RM does not contribute to the adsorptive properties of the composite, while being the most recalcitrant starting material, meaning that the final product is mostly the non-adsorptive RM and not the biomass. To correct for this, investigation into higher ratios of biomass to produce the magnetic composite are investigated in the following sections.

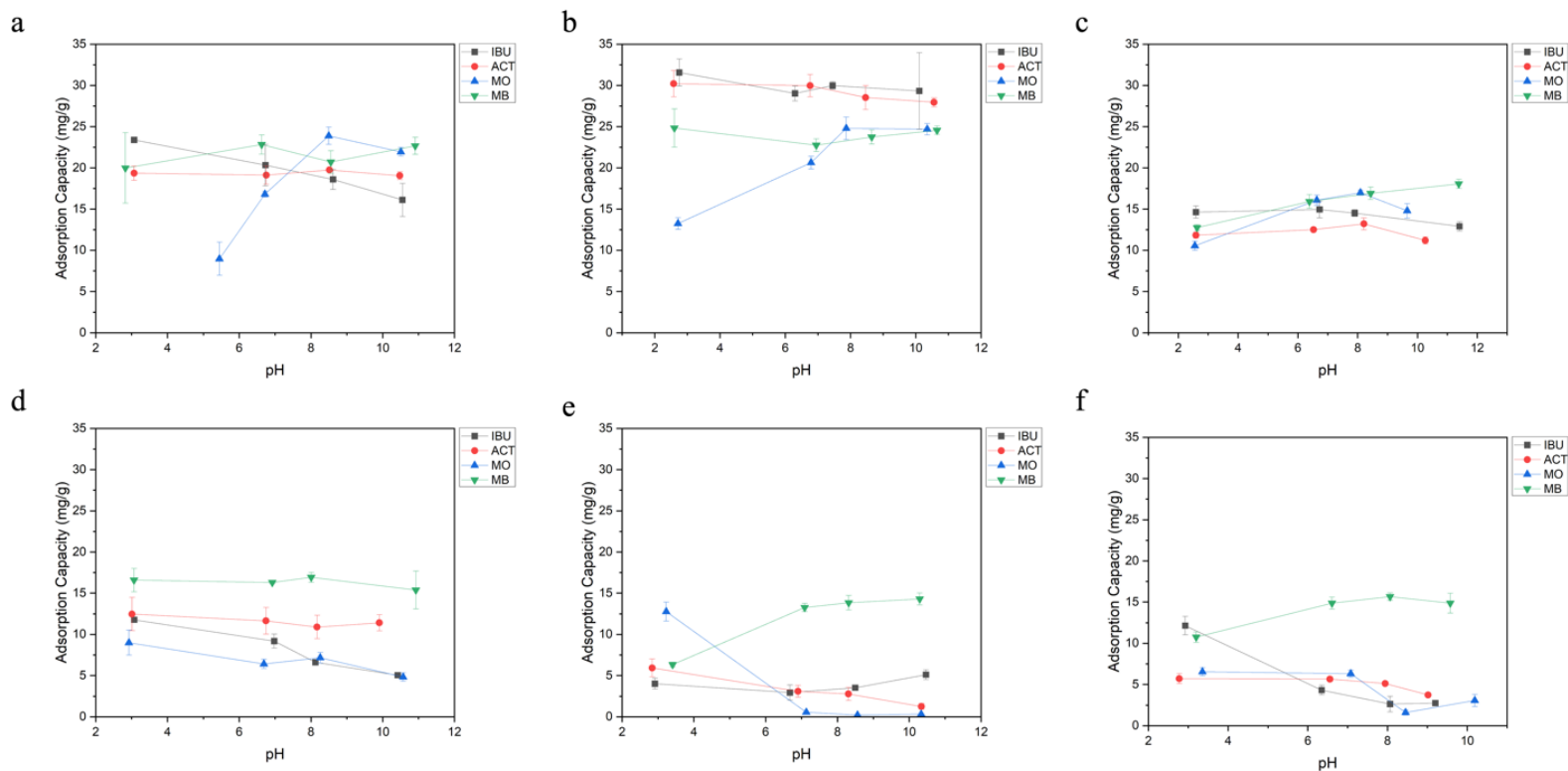


Figure 5.6 Adsorption capacities of IBU, ACT, MO, and MB with increasing pH for a) RC800-CO₂, b) DF800-CO₂, c) PW800-CO₂, d) MC800-CO₂, e) PH800-CO₂, and f) SG800-CO₂ where adsorption was performed using 50ppm of compounds and 50 mg of biochar in 15mL solutions

5.5.4 Effect of H₂O₂ Post-Treatments on Biochar RM Composites

To investigate the effect that post-treatment had on the biochar-RM composites, RM/PW-1/1 was chosen arbitrarily as a test adsorbent. The results of the adsorption tests for the composite before and after treatment are presented in **Figure 5.7a-b**, as well as the adsorption tests for the biochar analogue before and after comparison treatment. The adsorption for MB for R-PW-800-H₂O₂ at low pH was observed to be 15 mg/g and was significantly higher than the adsorption capacity before the post-treatment of 3.66 mg/g. This increase was attributed to an increase in electrostatic attraction due to more negatively charged sites after the treatment of R-PW-800 with H₂O₂. This is corroborated by the decreased adsorption of the anionic IBU after H₂O₂ treatment, from 21 mg/g to 7 mg/g at pH 4. The adsorption curves for both MB and IBU have similar trends before and after treatment with the oxidizing agent. MB and IBU have equal and

opposite trends over the exact change in pH but with a greater separation between the adsorption capacities seen after the post-treatment. The adsorption capacity of MB is seen to be nearly 5 times that of ACT at pH 4 for R-PW-800-H₂O₂ while being nearly 5 times less than that of ACT for R-PW-800 at the same pH. This indicates the overall positive surface charge of R-PW-800 becoming negative due to an increase in oxygenated surface functionality. Oxygen-containing functional groups, including hydroxyls, esters, and ether groups, can also increase the electron density of the aromatic surface through electron-donating inductive and resonance effects. This is expected to increase EDA interactions as it was indeed observed for R-PW-800-H₂O₂, where the adsorption capacity of MO increased between pH 3 and 6. MO gains electron-withdrawing characteristics as it becomes deprotonated, which will allow for interaction with surface EDGs. The overall increase of MO adsorption indicates a more substantial influence of the EDA interactions over electrostatic repulsion. However, the electrostatic repulsion was shown to increase at alkaline pH, as indicated by MO adsorption decreasing in this range. The π stacking adsorption mechanism decreases in influence upon treatment with H₂O₂, demonstrated as the adsorption of IBU decreases such that it is equal to that of the adsorption capacity of ACT, even with the presence of electrostatic repulsion. All of these changes in adsorption were also seen after treating the biochar without RM, further indicating the singularly important role the biomass portion of the composite has in adsorption, as well as showing that the H₂O₂ post-treatment similarity works on the composted as it does on biochars.

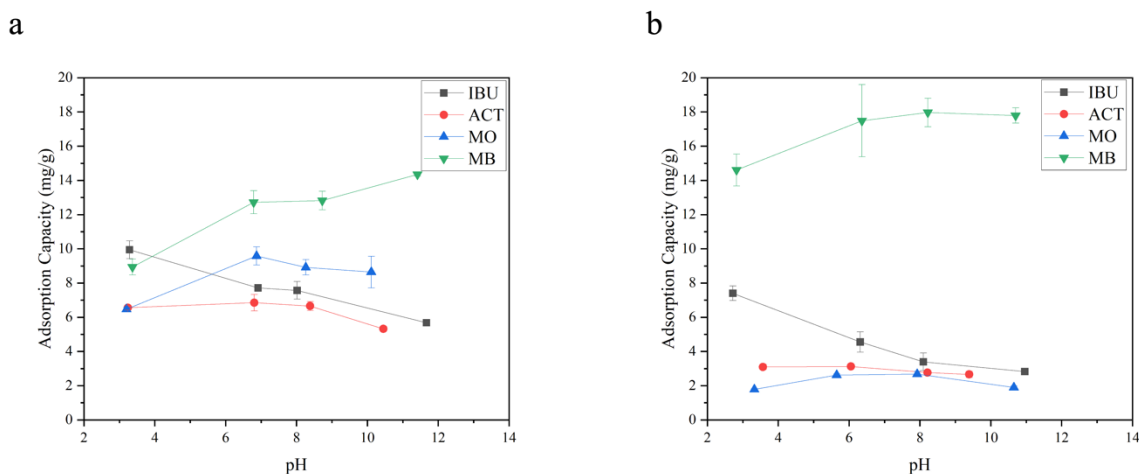


Figure 5.7 Adsorption capacities of IBU, ACT, MO, and MB with increasing pH for a) RM/PW-1/1, and b) RM/PW-1/1-H₂O₂

5.5.5 Optimization of RM and Biomass Ratio for Adsorptive and Magnetic Properties for Biochar RM Composite

When looking at the adsorption capacity of both RM and biochar derived from woody biomass alone, reported in **Table 5.1**, the adsorption of RM and RM800 is 0 mg/g for all of the organic compounds tested. There is a negative correlation between the ratio of RM to biochar and overall adsorptive capacity. In other words, the greater the mass of biomass in the feedstock, the greater the adsorption capacity of the pyrolytic product. This indicates that the biochar portion of the composite contributes entirely to the adsorptive character of the composite. The RM is then only added to provide magnetic properties to the final composite due to the presence of iron oxide in the RM particles. This is important to remember when investigating adsorption mechanisms, as it is only the biochar portion that significantly affects the adsorptive properties of the resulting final composite.

As discussed above, the mixing ratios of the biomass and RM and the reaction conditions determine the composition of the produced bio-magnetic adsorbent. RM/PW and RM/MC were chosen to investigate the effect of the mixing ratio of RM to biomass before pyrolysis since it performed best in adsorption studies, and the results are shown in **Figure 5.8**, where the adsorption capacities were all taken in triplicate with the error bars indicating the standard deviation. As shown in the figure, with the decrease of the biomass and the increase of RM in the co-pyrolysis feed, the bio-magnetic adsorbents' removal performance decreased. The results report that PW800 and MC800 had similar adsorption capacities of ACT of 39.0, and 37.0 mg/g, respectively. As the RM/Biomass ratio increased from 1/2 to 2/1, the removal of ACT decreased significantly for each of the biomasses investigated. It is worth noting that the PW and MC biochars produced under similar reaction conditions (with no RM) only showed similar ACT removal to that of the 1/2 adsorbents, suggesting that when prepared with appropriate ratios, the addition of RM will not cause significant negative effect on the adsorption performance of the adsorbent. These results demonstrate that the composite can perform equally or even better as an adsorbent than traditionally produced biochar made from the same biomass.

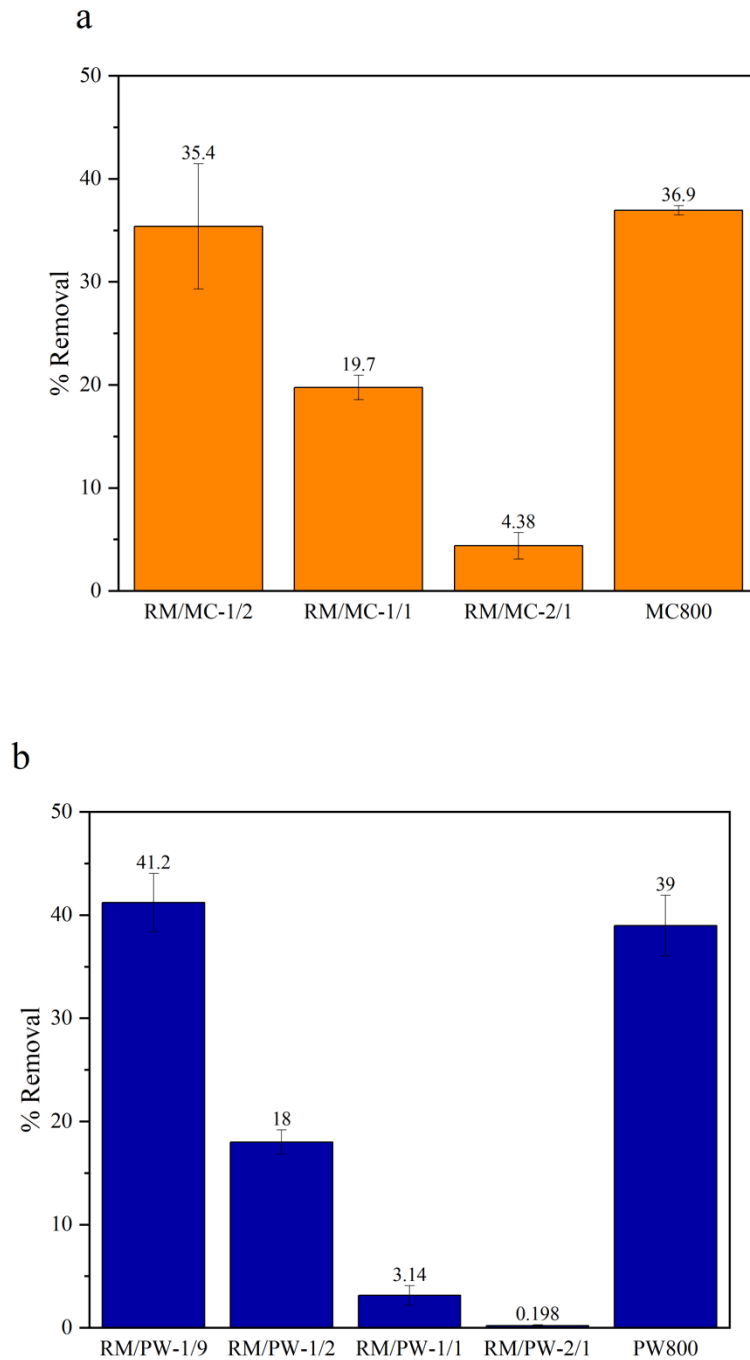


Figure 5.8 Adsorption capacity of ACT in 15 mL solution with 50 ppm ACT at neutral pH with 10 mg of a) RM/MC adsorbents and MC800-CO₂, and b) RM/PW adsorbents and PW800-CO₂ with different RM to biomass mass ratios

The images shown in **Figure 5.9** show that there is a much greater amount of the smaller RM particles in the composites produced at a 2 to 1 ratio of RM to biomass. The lighter particles, confirmed to be the RM due to high metal content in EDX spectra, are found to be in sizes similar to the biochar pieces ranging from 10-100 μm seen in the samples. While there are significant RM particles in the 2/1 composites, the magnetic properties were still found to be retained which is another important criterion to evaluate the performance in terms of ease of separation, correlated with its magnetic properties (31). The change of magnetic properties versus the changes in the RM to biomass mixing ratios was measured and presented in the form of hysteresis cycles up to 30 kA/m and shown in **Figure 5.10**. From this figure, qualitative and quantitative differences can be noted between the adsorbent with RM or biochar alone, which are paramagnetic and therefore attracted to any external magnetic field. The greater the coercive force for the composite, the greater the attraction to a magnetic field which was found to be greatest for the 2/1 ratio and lowest for the 1/2 ratio for all of the composites made from the three PW, and MC biomasses. The composite samples showed a typical ferromagnetic behaviour with clear hysteresis loops. The general trend is that the magnetic properties were seen to have a negative correlation with the content of the biomass, but a positive correlation with the RM content in the feedstock mixture. Because iron is available in the RM in the form of Fe_2O_3 , when it is co-pyrolyzed with the lignocellulosic biomass the sequential conversion of $\alpha\text{-Fe}_2\text{O}_3$ to metallic Fe might occur depending on the reaction temperature(32). Alone, pyrolyzing RM does not produce a magnetic product, however, the thermal decomposition of the biomass released electrons that caused the reduction of Fe_2O_3 , and the reducing agent may be the in-situ produced reductive gaseous products like CO , H_2 , and various condensable hydrocarbons(33). During this process, the consecutive reduction of Fe_2O_3 occurs in the temperature range of 380-700 $^\circ\text{C}$ and could lead to the formation of the different metallic Fe phases following the reaction order of " $\text{Fe}_2\text{O}_3 \rightarrow \text{Fe}_3\text{O}_4 \rightarrow \text{FeO} \rightarrow \text{Fe}$ ". This supports the deduction that the magnetic particles are obtained from the reduction of the RM oxides. Qualitative tests using a neodymium magnet were performed before and after adsorption where it was found that all composites produced were separable even after adsorption, with no significant difference in attraction to neodymium magnets between any composites tested.

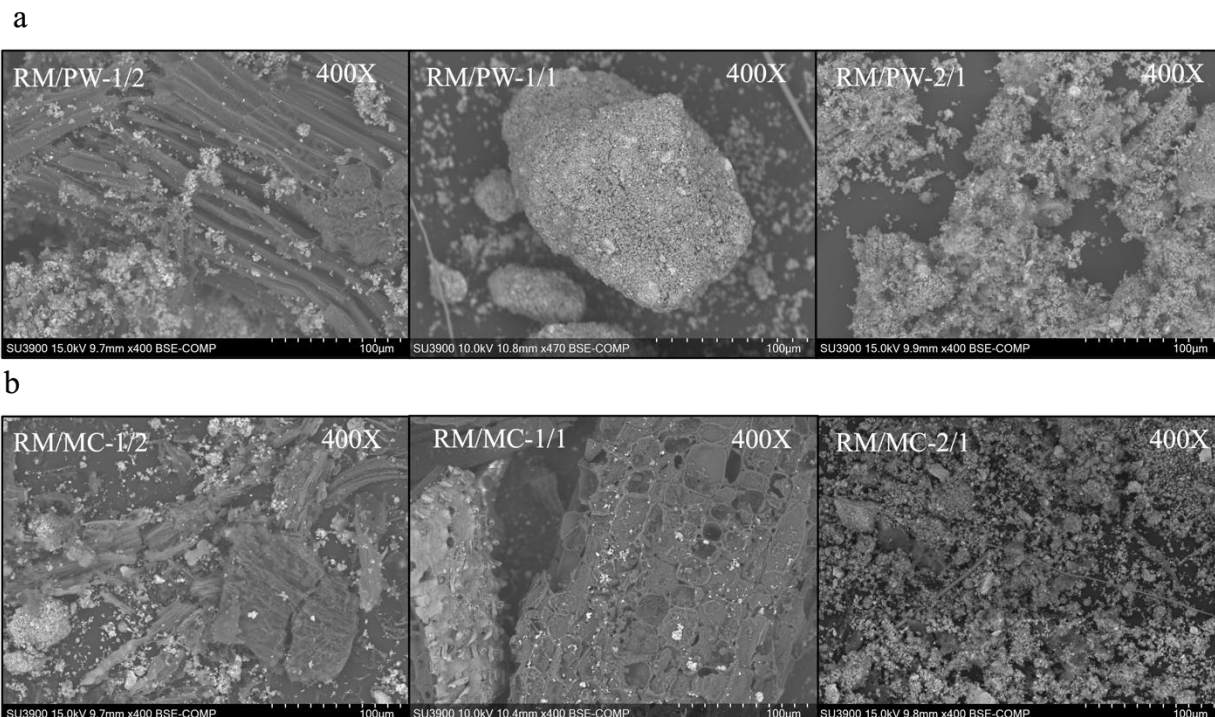


Figure 5.9 SEM images and EDX spectra at 400X Magnification for a) a) RM/PW, and b) RM/MC

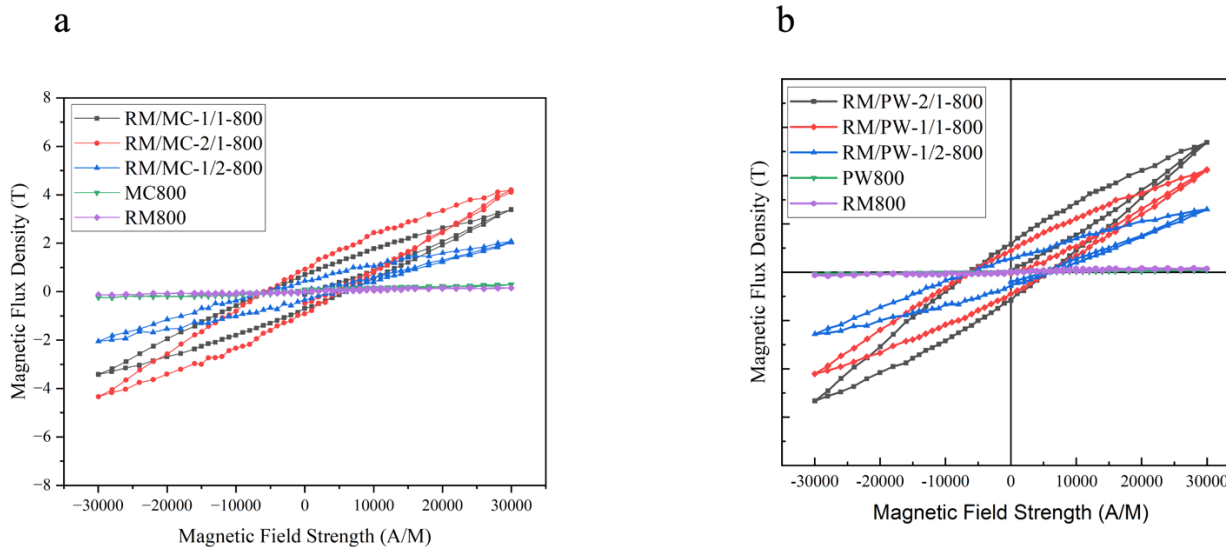


Figure 5.10 Magnetic susceptibility properties of a) RM/MC, and b) RM/PW adsorbents prepared with different RM to biomass mass ratios

5.6 Conclusion

In this study, bio-magnetic adsorbents produced from different woody and non-woody biomasses including RC, DF, PW, HL, MC, PH, SG, and RH were produced via co-pyrolysis with RM. This also proposes a method of using underused non-woody waste products and potentially environmentally harmful RM to create a product that can also remove dangerous compounds from water. This straightforward and practical procedure was found to be successful in converting all biomass species and RM into bio-magnetic adsorbents, evidenced by the good adsorption and magnetic properties of the produced composites. The adsorption capacities were found to vary for the adsorbents derived from different biomasses and the compound being adsorbed. The adsorption performance is attributed to the surface functional groups, specifically hydroxyl and carbonyl functional groups, which along with the surface porosity greatly aided in the adsorption of organic compounds. Moreover, for mixing with RM, a greater mass ratio of biomass yielded better adsorption performance with the best ratio being 1:2 for RM/biomass, demonstrating the best overall adsorption capacities of ACT for PW, DF, and MC. Also, within the range tested, the magnetic properties of the adsorbents decreased gradually when a greater ratio of biomass to RM was used, indicating that when using this method for preparing magnetic adsorbent, there will be a threshold of biomass to RM ratio to hold the separability. Finally, the 1:9 RM: DF led to the optimal properties of all composites tested in this study.

5.7 References

1. Li, C.; Xie, S.; Wang, Y.; Jiang, R.; Wang, X.; Lv, N.; et al. Multi-functional biochar preparation and heavy metal immobilization by co-pyrolysis of livestock feces and biomass waste. *Waste Management* **2021**, *134*, 241–250. doi:10.1016/j.wasman.2021.08.023.
2. Tao, Q.; Li, B.; Chen, Y.; Zhao, J.; Li, Q.; Chen, Y.; et al. An integrated method to produce fermented liquid feed and biologically modified biochar as cadmium adsorbents using corn stalks. *Waste Management* **2021**, *127*, 112–120. doi:10.1016/j.wasman.2021.04.027.
3. Nematian, M.; Keske, C.; Ng'ombe, J. N. A techno-economic analysis of biochar production and the bioeconomy for orchard biomass. *Waste Management* **2021**, *135*, 467–477. doi:10.1016/j.wasman.2021.09.014.
4. Yi, Y.; Huang, Z.; Lu, B.; Xian, J.; Tsang, E. P.; Cheng, W.; et al. Magnetic biochar for environmental remediation: A review. *Bioresource Technology*. Elsevier Ltd February 1, 2020. doi:10.1016/j.biortech.2019.122468.
5. Shen, X.; Yan, F.; Zhang, Z.; Li, C.; Zhao, S.; Zhang, Z. Enhanced and environment-friendly chemical looping gasification of crop straw using red mud as a sinter-resistant oxygen carrier. *Waste Management* **2021**, *121*, 354–364. doi:10.1016/j.wasman.2020.12.028.
6. Shi, W.; Ren, H.; Li, M.; Shu, K.; Xu, Y.; Yan, C.; et al. Tetracycline removal from aqueous solution by visible-light-driven photocatalytic degradation with low cost red mud wastes. *Chemical Engineering Journal* **2020**, *382*. doi:10.1016/j.cej.2019.122876.
7. Li, C.; Yu, J.; Li, W.; He, Y.; Qiu, Y.; Li, P.; et al. Immobilization, enrichment and recycling of Cr(VI) from wastewater using a red mud/carbon material to produce the valuable chromite (FeCr₂O₄). *Chemical Engineering Journal* **2018**, *350*, 1103–1113. doi:10.1016/j.cej.2018.06.072.
8. Wang, X.; Sun, T.; Wu, S.; Chen, C.; Kou, J.; Xu, C. A novel utilization of Bayer red mud through co-reduction with a limonitic laterite ore to prepare ferronickel. *Journal of Cleaner Production* **2019**, *216*, 33–41. doi:10.1016/j.jclepro.2019.01.176.
9. Mukiza, E.; Zhang, L. L.; Liu, X.; Zhang, N. Utilization of red mud in road base and subgrade materials: A review. *Resources, Conservation and Recycling*. Elsevier B.V. February 1, 2019, pp 187–199. doi:10.1016/j.resconrec.2018.10.031.

10. Tandekar, S.; Korde, S.; Jugade, R. M. Red mud-chitosan microspheres for removal of coexistent anions of environmental significance from water bodies. *Carbohydrate Polymer Technologies and Applications* **2021**, *2*, 100128. doi:10.1016/j.carpta.2021.100128.
11. Qiu, B.; Tao, X.; Wang, H.; Li, W.; Ding, X.; Chu, H. Biochar as a low-cost adsorbent for aqueous heavy metal removal: A review. *Journal of Analytical and Applied Pyrolysis*. Elsevier B.V. May 1, 2021. doi:10.1016/j.jaap.2021.105081.
12. Yoon, K.; Cho, D. W.; Bhatnagar, A.; Song, H. Adsorption of As(V) and Ni(II) by Fe-Biochar composite fabricated by co-pyrolysis of orange peel and red mud. *Environmental Research* **2020**, *188*. doi:10.1016/j.envres.2020.109809.
13. Yoon, K.; Cho, D. W.; Tsang, Y. F.; Tsang, D. C. W.; Kwon, E. E.; Song, H. Synthesis of functionalised biochar using red mud, lignin, and carbon dioxide as raw materials. *Chemical Engineering Journal* **2019**, *361*, 1597–1604. doi:10.1016/j.cej.2018.11.012.
14. Cho, D. W.; Yoon, K.; Ahn, Y.; Sun, Y.; Tsang, D. C. W.; Hou, D.; et al. Fabrication and environmental applications of multifunctional mixed metal-biochar composites (MMBC) from red mud and lignin wastes. *Journal of Hazardous Materials* **2019**, *374*, 412–419. doi:10.1016/j.jhazmat.2019.04.071.
15. Mehta, D.; Mazumdar, S.; Singh, S. K. Magnetic adsorbents for the treatment of water/wastewater-A review. *Journal of Water Process Engineering*. Elsevier Ltd September 1, 2015, pp 244–265. doi:10.1016/j.jwpe.2015.07.001.
16. Yi, Y.; Huang, Z.; Lu, B.; Xian, J.; Tsang, E. P.; Cheng, W.; et al. Magnetic biochar for environmental remediation: A review. *Bioresource Technology*. Elsevier Ltd February 1, 2020. doi:10.1016/j.biortech.2019.122468.
17. Wang, H.; Cai, J.; Liao, Z.; Jawad, A.; Ifthikar, J.; Chen, Z.; et al. Black liquor as biomass feedstock to prepare zero-valent iron embedded biochar with red mud for Cr(VI) removal: Mechanisms insights and engineering practicality. *Bioresource Technology* **2020**, *311*. doi:10.1016/j.biortech.2020.123553.
18. Liu, L.; Liu, X.; Wang, D.; Lin, H.; Huang, L. Removal and reduction of Cr(VI) in simulated wastewater using magnetic biochar prepared by co-pyrolysis of nano-zero-valent iron and sewage sludge. *Journal of Cleaner Production* **2020**, *257*. doi:10.1016/j.jclepro.2020.120562.

19. Kazak, O.; Tor, A. In situ preparation of magnetic hydrochar by co-hydrothermal treatment of waste vinasse with red mud and its adsorption property for Pb(II) in aqueous solution. *Journal of Hazardous Materials* **2020**, *393*. doi:10.1016/j.jhazmat.2020.122391.
20. Huff, M. D.; Lee, J. W. Biochar-surface oxygenation with hydrogen peroxide. *Journal of Environmental Management* **2016**, *165*, 17–21. doi:10.1016/j.jenvman.2015.08.046.
21. Sewu, D. D.; Boakye, P.; Jung, H.; Woo, S. H. Synergistic dye adsorption by biochar from co-pyrolysis of spent mushroom substrate and *Saccharina japonica*. *Bioresource Technology* **2017**, *244*, 1142–1149. doi:10.1016/j.biortech.2017.08.103.
22. Yi, S.; Gao, B.; Sun, Y.; Wu, J.; Shi, X.; Wu, B.; et al. Removal of levofloxacin from aqueous solution using rice-husk and wood-chip biochars. *Chemosphere* **2016**, *150*, 694–701. doi:10.1016/j.chemosphere.2015.12.112.
23. Navarathna, C. M.; Bompuwala Dewage, N.; Keeton, C.; Pennisson, J.; Henderson, R.; Lashley, B.; et al. Biochar Adsorbents with Enhanced Hydrophobicity for Oil Spill Removal. *ACS Applied Materials and Interfaces* **2020**, *12*(8), 9248–9260. doi:10.1021/acsami.9b20924.
24. Yi, Y.; Huang, Z.; Lu, B.; Xian, J.; Tsang, E. P.; Cheng, W.; et al. Magnetic biochar for environmental remediation: A review. *Bioresource Technology*. Elsevier Ltd February 1, 2020. doi:10.1016/j.biortech.2019.122468.
25. Nath, H.; Sahoo, P.; Sahoo, A. Characterization of Red Mud treated under high temperature fluidization. *Powder Technology* **2015**, *269*, 233–239. doi:10.1016/j.powtec.2014.09.011.
26. Shim, W. G.; Nah, J. W.; Jung, H. Y.; Park, Y. K.; Jung, S. C.; Kim, S. C. Recycling of red mud as a catalyst for complete oxidation of benzene. *Journal of Industrial and Engineering Chemistry* **2018**, *60*, 259–267. doi:10.1016/j.jiec.2017.11.012.
27. Alharthi, A. I.; Hargreaves, J. S. J.; Pulford, I. D.; Gupta, N.; Balakrishnan, M.; Batra, V. S.; et al. Hydrocarbon Cracking Over Red Mud and Modified Red Mud Samples. *Journal of Sustainable Metallurgy* **2016**, *2*(4), 387–393. doi:10.1007/s40831-016-0082-4.
28. Nath, H.; Sahoo, P.; Sahoo, A. Characterization of Red Mud treated under high temperature fluidization. *Powder Technology* **2015**, *269*, 233–239. doi:10.1016/j.powtec.2014.09.011.
29. Liu, Y.; Lin, C.; Wu, Y. Characterization of red mud derived from a combined Bayer Process and bauxite calcination method. *Journal of Hazardous Materials* **2007**, *146*(1–2), 255–261. doi:10.1016/j.jhazmat.2006.12.015.

30. Lorphensri, O.; Intravijit, J.; Sabatini, D. A.; Kibbey, T. C. G.; Osathaphan, K.; Saiwan, C. Sorption of acetaminophen, 17 α -ethynyl estradiol, nalidixic acid, and norfloxacin to silica, alumina, and a hydrophobic medium. *Water Research* **2006**, *40*(7), 1481–1491. doi:10.1016/j.watres.2006.02.003.
31. Li, X.; Wang, C.; Zhang, J.; Liu, J.; Liu, B.; Chen, G. Preparation and application of magnetic biochar in water treatment: A critical review. *Science of the Total Environment* **2020**, *711*. doi:10.1016/j.scitotenv.2019.134847.
32. Zhao, Y.; Zhang, R.; Liu, H.; Li, M.; Chen, T.; Chen, D.; et al. Green preparation of magnetic biochar for the effective accumulation of Pb(II): Performance and mechanism. *Chemical Engineering Journal* **2019**, *375*. doi:10.1016/j.cej.2019.122011.
33. Cho, D. W.; Yoon, K.; Ahn, Y.; Sun, Y.; Tsang, D. C. W.; Hou, D.; et al. Fabrication and environmental applications of multifunctional mixed metal-biochar composites (MMBC) from red mud and lignin wastes. *Journal of Hazardous Materials* **2019**, *374*, 412–419. doi:10.1016/j.jhazmat.2019.04.071.

Chapter 6

6 Conclusions and Future Work

6.1 Conclusions

Biochar research is a quickly growing field in analytical chemistry, chemical and environmental engineering given its proven effectiveness in environmental remediation, as it provides unique solutions to a wide range of important environmental issues. Biochar has the potential application as a promising adsorbent for the elimination of a variety of pollutants in both soil and aqueous environments due to its favourable adsorption properties. Compared to current water treatment methods, biochar presents a potentially more sustainable approach as it is a low-cost and renewable adsorbent made using readily available biomaterials with the potential to be optimized for specific adsorbates. This thesis focuses on the adsorption of organic compounds specifically in aqueous media, intending to optimize physical characteristics of the biochar for selective adsorption of desired compounds. Chapter 1 begins with a background discussion on the environmental motivations of investigating biochar for the removal of organic compounds, chosen specifically due to biochar's high affinity for aromatic compounds given its highly aromatic surface structure. Common characterization techniques such as.....are explained in detail as well, defining how these can be used to determine how these characteristics affect adsorption mechanisms.

Chapter 2 proposes a detailed method to investigate the adsorption mechanisms of biochar towards organic compounds in water, which was used to investigate a range of biochars to determine what compounds biochars are best suited to adsorb in real-world applications. IBU, ACT, MO, and MB were selected as four test compounds as representative organic pollutants and were used to investigate adsorptive capacities of biochars produced by four woody (RC, DF, PW, and HL) and four non-woody (RH, MC, PH, and SG) biomasses under different pyrolysis temperatures and flow gases, N_2 and CO_2 . π - π interactions were found to be dominant mechanisms for biochars that had high aromaticity, and oxygen-containing functional groups influenced the electrostatic interactions due to negative sites, as well as strengthening π - π EDA interactions. These results helped to support the efficacy of this test procedure, while the results also alluded to the importance of oxygen-containing groups in controlling the adsorption of organic compounds. While biochars that were found to have mainly hydroxyl functional groups showed good adsorption of aromatic compounds with EWGs, biochars with carbonyl groups were found to have greater adsorption capacities for aromatic compounds with EDGs. This suggests that the electrostatic interactions and π - π EDA interactions are both heavily influenced by the same

functional groups, resulting in possible competition between the mechanisms. There is a point where electrostatic interactions from negatively charged oxygen sites are stronger than the π - π interactions due to aromaticity, at which point the electrostatic interactions will dominate over π - π EDA and stacking interactions. Further evaluation of the composition of the biomasses showed that hemicellulose content contributed to greater hydroxyl groups, while greater cellulose and lignin content of the woody biochars produced chars with greater carbonyl groups.

Chapter 3 subsequently takes a deeper look at the effect of the physical properties on the adsorption mechanisms of biochar. HNO_3 , H_2O_2 , and KOH , post-treatment on different RC and DF biochars prepared under CO_2 at 800°C were chosen as they differ widely in their aromaticity, surface area, oxygen-containing functional groups etc. The use of HNO_3 treatment introduced hydroxyl groups and decreased ash content, both of which played the largest role in the electrostatic interactions of the biochar. While the mineral content was not seen to have a significant role in these interactions, oxygen-functional groups dominated in contributing to negatively charged sites and thus electrostatic interactions of biochar. Knowing this, H_2O_2 post-treatment was done to RC500- CO_2 , DF500- CO_2 , RC800- CO_2 , and DF800- CO_2 biochars, as this functionalized the biochar with hydroxyl groups while mostly maintaining the other physical properties of the biochar. It was found that OH groups increased electrostatic interactions for all the biochars while increasing π - π EDA interactions with compounds with EWGs so long as the aromaticity was great enough, as was seen for the RC800- CO_2 , and DF800- CO_2 biochars. The effect of carbonyl groups was investigated as well using chemical activation with KOH as a post-treatment, which increased both $\text{C}=\text{O}$ surface groups and aromaticity of the DF500- CO_2 , and DF800- CO_2 biochars. Higher aromaticity had the effect of increasing the relative strength of the EDA interactions, and carbonyl functional groups increased these interactions with compounds containing EDGs. It was found that there were five types of adsorption mechanisms that biochar may have, given the constrictions of the physical properties and how they can contribute to these adsorption mechanisms. The biggest contributing properties towards adsorption mechanisms were determined to be aromaticity and oxygen-containing functional groups (predominantly hydroxyl and carbonyl groups) with surface area and porosity being more determinant of overall adsorption capacities. Knowing this, five biochars were selected that displayed each of these five main mechanisms, which were investigated in the preceding chapter for the more real-world-like adsorption settings with complex mixtures of aromatic compounds.

Chapter 4 considers the effect that competitive adsorption may have on the adsorption mechanisms of biochars by investigating the changes in the adsorption capacities of three aromatic compounds: MO, MB, and ACT in pairs. Five biochars were chosen for this study, DF800-CO₂, DF800-CO₂-KOH, DF800-CO₂-H₂O₂, DF500-CO₂-KOH, and MC500-CO₂, whose adsorption mechanisms were found to be the most common adsorption mechanisms of biochars. This study was designed with the intent to observe interactions between competing adsorbates as this would more closely parallel real-world applications for adsorption, where understanding the effects of this would allow the designing of more effective water purification methods. The results therefore provide valuable and novel insight into the role that biochar adsorption mechanisms may have on the intermolecular interactions between aromatic compounds. Again, the oxygen-containing functional groups were found to have the largest influence on competitive adsorption, as they often provide the greatest number of adsorption sites for organic compounds via both electrostatic and π - π EDA interactions. In general, it was found that the biochars with more variance in oxygen functional groups, i.e., both hydroxyl and carbonyl groups present in FTIR, had greater synergetic adsorption when present in a mixture. Biochars with only hydroxyl groups exhibited competing adsorption mechanisms and poorer adsorption capacities of aromatic compounds in complex solutions.

MO is readily able to form intermolecular interactions with MB both through a π - π charge transfer and ionic charge interactions and it is more likely they can interact both with each other and the biochar. MO and ACT can transfer charges between their aromatic groups, however unlike with the cationic MB, MO is unable to form ionic interactions with ACT as it has no charge under the conditions of this study. If biochar has adsorption mechanisms suited to adsorb both compounds that do not compete, such as π - π EDA interactions, the adsorption capacities of both compounds were found to increase, as seen for DF500-CO₂-KOH. Alternatively, if the adsorption mechanisms compete with one another for two compounds, such as electrostatic and π - π EDA interactions, the competition for sites resulted in the decreased adsorption of the compound adsorbed by the weaker adsorption mechanism. This was observed for DF800-CO₂, and DF800-CO₂-H₂O₂. When only one of the compounds is strongly adsorbed by a biochar, the adsorption of the other compound was shown to increase relative to when adsorbed alone, such as was seen for DF800-CO₂ and MC500-CO₂.

In the case of ACT and MB, both have EDGs and are not likely to interact with one another via charge transfer interactions and there is more likely to be competition for adsorption sites since both are adsorbed by π - π EDA interactions with EWGs. Because MB is also able to be adsorbed by electrostatic interactions however, this does not increase ACT when adsorbed together since there is not a strong enough electrostatic interaction for most biochars. This may be because this biochar allowed for weak cation- π intermolecular interactions between the compounds, as was seen for DF800-CO₂-H₂O₂ and MC500-CO₂.

Finally, chapter 5 addresses the issue of the removal of biochar from wastewater after adsorption takes place, as this is a real-world problem with adsorption. Bio-magnetic adsorbents produced from RC, DF, PW, HL, MC, PH, SG, and RH were produced via co-pyrolysis with RM, a waste product of the aluminum industry rich in iron oxide. This also has the benefit of using an underused non-woody waste product and potentially environmentally harmful RM to create a value-added product for water treatment. Co-pyrolysis with RM was successful in converting all biomass species and RM that were investigated into bio-magnetic adsorbents, evidenced by the good adsorption and magnetic properties of the produced composites. The adsorption capacities varied for the adsorbents based on what biomasses they were produced from as well as the compound being adsorbed. The adsorption performance is attributed mainly to the surface functional groups, specifically hydroxyl and carbonyl functional groups, which along with the surface porosity greatly aided in the adsorption of organic compounds. Mixing ratios of biomass and RM were also tested to determine optimal conditions for magnetic and adsorptive properties of the composites, where better adsorption performance was found with a ratio of 1:2 for RM/biomass. A minimum ratio of RM to biomass of XX was required in order to maintain magnetic properties. Magnetic properties of the adsorbents decreased gradually when a greater ratio of biomass to RM was used, with the 1:9 RM: DF having the optimal properties of all composites tested in this study.

6.2 Future Work

This thesis has shown the efficacy of biochar as an adsorbent for aromatic organic compounds, with the adsorption mechanisms being dependent mainly on the aromaticity and oxygen-containing surface groups. Future research into biochar may include an investigation of biochar's affinity towards aliphatic compounds. While the highly aromatic surface structure of

biochar makes it well suited for adsorption of aromatic compounds, adsorption of non-aromatic compounds is usually found to be much lower and done primarily through electrostatic, pore filling and hydrophobic interactions (1,2). Aliphatic compounds make up a large portion of organic compounds in water sources, specifically, perfluoroalkyl and polyfluoroalkyl substances (PFAS) compounds are of growing concern (3). PFAS compounds have been used extensively in commercial products such as textiles, paints, packaging materials etc. due to their high thermal and chemical stability from the strong C-F covalent bond, however, this high stability is also responsible for these compounds persisting as they are deposited in water sources (4). These compounds are ubiquitous in soil and water and have been found to accumulate over time in the human body as a result of their ability to bioaccumulate in food chains (5,6). This has also been linked to diseases such as heart attacks, chronic inflammatory diseases, central nervous system disorders and cancer (4,7). This thesis provides a detailed understanding of biochar adsorption mechanisms towards organic compounds and how their properties may be engineered and altered to fit specific compounds, allowing for the possibility of designing an adsorbent for specific adsorption of difficult-to-remove aliphatic PFAS compounds. While these compounds are unable to interact via π - π interactions, electrostatic interactions will most likely be the dominant mechanism responsive to the adsorption of these compounds. The development of biochar with strong electrostatic interactions towards anions is projected to be the most effective for this purpose.

As well, further research into the desorption of organic compounds would also be valuable in the recycling of adsorbed compounds, which can be used in a variety of applications depending on the target compound for desorption. Understanding the mechanisms responsible for adsorption may provide insight into how these mechanisms may be weakened to allow for the retrieval of compounds. Furthermore, in combination with specific adsorption, biochar may provide a method to remove and reuse specifically desirable compounds from waste-water sources. This work provides a comprehensive evaluation of the surface chemistry of biochar for the application for adsorption of organic compounds, facilitating this future work.

6.3 References

1. Chu, G.; Han, Z.; Wang, Z.; Kong, D.; Qin, W.; Si, Y.; et al. The Sorption of Sulfamethoxazole by Aliphatic and Aromatic Carbons from Lignocellulose Pyrolysis. *Agronomy* **2022**, *12*(2). doi:10.3390/agronomy12020476.
2. Song, Z.; He, J.; Kouzehkhanan, S. M. T.; Oh, T.-S.; Olshansky, Y.; Duin, E. C.; et al. Enhanced Sorption and Destruction of PFAS by Biochar-Enabled Advanced Reduction Process. *Chemosphere* **2024**, 142760. doi:10.1016/j.chemosphere.2024.142760.
3. Militao, I. M.; Roddick, F.; Fan, L.; Zepeda, L. C.; Parthasarathy, R.; Bergamasco, R. PFAS removal from water by adsorption with alginate-encapsulated plant albumin and rice straw-derived biochar. *Journal of Water Process Engineering* **2023**, *53*. doi:10.1016/j.jwpe.2023.103616.
4. Zhang, Y.; Tan, X.; Lu, R.; Tang, Y.; Qie, H.; Huang, Z.; et al. Enhanced Removal of Polyfluoroalkyl Substances by Simple Modified Biochar: Adsorption Performance and Theoretical Calculation. *ACS ES and T Water* **2023**, *3*(3), 817–826. doi:10.1021/acsestwater.2c00597.
5. Garcia-Barrios, J.; Drysdale, M.; Ratelle, M.; Gaudreau, É.; LeBlanc, A.; Gamberg, M.; et al. Biomarkers of poly- and perfluoroalkyl substances (PFAS) in Sub-Arctic and Arctic communities in Canada. *International Journal of Hygiene and Environmental Health* **2021**, *235*. doi:10.1016/j.ijheh.2021.113754.
6. Brusseau, M. L.; Van Glubt, S. The influence of molecular structure on PFAS adsorption at air-water interfaces in electrolyte solutions. *Chemosphere* **2021**, *281*. doi:10.1016/j.chemosphere.2021.130829.
7. Cao, Y.; Lee, C.; Davis, E. T. J.; Si, W.; Wang, F.; Trimpin, S.; et al. 1000-Fold Preconcentration of Per- And Polyfluorinated Alkyl Substances within 10 Minutes via Electrochemical Aerosol Formation. *Analytical Chemistry* **2019**, *91*(22), 14352–14358. doi:10.1021/acs.analchem.9b02758.

Curriculum Vitae

Griffin Loeb sack

EDUCATION

2024-**Ph. D.**, Chemistry, University of Western Ontario, Institute for Chemicals and Fuels from Alternative Resources (ICFAR)

- *Thesis Title:* A Study on Biochar Properties Toward their Effects on Adsorption Mechanisms for Aromatic Organic Compounds in Water
- *Supervisors:* Dr. Ken Yeung, Dr. Franco Berruti, and Dr. Naomi Klinghoffer
- *Courses:* CHEM9522A Analytical Separations (Grade: 90), CHEM9754R Powder Diffraction (Grade: 85), CHEM9674A Advanced Optical Spectroscopy and Microscopy (Grade: 82), CHEM9532B Analytical Instrumentation (Grade: 92), Surface Chemistry of Nanoparticles (Grade: 93).

2019-**Honours B.Sc.**, Synthetic and Catalytic Chemistry Specialist, University of Toronto

- *Thesis Project:* Antifouling Effects of 3-(3-(trichlorosilyl)propoxy)propanoyl (MEG-Cl) chloride on Iridium and Steel
- *Supervisor:* Dr. Michael Thompson
- *Relevant Courses:* Organic Spectroscopic Analysis, Instrumental Analysis, Separation Science, Lab Instrumentation, Organometallic Chemistry, Organic Reaction Mechanisms.

TEACHING EXPERIENCE

2019-2024, **Laboratory Teaching Assistant**, Organic Chemistry for Life Sciences (CHEM2213A/CHEM2223B), University of Western Ontario

- *Supervisor:* Dr. Mark Workentin

2023-2024 **Laboratory Teaching Assistant**, Discovering Chemical Energetics (CHEM1302A), University of Western Ontario

- *Supervisor:* Dr. Augusto

2022-2023, **Course Teaching Assistant**, Organic Chemistry for Life Sciences, (CHEM2213A/CHEM2223B), University of Western Ontario

- *Supervisor:* Dr. Mark Workentin

2021-2022, **Course Teaching Assistant**, Chemistry: Everywhere and Everything (CHEM1027A), University of Western Ontario

- *Supervisor:* Dr. Gurpaul Kochhar

CONFERENCES

Oral Presentations

Loeb sack, G.; Berruti, F.; Yeung, K.; Klinghoffer, N. Investigation of Biochar Properties Responsible for Adsorption Mechanisms of Aromatic and Aliphatic Compounds in Water. The Third International Biochar Conference, Tomar, Portugal, September 17-22 2023.

Loebsack, G.; Berruti, F.; Yeung, K.; Klinghoffer, N. Biochar Adsorption: Investigation of Adsorption Mechanisms. The 6th Italian Biochar Association (ICHAR) Biochar School Conference, Virtual, Florence, Italy, October 13-14 2022.

Loebsack, G.; Kang, K.; Berruti, F.; Yeung, K.; Klinghoffer, N. Biochar Formation Pathways and Adsorption Mechanisms of Red Mud-Biomass Pyrolytic Composites with Magnetic Properties. The 23rd International Conference on Analytical and Applied Pyrolysis (PYRO), Ghent, Belgium, May 2022.

Loebsack, G.; Berruti, F.; Yeung, K.; Klinghoffer, N. Biochar as an Adsorbent for Removal of Organic Compounds in Water: Investigation of Adsorption Mechanisms. The 8th International Conference on Engineering for Waste and Biomass Valorisation, Virtual, Guelph, Ontario, Canada, May 2021.

Loebsack, G.; Berruti, F.; Yeung, K.; Klinghoffer, N. Biochar Applications of Biochar as an Adsorbent in Gas/Water Purification. International eConference on Analytical and Applied Pyrolysis (PYRO), Virtual, Ghent, Belgium, April 12-13 2021.

Poster Presentations

Loebsack, G.; Berruti, F.; Yeung, K.; Klinghoffer, N. Investigation of Biochar Properties Responsible for Adsorption Mechanisms of Aromatic and Aliphatic Compounds in Water. The Third International Biochar Conference, Tomar, Portugal, September 17-22 2023.

Loebsack, G.; Berruti, F.; Yeung, K.; Klinghoffer, N. Biochar Characterization of Soft Wood Biochar Adsorption Mechanisms through Adsorption of Four Model Organic Compounds. The 23rd International Conference on Analytical and Applied Pyrolysis (PYRO), Ghent, Belgium, May 2022.

PUBLICATIONS

Articles

Loebsack, G.; Kang, K.; Yeung, K-C.; Bartoli, M.; Berruti, F.; Klinghoffer, N. Magnetic Adsorbents from Co-Pyrolysis of Non-woody Biomass and Red Mud for Water Decontamination. *Can. J. Chem. Eng.* **2024**. doi:10.1002/cjce.25407.

Loebsack, G.; Kang, K.; Klinghoffer, N.; Yeung, K.; Torsello, D.; Gerbaldo, R.; Berruti, F. Adsorption Mechanisms and Optimal Production of Magnetic Red Mud Biochar Composites from Soft Wood Biomass. *J. Anal. Appl. Pyrolysis.* **2023**, 106340, doi:10.1016/j.jaap.2023.106340

Zecchi, S.; Ruscillo, F.; Cristoforo G.; Bartoli, M.; **Loebsack, G.;** Kang, K.; Piatti, E.; Torsello, D.; Ghigo, G.; Gerbaldo, R.; Giorcelli, M.; Berruti, F.; Tagliaferro. Effect of Red Mud Addition

on Electrical and Magnetic Properties of Hemp-Derived-Biochar-Containing Epoxy Composites. *Micromachines*. **2023**, *14*(2), 429. doi:10.3390/mi14020429.

Kang, K*.; **Loeb sack, G.**; Sarchami, T.; Klinghoffer, N.; Papari, S.; Yeung, K.; Berruti, F. Production of a bio-magnetic adsorbent via co-pyrolysis of pine wood waste and red mud. *J. Waste Manag.* **2022**, *149*, 124-133. doi:10.1016/j.wasman.2022.06.009.

Book Chapter

Bamdad, H.; **Loeb sack, G.**; Klinghoffer, N.; Hawboldt, K.; Yeung, K.; Berruti, F. Biochar: Emerging Applications. Chapter 15: Applications of Biochar in Gas and Water Purification and in Contaminated Soil Remediation. **2020**. IOP Publishing.